AN INTERMITTENT PREDICTIVE CONTROL APPROACH TO MODELLING SUSTAINED HUMAN MOTOR CONTROL

Adamantia S. Mamma-Graham

A thesis for the degree of Doctor of Philosophy (PhD)

Submitted to the College of Science and Engineering,
University of Glasgow

July 2014

[This page is intentionally blank]

I dedicate this thesis to my beloved husband Ross Samuel Graham who makes a lovely difference in my life.

When you start on the way to Ithaca,
wish that the way be long,
full of adventure, full of knowledge.
The Laestrygones and the Cyclopes
and angry Poseidon, do not fear:
such, on your way, you shall never meet
if your thoughts are lofty, if a noble
emotion touch your mind, your body.
The Laestrygones and the Cyclopes
and angry Poseidon you shall not meet
if you carry them not in your soul,
if your soul sets them not up before you.

extracted from the Poem ITHACA of **Constantinos C. Cafavy (1863–1933)**
(Translated by George Valassopoulo. The Criterion 2/8, July 1924)

Abstract

Although human sustained control movements are continuous in nature there is still controversy on the mechanisms underlying such physiological systems. A popular topic of debate is whether human motor control mechanisms could be modelled as engineering control systems, and if so, what control algorithm is most appropriate.

Since the early years of modelling sustained control tasks in human motor control the servomechanism has been an adequate model to describe human tracking tasks. Another continuous-time system model that is often used to model sustained control tasks is the predictive controller which is based on internal models and includes prediction and optimisation. On the other hand, studies have suggested intermittent behaviour of the "human controller" in sustained motor control tasks.

This thesis investigated whether intermittent control is a suitable approach to describe sustained human motor control. It was investigated how well an intermittent control system model could approximate both the deterministic and non-deterministic parts of experimental data, from a visual-manual compensatory tracking task. Finally, a preliminary study was conducted to explore issues associated with the practical implementation of the intermittent control model.

To fit the deterministic part of experimental data, a frequency domain identification method was used. Identification results obtained with an intermittent controller were compared against the results using continuous-time non-predictive and predictive controllers. The results show that the identified frequency response functions of the intermittent control model not only fit the frequency response functions derived from the experimental data well, but most importantly resulted in identified controller parameters which are similar to those identified using a predictive controller, and whose parameter values appear to be physiologically meaningful.

A novel way to explain human variability, as represented by the non-deterministic part of the experimental data (the *remnant*), was developed, based on an intermittent control model with variable intermittent interval. This model was compared against the established paradigm, in which variability is explained by a predictive controller with added noise, either signal dependent control signal noise, or observation noise. The study has shown that the intermittent controller with a variable intermittent interval could model the non-deterministic experimental data as well as the predictive controller model with added noise. This provides a new explanation for the source of remnant in human control as inherent to the controller structure, rather than as a noise signal, and enables a new interpretation for the physiological basis for human variability.

Finally, the theoretical intermittent control model was implemented in real-time in the context of the physiological control mechanism of human standing balance. An experimental method was developed to apply automatic artificial balance of an inverted pendulum in the context of human standing, via functions electrical stimulation control of the lower leg muscles of a healthy subject.

The significance of this study is, firstly, that frequency domain identification was applied for the first time with intermittent control, and it could be shown that both intermittent and predictive control models can model deterministic experimental data from manual tracking tasks equally well. Secondly, for the first time the inherent variability, which is represented by the remnant signal, in human motor control tasks could be modelled as part of the structure of the intermittent controller rather than as an added noise model. Although, the experimental method to apply automatic artificial balance of an inverted pendulum in the context of human standing was not successful, the intermittent controller was implemented for the first time in real-time and combined with electrical muscle stimulation to control a physiological mechanism.

Acknowledgements

I would like to thank everyone who has been involved either directly or indirectly in this PhD journey.

I would like to thank my supervisor Dr. Henrik Gollee for his support throughout my PhD and especially for his important corrections while I was writing the thesis.

Thanks to Ian Loram, Cornelis Van de Kamp, Martin Lakie, Peter Gawthrop, Cristiano Spiga and Timothy Osborne.

I would like to thank the Mechanical engineering department of Glasgow University, especially Mrs. Elaine Mcnamara for her suggestions during my writing and for listening to my worries. Elaine, thank you very much for being a good friend to me. My thanks also go to Ms. Marylin Dunlop and Mrs. Mari-Carmen Garcia-Perez for their friendship throughout my studies at university. A special thanks to all the staff of the library of Glasgow University for the great facilities and study areas you provide for the students so that it is pleasant and comfortable for them to study there.

I would like to thank the EPSRC for funding the project.

Very special thanks to my friends Dimitris Chalas, Margaret Armentano and Bethel (Bethos) Chika who made the process of writing more tolerable, by going for coffees.

I am very grateful to the Greek, and Greek-Cypriot community of Glasgow. Thank very much for making my stay to Glasgow more fun and embracing me from the very beginning as part of the community. I owe you a lot. Especially I would like to thank the late Mrs. Giorgina, Mrs. Sofia Gilmore, Mr. Costantino Papamichahl, Father Costantino Papageorgiou and his family, Father Rafeal Pavouri and Father Markos.

I would also like to thank Dr. Stan Gilmore who very kindly and patiently corrected my thesis. Stan, thank you so much.

I would like to say a BIG thank you to my family, who were supporting me from

afar, but they always felt near in my heart. Thank you very much for your kind support, love and patience. Especially I would like to thank my mother Charikleia who has always supported me and made me feel much stronger after talking to her. Dad and Mum thank you for teaching us that hard work and love for what we do are the ingredients for success. Also thank you both for your encouragement to try always for better things.

I would like to thank my lovely brother Dr. Costantanino Mamma and lovely sister Ms. Diomi Mamma. Diomi I am grateful to you for your visits to Glasgow when I couldn't come to Greece and making me laugh on the phone. Thank you Dr. Constantino Mamma for making me believe that everything is possible with hard work and patience, especially I would like to thank you for advising me when things felt like they were going wrong or I was off track.

Finally, I would like to thank my husband, Ross Samuel Graham, without whose unflinching support, GREAT patience and gentle encouragement this would not have been possible.

Contents

List of Tables

List of Figures

Chapter 1

Introduction

Movement control is concerned with the following questions: How is the sensory information from the environment and the body used to select and control movement? How do our perceptions of ourselves, the task we perform, and the environment in which we are moving influence our movement behaviour? In our everyday life neurologically normal people can control their movements, reasonably well, but people typically cannot explain in detail how this movement is achieved except for physiologists or scientists who probably could explain this to some degree. Although "movement science" as a new field of study could be recognised during the scientific revolution in the eighteenth century, the origins of motor control can be traced as far back as ancient Greece. The Greek philosophers were the first to study the relationship between human movements and the subject that controls the movements, i.e "the controller" ([1], Ch.1, [2], pp. $19-20$).

There are two types of movements, discrete and sustained ([3] pp. $21-24$). Discrete movements are conceptualised as those which are implemented as one unit long, with a fixed beginning, and ending. Kicking or throwing a ball, or shifting the gears on a car are examples. These movements can either be rapid (throwing, or blinking an eye) or may take some time for completion (writing a word). It has been established that discrete actions are ballistic (open-loop), executed in a pre-programmed manner and moderated by different kinds of feedback, such as visual, vestibular etc., only when the movement has been completed and approaches the target [4]. Discrete movements can be learned and joined together so that they can appear to be executed smoothly and

sustained. Examples are in sports and especially in gymnastics and swimming where athletes execute movement routines, other examples are in piano playing, handwriting and speech performances [3].

On the other hand, sustained movements are movements which do not have a definite beginning and an end. Examples of these movements are human balance, tracking tasks and control of external loads such as steering the wheel of a car. These are arbitrary tasks. In these types of movements the subject intends to continuously respond to perturbations that occur in the system either the muskuloskeletal system or in the environment by following a track via certain limb movements ([3] pp. $21 - 23$). For instance, quiet standing is a dynamic process which is characterised by small amounts of spontaneous sway in the saggital plane which make the body deviate from the upright position [5–7], therefore continuous regulation is required. The human motor control of these movements is sustained which means that it appears to be continuous in nature. This logically concludes that sustained control should be explained and described within the continuous control theory framework. Indeed, sustained control is commonly modelled within the framework of "servo control theory". Non predictive models have been applied to modelling both physiological and engineering mechanisms [8–15]. In addition in recent years, optimal or predictive continuous-time models using internal predictive models [16] have been used which are currently the dominant paradigms in the computational modelling of sustained movements [17–21]. However, while sustained control tasks appears to be continuous they may be comprised of sub-movements with a beginning and an end (i.e. they are ballistic actions) [6, 22–25].

Although the above models and especially the optimal control models are considered as paradigms there are physiological constraints such as the long neural processing time-delays and the inherent variability of the information that is transmitted within the nervous system that limits the application of these computational models.

The human body is equipped with a variety of sensors that allow adequate knowledge of one's own body. They are classified into three groups, the interoceptors, the exteroceptors and the proprioceptors ([3] pp.$135 - 136$). The interoceptors provide information about the state of the organs, the exteroceptors provide sensory

information about the movement of objects in the environment and include skin sensation, vision and other chemical senses. The proprioceptors provide information about the movement of the body, they are specialised receptors that are located in the muscles, tendons and joints and in the vestibular system of the inner ear to provide information about the position of the body parts relative to each other and the general orientation of the body in space. There are many proprioceptors that are important in motor control. One example are the muscle spindles, whose main role is to inform the nervous system about any changes in the length of the muscle, stretch velocity and velocity changes in muscle fibres, another example is the Golgi tendon organ which provides information about muscle tension ([3] pp.154 − 156). All these receptors could be considered as part of an internal observer system of the Central Nervous System (CNS) that monitors and gives information about the current changes of the various systems. In human motor control, the neural information that is transmitted by the various receptors to the CNS is both delayed and inherently variable [26, 27]. At a peripheral level, control processes such as reflex mechanisms take place with rather small delays (40 − 100ms). These loops can be modulated centrally by varying their gain and threshold. On the other hand, in higher levels which involve central processes, including brain processing, the delays are even larger ($>$ 200ms) and depend on the order (i.e. complexity) of the load to be controlled with low frequency bandwidths [24, 28].

At an engineering level, continuous systems with delays need a predictor to compensate for the effect of a delay in the feedback loop [22, 29–31]. Predictors, are feed-forward system models which can eliminate the time delay from the feedback loop [29]. However, for the predictor to be able to funtion as intended it is required for the system to be known, time-invariant, and therefore predictable. In this case, the controller parameters such as gains of simple or optimal feedback controllers are computed offline. In human motor control both the actuators, and the sensory signals are inherently variable and noisy. Thus, it is clear that there is a need for an online optimisation and computations of the control signal that will deal with the above constraints.

Craik and Vince in their seminal studies hypothesised the intermittent behaviour of

the "human controller" in motor control tasks [32–34]. They suggested that the human operator acts as servo but operates intermittently. They suggested serial ballistic control, based on the observations from the experiments, which showed a dominant frequency of 2Hz, hence ballistic control is executed at a rate of two to three actions per second [32,34]. In serial, ballistic actions control is a sequence of sub-actions, which appear to be smooth. Craik, argued that the intermittent control is not only evident in discrete-like movements but it is a mechanism even when the control is continuous [33] however this is not supported by experimental evidence.

Craik and Vince [32–34] attributed the intermittent nature of tracking movements due to the refractory period of the nervous system. In their seminal studies [32–34], they demonstrated the refractory nature of tracking following (i.e pursuit tracking) an initial response to an unpredicted, discrete step stimulus. They showed that the reaction time $RT2$ to a second stimulus was delayed as compared to the reaction time $RT1$ due to a first stimulus, based on the interval of time between the two stimuli. This delay, according to Vince [34] ranging between $200-500$ms, characterises the refractory nature of the sensory-motor system. Therefore, a second stimulus will not evoke a second corrective response until an interval of 500ms has elapsed. The refractory period can be associated with the stages of sensorimotor processing, response planning and response selection. When, a response is selected, programmed and executed, selection and execution of a second response is delayed until a certain time has elapsed. This duration is known as the "psychological refractory period".

The intermittent nature of human motor control, has inspired engineers to define theoretical models of human motor control mechanisms within discrete control paradigms [35, 36]. The results of the studies of Craik and Vince [32–34] have been developed into computational models by Navas and Stark and Neilson et al. [35, 36]. Neilson et al's. [36] theoretical intermittent model was based on three processing stages: sensory analysis (SA), response planning (RP) and response execution (RE) in which the first and the third stages operate in continuous-time and the second intermittently as it needs an interval of time to preplan a movement before passing the information to the next stage.

The refractory period and the hierarchical level processing is well established in

ballistic actions, however, until recently there was no concrete evidence for supporting the intermittent behaviour in all situations, for example during sustained control. Lakie and Loram [37] and Loram et al. [6] using ultrasound tracking during human balance have shown that the calf muscles rearranges intermittently with an average of 2.6 times per second which corresponds to a processing delay per muscle rearrangement of 400ms. These experiments also showed a frequency bandwidth of $0 - 3$Hz which is consistent with the postular bandwidth established by Fitzpatrick et al. [38]. In addition, the frequency bandwidth found in Loram et al. [6] is similar to the hand movements of a subject manually balancing an equivalent load [37] and of Neilson et al. [36] and Navas and Stark [35]. Thus it may be concluded that sustained control mechanisms involve neural processes that are consistent with the intermittent control hypothesis first proposed by Craik. Indeed, there is experimental evidence for intermittency during sustained control. The question is: Can sustained control be modelled using an intermittent control paradigm?

In continuous control systems the controller continuously changes the control signal, however in intermittent control [39] the control signal is not continuously calculated, but rather the control signal consists of a sequence of open-loop trajectories whose parameters are adjusted at certain sparse points in time, according to the control law. Intermittent control is based on switched systems, which are a particular case of hybrid systems, that combine behaviours that are both continuous-time and discrete-time and a logical rule which orchestrates the switching between these two modes. It is different from discrete-time control in that the control between samples is not constant and different from continuous-time in that trajectories are reset intermittently [40, 41], however, intermittent control can masquerade as continuous-time control even if there are disturbances [42]. The reason is that the intermittent control introduces high-frequency components which are not visible at the measurements points due to the low-pass characteristics of the neuromuscular and biomechanical systems. Therefore the control paradigm combines aspects of continuous-time control, sampled data and event driven control. In engineering, intermittent control is used in a range of system applications, either simple such as switching circuits or in systems that involve long time delays and hence processes that require slowly responding loops [39, 43, 44]. It is

also used for systems with open-loop instabilities and systems with poor models of the real time systems [45, 46].

Intermittent control was initially developed by Ronco et al. [47] as a practical approach to continuous-time generalised predictive control (GPC) [48] which was based on the discrete-time GPC [49, 50]. The GPC is a form of the model-based predictive control (MPC) [51, 52] and hence intermittent control can be used to implement MPC with hard constraints. In engineering literature the intermittent control theory has been subsequently developed both in time and frequency domain in a series of studies [25, 39, 47]. The IC model developed by Ronco et al. [47] is a feedback system and a combination of a continuous and discrete-time design based on a state observer-predictor-feedback (OPF) model of Kleinman [53]. The continuous-time state observer is intermittently sampled over an interval of time in which the system is open loop resulting in an intermittent continuous trajectory of the control signal. A system matched hold (SMH) element is used to reconstruct the sampled signal. The intermittent interval in which the control is open-loop can either be fixed or variable.

The purpose of this research study is to determine whether or not sustained movements can be modelled as intermittent control mechanisms. It is not intended to show whether intermittent control is the only theory in which sustained control can be modelled.

1.1 Aims and objectives

The main aim of this research was to investigate whether intermittent control is a way to describe sustained human motor control. In particular it was investigated how the intermittent control system model could approximate experimental data from a visual-manual compensatory tracking task.

The first objective was to establish how well the intermittent controller could approximate the deterministic behaviour of the human controller. The performance of the intermittent control model was compared against the performance of the continuous-time non-predictive and predictive control systems [54].

The second objective was to investigate how the intermittent control model could

be used to explain the inherent human variability during a sustained motor control task. A comparison was made with the established explanation of continuous-time predictive control system with added noise [55]

The third objective was to explore issues associated with the practical implementation of the intermittent control model.

1.1.1 Contributions

Based on the frequency domain presentation study of Gawthrop [56], in this research study frequency domain identification was used for the first time with intermittent control. The study has shown that both intermittent and predictive control system models can explain experimental data equally well. Importantly, this study has demonstrated for the first time that inherent variability of human motor control tasks (as manifested by the remnant signal) could be modelled as a structure of the controller rather than as added noise. Finally, the theoretical intermittent control model was implemented for the first time in real-time and combined with electrical muscle stimulation to control a physiological mechanism.

1.2 Overview and Structure of the thesis

This thesis is divided into seven chapters as follows:

Chapter one is the introduction, which explains the motivations of this work and considerations for modelling sustained motor control tasks in terms of continuous-time models.

Chapter two is a literature review, covering a description of human control of sustained and ballistic movements. The continuous-time models that are used in computational modelling to describe sustained movements are explained in detail and their physiological basis is explored. In addition the concept of intermittency in motor control is presented.

Chapter three describes the materials and methods used in this study. The controller models are described in this section. These are the continuous-time non-predictive (NPC) and predictive control (PC) systems, and the intermittent

control (IC) system model. Also, the experimental methods of the human sustained compensatory tracking control task are introduced.

Chapters four and five describe the main parts of the evaluation of the proposed method to model the sustained control task using the intermittent control model. Chapter four describes the materials and methods that were used for the frequency domain identification study. The results of this study are also presented with an analytical discussion. The main purpose of this chapter was to determine whether the IC system model could approximate the deterministic characteristics of human motor control, based on experimental data.

Chapter five describes the materials and methods that were used to model human variability during the motor control task. The remnant signal model control structure of the IC model is presented along with the noise signal models that were used for the continuous-time PC model. The results derived with these methods are evaluated and discussed.

Chapter six describes the preliminary study to explore the implementation issues of the IC model in the context of electrical muscle stimulation. The study protocol is described along with the methods and the results obtained from this method.

Chapter seven is the discussion which examines the results from the intermittent control modelling and compares them with that of the results shown using the continuous-time predictive model. In addition it contains an outline of future work along with the conclusions drawn from this work.

1.3 Publications

1. A. Mamma, H. Gollee, P. J. Gawthrop and I. D. Loram (2011), "Intermittent Control Explains Human Motor Remnant Without Additive Noise" , In Proc 19th IEEE Mediterranean Conf Control Automation. Corfu, Greece , June, 2011. , pp. 558-563.

2. A. Mamma, H. Gollee, P. J. Gawthrop and I. D. Loram (2011), "Modelling the Human Remnant during Manual Control Tasks" , In Proc. 6th Int. Posture Symposium. Smolenice Castle, Slovakia , September, 2011. , pp. 60.

3. H. Gollee, A. Mamma, P. J. Gawthrop and I. D. Loram (2011), "Frequency-domain Identification of Human Balance Control", In Proc. 6th Int. Posture Symposium. Smolenice Castle, Slovakia , September, 2011. , pp. 40.

4. H. Gollee, A. Mamma, I.D. Loram, P.J. Gawthrop " Frequency-domain Identification of the Human Controller", Biol.Cybern, 2012, vol.106, pp.359-372

5. P.J. Gawthrop, H. Gollee, A. Mamma, I.D. Loram and M. Lakie (2013), "Intermittency explains variability in human motor control", In NeuroEng 2013: Australian Workshop on Computational Neuroscience. Melbourne, Australia , January, 2013.

Chapter 2

Literature Survey

2.1 Introduction

Computational theories attempt to explain mathematically, by providing computational algorithms, human behaviour in all aspects of life. Research has been carried out on the development of computational models in human motor control involving sustained motor control mechanisms which includes continuous movements during postural balance. Human sustained control appears to be continuous in nature and feedback regulation is essential. A straightforward approach is therefore to use negative feedback continuous-time models taken within the framework of continuous control theory to model human motor control behaviour. For many years the "servo control" mechanism has been used as a model for sustained control behaviour in man-machine systems [9, 57] which has later been applied to model human neural control systems [10,11,58]. Optimal continuous control using internal predictive models is currently the dominant paradigm both in engineering and physiological modelling [14, 18, 20, 53, 59]. In both of the above feedback models, "servo" and optimal continuous-time, the inherent variability [27, 60] which is exhibited during continuous movements is treated as signal-dependent motor or observation noise [8, 26], or as observation noise with Gaussian characteristics [12, 61] or as combination of both dependent motor noise and observation noise which is independent on the control or response signal [62]. However, there are studies which support that variability encompass more than just noise [27, 60] ([63] pp. $3 - 23$).

On the other hand Craik [32,33] supported that the human operator, during discrete tasks, behaves as an intermittent controller rather than a continuous servo due to refractoriness. Due to the psychological refractory period, which is the minimum interval of time for which control output appears not to be modulated by sensory feedback, control proceeds as a series of ballistic actions (open-loop), each of which lasts for one refractory period. Vince [34] demonstrated that humans behave this way in both pursuit and compensatory discrete tracking tasks involving discrete stimuli, exhibiting $2-3$ actions per second, hence the response is updated approximately every 500 ms, rather than continuously. Evidence for this limit in human response bandwidth was found by Navas and Stark [35] in discrete hand movement tasks. The rate of $2-3$ actions per second was also observed in the human response during experiments in which subjects were required to continuously balance a real inverted pendulum [64], and most importantly, by the study of Lakie and Loram [37] who demonstrated that the rate of control actions did not change during the manual sustained control task even when different sensory information was provided. The above findings raise the question whether or not sustained control could be described by intermittent control systems [39, 40].

In this chapter, the two different classes of voluntary movements, discrete and continuous ([3] pp. $21-22$), will de described in detail. The current computational models, that are used to describe voluntary movements are reviewed with a focus on the sustained control mechanisms. In addition the human variability which is present in all stages of human behaviour is discussed and its relationship to the remnant signal is explained. The current models that are used to describe the remnant signal during human motor control tasks are reviewed. Finally, the different intermittent control models that are applied in engineering will be reviewed with a view towards evidence of intermittency in physiological systems.

2.2 Voluntary movements

The thesis is concerned with modelling human motor control behaviour during a sustained movement control task. Therefore it is important first to understand the different types of human movements that exist in human motor control which determine the control law that is used to describe the control tasks.

In the literature of human motor control and behaviour, voluntary movements are classified in two major ways: discrete and sustained (continuous) ([3] pp. $21-22$).

Discrete movements are those with a definite beginning and a definite ending. Examples of discrete movements are hand reaching, grasping, kicking or even blinking an eye. They are typically fast movements associated with short delays to complete a task. They are pre-programmed movements [65, 66] based on build-in models of the controlled object which is achieved through motor learning and are executed in a ballistic manner in which sensory information only takes place after the execution of the movement [67]. The internal models of the controlled object are located and stored in the cerebellar cortex [16, 67, 68]. Different computational models based on the internal models are used to describe discrete movements [69, 70].

Unlike discrete movements sustained movements are those movements which do not have a definite beginning and an end. They involve movements that require muscular control adjustments of some degree during the movement, as in operating the steering wheel of a car or during human quiet stance. The human continuously operates these movements until they stop.

These two types of movements, discrete and sustained, may be combined in sequence so that they blend into one another which are called serial movements ([3] pp.$21-23$). For example, placing the foot on a car accelerator pedal is a discrete movement, but this may be followed by a continuous movement of adjusting the amount of pressure on the pedal to the conditions of traffic or static positioning.

2.3 Control modelling of voluntary movements

Discrete movements are fast and coordinated movements [71], for that reason they cannot be executed under simple feedback control mechanisms due to the biological large feedback delays [67]. In computational modelling these movements are modelled as open-loop control systems which are pre-programmed trajectory based on paired internal models [16, 67]. Internal models are used in control theory, and they are mathematical representations of the actual system to be controlled. The internal model mimics the behaviour of the controlled object which interacts with the environment. Studies have shown that the brain integrates those internal models during fast arm movements in the absence of feedback [4, 16, 67, 68]. The internal models are of two types: a) inverse models which invert the controlled system by providing the desired motor command that will cause a desired change in state. b) forward models, which represents the relationship between the input to the system (motor command) and the output. Hence, the inverse model acts as a controller, or generally can provide the motor command which is necessary to achieve some desired state estimation. A forward model predicts the next state (eg. velocity and position) based on the knowledge about the current states and the motor command [4, 16, 72].

A common class of sustained movements is tracking [73] which requires apparently continuous regulation since it has to conform to some external input signal (i.e. disturbance signal) which is applied to the system continuously and causes the system to deviate from its desired trajectory. Sustained control such as during tracking is modelled as a closed-loop system which is guided by feedback, for instance visual or vestibular or proprioceptive, or a combination of those. The basic characteristic of a tracking task is to execute corrective movements at correct time in response to disturbances. In tracking tasks a reference signal trajectory specifies the desired output of the system. For example the curves in a road represent the reference trajectory and specify the desired path to be followed by the auto-mobile which represents the "system".

The reference signal trajectory in sustained tasks is considered the target to be followed and can be constant or predictable (eg. steering a ship to a specified heading or maintain quiet stance during human balance), variable, and unpredictable (eg.

following a winding road). The output is accomplished by a physical response and feedback is provided, for example on a display in visual-manual tracking tasks.

Figure 2.1 depicts a simplified control model during human motor control compensatory tracking tasks.

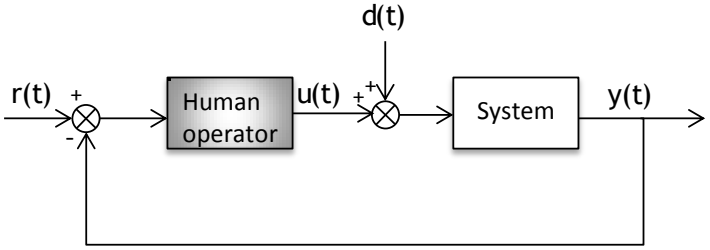

Figure 2.1: Simplified control system model during human motor control compensatory tracking tasks. The block "System" represents the controlled object, the block "Human operator" represents the human who is obliged to control the "System". The reference signal $r(t)$ is considered the desired trajectory which the "System" need to follow and $y(t)$ is the response signal. The control of the "System" is accomplished by the "Human operator" who produces a control signal $u(t)$ in the presence of a disturbance signal $d(t)$ which can be predictable or unpredictable.

Pursuit and compensatory tracking are common tasks in sustained control [73]. In pursuit tracking both the reference (target) and the output (response) are shown on a display. The task of the "Human operator" is to align the moving controlled system with the target which can move in either predictable or in an uncertain way. For example while steering the wheel of a car the target is the road and the "System" is the car which is required to follow the shape of the road. In compensatory tracking control only one of the signals moves, the response signal, whereas the desired trajectory target remains fixed. The task of the "Human operator" is to get the response to align with the fixed target. An example is steering the wheel of a car in windy weather. The driver, hence the "Human operator" is required to keep the car in the center of the lane when a wind gust pushes the car off the centre of the lane [73] , thereby compensating for the effect of the disturbance.

Tracking tasks can be classified according to the dynamic order of the "System" that is controlled. In zero-order tracking tasks (position control) the movement of the "Human operator" controls the position of the "System". For example when the subject moves the mouse of the computer from one position to another and then stops,

the cursor which is displayed on the screen of the computer has moved a proportional amount and also stops. In first order tracking tasks (velocity control) the operator's movement is used to control the rate at which the output of the controlled system is being changed. Many cursor keys are velocity control such that constant depression of the cursor will lead to a constant rate movement of the cursor across the screen. In second order tracking tasks (acceleration), the movement of the control produces changes in the acceleration of the system. The pure second-order system is typical of any system with mass and therefore inertia. In addition system delays may appear due to the neuromuscular dynamics of these systems. Such a system can be used to describe the physiological mechanism of human standing [11, 74]. The task of human quiet standing can be simplified to the task of balancing a single axis inverted pendulum which is perturbed by small oscillations acting on the axis of rotation [11, 74, 75].

During tracking tasks, there are performance limitations that depend mainly on the human operator's characteristics and secondarily on the system to be controlled. People do not process information instantaneously, therefore there is a time delay between a stimulus action or a change in a target and the initiation of the motor control response required to track the target or to respond to the stimulus. The operator's motor control process introduces a time lag into the task which degrades the tracking performance due to the fact that the operator is always "chasing" the target and is always behind it. In control theory this is considered as the feedback time delay which includes the time for the operator to receive the sensory information, process it and plan the execution of the motor command. In addition there is another time-delay which is the time between the motor control action and the response of the system under control. The "effective time delay" includes the feedback delay and the control-system delay.

According to the motor control review studies of Elliott et al. [76] and Hoffmann [77], in 1899 Woodworth was the first to determine the processing time for visual feedback using an experimental method based on goal-directed movements and the study revealed the human processing time-delay of $400 - 500$ms. The study of Keele and Posner [78] on goal-directed movements using visual feedback avoided the problem which occurred in Woodworth's work and revealed a minimum duration for processing visual feedback to be between $190 - 260$ ms which is half the minimum duration

suggested by Woodworth. Also a processing time delay of $300 - 350$ms revealed in Pew [79] in which subjects were required to maintain a target at the centre of an oscilloscope, which moved horizontally, by sequentially pressing two keys. The controlled system had pure acceleration dynamics and by pressing each of the keys caused the target to accelerate either to the left or right. In this study when the oscilloscope was blanked up to 410ms after the response, the time delay before the next corrective response was $300 - 350$ms after the end of blanking. In addition McRuer and Jex [57] and later Loram et al. [24] found that the magnitude of the time delay is dependent on the order of the system being controlled in continuous compensatory tasks. Both studies have shown that for first order systems the "effective delay" is $150 - 300$ms and for second order unstable systems during tracking tasks it is $400 - 500$ms. The feedback time delay, which is the processing time delay before the human response, for first order systems was estimated by Loram et al. [24] to be 124 ± 20ms and for second order systems 220 ± 30ms.

In addition to the time lag limitation during tracking tasks another limitation during the operator's information processing activity is the upper frequency limit with which corrective decisions can be made. This in engineering control theory is described as the bandwidth which is the maximum frequency of a random input signal that can be successfully tracked. In control theory the bandwidth of any feedback control system is limited by the feedback time delay ([80] pp. 172). Woodworth (1899) conducted the first study to determine the maximum response reaction time in goal-directed movements using visual feedback [76]. During the experiments subjects were required to determine reciprocal (back and forth) goal-directed sliding movements to the beat of a metronome which was set at different speeds. The study showed that the maximum reaction time was limited to ~ 500ms therefore sequential discrete movements could be applied at ~ 2 times per second hence that reveals a bandwidth of ~ 1Hz since two corrections are required for each cycle. Vince [34], applied a series a discrete double stimulus experiments with different intervals between the stimuli. When stimuli were presented in succession a normal response was not made unless the interval between stimuli was more that 500ms. When the interval between stimuli was 500ms or less a response to the second stimulus did not begin until 500ms have elapsed.

The results showed that when unpredictable paired discrete stimuli were presented in rapid succession of more than $2-3$ stimuli per second, the response to the second stimulus was delayed when compared to the first stimulus. The results were explained by the refractoriness of the human operator. The human sensory system is refractory after responding to the first stimulus and must wait until the refractory period (500ms) has been processed before the response to the second stimulus can be formulated. In later years, Loram et al. [81] estimated a control frequency bandwidth of $\sim$ 1Hz when subjects were required to control an unstable inverted pendulum in a visual-manual compensatory tracking task. The frequency of the controller's response remained the same even when the tracking task becomes more difficult and demanding in balancing the unstable load. Various studies on pursuit and compensatory tracking tasks have revealed a control bandwidth range of $1-2$Hz [24, 35, 82].

The human factors, such as processing time delay and bandwidth during tracking tasks determine the variables that should be taken into account in modelling human motor sustained control tasks, since they constrain the operator's behaviour during tracking tasks. In addition to the human factors which limit the performance during tracking task, another human factor which is essential during human motor control modelling is the inherent variability which is exhibited during continuous movements. The section below reviews the inherent variability as a human factor and how it is characterised in computational modelling.

2.4 Human motor variability

A factor which is essential in the computational modelling of human motor control tasks is variability [60]. Variability is inherent in humans and it is exhibited in all stages of behaviour such as planning, learning and execution [27, 83]. It is observed both in discrete [3, 84, 85] and sustained movements [3, 27].

Variability could be observed in trial-to-trial tasks, like that of continuous movements. For instance when someone undertakes the same task many times the output response trajectory fluctuates between repetitions (cycles) and is never an exact duplicate of one another [3, 27, 60]. In addition, in discrete control tasks, when a movement is required to end at a particular time and location in space the output motor response is variable among its repetitions. The duration and end-points deviate from the specified targets. The fluctuations that are observed in the movement repetitions or the end-points are due to the human variability.

Variability is often considered as a measurement of performance. For instance, in some sports and especially those that require accuracy from athletes (e.g golf, basketball, cricket, e.t.c) decreasing variability is important in order to gain accuracy and win. Although human variability may be considered a limiting factor in the performance of a motor control task, they are persistent in the face of perturbations and reproducible with a high degree of accuracy [83]. Standard deviation (SD) is the major measurement variable of the amount of human variability and is considered as an index of the magnitude of variations from the mean of the distribution [86]. However, it does not present the structure of variability which is an important factor ([63], Ch,1).

Qualitatively, human variability in motor control tasks is revealed as a response signal called, the remnant signal. The remnant signal is easily observed in tasks where subjects are asked to control a system which is excited by a periodic input at a range of discrete frequencies. The operator's Fourier transform response signal will contain components at the excited frequencies (i.e. those frequencies which are contained in the excitation signal) but will also show components unrelated to the input frequency components. The latter Fourier components will form a signal at non excited frequencies which is called remnant signal [8]. In repetitive motor control tasks, such that of sustained control tasks, the remnant signal is different at each cycle

(period).

In computational modelling of physiological systems the remnant signal is commonly modelled as a noise signal with statistical characteristics, added either at the input or output of the controller. Therefore, human variability is considered to be due to a stochastic (i.e random) process which is added to the deterministic part of the dynamic model that describes the linear input/output relationship of the human controller during the control task [57].

In man-machine systems early theoretical research on the characteristics of the remnant signal was implemented by Levison et al. [8]. The study was based on the fact that the remnant signal is the controller's random (stochastic) response signal shown at non excited frequencies and it is not related to the linear input/output transfer function. Levison et al. [8], suggested a theoretical remnant signal model based on the assumptions that 1) the plant dynamics of the controlled system during the compensatory tracking task are linear, and 2) the subject operates a single control task. Based on these assumptions they described the remnant signal model as an observation noise signal (i.e a noise process which is added to the controller's input) with white characteristics and power density levels that are proportional to the variance of the signal that is being disturbed. The remnant signal model is additive to a deterministic continuous-time linear controller model. The theoretical remnant signal has been shown to fit equivalent experimental remnant data from simple compensatory tracking tasks well. The study has shown that the observation remnant signal model could be described as white noise with power density level of -20db for control tasks in which the plant dynamics are either zero or second order. In addition, the remnant signal has been modelled as a white Gaussian motor noise signal added to the continuous-time controller's output response, and as white Gaussian observation noise added to the system's response signal [18]. These two signals, motor noise and observation noise signals, have been considered to be representations of the remnant signal to a deterministic continuous-time model during compensatory tracking tasks [18].

In addition, in the computational modelling of human postural control, the remnant signal has been modelled as a motor noise signal with low-pass filtered white noise characteristics which is added to the deterministic part of the output response

of a continuous-time Proportional-Integral-Derivative (PID) controller [5, 12]. The corresponding models of Peterka [5] and Maurer and Peterka [12] have shown to fit experimental data well. In addition, van der Kooij and Peterka [62] modelled the remnant signal during human stance control both as observation noise and motor dependent noise. In goal-directed movements such as that of saccadic movements or discrete arm movements it has been suggested that the variability in the motor control trajectories is due to a noise signal which is dependent on the mean level of the motor response signal during the goal-directed tasks [26].

The studies described above support the assumption that the remnant signal during human motor control tasks can be described as an additive noise source with statistical characteristics injected either at the input or the output of the continuous-time linear controllers. Especially, the optimal control system with motor dependent noise has received a lot of attention in engineering and has been used to describe physiological systems [72, 87].

Noise in physiological systems has been linked to the cause of inherent variability of motor output response at the behavioural level [27,85,88]. A distinguished study which attributes noise to human performance limitation is Fitts' Law [89] which describes the speed-accuracy trade-off during discrete movements. Fitts, using goal-directed control tasks, proposed that the channel capacity of the sensorimotor system is the rate at which it can transmit information. He assumed that the capacity to transmit information is limited by the amount of the noise in the system. In addition to Fitts' law, Schmidt et al. [84] supported that biological systems have inherent noise which causes motor control variability in which the variance varies with the size of the signal. They carried out an experiment in which volunteers were required to make rapid reaching movements to a target and the measured target variability was measured. The experiment showed that there is a linear relationship between the amplitude of the motor output signal and the signal variability. In eye and arm movements the motor noise signal is modelled as noise with zero mean and variance which increases with the size of the control signal [26]. In systems with signal-dependent motor noise, a minimum-variance theory accurately predicts the trajectories of both saccades and goal-directed movements and the speed-accuracy trade-off [26]. Other studies support

that the variability measured at the motor output tends to have structure consistent with low pass filtering of white noise [7, 12]. A different approach to the linear time-invariant predictive control model was presented by Metz [90] in which he suggested that the variability on human control tasks is due to the time-varying behaviour of the human controller. Metz based his model on the study of McRuer [57] that suggested that a potential source of remnant could be due to the non-stationary subject performance. Metz [90] proposed that significant time variations in the subject's parameters occur during tracking with variations in subject's gain and time delay. In the study optimal control was used in which the primary feature of the model was that the state $x(t)$ is processed by a time-varying gain vector $l(t)$ which is utilized to generate the control $u(t)$. Although the model presented an alternative approach to describe the remnant signal, the simulation results using that time-varying model were not consistent with the observations derived from compensatory tracking experiments.

On the other hand the approach to describe the remnant signal, i.e. human variability, during sustained control as an observation or motor noise with white Gaussian characteristics does not have a natural explanation ([63] Ch1). White noise is a mathematical model and not a physical process [83]. In addition, with this noise the variance of the measured signal (control signal) that is observed is independent of its mean. This means that even if the measured signal varies by some amount the variance is the same whether the signal has a small amplitude or large amplitude. Faisal et al. [27] and Slifkin and Newell [60] argued that the notion to describe the remnant signal as noise with white Gaussian distribution with a carefully chosen frequency spectrum cannot naturally explain variability during sustained control tasks since noise levels which appear to be outside the normal distribution are ignored or underestimated. Noise signals are often characterised by their mean and standard deviation. The standard deviation is a measurement variable which gives only an index of the degree of the deviation from a mean value in a distribution [60], therefore it captures only the magnitude of the fluctuations in the system output. However, variations in system output could be measured using another dimension which is independent of the magnitude. This dimension is the way the system output changes over time, and it is the structure of the system dynamics.

Slifkin and Newell [86] applied an isometric force task experiment in subjects to study the relationship between the magnitude and structure of force variability over a range of force levels. During the task the subjects were required to match the force they produced to the force targets (ten different force targets) displayed on a computer monitor. The results revealed that increasing the force level increased in an exponential relationship the magnitude of the force variability measured as force standard deviation. Therefore the force variability was increased incrementally in relation to force level. This contradicts the linear relationship between the amplitude of the motor output signal and the signal variability in the study of Schmidt et al. [84]. Slifkin and Newell [86] measured the entropy which revealed that noisiness in time domain changed to an inverted U-shaped function over the different range of force levels. The same observations were found in frequency domain analyses. The different shapes of the force variability against force levels and noise against the force levels suggested that isometric force variability is not directly related to noise. Therefore, increases in the magnitude of variability (i.e. SD) do not necessary correspond to increases in system noise.

The inverted U-shaped function between the level of force output range and noisiness reveals that the greater noisiness in force output occurs just below the midrange of maximum force production. Therefore greater noisiness in force output is associated with an improvement in information transmitted in task performance. This is in contrast to the current notion which supports that noise is a detrimental factor in the motor control task [89].

Faisal et al. [27] Slifkin and Newell [60] and Davies et al. ([63] Ch.1) supported that the remnant signal is based more on structure rather than on randomness. Rilley and Turvey [83] argued that it is first important to search for simple deterministic mechanisms that produce simple and predictable motor behaviour.

In summary, human variability is commonly modelled as an additive observation or motor noise process which is injected into a linear continuous-time controller. Therefore motor behaviour is modelled in two parts. That means that human variability is considered as a signal which is not part of the "human controller". Rilley and Turvey [83] suggested that if a deterministic model can generate realistically variable behaviour

then the assumption of the model with the two factors in not needed.

2.5 Continuous-time models of sustained movements

Sustained movements are continuous in nature; for this reason continuous-time algorithms have been applied to model such mechanisms. A common continuous-time algorithm is the simple "servo control" mechanism.

McRuer and Jex and McRuer and Kredel [57, 91] supported the servo behaviour of the human operator in man-machine systems. They demonstrated the simple quasi-linear function behaviour of the human operator when controlling stable systems, and suggested a lead-lag transfer function as a model to describe the human operator with a static gain and delay which depends on the order of the controlled system plus a "remnant" signal with Gaussian characteristics which represents the output signal that cannot be described as a linear operation on the input signal. For simple compensatory tracking tasks where the controlled system is stable and the time delays are relatively small ($\sim$ 90ms) the human operator can adequately be modelled as a quasi-linear transfer function.

In addition the "servo" mechanism approach to modelling sustained control mechanisms has been applied in physiological systems. Johansson et al. [10] have shown that the physiological mechanism of the continuous motor control of human upright stance could be adequately controlled by a PID controller with no time delay. The PID controller whose components are determined by three gains was found to balance an inverted pendulum which continuously sways in the saggital plane and characterises human stance during quiet balance. System identification was used to tune the three gain parameter controller using experimental data taken from a postural control experiment in which subjects were exposed to a vibration stimulus when standing on a force plate with their eyes closed. The identification method showed that the three gain parameter controller fit the experimental data well.

The Proportional Integral Derivative (PID) with time delay has received a lot of attention in modelling human balance [5, 11, 12]. The three gain parameter and time

delay of the PID model have been tuned to simulate spontaneous sway [12], and it has been shown that the servo mechanism can reproduce realistic sway behaviour with an identified control loop time delay of about 170ms. Furthermore, the PID model has been tuned using optimisation methods to fit experimental data from procedures where the support surface, during human balance, has been pseudo-randomly rotated [11] or translated [13]. The studies have shown that the PID system with time delays between $60 - 170$ms fits experimental data taken from the sustained control task of human postural balance with high or low frequency perturbations.

The above studies have shown that a PID controller by being carefully tuned can simulate or fit experimental data from standing tasks well. It is true, that during real human balance tasks reflex and central processes take place therefore the feedback time delays are considered to be around 90ms. However, for control tasks that replicate sustained control mechanisms such as those of human balance and especially in the case where the reflex mechanisms during these tasks are excluded, responses obtained with PID control do not explain the long processing time delays and the limited control bandwidth that are observed during these tasks.

Loram et al. [81] have shown that a PID controller with a time delay fitted experimental data taken from a tracking task very well, however it did not succeed to meet the controller's physiological control constraints. The optimised PID time delay was too low in relation to the mean response time delay found from the subjects who took part in the task. In addition Gawthrop et al. [25], using a non-parametric identification method have shown that although the simple non-predictive PID control system could fit experimental data from a visual-manual compensatory tracking task, the identified time-delay was consistently smaller than that found from the experimental data. In addition the simulations applied by Peterka [5] on a PID system with a feedback time delay higher than 190ms resulted on an unstable feedback system due to the delay in the feedback loop. This strongly shows that more sophisticated controllers should be used to model sustained control tasks.

The servo PID paradigm of human control has been increasingly replaced by the optimal predictive control theory [21, 53, 87] which is based on the engineering control methodology of internal models [16] including prediction and optimisation.

The major reason for this is the presence of long processing time delays in physiological mechanisms.

The human sensorimotor system is the product of processes that continuously act to improve the behavioural performance [4, 92]. One such control process is optimal feedback control which is concerned with operating a dynamic system at minimum cost. Optimal feedback control deals with the problem of finding a control law for a given system such that a certain optimality criterion is achieved based on constraints. A special case of optimal control is the linear quadratic (LQ) optimal control problem in which the optimality criterion is described as a linear quadratic function. The LQ problem states that the optimal control law minimises a quadratic continuous-time cost functional J within a time frame $[t_0, t_1]$ subjected to the linear dynamic system in state-space form with initial conditions. A particular form of the LQ problem is the linear quadratic regulator (LQR). In LQR the state matrices of the linear dynamic system are constant and the terminal time t_1 is taken to infinity. The optimal feedback control law minimises the linear infinite horizon quadratic continuous-time cost functional subject to linear system dynamics. The optimal control signal that is calculated and is then applied by the controller is an optimal movement trajectory that maps the system's states ([30] Ch.22).

However, physiological systems are observable only through delayed and noisy sensors, and for that reason the controller has to rely on an internal estimate of the state. Observers take into account motor control output signal data such as current control signals and knowledge of the system's dynamics, it weights all these input and estimates the current state. An observer system is required to have explicit knowledge of the dynamics of the system to be controlled, hence an "internal model" in often used. Studies on movement planning [16, 67, 68, 70] have shown the potential existence of internal models within the brain during reaching and grasping. In systems with pure time delays a predictor is required to eliminate the problem in the loop [25, 31, 68]. Predictors [29] are feed-forward models based on an internal system model which are used in control theory to eliminate time-delays in the feedback loop. Therefore the feedback controller is driven by the state estimate predicted in the future.

Kleinman [53] proposed a predictive control model in modelling man-machine

systems. The human operator is described as an controller whose strategy is to minimise a quadratic cost function when the system output is a delayed linear combination of system states corrupted by additive observation noise. To provide the most precise and current estimate of the actual state of the system on which to base the optimal control the "human controller" consists of two processing operations: 1) prediction in order to compensate for the time delays, taking into account the manner in which future states may be predicted from the past state, and 2) an observer to give an estimate of the true state of the system. In the control model of Kleinman [53] human variabilty is modeled either as an observation noise signal added to the system response or as a motor noise signal, both random with white characteristics [8,18]. The predictive control model of Kleinman [53] has been extensively used to model man-machine systems in engineering applications. The continuous-time state Observer, Predictor, Feedback (OPF) structure provides a model of human control systems. Simulated data derived from the OPF system model with a remnant source modelled as additive noise signals with white characteristics have shown to fit experimental data taken from different visual-manual compensatory tracking tasks well [18], using as controller a gain, a single integrator (velocity control) and a double integrator (acceleration control). In addition the predictive control model of Kleinman [53] with an additive noise signal has been used to fit experimental data from two degrees of freedom compensatory tracking tasks. The simulated data fit the experimental tracking responses well with time delays of 250 ms. The continuous-time state-observer, state-predictor, state-feedback structure of Kleinman [53] has been shown to be applicable under a range of experimental conditions taken from man-machine visual-manual compensatory tracking tasks [17–19] with a feedback delay of $150-250$ms. McRuer [9] has stated that the OPF model is an algorithmic model of the human operator which "works well for imitating human behaviour". In addition the OPF model has been shown to model the speed-accuracy trade off equation of Fitt's law [93]. Also, Gawthrop et al. [25] have shown that a predictive control system, using a system identification method in time domain, fitted experimental data of balancing an inverted pendulum better than that of a PID controller. This study revealed that the optimised feedback loop time-delay using a predictive control system was found to be very close to the

estimated time delays derived from the experiments for each subject.

In addition, the OPF model of Kleinman in relation to internal models in physiological systems became the algorithmic paradigm for interpreting human motor control. Variations of the OPF model have been shown to successfully fit experimental data from perturbed human balance with a feedback time delays of around 100ms [20,59] or fit experimental data using balancing of an inverted pendulum which imitate human standing [25]. The continuous-time OPF model fits experimental data well and it is considered as a paradigm in modelling continuous-time sustained control mechanisms. Sustained control, as it is shown above is investigated and explained using continuous non-predictive or using optimal internal predictive models with additive or signal-dependent noise to model variability. In the absence of any contradictory evidence, these results support that continuous models can explain human sustained motor control and can be interpreted within the framework of continuous-time control theory [14].

However, there are sustained control tasks in the literature which are not interpreted by a continuous-time model. Vince [34] conducted three similar tracking experiments in which subjects were required to balance the position of a pointer, on a rotating drum, when it was disturbed by a zero-order continuous external stimuli (i.e. position control tasks) at different constant frequencies for each experiment. From the experimental results they showed that the frequency of the subject's response actions did not depend on the frequency of the external disturbance signal but rather it was constant at 0.5 sec (i.e. $2-3$ actions per second). In addition, it was shown that the mean tracking error (the measurement of the performance) was found to be proportional to the frequency of the disturbance. Therefore, the subjects were unable to correct for higher frequency disturbances due to their limited rate of corrective action. The low rate of corrective response is not attributed to sensory threshold. Indeed, Craik [32] found that visual resolution of the disturbance signal during tracking tasks had no effect on the periodicity of corrective actions. The results from the experiments [34] showed that subjects were not applying corrective movements to the stimuli continuously but rather every 0.5 secs, limiting the human response frequency to 2Hz.

Vince and Craik [32–34] following the work of Telford [94] on double auditory

stimulus time experiments attributed the human motor response frequency of 2 Hz in tracking tasks due to the "psychological refractory period" [95].The refractory period is the time during which the control output is not modulated by sensory feedback. Due to the refractory period, control is executed as a sequence of discrete ballistic control actions, each of which has a minimum duration of one refractory period. Therefore control adjustments are made intermittently and not continuously.

Vince [34] has shown direct evidence of refractoriness during a zero-order manual tracking task. In the study, Vince applied a series of zero-order discrete double step-stimulus experiments with different intervals between the stimuli. When stimuli were presented in succession a normal response was not made unless the interval between stimuli was more that 500ms. When the interval between stimuli was 500ms or less a response to the second stimulus did not begin until 500ms have elapsed. The results showed that when unpredictable paired discrete stimuli were presented in rapid succession of more that $2-3$ stimuli per second, then response to the second stimulus was delayed when compared to the first stimulus. Therefore, the human sensory system is refractory after responding to the first stimulus and must wait until the refractory period (500ms) before the response to the second stimulus can be formulated.

Craik and Vince [32–34] suggested a theoretical intermittent control model to describe human behaviour due to the refractory period [32, 33]. The intermittent control model of the human operator suggests that the human applies a series of corrective sub-movements every 500ms (one refractory period). The operator's smooth response consists of a sequence of sub-movements, each planned in advanced using current information, however they are executed ballistically (open-loop), without being influenced by the feedback of the result. The ideas of intermittency in human behaviour was suggested to explain tracking tasks associated with zero-order loads and it clearly required response planning and selection. However the questions that arises is: Could Craik's hypothesis of serial ballistic control also be applied to sustained control of higher order loads? A recent study of Van de Kamp et al. [96] has investigated whether refractoriness is applied in sustained visual-manual control tasks using double-stimuli. The study found evidence of intermittency during sustained motor control tasks, even for second order loads. The results revealed that refractoriness is a physiological control

mechanism and that its magnitude depends on the system properties (order of the system to be controlled) but not on the stability. For zero order systems the maximum refractory period is 250ms, for first order systems 350ms, and for second order unstable systems 550ms. Refractoriness can only be explained using intermittent control and not continuous-time control.

The limited bandwidth of 2 Hz in human voluntary movement control found in Vince [34] and explained based on the intermittent behaviour of the human operator during discrete movements [32, 33] was demonstrated in a series of sustained control tasks where Lakie et al. [64] requested participants to manually balance a real inverted pendulum with human dynamics and low intrinsic stiffness. This manual control task related to human standing using hand movements. During the experiment balance of the inverted pendulum was succeeded by pulling on a handle which was attached to the inverted pendulum via a weak spring. The experiment revealed that the load was balanced through discrete hand movements at a rate of about two to three adjustments per second. Therefore it is an intermittent control process similar to manual pursuit tracking of Vince [34] and Loram et al. [97]. The rate of corrective control (2 to 3 actions per second) during manual control of an inverted pendulum found to be irrelevant to the nature of feedback or to the dynamics of the load. Lakie et al. [37] showed that the rate of control actions did not change when subjects used visual, vestibular or proprioceptive feedback either alone or in a combination. In addition Loram et al. [81] have shown that the rate of corrective control actions did not change in the case where the time constant of the inverted pendulum was changed by a factor of two. The above cases involving the manual control of an inverted pendulum cannot be explained by the continuous-time OPF model, however they fall within the concept of intermittent control which includes event and clock-drived actions [39, 40].

2.6 Intermittent control

2.6.1 Intermittent control models in engineering

In engineering theory, intermittent control is related to hybrid control since it combines aspects of continuous-time control, sampled data and event driven control. It is

different from discrete-time control in that the control between samples is not constant and different from continuous-time in that trajectories are reset intermittently. In addition the control signal is not continuously calculated, as in continuous-time systems, but rather the control signal consists of a sequence of open-loop trajectories initiated by intermittent feedback [39–41].

Intermittent control was initially developed by Ronco et al. [47] as a practical approach to continuous-time generalised predictive control (GPC) [48] which was based on the discrete-time GPC [49, 50]. The GPC is a form of the model-based predictive control (MPC) [51, 52] and hence intermittent control can be used to implement MPC with hard contraints. The continuous-time moving horizon within which optimisation and prediction takes place in MPC is replaced by an intermittent moving horizon approach, in which the moving horizon axis remains fixed for an interval of time. Within this period of time optimisation and the moving horizon evolve in an open-loop fashion. After the interval of time the axis of the moving horizon is moved and a new optimisation takes place. It was shown by Ronco et al. [47] that the intermittent approach not only allowed an online optimisation, hence it could handle cases in which the system is time varying, but also that it avoided the computational burden due to the on-line computational optimisation requirement. The intermittent control approach removes the computational inflexibility due to the fact that there is no need for a continuously moving horizon. The intermittent generalised predictive controller (IGPC) showed better control performance and stability performance, as opposed to the continuous generalised predictive control (CGPC), in controlling an inverted pendulum when the on-line optimisation time increased (intermittent intervals for the IGPC where $\Delta_{ol} = 0.01, 0.1, 0.5$sec and sample interval for the CGPC were $\Delta = 0.01, 0.1, 0.5$ sec). The main form of intermittent control is event driven [40] where sampling is determined by events such as an error crossing a threshold. A special form of the event-driven intermittent control is the clock-driven [39] in the case where the threshold is always exceeded (i.e. there is always an event) then the intermittent interval becomes regular. This could for example, be the case in a very challenging task, for instance when the task includes lots of disturbances. Clock driven intermittent control can be analysed in the frequency domain [56].

A special case of intermittent control was suggested by Gawthrop and Wang [39, 41] in which the intermittent control is designed to give system responses which approximates that of an underlying continuous-time control design. The intermittent hold, is designed to match the continuous-time closed loop system and it is referred to as a system matched hold (SMH). The behaviour can be mistaken for that of a continuous-time controller, a characteristic which has been termed the masquerading property of intermittent control [42]. Indeed, one effect of the SMH is that the intermittent controller in the absence of a disturbance signal masquerades like an underlying continuous-time controller and the response is similar to that of the continuous-time controller only delayed by Δ_{ol} due to the intermittent interval. On the other hand, in the case where there is a disturbance in the feedback loop the observer error is not zero and the performance of the intermittent controller is degraded in contrast to that of the underlying continuous controller [42].

The intermittent control model of Gawthrop and Wang [39] was shown to have applications in engineering control systems and fit either simulated or experimental data with loop delays in the range between $100 - 200$ms [39, 40, 47, 56, 98, 99]. In addition it was shown to simulate physiological models [93].

A different intermittent control approach has been suggested by Estrada and Antsaklis [44] and Insperger [100]. Estrada and Antsaklis [44] have proposed a model named "Intermittent control" for both continuous and discrete time models in which the feedback control is applied for some time either periodically or non-periodically and zero control for the rest. Insperger [100] proposed a model called "Act-and-Wait' to overcome infinite dimensional pole placement problems which were induced in time-delayed systems. The study has shown a simple way to reduce the system to a n-dimensional pole placement problem by switching off and on the feedback periodically and especially having "off" intervals longer than the time delay. The "Act-and-Wait" intermittent feedback model of Insperger [100] is found to be related to the intermittent predictive control of Gawthrop and Wang [39] due to the generalised interpretation of the intermittent control model [101].

2.6.2 Intermittent control in human motor control

In general, event-driven intermittent control based on an error crossing threshold in visual-manual tracking tasks has been observed in manual tracking task experiments. An event-driven intermittent feedback predictive control model based on a positional error threshold has been suggested by Mial et al. [82]. They argued that in visual-manual tracking tasks, corrective movements are characterised by step-and-hold sub-movements which are caused by a tracking error deadzone, hence tracking movements are likely to be threshold triggered [102]. Hanneton et al. [103] argued that the intermittent step and hold control in hand corrective movements, during tracking, are based on sliding variables (a combination of the instantaneous tracking error and its temporal derivatives) crossing a constant threshold such that a stability criterion is fullfilled. The same intermittent control step and hold model in hand tracking tasks was suggested in an experiment involving a two degree of freedom arm movement [104].

A bang-bang intermittent controller with an intermittent interval of 250 ± 25ms has been shown to provide stability and control to an unstable system in relation to human standing [31, 105]. The controller was designed as proportional derivative (PD) intermittent controller in which control is triggered only when state-dependent thresholds are passed. The feedback delay was 180ms. The intermittent controller was compared against the continuous-time PD control and it was shown that the bang-bang intermittent control model maintained stability for increases in the feedback loop delay up to 30% as opposed to the simple continuous-time PD which maintained stability up to 10% increase. Also, in the dynamics control of stick balancing [23], intermittent control with a state-dependent threshold has been suggested to overcome unpredictable noise.

The work of Gawthrop et al. [42] revealed that an event driven SMH intermittent controller based on the OPF internal models could fit experimental data from a compensatory tracking task in which humans were required to control an inverted pendulum with humans dynamics. Event driven feedback control model, was applied only when a quadratic function of a system state difference exceeded a threshold. The study demonstrated cases of human tracking tasks which could not be described by the OPF continuous-time control model of Kleinman [53]. Human compensatory tracking

control of an inverted pendulum with human dynamics was successfully modelled both using the continuous-time predictive controller of Kleinman [53] and the event driven intermittent control in the case where the system was disturbed by a continuous-time multisine signal. When the system was disturbed by a double stimulus the event driven intermittent controller could fit the experimental data whereas the continuous-time control system could not.

Intermittent control, by serial ballistic trajectories naturally includes triggering related to both temporal processes and thresholds [102]. When thresholds are large, such that there are durations below and above the threshold, they determine the triggering of actions [40, 42]. When thresholds are small, such that they are always exceeded, triggering is related to the intermittent interval governed by the psychological refractory period [106].

The first clock driven theoretical intermittent control model [36] was based on the three-stage intermittent human behaviour model of Craik [32, 33]. The theoretical algorithm, has been advocated in the form of Adaptive Model Theory. The theoretical controller is based on the notion that the central nervous system (CNS) incorporates internal inverse models of the various controlled systems that takes part in a pursuit tracking movement. The controlled system consists of the muscle control system (MCS), biomechanics (BM) and the tracking or external system (E). The controller algorithm consists of a response planning (RP) stage, response selection (RS) stage and a response execution (RE) stage. Intermittency is inherent because the (RP) stage operates in ballistic manner as it requires an interval of time to pre-plan an optimum movement trajectory before it passes the information to the next stage. Response planning of a new movement by the (RP) stage is not commenced until the planning of the old movement response has been completed. Each movement is pre-planned intermittently by the (RP) stage and executed in an open-loop fashion by the (RE) stage. During response execution, the inverse internal models are employed to translate the optimum pre-planned response into motor control trajectory that will initiated to the controlled system. In the (RP) stage the optimum motor response trajectory is pre-planned at least one reaction time interval into the future. The optimum response selection is based on the criterion to improve accuracy, hence a subject might choose the

optimum response trajectory slower than the fastest possible response.That relies on the speed-accuracy trade-off of Fitt's law [89]. The theoretical model has been shown to account not only for results of discrete response, double stimulation reaction time experiments but also for the behaviour of human operators performing continuous tracking tasks. This intermittent control model has been developed in a series of studies [107,108] and represents a neural intermittent clock-driven control model with a relatively high frequency, (intermittent interval of $50-100$ms) and a ZOH to reconstruct the discrete signal to continuous-time.

In contrast, a low frequency ($1-3$Hz) clock-driven intermittent control mechanism was suggested in a task where subjects manually controlled a real inverted pendulum using hand movements [64]. This study argued that human control is subject to a refractory period which is similar to the intermittent control process found during manual pursuit tracking [97,109]. Furthermore, the same rate of human motor response and the same intermittent control mechanism was found in a similar task [37] when different sensory information was available to the subjects. In addition the same intermittent control mechanism of $2-3$ actions per second was suggested in a sustained control task in which subjects were required to control an inverted pendulum using a joystick [81]. The rate of corrective actions did not change when the time constant of the inverted pendulum was changed by a factor of two. Also, Loram et al. [28] showed that tapping control of a joystick at a rate of $2-3$ actions per second, similar to the intermittent human motor control behavioural observations of Craik and Vince [32,34], was a natural process during a manual compensatory tracking task.

The above observations require to discover whether or not a sustained control, such that of controlling an inverted pendulum, could be modelled as an clock-driven intermittent control mechanism.

2.7 Chapter summary

In this chapter we have presented the two different classes of voluntary movements, discrete and continuous. We focused on the continuous movements (or sustained movements) and presented how control of such as movements is achieved. The human behaviour limitations during sustained control mechanisms, such as that of bandwidth and time-delay were discussed. The continuous time models that are used in computational modelling of sustained control models were discussed and reviewed in detail. Some human sustained control experiments were shown not to be able to be modelled by continuous time controllers due the human behaviour associated with refractoriness, however they could be modelled using an intermittent controller. In the following chapter of this thesis we present the materials and methods that were used to investigate whether an intermittent controller could model a sustained control balance task. The intermittent controller will be compared against the continuous time controllers that are used in modelling human sustained control behaviour.

Chapter 3

Materials and Methods

3.1 Introduction

The purpose of this chapter is to provide the materials and methods that were used for the computational modelling of the experimental data collected from a sustained balance control task.

In linear control theory closed-loop systems, either continuous or sampled-based, can be represented either in transfer function form, based on Laplace transforms or in state-space based on differential equations. This study used a state-space framework for both the plant and the control systems. A state-space form was more convenient in order to make use of the state-space predictor formulation of Kleinman [53] and because it is a natural setting for intermittent control [42].

The general state-space form of the linear dynamic system that was required to be controlled by the participants during the experimental task is presented. In addition, the artificial controller models, that were used for the computational modelling of the "human controller" during the physiological sustained control task, are also presented analytically. This includes the equations of motion that describe the artificial models along with their graphical representations. The similarities and differences between the artificial models are also discussed using a simple example.

The design of the physiological experimental task is presented along with the apparatus and the recordings that were used for the experimental setup. Physiological sustained control systems can be considered as closed loop systems, therefore the

"human controller" is embedded within the closed-loop system during these tasks. The identification of these systems, using identification methods from measured data [110, 111] can be successful only when the physiological system is perturbed by an external measured disturbance signal $d(t)$ and an output signal $u(t)$ or $y(t)$ is recorded [61]. If the disturbance $d(t)$ is added to the control signal, then the closed-loop transfer function from the disturbance to the controller's response signal $u(t)$ reveals the complementary sensitivity transfer function of the feedback system which is dependent on both the dynamics of the "human controller" and the dynamics of the system. Knowing the dynamics of the system to be controlled, the dynamics of the "human controller" can then be estimated from the sensitivity transfer function. On the other hand, the identification of physiological systems using unperturbed measured data not only defines the need to estimate a disturbance signal model but most importantly it treats both the system and the "human controller" as open-loop systems therefore ignores that both of these systems are within a feedback system. Hence it can lead to ambiguity when interpreting the results [61]. For the above reasons, during the experimental task an external signal excited the system. The signal that excited the system during the task and the procedure that took place during the experiments are described analytically in this section. Finally the physiological relevance between the experimental compensatory tracking task and the physiological mechanism of human quiet standing is also discussed.

Frequency domain analysis ([111], Ch.2) was applied in the study. The time domain input and output signals that were generated from the experiments and the simulations respectively were analysed in frequency domain using the Discrete Fourier Transformation (DFT) algorithm.

Following Pintelon and Schoukens ([111], Ch.4) a band-limited periodic signal excited the system during the experiments and simulations. The use of a band-limited periodic disturbance signal gave the opportunity to apply frequency domain analysis in both the experimental and simulated data which is presented in Chapter 4. In addition the use of a band-limited periodic signal as the disturbance signal during the physiological task allowed to quantify and qualify the non periodic data, due to the inherent variability, which creates a signal called remnant signal and which is analysed

in Chapter 5.

Section 3.2 describes the linear system and the artificial controller models that were used in the study. Section 3.3 describes the experimental setup. Section **??** presents the system model that was controlled by the participants during the experiments and the controllers during simulations. Section 3.4 describes the type of analysis that was applied to the input and output experimental data and Section 3.5 concludes the chapter.

3.2 System and control models

The section presents the linear dynamic controlled system. In addition the three controller models that were used for the computational modelling of the physiological sustained control balance mechanism are presented. The state-space equations of motion of both the linear dynamic system and the controllers are presented.

Section 3.2 describes the general form of the linear dynamic system, section 3.2.1 describes the artificial non predictive controller (NPC), section 3.2.2 describes the predictive controller (PC) [53] and section 3.2.3 describes the artificial intermittent controller (IC) [42].

This research study considered a single-input single-output (SISO) time delay dynamical system which is excited by a disturbance signal $d(t)$. The state-space form ([30], Ch.17) of this system is given by

$$\dot{x}(t) = Ax(t) + B[u(t) + d(t)] \tag{3.1}$$

$$y(t) = Cx(t) \tag{3.2}$$

$$u(t) = u_o(t - \Delta) \tag{3.3}$$

$$x(0) = x_o \quad \text{initial conditions} \tag{3.4}$$

where $A \in \mathbb{R}^{n\times n}$, $B \in \mathbb{R}^{n\times 1}$ and $C \in \mathbb{R}^{1\times n}$ are the system matrices, $x \in \mathbb{R}^n$ is the state vector of the state variables, $\dot{x}(t)$ denotes the first derivative of $x(t)$ with respect to time, $u \in \mathbb{R}^n$ is the system input (control signal), $u_o(t)$ is the non-delayed

control signal, $y \in \mathbb{R}$ is the system response, Δ is the time-delay due to neural and computational delays which exist in physiological systems and $d(t)$ is the disturbance signal to the control signal.

3.2.1 Non-predictive controller (NPC)

Figure 3.1 shows the non-predictive control system.

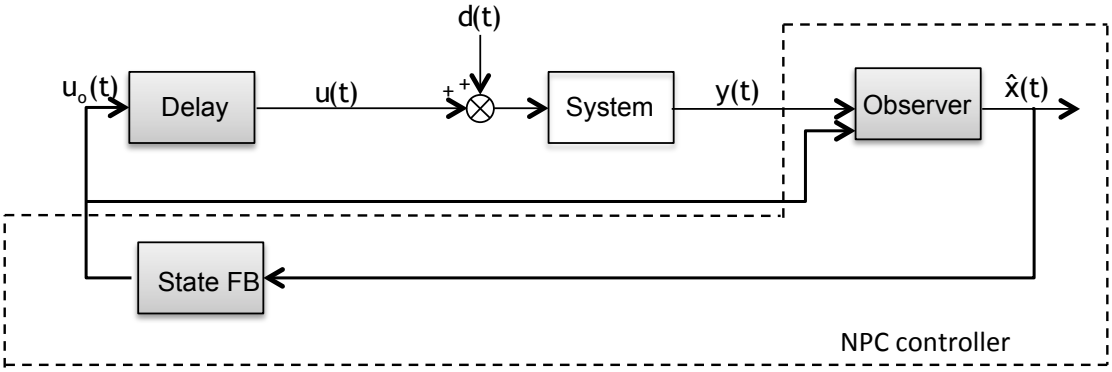

Figure 3.1: General form of the NPC system. The controller shown inside the dotted lines is comprised of an observer and a state feedback. The time delay is not part of the controller design.

The NPC controller consists of a standard state observer and state feedback. The control system state-space equations are given below:

$$\dot{\hat{x}} = A\hat{x}(t) + Bu_o(t) + L(y(t) - \hat{y}(t)) \tag{3.5}$$

$$= A\hat{x}(t) + Bu_o(t) + LC(x(t) - \hat{x}(t)) \tag{3.6}$$

$$= A_o\hat{x}(t) + Bu_o(t) + Ly(t) \quad \text{(Observer)} \tag{3.7}$$

$$\hat{y}(t) = C\hat{x}(t) \tag{3.8}$$

$$\hat{x}(0) = x_0 \quad \text{initial conditions} \tag{3.9}$$

The control signal is given by

$$u_o = -K\hat{x}(t) \quad \text{(Controller)} \tag{3.10}$$

where $\hat{x}(t)$ is the observer state which is used to give an estimate of the current

state $x(t)$. This is implemented by using a forward model of the system together with the measured system output $y(t)$ and the system input $u_o(t)$ (Fig. 3.1) [30].

Below an analysis is given for the case where $\Delta = 0$. Therefore, the observer matrix A_o is given by:

$$A_o = A - LC \tag{3.11}$$

K, L are the controller and observer gains respectively. The closed loop system poles are the eigenvalues of A_o (equation (3.11)) together with the eigenvalues of the state matric A_c where:

$$A_c = A - BK \tag{3.12}$$

The observe state error $\tilde{x}(t)$ is defined as

$$\tilde{x} = \hat{x}(t) - x(t) \tag{3.13}$$

Combining equations (3.1) and (3.7) the dynamics of the observer state error $\tilde{x}$ is defined as

$$\dot{\tilde{x}}(t) = A_o\tilde{x}(t) + B(u_o(t) - u_o(t-\Delta) - d(t)) \quad \text{observer state error} \tag{3.14}$$

$$\tilde{x}(0) = 0 \quad \text{initial conditions} \tag{3.15}$$

The combined state X (equations (3.1) and (3.14)) is given by

$$X = \begin{bmatrix} x(t) \\ \tilde{x}(t) \end{bmatrix} \tag{3.16}$$

Equations (3.1) and (3.14) can be combined as:

$$\begin{bmatrix} \dot{x}(t) \\ \dot{\tilde{x}}(t) \end{bmatrix} =$$

$$\begin{bmatrix} A_c & -BK \\ -BK & A_o - BK \end{bmatrix} \begin{bmatrix} x(t) \\ \tilde{x}(t) \end{bmatrix} - \begin{bmatrix} 0 \\ -BK \end{bmatrix} x(t-\Delta) + \begin{bmatrix} 0 \\ -BK \end{bmatrix} \tilde{x}(t-\Delta) + \begin{bmatrix} B \\ -B \end{bmatrix} d(t) \tag{3.17}$$

Although there is a delay Δ in the feedback loop the NPC was designed without considering the time delay in the feedback loop. Therefore the NPC does not use a predictor, therefore the closed loop system is not robust and instabilities could occur due to presence of the delay in the feedback loop. This can be explained by refering to equation (3.14), the observer error which defines how well the observer generates a good estimate of x is dependent on both the disturbance signal and the delayed control signal $u_o(t-\Delta)$, therefore the closed loop system is not robust due to the presence of the disturbance and the delayed control signal in the observer error.

3.2.2 Predictive controller (PC)

Figure 3.2 shows the predictive control system. The design of the predictive controller is based on Kleinmann [53]. The model consists of a state observer, predictor, feedback (OPF) structure and it has been used in series of studies modelling the "human controller" in physiological control tasks [8, 17–19].

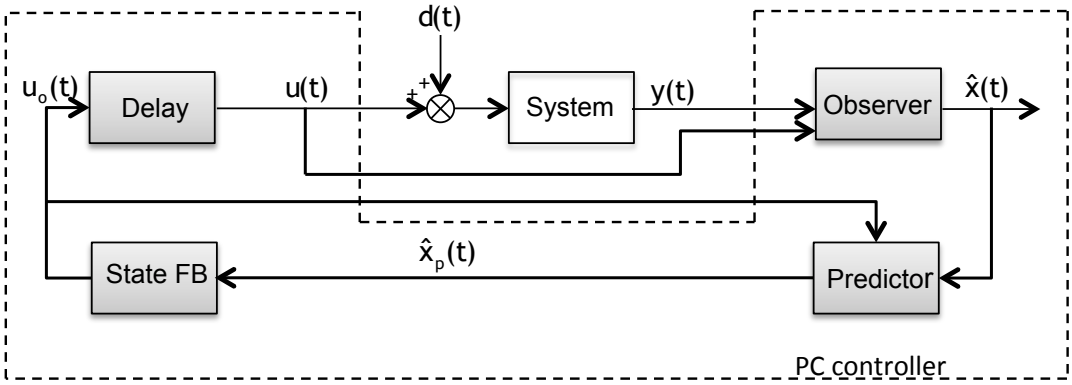

Figure 3.2: General form of the PC system. The block "System" represents the system to be controlled. The controller shown inside the dotted lines is comprised of an observer, predictor, feedback system model. The delay is part of the controller design.

The control system state-space equations are:

The observer system equation is given by

$$\dot{\hat{x}} = A\hat{x}(t) + Bu(t) + L(y(t) - \hat{y}(t)) \tag{3.18}$$

$$= A_o\hat{x}(t) + Bu(t) + Ly(t) \qquad \text{(Observer)} \tag{3.19}$$

$$\hat{y}(t) = C\hat{x}(t) \tag{3.20}$$

$$\hat{x}(0) = x_0 \quad \text{initial conditions} \tag{3.21}$$

$$\hat{x}_p(t) = e^{A\Delta}\hat{x}(t) + \int_0^{\Delta} e^{A\tau}Bu_o(t-\tau)d\tau \qquad \text{(Predictor)} \tag{3.22}$$

The controller state-feedback is given by

$$u_o(t) = -K\hat{x}_p(t) \qquad \text{(Controller)} \tag{3.23}$$

the delayed control signal $u(t)$ is given by

$$u(t) = -K\hat{x}_p(t-\Delta) \qquad \text{(Delayed State Feedback)} \tag{3.24}$$

The state estimate $\hat{x}(t)$ is given by (equation (3.19)), $\hat{x}_p(t)$ is the predicted state at

time $t + \Delta$. The optimum predictor $\hat{x}_p(t)$ is obtained by solving the system (equation (3.1)) from time t to time $t + \Delta$ using the observed state $\hat{x}(t)$ (equation (3.19)) as the initial state. The first term of (equation (3.22)) represents the transient response of the system to the state estimate $\hat{x}(t)$ at the time t whereas the convolution integral of the last term gives the response to the control signal over the time-delay period, $u(t)$ (equation (3.24)) is the delayed control signal.

Combining equations (3.1)-(3.3) and equation (3.19) the dynamics of the observer system error $\tilde{x}(t)$ (equation (3.13)) for the PC are

$$\dot{\tilde{x}}(t) = A_0\tilde{x}(t) - Bd(t)) \tag{3.25}$$

$$\tilde{y}(t) = C\tilde{x}(t) \tag{3.26}$$

$$\tilde{x}(0) = 0 \quad \text{initial conditions} \tag{3.27}$$

$$\tag{3.28}$$

The combined system is equal to

$$\begin{bmatrix} \dot{x}(t) \\ \dot{\tilde{x}}(t) \end{bmatrix} = \begin{bmatrix} A_c & -BK \\ 0_{n\times n} & A_0 \end{bmatrix} \begin{bmatrix} x(t) \\ \tilde{x}(t) \end{bmatrix} + \begin{bmatrix} B \\ 0 \end{bmatrix} d(t) \tag{3.29}$$

The use of a predictor in a feedback loop ensures closed loop stability in the presence of time delays since the predictor moves the time delays outside the feedback loop [30]. Equation 3.25 shows that the observer state error $\tilde{x}$ is affected only by the disturbance applied to system and not by the delay in the feedback loop.

3.2.3 Intermittent controller (IC)

Figure 3.3 shows the structure of the intermittent control system [42].

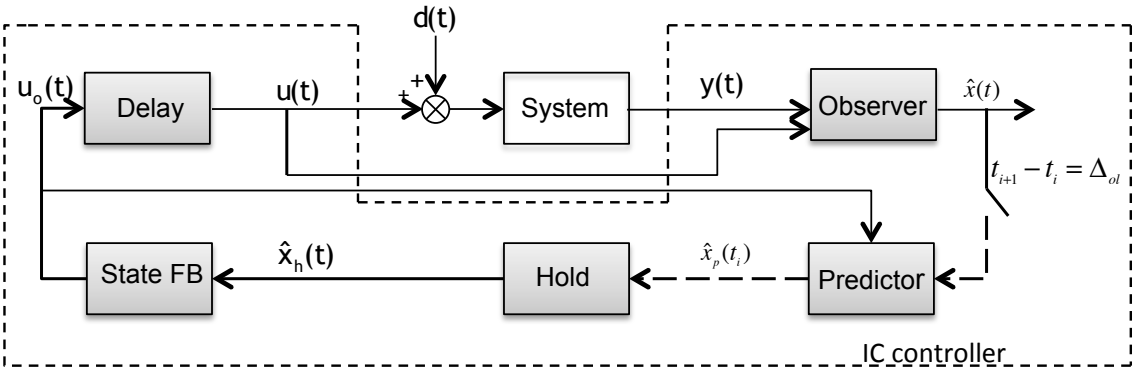

Figure 3.3: General form of the IC system. The block "System" represents the system to be controlled. The controller shown inside the dotted lines is comprised of an observer, predictor, feedback system model. The time delay is part of the controller design. The control signal is updated every Δ_{ol}. In addition, the continuous-time state observer vector $\hat{x}(t)$ is sample every Δ_{ol} , using a sampling element, resulting in a sampled state estimate $\hat{x}(t_i)$. Therefore, the predictor operates on the sampled signal and it is evaluated at the sampled instant t_i resulting in the sampled vector $\hat{x}_h(t)$. The block "Hold" constructs the continuous-time vector signal $\hat{x}_h(t)$ from the sampled signal $\hat{x}_p(t_i)$.

The IC controller structure is similar to the PC controller (Fig.3.2). In particular, it shares the same state observer, predictor and feedback (OPF) system of Kleinman [53]. However, the intermittent controller (IC) differs from the predictive controller (PC) (Fig.3.2) in the following ways:

The IC is a sampled version of the continuous-time predictive controller (Fig.3.2). More particularly, the observed continuous-time state vector $\hat{x}(t)$ is sampled every intermittent interval Δ_{ol}, using a sampling element, resulting in a sampled state estimate $\hat{x}(t_i)$ at instants t_i. Therefore, the predictor operates on the sampled signal and it is evaluated at the sampled instants t_i resulting in the sampled vector $\hat{x}_p(t_i)$. There is a block element labelled "Hold" which constructs the continuous-time vector signal $\hat{x}_h(t)$ from the sampled signal $\hat{x}_p(t_i)$. This hold element is a generalised hold element, and it is discussed below. The "state feedback" block is driven by the open-loop state estimate $\hat{x}_h(t)$ rather than the closed-loop state estimate $\hat{x}(t)$. The hold state $\hat{x}_h(t)$ is updated at the intermittent sample instances t_i, whereas $\hat{x}$ is continuously

changing. The IC is a combination of continuous-time and discrete time, therefore it makes use of three time frames:

1. **continuous-time**, t in which the controlled system operates (equations (3.1),(3.2)).

2. **discrete-time** at which feedback occurs and indexed by i. The discrete instants are denoted by t_i and the estimated state is $\hat{x}_i = \hat{x}(t_i)$. Feedback occurs intermittently, every intermittent interval Δ_{ol}, therefore The i^{th} intermittent interval, is defined as:

$$\Delta_{ol}^{i} = t_i - t_{i-1} \tag{3.30}$$

   The intermittent interval can either be variable or fixed [40].

3. **intermittent-time** is a continuous-time variable denoted by τ and restarts at each intermittent interval. Hence, within the intermittent interval τ is given by

$$\tau = t - t_i \tag{3.31}$$

   Every intermittent interval Δ_{ol} an open-loop control trajectory u_i is generated indexed by the integer i. Therefore the open-loop intermittent control signal trajectory that is generated within an intermittent interval Δ_{ol} is equal to

$$u_0(t) = u_0(t_{i-1} + \tau) = -K\hat{x}_h(t - t_{i-1}) \quad \text{for } t_{i-1} \leq t < t_i \tag{3.32}$$

where $\hat{x}_h(\tau) = \hat{x}_h(t - t_{i-1})$ is the generalised hold state which evolves in the intermittent time τ (equation (3.31)) and is given by the state space form

$$\dot{\hat{x}}_h(\tau) = A_h\hat{x}_h(\tau) \tag{3.33}$$

$$\hat{x}_h(0) = \hat{x}(t_i) \quad \text{initial conditions} \tag{3.34}$$

Solving the differential (equation (3.33)), $\hat{x}_h(\tau)$ becomes

$$\hat{x}_h(\tau) = e^{A_h(\tau)}\hat{x}_h(0) \tag{3.35}$$

and the control signal $u(t)$ is given by

$$u_0(t) = -Ke^{A_h(t-t_{i-1})}\hat{x}_p(t_{i-1}) \quad \text{for } t_{i-1} \leq t < t_i \tag{3.36}$$

Therefore every intermittent interval an open-loop control action trajectory $u_0(t)$ is generated based on the current state $x(t_i)$.

Figure 3.4 shows a typical sampled intermittent control signal $u_0(t)$ which is generated within an intermittent interval Δ_{ol}^i. At each instance t_i there is a jump due to the sampling process, however the control signal $u_0(t)$ appears smooth unlike the jump at the discrete time t_i

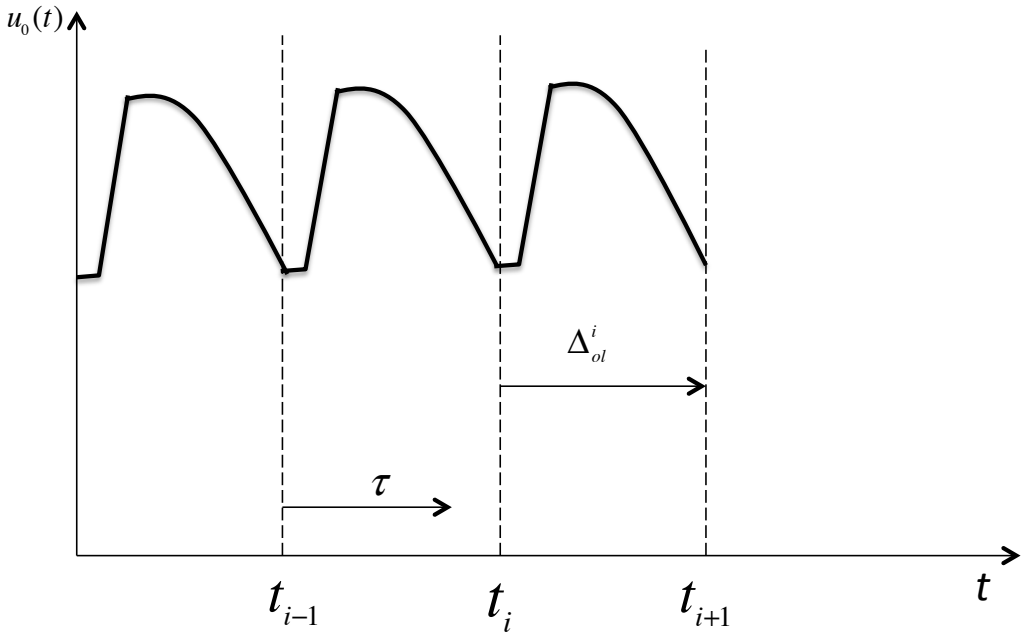

Figure 3.4: Intermittent control sampled signal $u_0(t)$. The control signal is generated every Δ_{ol}^i and it appears smooth unlike the jumps in the discrete time t_i.

The are three ways in which the discrete times t_i could be generated:

1. In a **periodic way** "clock-driven". In this case the intermittent interval Δ_{ol} (equation (3.30)) is fixed therefore sampling occurs at regular instants $t_i = i\Delta_{ol}$. The use of a periodic sampling every Δ_{ol} in a sampled-data feedback system such that of the intermittent control (Fig. 3.3) gives analytical properties such as the Fourier representation of the closed loop system containing the intermittent controller [56, 112]. The frequency response of the intermittent

controller approximates that of the underlying continuous-time control in case the system to be controlled is not excited by a disturbance signal [39, 56].

2. In an **event driven way** according to some error exceeding a threshold [40, 42]. Unlike the "periodic way" in the "event -driven way" the intermittent interval is not fixed. There is an event detector which continuously monitors the difference between two states, for example the error between the open-loop hold state $\hat{x}_h$ and the closed-loop state observer $\hat{x}$ [42] or the error between the predicted state $\hat{x}_p$ and the closed loop state observer $\hat{x}$ [40]. In either cases if the state error exceeds a threshold the detector generates an event and intermittent sampling occurs until the error threshold is satisfied. Therefore the generation of the instants t_i are "event driven". The times at which discrete instants t_i are generated determines the length of the intermittent interval Δ_{ol}^i. Therefore the discrete instants are equal to $t_i = \sum_{j=1}^{i} \Delta_{ol}^j$. In "event driven" each intermittent interval Δ_{ol}^i has maximum and minimum values

$$\Delta_{min} \leq \Delta_{ol}^i \leq \Delta_{max} \tag{3.37}$$

3. **In a variable way** (i.e not event driven). The intermittent interval occurs neither "periodic" nor based on "event-driven". In the "variable" way the intermittent interval Δ_{ol}^i follows a statistical distribution with a mean. Therefore sampling occurs at different instants $t_i = \sum_{j=1}^{i} \Delta_{ol}^j$ where Δ_{ol}^i is taken from the distribution. This method was applied in Chapter 5.

As shown in equation (3.33) the hold dynamics are determined by the square matrix A_h (equation (3.33)). In Gawthrop and Gollee [99] it was shown that A_h can be chosen in such a way that different types of intermittent control can be used, such as tapping control. This study, makes use of a special case of the generalised hold, the system matched hold (SMH), where the dynamics of the hold state match those of the underlying closed loop continuous time system (equation (3.12)). The system matched hold is discussed in the next section.

3.2.4 System matched hold (SMH)

The intermittent controller is based on an underlying continuous-time controller using a standard state estimate feedback however periods of open-loop are combined with intermittent feedback. Therefore this intermittent controller combines both continuous-time and discrete time features hence it is hybrid and it results in a hybrid dynamical system. A sampling element is used for the discritisation of the continuous-time controller and observer state and a hold element is used for the exactly opposite reason which is the conversion form the discrete to continuous.

Gawthrop and Wang [39] have shown that the intermittent controller uses a generalised hold to convert the discrete-time signals to continuous-time. The IC uses basis functions [39], therefore that permits to make use of a particular hold which is based on the closed-loop dynamics of the underlying continuous-time control design. This special hold is the SMH. The SMH is a disturbance free open-loop simulation based on the closed-loop system dynamics of the continuous-time control system [41].

Therefore the state matrix A_h of the generalised hold (equation (3.33)) will be equal to the closed-loop system matrix A_c (equation (3.12)).

$$A_h = A_c \tag{3.38}$$

Hence, the generalised hold state $\hat{x}_h(\tau)$ (equation(3.35)) using the SMH will be equal to

$$\hat{x}_h(\tau) = e^{A_c(\tau)}\hat{x}_h(0) \tag{3.39}$$

This particular hold design is associated with the separation principle ([30], Section 18.4) which is similar to that of the continuous-time predictive controller [39, 41, 56]. The consequence of the separation principle is that neither the design of the hold nor the stability of the closed-loop system are affected by the variability of the intermittent sampling [41] for zero time delay. The use of the SMH is independent of the intermittent interval and the stability is not affected. One effect of the hold is that the loop time delay Δ of the intermittent control system is not constant but depends on when the intermittent interval is restarted [41]. On average the effective loop-time delay is

$$\Delta_{eff} = \Delta + 0.5\Delta_{ol} \tag{3.40}$$

Another important effect of the SMH hold is that the intermittent controller in the absence of a disturbance signal behaves exactly like an underlying continuous-time controller. The intermittent control signal is identical to that of the underlying continuous-time controller, resulting in a system response which is similar to that of the underlying continuous-time controller only that is delayed due to additional intermittent interval Δ_{ol}. The intermittent control signal is identical to that of the underlying continuous-time controller due to the fact the observer error is zero (equation (3.25)). On the other hand in the case of a disturbance the performance of the intermittent controller is degraded, due to the fact that the observe error is not zero any more. It might take some events before the observer error is eventually zero. However even in the case of a disturbance the control signal looks similar to that of the underlying continuous-time controller.

3.2.5 Intermittent predictor

Unlike equation (3.22) in which the predictor uses the convolution integral and therefore it is infinite-dimensional the formula of the predictor for the IC model is much simpler than that for the continuous PC [42].

Equation (3.22) is the solution of the differential equation, in the time frame τ (equation (3.31)) evaluated at time $\tau = \Delta$

$$\dot{\hat{x}}_p(\tau) = A\hat{x}_p(\tau) + Bu(\tau) \tag{3.41}$$

$$\hat{x}_p(0) = \hat{x}_h(t_i) \tag{3.42}$$

Combining equations (3.33),(3.41) results in:

$$\begin{cases} \dot{\hat{X}}(\tau) = A_{ph}X(\tau) \\ X(0) = X_i \end{cases} \tag{3.43}$$

where

$$X(\tau) = \begin{pmatrix} \hat{x}_p(\tau) \\ \hat{x}_h(\tau) \end{pmatrix} \tag{3.44}$$

$$X_i = \begin{pmatrix} \hat{x}_p(t_i - \Delta) \\ \hat{x}(t_i) \end{pmatrix} \tag{3.45}$$

and

$$A_{ph} = \begin{bmatrix} A & -BK \\ 0_{n\times n} & A_h \end{bmatrix} \tag{3.46}$$

where 0 is a zero matrix of the indicated dimensions and the hold matrix A_h is A_c (SMH).

Equation (3.41) has an explicit solution at time $\tau = \Delta$ given by:

$$X(\Delta) = e^{A_{ph}\Delta} X_i \tag{3.47}$$

The prediction $\hat{x}_p$ can be extracted from equation (3.47) to give:

$$\hat{x}_p(t_i) = E_{pp}\hat{x}(t_i) + E_{ph}\hat{x}_h(t_i) \tag{3.48}$$

where the $n \times n$ matrices E_{pp} and E_{ph} are partitions of the $2n \times 2n$ matrix E:

$$E = \begin{bmatrix} E_{pp} & E_{ph} \\ E_{hp} & E_{hh} \end{bmatrix} \tag{3.49}$$

where

$$E = e^{A_{ph}\Delta} \tag{3.50}$$

Using equation (3.48) is more practical than equation (3.22). Matrices E_{pp}, E_{ph} can be computed off-line therefore the computational load is lower than that using the convolution integral (equation (3.22)) in real time.

The time taken to compute the control signal can be up to Δ_{min} [47] and for practical reasons the predictor equations are simpler if the system time delay $\Delta \leq \Delta_{min} = \Delta_{ol}$ (equation (3.37)) [42].

3.2.6 Controller comparison

The three controller models NPC, PC, IC have been compared with one another in a simple example. A system with a transfer function in the s-domain representation was considered:

$$y(s) = \frac{1}{s^2}u(s) + \frac{1}{s^2}d(s) \tag{3.51}$$

The state-space representation of the above system in the form of equation (3.1) comprises of the state matrices given below

$$A = \begin{bmatrix} 0 & 0 \\ 1 & 0 \end{bmatrix}, B = \begin{bmatrix} 1 \\ 0 \end{bmatrix}, C = \begin{bmatrix} 0 \\ 1 \end{bmatrix}^T \tag{3.52}$$

The time delay was considered $\Delta = 0.25$sec and for the intermittent controller the intermittent interval $\Delta_{ol} = 0.5$sec. The control gain K and the observer gain L were designed using the LQR method for all three controllers.

A constant reference signal $r(t) = 1$ was considered during the simulations and the disturbance signal $d(t)$ was initially $d = 0$ and then changed to -1 at time $t = 5$ s.

$$d(t) = \begin{cases} 0 & 0 \leq t < 5 \\ -1 & t > 5 \end{cases} \tag{3.53}$$

Figures 3.5a and b show the system output $y(t)$ and control input u respectively in the case where there is no disturbance signal added to the systems. The results show that the IC masquerades as the PC except for the extra delay due to the intermittent interval Δ_{ol}.

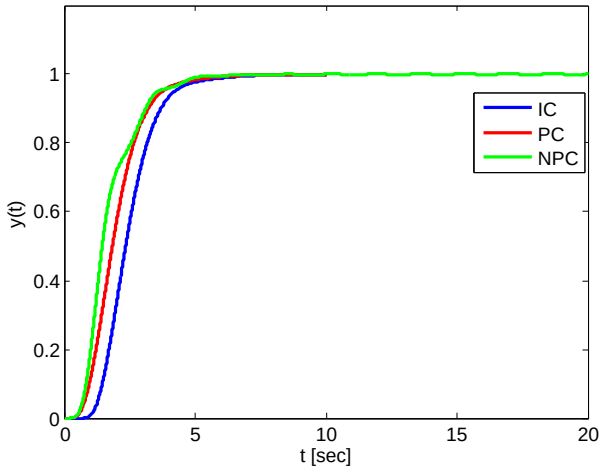

(a) Output response, y

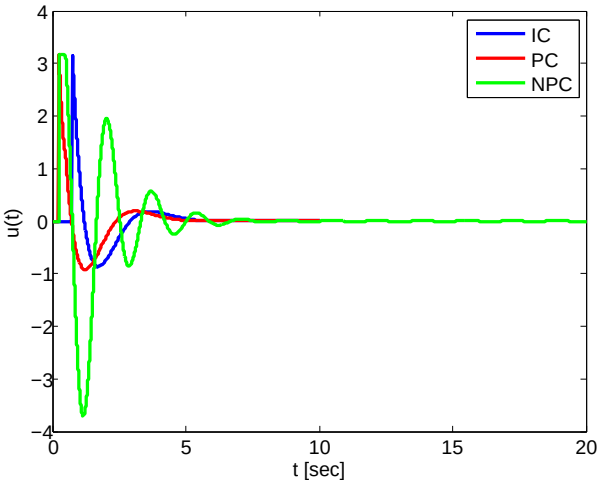

(b) control signal, u

Figure 3.5: Controller comparisons using a simple example. The figures show the output responses $y(t)$ and control signals $u(t)$ from simulations using the NPC, PC and IC controllers when there is no disturbance added to the systems. a) The figure shows the response signal $y(t)$ for the NPC (green line) PC (red line) and the IC(blue line). b) The figure depicts the control signals. For the NPC controller (green line) the control signal generated is oscillatory due to the absence of the predictor in the controller. The control signals of the PC and the IC are very similar. The IC masquerades like the PC except for the extra delay due to the intermittent interval Δ_{ol}.

Figure 3.6 a and b show the system output $y(t)$ and control input $u(t)$ respectively in the case where there is a disturbance signal added to the system at $t = 5$ s. Up to $t = 5$ s the IC controller behaves like the underlying continuous-time PC controller and the control response $u(t)$ is identical to that of the PC except for the extra delay of $\Delta_{eff} = 0.5$ s due to the intermittent interval Δ_{ol}. This is because the observer error (equation (3.25)) is zero. On the other hand at time $t = 5$ s a disturbance is added to the control loop system therefore the observer error is not zero any more. Figure 3.6b shows that almost four events occur until the observer error is zero. From the simple example it was shown that in the absence of a disturbance signal the IC with a SMH and a fixed Δ_{ol} behaves exactly like the underlying continuous-time controller, however in the presence of a disturbance the performance of the IC is degraded (ie. "spikeness " is shown in the control response) because the observer error is not zero any more but the response is similar to that of the underlying continuous-time controller.

On the other hand, Figure 3.6b shows that the control signal for the NPC controller is oscillatory before and after the initiation of the disturbance signal at $t = 5$ s. The control signal is oscillatory due to the absence of a predictor in the control system loop, therefore any change in the time delay could produce instabilities to the system.

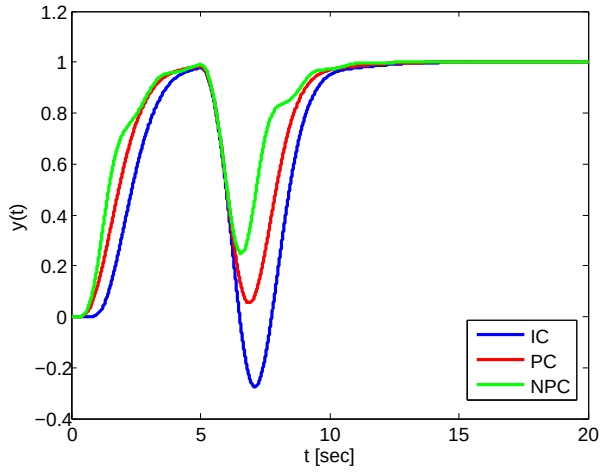

(a) response output, y

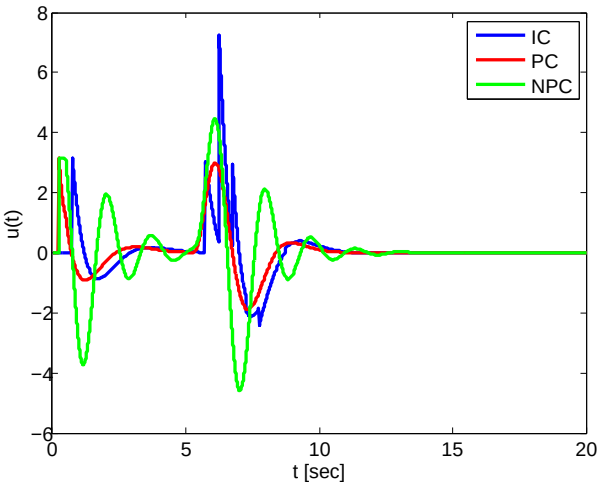

(b) control signal u

Figure 3.6: Controller comparisons using a simple example. The figures show the output responses $y(t)$ and control signals $u(t)$ from simulations using the NPC, PC and IC controllers when there is disturbance added to the systems. a) The figure shows the response signal $y(t)$ for the NPC (green line) PC (red line) and the IC(blue line. b) The figure depicts the control signals. For the NPC controller (green line) the control signal generated is oscillatory due to the absence of the predictor in the controller. Up to $t = 5$ s the IC controller behaves like the underlying continuous-time PC controller and the control response $u_0(t)$ is identical to that of the PC except for the extra delay of $\Delta_{eff} = 0.5$ s due to the intermittent interval Δ_{ol}. On the other hand at time $t = 5$ s a disturbance is added to the control loop system therefore the observer error is not zero any more. Almost four events occur until the observer error is zero.

3.3 Experimental setup

The physiological compensatory tracking task that was used for the computational modelling is described in this section.

The experimental data from the tracking task were collected in Loram et al. [28] and the experiments took place at the Institute for Biomedical Research into Human Movement and Health at Manchester Metropolitan University, Manchester, UK.

Experimental data were collected from visual-manual SISO sustained control compensatory tracking of an unstable second order system with a time constant equivalent to that of an upright standing human [24]. The unstable system had to be actively controlled otherwise stability was lost. The participants were required to balance the unstable system by continuously moving a single-axis joystick in the presence of an unpredictable disturbance signal $d(t)$. The task was compensatory since the aim was to keep the system still in a fixed position when the only information that was available to the participants was the response system signal that was denoted as a dot on an oscilliscope during the task. Therefore only visual feedback was availiable.

The initial aim of the experiment of Loram et al. [28] was to study human quiet standing in the case where all reflexes are ignored therefore peripheral processes [14,20] are not present whereas central processes are, during quiet standing, and in addition vestibular and proprioceptive feedback all excluded. The rationale behind the study is presented in detail in Loram et al. [24]. As stated in Loram et al. ([28], pp. 309) "the apparatus, historical evolution of the study of the sustained control mechanism of quiet standing, measurements, methods of analysis and rationale for these methods have already been described in detail in Loram et al. [24]". We refer to the reader to the previous work and restrict here to the minimum necessary.

It is rather true that human upright stance is a complex process involving the sensory, nervous and motor systems. In addition it is inherently unstable, as small deviations from upright stance result in torques due to gravity which drive the system further away from the upright position [11]. To maintain a human upright stance the vertical location of the Centre of Mass (CoM) of the human body should not exceed the limits of the base of support (the feet). Therefore the aim is to keep the CoM location of the body within a relatively small range provided by the feet. This

is complex as humans use multiple joints and muscles which serve as the actuators to keep the projection of the CoM within the area of support. Therefore the human body is considered as a multi-segment system which receives multiple input signals and generates multiple output signals. In addition during the human upright stance the nervous system receives delayed information from the multisensory system. Delayed sensory information from the somatosensory, visual and vestibular systems must be integrated in the higher level of the nervous system to send appropriate control signals to activate the various muscles and joints in order to maintain human stance. For these reasons the physiological mechanism of human standing is considered as a multiple-input multiple-output (MIMO) feedback system with a feedback time-delay.

During quiet standing medial/lateral sway is present but is smaller than in saggital sway [75]. Gatev [113] using a multi-camera system have shown that the ankle mechanisms (dorsiflexors/plantarflexors) in the saggital plane dominate quiet standing control. For that reason human quiet standing could be reasonably simplified to the task of balancing a single axis inverted pendulum rotating around the ankle joint. Studies of Fitzpatrick and Taylor [114] and Loram et al. [115] have shown that subjects could balance a real inverted pendulum using only ankle torques. In addition Loram et.al. [116] have shown that the simple inverted pendulum model could be used to predict muscle changes during quiet standing. Therefore, for small changes as in quiet standing the miltiple complex mechanism of quiet standing could be considered as a SISO system with a delay. Therefore, the physiological mechanism of human quiet standing could be considered as a single-input single-output (SISO) delayed system. Especially for small angles observed in the inverted pendulum the mechansim of quiet standing is considered a linear SISO system with a delay [5, 14, 24, 38].

The neural control processes that take part during human quiet standing are complicated and still controversial among researchers. There are two conflicting views on the processes during human balance control. The first view which is based on identification analysis of disturbed standing, supports that human standing balance is a linear continuous-time feedback system which includes short time delays (up to 200ms) and the feedback gains are altered according to the task [11, 13, 14, 61]. That means that the intrinsic properties of the ankle joints such as stiffness and damping

can adequately provide a torque response to unexpected disturbances during quiet standing. The second view has come from observations in tasks in which subjects are required to balance inverted pendula with human dynamics or during quiet standing. In these studies it was found that human balance is variable, it is poorly described as a continuous-time process and is associated with long time delays in which central processes such as prediction, decision and making trajectory formation are involved [37,105,117]. Loram et al. [115,116,118] in experiments on postural sway have suggested that the muscle length changes in a non-spring-like manner. They supported that the ankle stiffness is only 92% of that required to provide human balance supported by Casadio et al. [119] who suggested an intrinsic stiffness of 64% of the load stiffness of the human body. Morraso et al. [117] suggested that quiet standing requires prediction, decision making and trajectory formation planning [4,16] for its accomplishment. Also, Loram et al. [6] have shown using ultrasound tracking that the movements of the calf muscles during human quiet standing are similar to hand movements of a subject manually balancing an equivalent body (inverted pendulum with human dynamics). Hence, human quiet standing is essentially a sustained compensatory tracking task. In such tasks humans have available only information about the state of the controlled load, position and velocity, and the control task is to minimise deviation in this state from the desired fixed reference.

3.3.1 Subjects

Eleven healthy subjects, 9 male, 2 female, aged $21 - 59$ years (36 ± 13 years, mean $\pm$ S.D) participated voluntarily in the experiment which was carried out at Manchester Metropolitan University. The protocol of the experiment was approved by the Academic Ethics Committee of the Faculty of Science and Engineering, Manchester Metropolitan University. All participants gave written, informed consent to these experiments which conformed to the standards set by the latest revision of the Declaration of Helsinki [28].

3.3.2 Apparatus and System model

Figure 3.7 shows a diagram of the experimental setup that was used in Loram et al. [28].

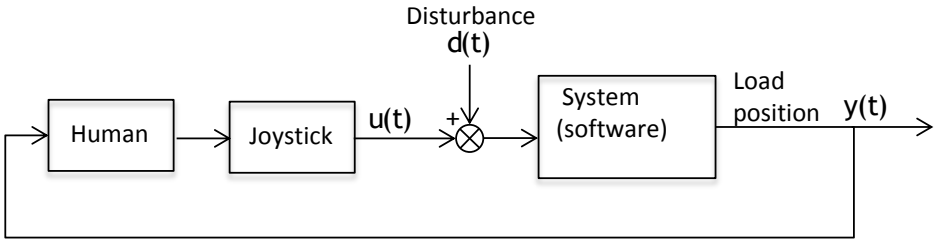

Figure 3.7: Experimental setup.

The block "Joystick" (Fig.3.7) represents the single-axis joystick (HFZ Magnetic, CH Products, Ltd, UK) in which the internal restoring spring was removed. The joystick voltage was used as analogue input to the virtual "System" and offset so that the central position of the joystick applied a small virtual force to the "System". During the task the participant, which is represented as the block "Human" applied a force to the "System" by moving the joystick upward or downward. The joystick position specified the control force which was applied in the "System". Continuous forward and backward adjustments of the joystick, using the flexors of the fingers and abductors of the thumb, were required by the participants in order to control the "System". The joystick movement in all trials was 2.5mmV^{-1}.

The block "System" represents the virtual load that was constructed using Real-Time Workshop and executed on a laptop using Real-Time Windows Target within Matlab v7 at a sample rate of 1000 samples per second.

The virtual load to be controlled was a single-link inverted pendulum with dynamics of a human standing balanced by the calf muscles acting through the Achille's tendon [6, 64, 116]. The mass of the load was m 70 kg, with gravitational acceleration g of 9.81 ms^{-2} and a centre of mass height h of 0.92 m. The load was subjected to a destabilising gravitational force (mgh) and the virtual passive stiffness (ankle stiffness) k was considered to be $c = 85\%$ of the gravitational moment (i.e. $k = 0.85$ mgh, with $c = 0.85$). According to Loram et al. [24] the moment of inertia of the inverted pendulum is 77 kgm^2 and the passive ankle viscosity B is 2.9 Nmrad^{-1}.

Figure 3.8b is the equivalent model that was used during the compensatory tracking

task experiments. θ_{in} is the input angle (system input) which corresponds to the spring angular position generated by the participant by moving one end of the spring (bias) using the joystick and θ represents the angular position of the pendulum.

Figure 3.8a is the physical model which represents the mechanism of human quiet standing. The human during quiet standing is described as an inverted pendulum which sways around the ankle joint via active muscles, the calf muscles, which are responsible for preventing forward toppling, through the Achille's tendon [6,25,28,116]. Generally, the calf muscles, soleus and gastrocnemius connect to the leg bones and the back of the knee through the Achille's tendon. In that physical model it is shown that the calf muscles are described by the single contractile element (CE) whereas the Achille's tendon, that connects the contractile element to the ground through the foot, is described as spring-like element with stiffness k [120]. The contractile element CE acts through the spring-like element. During standing the human body tends to topple forward. However, falling is prevented by restoring torques (T). The amount of the torque produced is dependent on the amount the angle θ is increased (increase in angle θ causes a forward lean of the body) or on the amount of the contraction θ_{in} of the CE element is decreased. In either cases, there is always a change in the length of the spring-like element with stiffness k (the Achille's tendon). Therefore the ankle torque is equivalent to

$$T = k(\theta - \theta_{in}) - B\dot{\theta} = -cmgl(\theta - \theta_{in}) - B\dot{\theta} \tag{3.54}$$

Equation 3.54 separates the ankle torque into the active $cmgh\theta_{in}$ and passive $-cmgh\theta - B\dot{\theta}$ components where c is the ratio of the tendon stiffness relative to the load stiffness mgl, θ_{in} is the neurally modulated bias or contractile element length and B is the passive ankle viscosity.

The general equation of motion for the inverted pendulum is given by

$$\Sigma M = I\ddot{\theta} \Rightarrow \tag{3.55}$$

$$I\ddot{\theta} = mgl\sin\theta + T \tag{3.56}$$

where I is the moment of inertial, θ is the angle from the vertical, m the mass of the inverted pendulum, g the gravitational acceleration, l the height of centre of mass and T the ankle torque.

For small changes, as that in quiet standing [6,116] $\sin\theta = \theta$, therefore the linearised equation of motion of the inverted pendulum with human dynamics (Fig. 3.8b) is given by

$$\Sigma M = I\ddot{\theta} \Rightarrow I\ddot{\theta} = mgl\theta + T \tag{3.57}$$

Combining equations (3.54), (3.55), (3.57), the Laplace transform equation is given by

$$I\ddot{\theta}(s) = mgl\theta(s) - cmgl(\theta(s) - \theta_{in}(s)) - B\dot{\theta}(s) \Rightarrow I\ddot{\theta}(s) + B\dot{\theta} + mgl\theta(c-1) + mgl\theta_{in} = 0 \tag{3.58}$$

Following (Franklin et al. [121] Ch.7) the state space form of the above ordinary differential equation (ODE) is given by

$$\begin{aligned} \begin{bmatrix} \ddot{\theta}(t) \\ \dot{\theta}(t) \end{bmatrix} &= \begin{bmatrix} \frac{B}{I} & \frac{mgl(c-1)}{I} \\ 1 & 0 \end{bmatrix} \begin{bmatrix} \dot{\theta}(t) \\ \theta(t) \end{bmatrix} + \begin{bmatrix} \frac{mgl}{I} \\ 0 \end{bmatrix} \theta_{in} \\ y(t) &= \begin{bmatrix} 0 & 1 \end{bmatrix} \begin{bmatrix} \dot{\theta}(t) \\ \theta(t) \end{bmatrix} \end{aligned} \tag{3.59}$$

The state-space representation of the linearised equation of motion of the "System" in numerical values is equivalent to:

$$\begin{bmatrix} \ddot{\theta}(t) \\ \dot{\theta}(t) \end{bmatrix} = \begin{bmatrix} 0.0372 & -1.231 \\ 1 & 0 \end{bmatrix} \begin{bmatrix} \dot{\theta}(t) \\ \theta(t) \end{bmatrix} + \begin{bmatrix} 8.2 \\ 0 \end{bmatrix} \theta_{in}$$
$$y(t) = \begin{bmatrix} 0 & 1 \end{bmatrix} \begin{bmatrix} \dot{\theta}(t) \\ \theta(t) \end{bmatrix} \tag{3.60}$$

θ_{in} is the input angle (system input) (equation(3.3)) which corresponds to spring angular position generated by the participant by moving one end of the spring while $y(t)$ ($\theta(t)$, second state) is the output signal which corresponds to the position of the inverted pendulum and it is equivalent to the ankle angle of the approximated standing human. The first state, $\dot{\theta}$ represents the angular velocity of the inverted pendulum. The system is unstable and requires active control to be stabilised. More details are given in [24, 28].

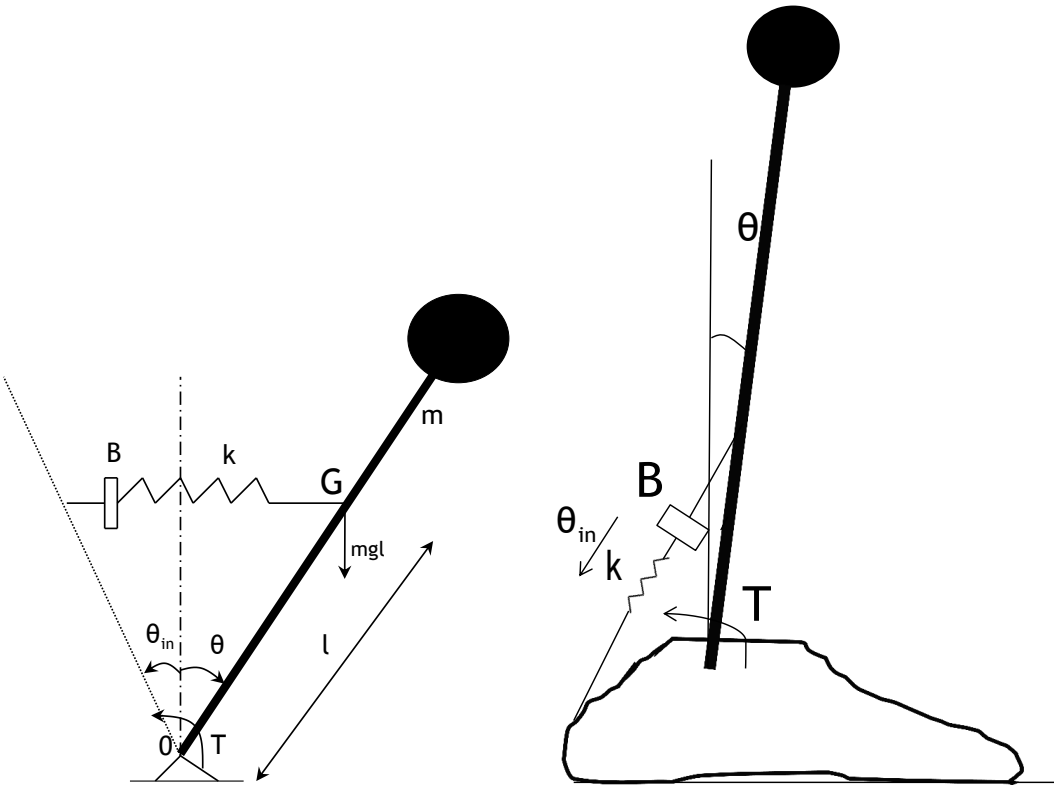

(a) Physical model (b) Equivalent model

Figure 3.8: Physical and equivalent models that represent the mechanism of human quiet standing a) represents the physical model during quiet standing. The human body is considered as an inverted pendulum which sways around the ankle joints via active muscles, the calf muscles which are responsible for preventing forward toppling, through the Achilles tendon. During standing passive stabilisation is accomplished by the intrinsic ankle stiffness k determined mostly by the Achilles tendon with viscosity B. θ_{in} represents the muscle shortening applied at the end of the compliant tendon and θ is the resulting angular position of the body (inverted pendulum). b) represents the equivalent system model that was used during the compensatory tracking tasks.The human body is considered an inverted pendulum with mass m and length l from the CoM (G). During the task the participants control the inverted pendulum by moving one end of the spring, with stiffness k, of the muscle-tendon unit. This is equivalent to lengthening and shortening the calf muscles during quiet standing. θ_{in} is the system input determined by the participant and θ is the corresponding angular position of the inverted pendulum.

3.3.3 Perturbation signal design

The use of an external perturbation in combination with the correct identification method identifies the dynamics of the sustained control mechanism and the dynamics of the system to be controlled separately [61].

According to Pintelon and Schoukens ([111], Ch. 4), the excitation signal that is applied during an experimental task is essential and determines the quality of the both non parametric and parametric models that are derived from the measurements of the input and output data.

In this study, it was essential to determine the deterministic part of the experimental data and in addition to study human variability, which is revealed from the stochastic measured data, therefore the selection of the excitation signal was very important to this study. Pintelon and Schoukens ([111], Ch. 4) suggest that the use of band-limited periodic signals as excitation signals during experimental tasks has advantages such that the noise-to-signal (NSR) ratio is improved for the raw data, also in periodic signals where integer number of periods are selected the phenomenon of leakage is avoided. In addition, it is possible to detect, qualify and quantify deterministic data (data at excited frequencies) from the stochastic data (remnant signals at non excited frequencies) in the case of non-linear dynamic systems, as in the case of human behaviour. For the above reasons this study used as an excitation signal a band-limited periodic signal [28].

Therefore, the signal $d(t)$ that excited the system during the compensatory tracking task was a band-limited periodic signal. In particular, a multisine periodic band-limited signal with carefully chosen frequency components was considered as the excitation signal during the experimental task. Such signals unlike binary periodic signals (eg. Pseudo Random Binary Signal (PRBS)) excite the system at the frequency band of interest only whereas the pseudo-binary periodic signals excite other frequency bands as well.

The disturbance signal $d(t)$ was chosen to be unpredictable by the human during the experimental task. Therefore, the mulisine disturbance signal is equal to

$$d(t) = \sum_{e=1}^{N_e} A_e \cos(2\pi\omega_e t + \phi_e) \tag{3.61}$$

where ω_e represents the N_e discrete frequencies with resolution $\omega_0 = 2\pi f_0$. The period of the signal is given by its fundamental frequency component and is equal to

$$T_0 = 2\pi/\omega_0 \tag{3.62}$$

During the experiment [28] the period of the input signal $d(t)$ was $T_0 = 10$ s with fundamental frequency $f_0 = \omega_0/2\pi = 0.1$ Hz. The signal $d(t)$ was chosen to be band-limited to avoid aliasing artefacts introduced by the sampling process and was chosen to contain power at $N_e = 100$ discrete frequencies ranging from $f_e = \omega_e/2\pi = [0.1, ..., 10]$ Hz $(e = 1, 2, ..., N_e)$. The upper frequency limit was chosen to be above any possible human control bandwidth and the lower limit was chosen to avoid leakage effects due to the limited time span (200 s) of the data.

To obtain an unpredictable excitation, the phases ϕ_e were random values taken from a uniform distribution on the open interval $(0, 2\pi)$, while the amplitude was $A_e = 1$ for all frequencies ω_e to ensure that all frequencies were equally excited [28]. For each trial, the phases were re-randomised, and the crest factor (ratio of maximum deviation to standard deviation) [111] was limited to 3. For example, a sequence was generated and if the sequence had a crest factor larger than 3 then it was removed and a new sequence was applied. To meet the experiment requirements the amplitude A_e of the signal was scaled by dividing the amplitude by a factor of 60.

An example of 40 s of the disturbance signal $d(t)$ which was applied during the experiments is shown in Figure 3.9.

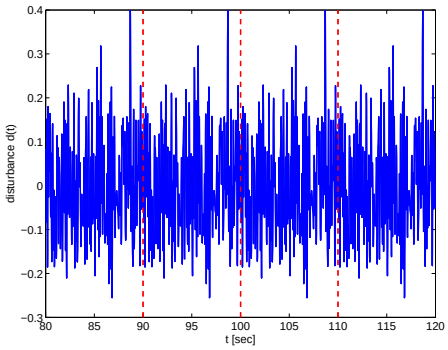

Figure 3.9: Example of the disturbance signal applied during the experiments. The signal was a band-limited periodic signal with contained $N_e = 100$ frequencies ranging from $f_e = 0.1, ..., 10$. The period of the signal was $T_0 = 10$ s with fundamental frequency $f_0 = 0.1$ Hz

The advantages of such a perturbation signal are that: it is periodic hence the estimation of Frequency Respone Functions (FRFs) is improved. Its power can be specified at any frequency that is being excited. By making a dedicated selection of the components of the excitation signal, it is possible to detect, qualify and quantify the presence of random distortions [111].

3.3.4 Procedure

During the experiment the participants sat quietly in a self-selected position and by holding continuously a sensitive single-axis joystick they were asked to control the position of a dot which was displayed in the oscilloscope and moved in the x-axis of the oscilloscope (Fig.3.10). The joystick position determined the control force applied to the system. The position of the dot represented the position of the inverted pendulum with human dynamics running in real time (Sect.3.2).

To reveal the human dynamics, during the experiment the unpredictable external disturbance $d(t)$ was added to the joystick signal $u(t)$. The disturbance signal was not added to the movement displayed on the oscilloscope (output response) due to the fact that humans easily perceive and filter out or are distracted by the artificial higher frequency components of the stimulus ([73] pp. 211). The summation of the joystick signal and the disturbance signal was applied to the "System" (Fig.3.8) which was denoted as a dot on the oscilloscope. The system position was the only information the subjects had during the experiment and it was shown on the oscilloscope. In any of the trials the participants were instructed to prioritise one of the two goals: a) the aim was to keep the system position as close to the centre of the oscilloscope as possible, (i.e "minimise position" control strategy) and b) the aim was to keep the system position still but it does not matter where the load is on the screen (i.e. "minimise velocity" control strategy).

During the experiment the participants controlled the virtual inverted pendulum by moving one end of the spring using the joystick. This is equivalent to shortening and lengthening the calf muscles in the active agonist muscle-tendon unit during quiet standing. The set-up replicated standing balance which is equivalent to a compensatory, manual tracking task.

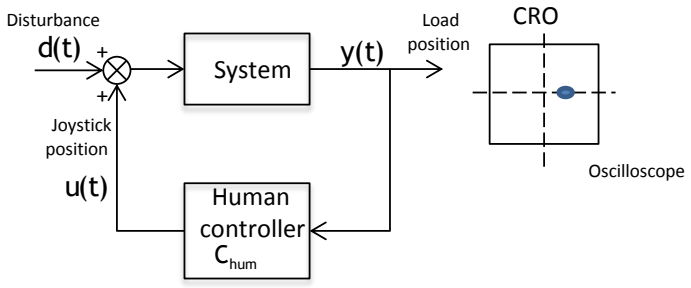

Figure 3.10: Experimental setup.

Each session lasted for 200 s comprising 20 periods of the disturbance and the virtual system run in real-time using Simulink (MathWorks, USA). The experiments were executed on a PC using Real-Time Windows target (Mathworks) and the source of the data was recorded at a sample rate of 100 samples per second ($T_s = 0.01$s).

The joystick voltage was acquired at 16 bit resolution and used as analogue input to the real-time model. During the experiment, if the load passed above the positional limits ± 10 V then the load "dropped" and automatically returned to the centre with zero velocity within a few tenths of a second. The continuous time t was replaced by the discrete sample time $t_n = nT_s$.

3.4 Analysis methods

3.4.1 Data analysis

The frequency response transfer function (FRF) of the "human controller" was generated both for the experimental data, derived during the experiments, and the simulated data derived for the three control system models NPC, PC, IC. That was achieved by obtaining the closed loop frequency response transfer function (FRF) relating the disturbance $d(t)$ ("input signal") to the control signal $u(t)$ ("output signal"). The FRF of the closed-loop system is dependent on both the dynamics of the controlled system and the dynamics of the "human controller" respectively. The a-priori knowledge of the dynamics of the system means that the dynamics of the "human controller" can be derived from the closed-loop FRF. Therefore frequency domain analysis ([111], Ch.2) between the excitation signal $d(t)$ and the control

signal $u(t)$ was applied in this study. The time domain signals $u(t_n)$ and $d(t_n)$ were tranformed in frequency domain using the Discrete Fourier Transform (DFT) algoritm. All experimental and simulated time domain data $u(t_n)$ and $d(t_n)$ were analysed with period

$$T_p = n_p T_0 \tag{3.63}$$

where $n_p \in \mathbb{N}$ is a multiple of the disturbance period, and T_0 is given by equation (3.62). Therefore, the resolution of the discrete frequency components ω_k which results for period T_p of analysis is equal to

$$\omega_k^0 = 2\pi/T_p = \omega_0/n_p \tag{3.64}$$

The sampled time signals $u(t_n), d(t_n)$ were transformed into frequency domain using the DFT ([111], Ch.2) and are equal respectively to

$$U(j\omega_k) = \sum_{n=0}^{N-1} u(t_n) e^{-j2\pi n \frac{k}{N}} \tag{3.65}$$

$$D(j\omega_k) = \sum_{n=0}^{N-1} d(t_n) e^{-j2\pi n \frac{k}{N}} \quad \text{with} \quad \omega_k = k\omega_k^0 \tag{3.66}$$

where ω_k is the k^{th} discrete frequency and $k = 1, 2, ..., N$, with $N = T_p/T_s$ the number of sample points over one period, T_p (equation (3.63)) and is equivalent to the frequency components obtained by the DFT. Note that due to symmetry, only the first N/2 frequency components need to be considered.

The N_e frequencies at which the disturbance signal has a frequency component (equation(3.66)) are denoted as excited frequencies

$$\omega_e = \omega_k \quad \text{if} \quad |D(j\omega_k)| > 0 \quad \text{with} \quad k = 1, 2, ..., N/2 \tag{3.67}$$

The remaining $N_n = N/2 - N_e$ frequencies are the non-excited frequencies,

$$\omega_n = \omega_k \quad \text{if} \quad |D(j\omega_k)| = 0 \quad \text{with} \quad k = 1, 2, ..., N/2 \tag{3.68}$$

If a sequence of data with total duration T_t is analysed, then this consists of $n_0 = T_t/T_0$ periods of the disturbance input signal $d(t)$ (for $n_p = 1$) and for $n_p > 1$

$$n_a = T_t/T_p \quad \text{periods} \tag{3.69}$$

For the experimental data the DFT signals for the l^{th} period can be denoted as $D^{[l]}(j\omega_k)$ and $U^{[l]}(j\omega_k)$ respectively. Although the disturbance signal will be the same for each period, the output signal will be generally different from period to period if non-linearities or noise are present.

Figure 3.11a presents the disturbance signal $d(t)$ that was applied both in the experimental procedure and the simulations using the three artificial control sytems, non-predictive control, predictive control and intermittent control. Figure 3.11b depicts a representation of the control signal $u(t)$ that was generated for one participant.

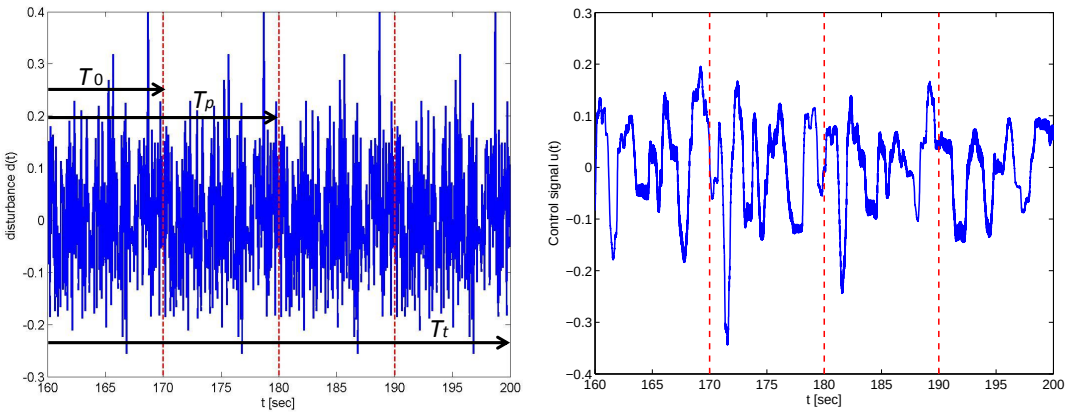

(a) Disturbance signal applied in the experimental task and simulations.

(b) Control signal that was derived from one participant during the experimental procedure

Figure 3.11: Examples of the multisine disturbance signal that was applied both in the experimental procedure and the simulations using the three artificial controllers, NPC, PC and IC. Also the figure depicts an example of the control signal that was derived from one participant during the experimental task. a) Depicts the disturbance signal $d(t)$ that was applied during the experimental task and simulations. In the figure, T_0 is the period of the disturbance signal, T_p is the period of analysis and T_t is the total duration of the applied disturbance signal. b) Depicts the control signal $u(t)$ that was generated by a participant during the experimental procedure. The vertical lines indicate periods of 10 sec.

Figure 3.12a depicts the disturbance signal $D(j\omega_k)$, in frequency domain for one period l whereas Figure 3.12b depicts the control signal $U(j\omega_k)$ in frequency domain

that was generated for a participant during the experimental task. Figure 3.12b shows that the signal includes components both at the excited ω_e (equation (3.67)) and non-excited frequencies ω_n (equation (3.68)) due to the inherent human variability. Although the disturbance signal will be the same for each period, the output control signal will be generally different from period to period if non-linearities, variability, or noise are present.

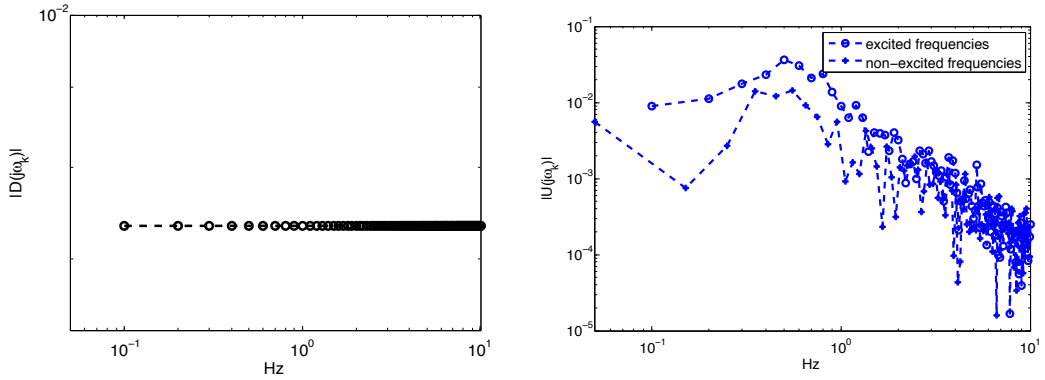

(a) $|D(j\omega_k)|$ (b) $|U(j\omega_k)|$

Figure 3.12: Disturbance and control signals derived from one subject in frequency domain. a) Illustrates the disturbance signal that was applied during the experimental task and simulation. b) Illustrates the control signal $|U(j\omega_k)|$. The control signal is shown to include components both in excited ω_e (continuous blue line) and non-excited frequencies ω_n (dotted blue line).

3.4.2 Analysis at excited frequencies

For the experimental data, in the case where $n_p = 1$ the DFT for the l^{th} period of the signals $d(t)$ and $u(t)$ at excited frequencies over one period T_p is given by equations (3.66) and (3.65) with $\omega_k = \omega_e$ (equation (3.67)). The DFT estimated disturbance and control signals for each experimental data over the n_a periods (equation (3.69)) are given by

$$D(j\omega_e) = \frac{1}{n_a}\sum_{l=1}^{n_a} D^{[l]}(j\omega_e) \tag{3.70}$$

$$U(j\omega_e) = \frac{1}{n_a}\sum_{l=1}^{n_a} U^{[l]}(j\omega_e) \tag{3.71}$$

The frequency response transfer function FRF for each participant s for one period l can be estimated as

$$T^{[l]}(j\omega_e) = \frac{U_s^{[l]}(j\omega_e)}{D_s^{[l]}(j\omega_e)} \quad \text{with,} \quad e = 1, 2, ..., N_e, \ \textbf{and}, \ s = 1, 2, ..., 11 \tag{3.72}$$

The mean estimated FRF over all periods n_a(equation (3.69)) for each participant is given by

$$T(j\omega_e) = \frac{1}{n_a}\sum_{l=1}^{n_a} T^{[l]}(j\omega_e) \quad e = 1, 2, ..., N_e \tag{3.73}$$

3.4.3 Analysis both at excited and non-excited frequencies

In the case where $n_p > 1$ the period of analysis T_p (equation (3.63)) is a multiple of the disturbance signal period T_0 with resolution ω_k^0 (equation (3.64)) being a multiple $1/n_p$ times the resolution $\omega_0 = 0.1$ of the disturbance signal applied during the experimental task. Therefore the time domain control signal $u(t_n)$, as expected, would contain power data both at excited, ω_e (equation 3.67)) and non-excited frequencies ω_n (equation (3.68)) frequencies.

For each analysis period T_p and each subject s the power spectra density (PSD), both at the excited ω_e and non-excited ω_n frequencies is defined for each segment l

followed by averaging over all segments.

The PSD for one subject and period segment l at the k^{th} frequency is given by

$$S^{[l]}(j\omega_k) = \frac{1}{\omega_k^0}|U^{[l]}(j\omega_k)|^2 \tag{3.74}$$

The estimated PSD for one subject averaging over all segments is given by

$$S(j\omega_k) = \frac{1}{n_a}\sum_{l=1}^{n_a} S^{[l]}(j\omega_k) \tag{3.75}$$

The frequency ω_k is the k^{th} frequency which can be either excited (equation (3.67)) or non-excited (equation (3.68)).

3.5 Chapter Summary

This chapter described analytically the materias and methods that were used for this study. Firstly, the three artificial controller models NPC, PC, IC were described both graphically and in state-space form. Secondly, the system model was also presented including a graphical representation. Thirdly, the frequency domain analysis that was used for both the experimental and simulated data has also been presented.

Chapter 4

Frequency domain identification of the human controller

4.1 Introduction

A robust method to identify physiological mechanisms is either to fit human experimental data into artificial control models or emulate these mechanisms using artificial models. In motor control area, two broad classes of methods to identify the mechanisms that describe physiological systems can be distinguished: an analytic examination of the physiological mechanism which includes a detailed analysis of suitable averaged small sections of data [115] and the more engineering approach of system identification [10, 11].

System identification builds accurate models of complex systems from noisy data. It has of three steps: 1. the design of an experiment 2. the construction of a model, black box or from physical laws and 3. the estimation of the model parameters from the measurements. Studies on computational modelling of the physiological mechanism of human upright balance control have used various identification methods, in either the time or frequency domain. Maurer and Peterka [12] have tuned the three gain parameters and the time delay of a PID control algorithm to simulate spontaneous sway during postural control. Identification from unperturbed simulated data has been applied using a single-link inverted pendulum with human dynamics as the system

model. The same linear controller model, PID, has been tuned to reproduce stimulus-response data from postural control tasks in which either the support surface has pseudo-randomly rotated [11] or translated using a three-link inverted pendulum with human dynamics as the system model [13, 15]. In addition a system identification approach has been applied to fit a third order linear model, which describes the human balance mechanism, to experimental data taken from a postural control task using either somatosensory stimuli such that of visual display motion or touch surface [122], or vibration stimuli [10]. Also, system identification methods have been applied to fit artificial linear models that emulate human arm dynamics to perturbed experimental data. For servomechanisms, PID has been shown many times to fit the data quite well. On the other hand, the predictive control model of Kleinman [53] has been shown to fit experimental data from a range of experimental conditions well. Kleinman et al. [18] and Baron et al. [19] have shown that this model explained many features of the human operator performing man-machine compensatory tracking tasks including the general features of the error signals, called remnant [8]. In addition, an earlier paper Gawthrop et al. [25] used time-domain identification and random non-periodic signals to compare the abilities of the predictive and non-predictive controller models to fit experimental data obtained from a compensatory tracking task which emulated human quiet balance. The results have revealed that both optimised controllers fit the data well; however, only the identified predictive controller resulted in values for the identified time delays which were physiologically meaningful.

One advantage using frequency domain identification methods is that they save on computational time. Usually time domain identification involves identifying models which are comprised by some thousands of time domain points. On the other hand, frequency domain identification usually deals with hundreds of frequency components, therefore computational time is saved when using frequency domain identification. Another advantage of frequency domain is the possibility to extract valuable information about the bandwidth of the system or the controller. Especially in man-machine systems or in physiological systems. in which the human is considered the operator, knowledge of the controller's bandwidth assists in the important understanding of the range of frequencies in which the human can follow an input

signal. With knowledge of the human bandwidth, machines can be designed to reflect human operator characteristics.

For system identification in the frequency domain, Pintelon and Schoukens ([111], Ch.2) and Pintelon et al. [123] have suggested a two stage identification method. In the first stage the non-parametric frequency response transfer function (FRF) is estimated from the experimental data and in the second stage a parametric frequency response transfer function, derived from the parametric models, is fitted to the non-parametric FRF using a non-linear optimisation. This method has been used by Peterka [11] to identify a computational model that describes human postural balance. In the study the gain parameters and the time delay of an artificial PID controller were optimised, using the two stage identification method of Pintelon and Schoukens ([111], Ch.2).

Identification of physiological control systems have been applied to both unperturbed [12, 124] or perturbed [11, 13, 15, 25] measured data. However, the identification from unperturbed measured data leads to erroneous identification results. It is rather true that physiological mechanisms, for instance human quiet stance, are closed loop systems therefore the "human controller" is embedded within the closed-loop system and the control signal applied by the "human controller" is dependent and varies according to the system output. Identification of these systems using unperturbed data treats the mechanism as a system in which the control signal derived from the "human controller" is independent from the system response therefore the dynamics of both the "human controller" and the system are generated by an open-loop system without considering feedback. Therefore, there is a need to estimate excitation models from the identification methods which do not lead to ambiguous results. These problems are avoided by using external measured perturbation signals to systems and by identifying the entire closed-loop dynamics [61]. The identification of the physiological systems using measured data from perturbations treats the system as a closed-loop system in which the closed-loop relation between the excitation signal and the system response or control signal includes the dynamics of the both the controller and system.

According to Pintelon and Schoukens ([111], Ch.4) the advantage of using band-limited continuous periodic signals as excitation signals, in identification methods, is that leakage errors are avoided. Also these signals excite the frequency band of interest

unlike to binary periodic signals (eg. PRBS) which excite the system at frequencies outside the frequency band. Especially, the importance of using a continuous excitation signal in the identification methods of physiological systems and especially to that of quiet standing has been discussed by Peterka [11]. Peterka suggests that for the identification of quiet balance control it is more appropriate to use continuous perturbations since human balance is a continuous process. On the other hand, using transient stimuli (e,g sudden support surface motions) is not natural process and therefore it may trigger motor programs which are not processes of human balance.

The aim of the work presented in this chapter was to investigate whether or not the IC controller could describe the deterministic part of the experimental data derived from the sustained visual manual compensatory tracking task (Sect. 3.3) which emulates human quiet balance. The IC controller was compared against the well know NPC and PC controllers [18,53]. The two-stage frequency domain system identification method of Pintelon and Schoukens ([111], Ch.2) was applied in the study. In the first stage the non-parametric FRFs were calculated from the perturbed input/output experimental data. In the second stage the non parametric FRFs of the artificial models were fitted to the parametric FRFs using non-linear optimisation.

The intermittent controller as it has been mentioned combines aspects of continuous-time and discrete time control therefore the frequency domain representation of the IC controller could be difficult. However, the basis function representation of the IC [39] was used to express the controller in sampled-data form with a vector generalised hold. Therefore, Gawthrop [56] represented a frequency domain representation of the IC based on the "sensitivity function" approach of Goodwin and Salgado [112]. Hence, the continuous-time sampled-based data IC system was described in the frequency domain.

Section 4.2 describes the closed-loop frequency responses of the three controllers, and the system identification method that was applied in the study. Section 4.4 describes the simulated and experimental data results. Section 4.5 includes the discussion of the chapter and section **??** concludes the chapter. The material presented in this chapter has been published in

1. H. Gollee, A.Mamma, P.J. Gawthrop and I.D.Loram (2011) "Frequency-domain

Identification of Human Balance Control", In Proc. 6th Int. Posture Symposium. Smolenice Castle, Slovakie, 2011, pp. 40

2. H. Gollee, A. Mamma, I. D. Loram and P. J. Gawthrop (2012), "Frequency-domain Identification of the Human Controller", Biol Cybern. Vol. $106(6-7)$, pp. $359-372$.

4.2 Materials and Methods

This section presents analytically the materials and methods that were used for the system identification approach of the human controller. In this section, the state-space representations of the artificial controllers (Sects.3.2.1, 3.2.2, 3.2.3) are presented in Laplace transform, with s denoting the complex Laplace operator ([121] Ch.7).

4.2.1 System and controller frequency responses

The closed-loop transfer function from the disturbance signal $d(t)$ to the control signal $u(t)$ for the two linear continuous-time systems, non-predictive control and predictive control (Figs. 3.1, 3.2) is given by

$$u(s) = -u(s)P(s)H(s)e^{-s\Delta} + d(s)P(s)H(s)e^{-s\Delta} \tag{4.1}$$

$$u(s)(1 + P(s)H(s)e^{-s\Delta}) = d(s)P(s)H(s)e^{-s\Delta} \tag{4.2}$$

$$\frac{u(s)}{d(s)} = \frac{P(s)H(s)e^{-s\Delta}}{1 + P(s)H(s)e^{-s\Delta}} \tag{4.3}$$

where the $P(s)$ represents the dynamics of the system (equation (3.1), (3.2)) given by

$$P(s) = \frac{y(s)}{u(s)} = C(sI - A)^{-1}B \tag{4.4}$$

where I the $n \times n$ unit matrix and $H(s)$ represents the dynamics of the controller with a transfer function given by

$$H(s) = -\frac{u_o(s)}{y(s)} \tag{4.5}$$

The loop gain for each of the linear systems, NPC, PC is given by:

$$L(s) = P(s)H(s)e^{-s\Delta} \tag{4.6}$$

From (equation ((4.3)) and (equation ((4.6)) the closed-loop transfer function is given by:

$$\frac{u(s)}{d(s)} = \frac{L(s)}{1 + L(s)} \tag{4.7}$$

$$\frac{u(s)}{d(s)} = T(s) \tag{4.8}$$

To estimate parametric models, the transfer function $T(s)$ (equation (4.8)) must be derived in terms of the system $P(s)$ and the controller $H(s)$. The system $P(s)$ (equation (4.4)) is exactly known since it describes the dynamics of the virtual inverted pendulum (equation (3.60)). Therefore the aim is to obtain $H(s)$ (equation (4.5)) and the feedback loop delay Δ in order to define parametric representations of the "human controller".

The $H(s)$ representations for the linear controllers NPC, PC are given in the next section.

4.2.2 Non-predictive control

Equations (3.7, 3.10) are transformed in Laplace domain:

$$\hat{x}(s) = (sI - A_o)^{-1}(Bu_o(s) + Ly(s)) \qquad \text{(Observer)} \tag{4.9}$$

$$u_o(s) = -K\hat{x}(s) \qquad \text{(Controller)} \tag{4.10}$$

From equations (4.5,4.9–4.10) the controller transfer function is equal to:

$$H(s) = K\left(sI - A_o + BK\right)^{-1} L \tag{4.11}$$

4.2.3 Predictive control

Equations (3.19, 3.22, 3.23) are transformed in the Laplace domain:

$$\hat{x}(s) = (sI - A_o)^{-1}\left(e^{-s\Delta}Bu_o(s) + Ly(s)\right) \quad \text{(Observer)} \tag{4.12}$$

$$\hat{x}_p(s) = e^{A\Delta}\hat{x}(s) + (sI - A)^{-1}\left(I - e^{-(sI-A)\Delta}\right)Bu_o(s)$$

$$\text{(Predictor)} \tag{4.13}$$

$$u_o(s) = -K\hat{x}_p(s) \qquad \text{(Controller)} \tag{4.14}$$

where I is the $n \times n$ unit matrix.

Equations (4.12)–(4.14) can be rewritten as:

$$u_o(s) = -H_y(s)y(s) - (H_1(s) + H_2(s))u_o(s) \tag{4.15}$$

$$\text{where } H_y(s) = Ke^{A\Delta}\left(sI - A_o\right)^{-1} L \tag{4.16}$$

$$H_1(s) = Ke^{A\Delta}\left(sI - A_o\right)^{-1} Be^{-s\Delta} \tag{4.17}$$

$$\text{and } H_2(s) = K\left(sI - A\right)^{-1}\left(I - e^{-(sI-A)\Delta}\right)B \tag{4.18}$$

From the above equations it follows that the controller transfer function $H(s)$ is given by:

$$H(s) = \frac{H_y(s)}{1 + H_1(s) + H_2(s)} \tag{4.19}$$

4.2.4 Intermittent control

The intermittent controller [42] combines aspects of continuous-time and discrete time control. Therefore as discussed in Gawthrop [56] the frequency domain analysis of the IC is not straightforward as in NPC and PC models. However, Gawthrop and Wang [39] have shown that if the intermittent controller is based on basis-functions, the controller can be reinterpreted in a sampled-based form using a generalised hold, SMH, in this study (Sect. 3.2.4). The use of basis functions and the use of a SMH as

the generalised hold [56] allow the frequency-domain analysis of the IC to be based on extensions of standard sampled-data systems as discussed and explained in Goodwin and Saldago [112]. Below there is an analysis of the IC based on Gawthrop [56] to derive the FRF representation of the controller.

For the delay-free case (i.e $\Delta = 0$) the Fourier Transform of the system (equation (3.1), (3.2)) in frequency domain is given by

$$j\omega X(j\omega) = AX(j\omega) + BU(j\omega) + BD(j\omega) \tag{4.20}$$

$$X(j\omega) = (j\omega I - A)^{-1}BU(j\omega) + (j\omega I - A)^{-1}BD(j\omega) \tag{4.21}$$

$$Y(j\omega) = CX(j\omega) \tag{4.22}$$

where $[(j\omega I - A)^{-1}]B$ is denoted as

$$G(j\omega) = [(j\omega I - A)^{-1}]B \tag{4.23}$$

Therefore from equations (4.21) and (4.23) the Fourier transform of the system (equation (3.1)) could be written as

$$X(j\omega) = G(j\omega)U(j\omega) + X^d(j\omega) \tag{4.24}$$

where

$$X^d(j\omega) = G(j\omega)D(j\omega) \tag{4.25}$$

The Fourier transform of the observer error dynamics (equation (3.25)) is given by

$$j\omega\tilde{X}(j\omega) = A_0\tilde{X}(j\omega) - BD(j\omega) \tag{4.26}$$

$$\tilde{X}(j\omega) = -(j\omega I - A_0)^{-1}BD(j\omega) \tag{4.27}$$

Denoting $[(j\omega I - A_0)^{-1}]B$ as

$$G_0(j\omega) = [(j\omega I - A_0)^{-1}]B \tag{4.28}$$

The Fourier transform of the observe error is finally given by

$$\tilde{X}(j\omega) = -G_0 D(j\omega) \tag{4.29}$$

For the delay-free case where $\Delta = 0$ the Fourier transform of the control signal $u(t)$ (equation (3.3)) is given by

$$U(j\omega) = -K\hat{X}(j\omega) \tag{4.30}$$

Figure 4.1 presents the closed-loop system by combining equations (4.21–4.30)

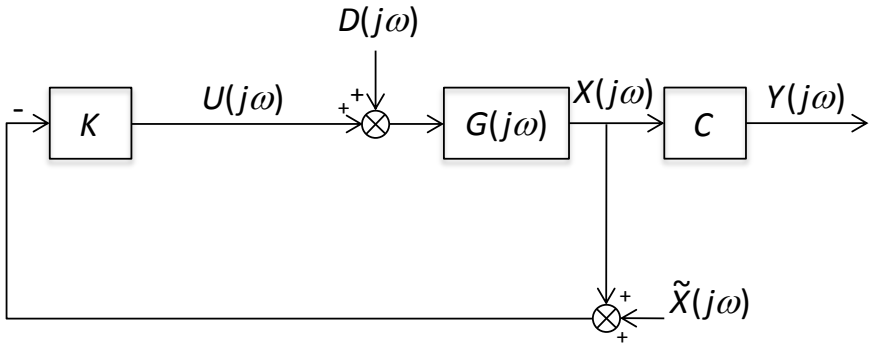

Figure 4.1: Closed-loop representation of the continuous-time control system in frequency domain.

From Figure 4.1 the closed-loop control signal $U(j\omega)$ and the system output $Y(j\omega)$ could be presented as:

$$\begin{aligned} U(j\omega) &= -(1 + KG(j\omega))^{-1} KG(j\omega)D(j\omega) - (1 + KG(j\omega))^{-1} K\tilde{X}(j\omega) && (4.31)\\ &= -KS(j\omega)G(j\omega)D(j\omega) - KS(j\omega)\tilde{X}(j\omega) && (4.32)\\ &= S(j\omega)KX^d(j\omega) - KS(j\omega)\tilde{X}(j\omega) && (4.33)\\ &= -S(j\omega)K(\tilde{X}(j\omega) + X^d(j\omega)) && (4.34)\\ &= -S(j\omega)KX^v(j\omega) && (4.35) \end{aligned}$$

and

$$Y(j\omega) = CG(j\omega)(D(j\omega - KS(j\omega)(X^v(j\omega)) \tag{4.36}$$

where $S(j\omega)$ is the sensitivity function of the closed loop system (Fig.4.1) and is equal to

$$S(j\omega) = \frac{1}{1 + KG(j\omega)} \tag{4.37}$$

$$= (1 + KG(j\omega))^{-1} \tag{4.38}$$

$X^d(j\omega)$ is given by equation (4.25) and X^v is equal to

$$X^v(j\omega) = \tilde{X}(j\omega) + X^d(j\omega) \tag{4.39}$$

Using equations (4.35)-(4.39) the closed-loop system (Fig.4.1) can be presented in open-loop form as shown in Figure 4.2.

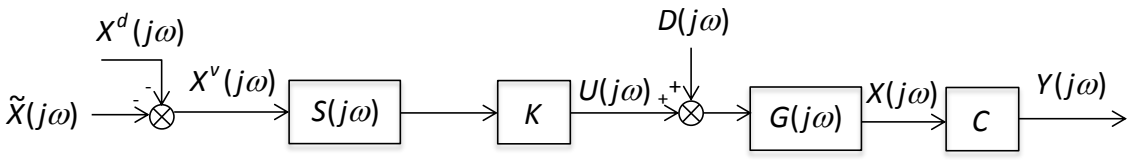

Figure 4.2: Open loop representation of the continuous-time closed loop system (Fig.4.1) represented in frequency domain. The figure describes the modified system where the feedback loop has been transformed using the sensitivity function $S(j\omega)$.

So far the continuous-time IC system with no delay has been analysed and presented in frequency domain. Below there is the analysis of the IC system in discrete-time. Using the forward-shift operator z, ([121] Ch.8) the discrete-time equation for the combined system including the system (equation (3.1)) and the hold dynamics (equation (3.33)) is given below

$$x_{i+1} = A_x x_i + B_x u_i \tag{4.40}$$

where A_x and B_x are the state-matrix and vector matrix of the combined discrete time equation of the system and generalised hold.

The discrete-time form of the dynamics of the system using the forward-shift operator z is given by

$$G_z(z) = [zI - A_x]^{-1} B_x \tag{4.41}$$

In addition, the transfer function of the controller gain is given by

$$K_z(z) = K \tag{4.42}$$

The z-transform of the continuous-time intermittent control $U(j\omega)$ (equation (4.35)) and the sensitivity function $S(j\omega)$ (equation (4.38)) are given below

$$U_z(z) = -K_z(z) S_z(z) X_z^v(z) \tag{4.43}$$

$$S_z(z) = [I + G_z(z) K_z(z)]^{-1} \tag{4.44}$$

The IC controller combines a sampling process which takes place in this study every intermittent interval Δ_{ol} in which the continuous-time observer state $\hat{x}$ is sampled to determine a discrete control signal u_i (equation (3.32)) which is translated to a continuous-time signal using the SMH hold, however, the sampling operation makes it difficult to derive a continuous-time frequency response. As discussed in Goodwin and Salgado [112] and in Gawthrop [56] the process of sampling can be mathematically represented as multiplication by an infinite sequence of impulse functions spaced in time by the constant sampling interval. In this study the sampling interval is periodic and every Δ_{ol}. The sampling sequence can therefore be represented as

$$\Delta_{ol} \sum_{p=-\infty}^{\infty} \delta(t - p\Delta_{ol}) \tag{4.45}$$

where δ is the Dirac delta function.

According to Goodwin and Saldago [112] and Gawthrop [56] the Fourier transform of a continuous-time signal $x(t)$ multiplied by the sampling sequence (equation (4.45)) is expressed as

$$[X(j\omega)]^s = \sum_{p=-\infty}^{\infty} X(j\omega - pj\omega_s), \quad \text{s denotes that the signal is sampled} \tag{4.46}$$

where the sampling frequency ω_s is given by

$$\omega_s = 2\pi f_s \tag{4.47}$$

with

$$f_s = \frac{1}{\Delta_{ol}} \tag{4.48}$$

The continuous-time frequency response corresponding to a discrete-time transfer function in z when the discrete-time input is impulse multiplied is obtained by replacing z with $e^{j\omega\Delta_{ol}}$. Therefore the sampled-based version of the Fourier transform control signal (equation (4.43)) is given by

$$U_z(e^{j\omega}) = K_z(e^{j\omega})S_z(e^{j\omega})[X^v(j\omega)]^s \tag{4.49}$$

where $U_z(e^{j\omega})$ is the Fourier transform of the impulse-multiplied intermittent control u_i and $S_z(e^{j\omega})$ is the sampled-based sensitivity function

$$S_z(e^{j\omega}) = [I + G_z(e^{j\omega})K_z(e^{j\omega})]^{-1} \tag{4.50}$$

The frequency response of the SMH hold including an impulse-modulated input is the series matrix $H(j\omega)$ given by Gawthrop et al. [42] and it is equal to

$$H(j\omega) = \frac{1}{\Delta_{ol}} K^T[j\omega I - A_c]^{-1}[I - e^{-(j\omega I - A_c)\Delta_{ol}}] \tag{4.51}$$

The vector SMH hold $H(j\omega)$ reconstructs the sampled signal u_i which with the disturbance signal $D(j\omega)$ feeds the continuous-time transfer function $G(j\omega)$ (equation (4.23)).

Figure 4.3 shows the sampled-based frequency domain intermittent controller which derives from the discrete and continuous-time equations described above. The sampler $[X^v]^s$ is outside the loop and drives the discrete time controller and the discrete time closed-loop sensitivity function $S_z(e^{j\omega})$ (equation(4.50)). The generalised hold $H(j\omega)$ (equation (4.51)) reconstructs the sampled-based signal to continuous time which together with the disturbance signal and feeds the continuous time transfer function $G(j\omega)$ (equation (4.23)).

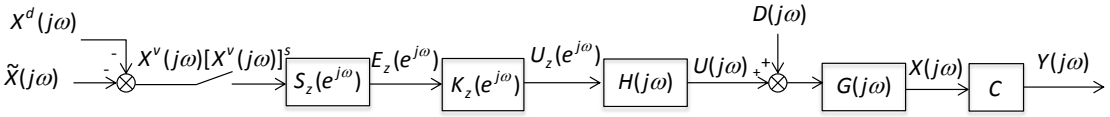

Figure 4.3: The figure describes the open loop system of the combination of the continuous and discrete intermittent control system.

From Figure 4.3 the continuous-time system (equations (3.1)-(3.2)) controlled by an intermittent controller with SMH hold and fixed intermittent interval Δ_{ol} gives a closed-loop system where the Fourier transform of the intermittent control signal $U(j\omega)$ is given in terms of the Fourier transform $X^v(j\omega)$ and is equal to

$$U(j\omega) = F(j\omega, \theta)\,[X^v(j\omega)]^s \tag{4.52}$$

where the FRF transfer function of the intermittent controller is given by

$$F(j\omega) = H(j\omega)K_z(e^{j\omega})S_z(e^{j\omega}) \tag{4.53}$$

where $H(j\omega)$, $K_z(j\omega)$ and $S_z(e^{j\omega})$ are transfer functions which are given by equations ((4.51), (4.42),(4.50)) respectively and $[X^v(j\omega)]^s$ is a sampling process for the signal $X^v(j\omega)$ (equation (4.39)).

The analysis presented in this section is a simplified version of Gawthrop et al. [42] for the special case in which a generalised SMH is used and the intermittent interval is constant (equation (3.30)).

Comments As discussed in Gawthrop et al. [42], the presence of the sampling operator $[X^v(j\omega)]^s$ in equation (4.52) means that the interpretation of the FRF transfer function $F(j\omega)$ (equation (4.53)) is not quite the same as that of the FRF transfer function $T(s)$ of (equation (4.8)). The reason is that the sampling operator $[X^v(j\omega)]^s$ generates an infinite number of intermittent control signals $U_i(j\omega)$ which are identical to each other except that the sampling sequence is different and equal

$$r(t, \Delta_i) = \Delta_{ol} \sum_{p=-\infty}^{\infty} \delta(t - (p\Delta_{ol} - \Delta_i)) \tag{4.54}$$

where

$$0 \leq \Delta_i < \Delta_{ol} \tag{4.55}$$

The above means that although the sample interval Δ_{ol} will be the same for all intermittent control signals $U_i(t)$ the sampling sequence will generate intermittent control signals $U_i(t)$ which will have different sampling delay Δ_i. Gawthrop et al. [42] has shown that $F(j\omega)$ can be treated as the theoretical frequency response transfer function of an average ensemble of closed-loop intermittent controllers and that average ensemble is similar to the equivalent $T(j\omega)$ (equation (4.8)). Therefore the frequency response $U(j\omega)$ (equation (4.52)) of the IC controller will masquerade as a frequency response of a continuous time underlying controller due to the average ensemble of the closed-loop IC.

Below an example of the average ensemble phenomenon is illustrated: The mulitisine periodic signal $d(t)$ (equation (3.61)) excites the unstable second order system (equation (3.60)) at n_k frequencies with $f_k = [0.1, 0.2, ...10]$Hz. The IC controller with fixed intermittent interval $\Delta_{ol} = 0.26$ sec and feedback time delay $\Delta = 0.1$ sec is used to control the system. The sampling frequency therefore is $f_s = \frac{1}{\Delta_{ol}} = 3.8$Hz. To illustrate the ensemble average phenomenon two hundred and sixty ($N = 260$) simulations took place which lasted for $t = 30$sec each one. Each simulation is exactly the same with the exception that the sampling is delayed by a different amount: For example the i^{th} simulation has a delay equal to $0.001i$ with $N_i = 1, 2, ...N = 260$.

For each simulation a control signal $u(t_i)$ is generated. The average control signal $\hat{u}(t)$ is equal to

$$\hat{u}(t) = \frac{1}{N} \sum_{i=1}^{N} u_i(t) \tag{4.56}$$

The input signal is periodic with amplitude $A = 1$ and random phase ϕ_k, therefore the theoretical control signal is given by

$$u(t_n) = \sum_{i=1}^{N_k} |F(j\omega_k)| \cos\left(\omega_k t_n + \angle F(j\omega_k) + \phi_k\right) \tag{4.57}$$

Figure 4.4 shows an example of the control signal that was generated for a number of

simulations (here 50 simulations out of 260) in which the sampling process is delayed by a different amount. The resulted control signals look like typical intermittent control signals (i.e they include the jumps due to the sampling process, (equation (4.51)). The figure also shows the ensemble average control signal (equation (4.56)) depicted against the theoretical control signal in time domain (equation (4.57)). Both time domain signals are similar to each other. The average of the individual elements of the ensemble is smooth and similar to that derived from the theoretical impulse response.

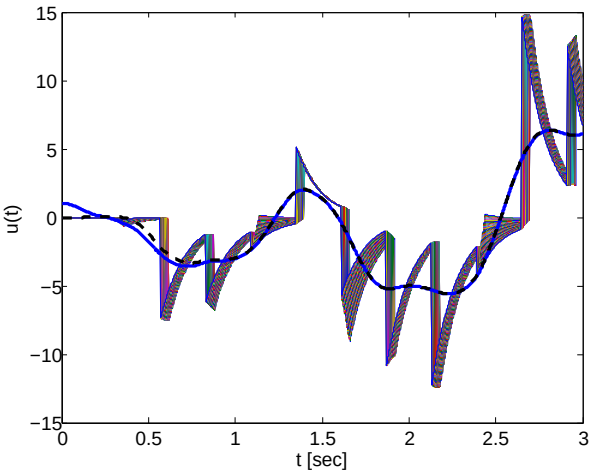

Figure 4.4: Example of the ensemble average phenomenon of the IC. The figure shows an example of the control signals that were generated for different simulations in which the start of the intermittent interval is different in each simulation. The resulting control signal for each simulation looks like a typical intermittent control signal (i.e it includes jumps due to the sampling process. The black dotted line illustrates the ensemble average control signal and the blue continuous line illustrates the theoretical control signal response. The ensemble control signal which results from the average of the individual control signal elements is smooth and similar to that derived from the theoretical impulse response.

Figure 4.5 shows the results in frequency domain. The figure shows the amplitude of the theoretical frequency response $|F|$ against the ensemble average along with the frequency responses derived from the simulations. The theoretical amplitude frequency response is identical to the ensemble average at low frequencies up to 2 Hz.

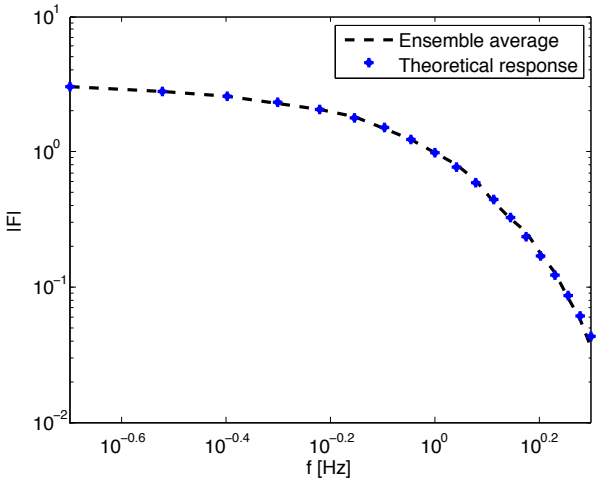

Figure 4.5: The ensemble average of the frequency response $|F(j\omega)|$ (in black) is derived from the individual frequency responses using simulations with different sampling delay. The figure shows that the ensemble average (black dotted lines) is identical to the theoretical frequency response (in blue) for low frequencies up to 2 Hz.

Figure 4.6 illustrates the magnitude of the theoretical frequency response of the IC controller against the magnitude of the frequency response of the PC controller. The figure shows that the theoretical frequency response is very similar to the frequency response derived from the PC controller at low frequencies up to 1.5Hz.

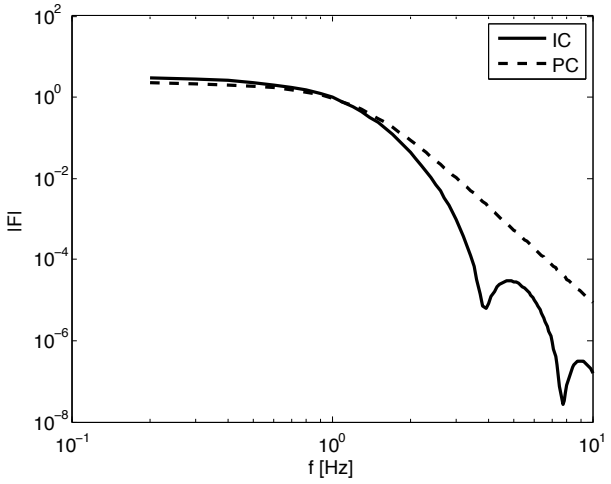

Figure 4.6: Figure illustrates the magnitude of the theoretical frequency response of the IC controller against the magnitude of the frequency response of the PC controller (dotted line). The figure shows that the theoretical frequency response is very similar to the frequency response derived from the PC controller at low frequencies up to 1.5Hz.

4.2.5 System identification

The system identification method that was applied is the two stage approach of Pintelon and Schoukens [111].

1. In the first stage a non-parametric Frequency Response Function (FRF) was estimated based on the measured input/output data.

2. In the second stage, a parametric model of the system was fitted to the estimated FRF using an optimisation procedure.

The next sections describe the two stages that were followed for the identification method.

4.2.6 Non-parametric estimation

The non-parametric FRF is based on the experimental data measurements derived from the sustained control task experiment (Sect.3.3). The FRF relates, in frequency domain, the closed-loop disturbance input signal d to the control signal u and is given by equation (3.72) for each subject s at each period l. The estimate FRF over all periods n_a for each subject is given by $T(j\omega_e)$ (equation (3.73)).

The coherence [111] was also obtained

$$\hat{\gamma}^2_{ud}(j\omega_e) = \frac{\left|\sum_{l=1}^{N_e} U^{[l]}(j\omega_e)D^{[l]}(j\omega_e)\right|^2}{\sum_{l=1}^{N_e}\left|D^{[l]}(j\omega_e)\right|^2 \sum_{l=1}^{N_e}\left|U^{[l]}(j\omega_e)\right|^2} \tag{4.58}$$

The coherence is a measurement of how much of the output power is coherent to the input power at each excited frequency ω_e. When a periodic excitation is used, the coherence is unity in the absence of noise and becomes smaller as noise increases.

4.2.7 Parametric estimation

For each of the control models NPC, PC, IC a parametric FRF $\hat{T}(j\omega_e, \theta)$ which approximates the closed-loop transfer function (equation(4.8)) was determined. For the linear control models NPC and PC the parametric $\hat{T}(j\omega_e, \theta)$ is based on equation (4.7) and is given by

$$\hat{T}(j\omega_e, \theta) = \frac{L(j\omega_e, \theta)}{1 + L(j\omega_e, \theta)} \quad \text{for NPC and PC} \tag{4.59}$$

where $L(j\omega_e, \theta)$ is the system gain (equation(4.6)) and it is parametrised by the vector θ.

For the IC the parametric FRF is based on equation (4.52) and is given by,

$$\hat{T}(j\omega_e, \theta) = F(j\omega_e, \theta), \quad \text{for IC} \tag{4.60}$$

There are many ways to parametrise the controllers. The main issue in the selection of the method is a) the number of parameters to be parametrised with enough freedom to fit the data and b) the stability of the system during the optimisation method. One method could be to parametrise the feedback and observer gains K and L together with the delay Δ and the intermittent interval Δ_{ol} for the case where the IC is used. This method is not only time consuming due to the number of parameters to be parametrised but most importantly it results in a closed-loop system in which stability is not explicitly known. For that reason an indirect method was used and it is described analytically below:

Firstly, the controller and observer gains K, L for each of the controllers NPC,

PC, IC (Sect.3.2.1, 3.2.2, 3.2.2) were designed. There are many ways to design the state feedback K and the observer gain L ([125], Ch.9 [121], Ch.7). For instance the pole-placement method which is based on fixing the eigenvalues of A_c (equation(3.12)) and A_o (equation(3.11)). In this study the standard Liner Quadratic Regulator (LQR) approach was used therefore it allowed the specification of boundaries for the design parameters which guarantee a nominally stable closed-loop system ([125], Ch.6). In the LQR method, the controller gain vector K is chosen in such a way that the control law $u = -Kx$ minimises the cost function

$$J_c(u) = \int_{t_0}^{t_1} (x^T(t)Q_c x(t) + u(t)R_c u(t))dt \tag{4.61}$$

subject to the system dynamics (equation (3.1)). Considering the steady state case $t_1 \to \infty$ for linear systems an algebraic solution (as opposed to finding the minimum of the criterion computationally) exists which uses the algebraic Ricatti equation

$$A^T P + PA - PBR_c^{-1}B^T P + Q_c = 0 \tag{4.62}$$

and the solution to optimisation is

$$K = R_c^{-1}B^T P \tag{4.63}$$

where P is the positive-definite solution of the algebraic Riccati equation (equation (4.62)) ([125], Ch.6).

The feedback gain vector K is then obtained by choosing the elements of the state-weighting matrices Q_c $(n \times n)$ and R_c. Nominal stability can be guaranteed when these matrices are positive symmetric.

The controlled system is a second order system (equation (3.60)) therefore the design of the controller K is based on the choice of the two positive scalars q_c, q_v with the weighting matrices Q_c and R_c given by

$$R_c = 1 \quad Q_c = \begin{bmatrix} q_v & 0 \\ 0 & q_c \end{bmatrix} \quad \text{with} \quad q_c, q_v > 0 \tag{4.64}$$

In the same way, the observer gain vector L is obtained by applying the same

approach to the dual system $[A^T, C^T, B^T, D]$ using the weighting matrices Q_o, R_o ([125], Ch.6). The gain L is designed by choosing the single variable q_o,

$$R_o = 1 \quad Q_o = q_o B B^T \quad \text{with} \quad q_o > 0 \tag{4.65}$$

R_o and Q_o correspond to R_c and Q_c in (equation (4.61)) for the dual system.

Having designed the controller and observer gains K, L for each of the artificial controllers and guaranteeing nominal closed-loop stability, then the controllers were parametrised by the vector θ

$$\theta = [q_v, q_c, q_o, \Delta] \text{ (augmented by } \Delta_{ol} \text{ for IC)} \tag{4.66}$$

A weighted mean squared error criterion J was used to measure the goodness of fit between the estimated FRF and its parametric fit, for each of the control models, and it is given by

$$J_s(\theta) = \frac{1}{N_e} \sum_{e=1}^{N_e} \gamma_e^2 [T(j\omega_e) - \hat{T}(j\omega_e, \theta)]^2 \quad N_e = 100 \tag{4.67}$$

where γ_e^2 is the weighting factor and it was chosen to be the estimated coherence (equation (4.58)). The choice of the estimated coherence as the weighting factor in the optimisation criterion J (equation (4.67)) ensures that frequencies which are contaminated by noise (i.e. for which the coherence is small) contribute less to the criterion. The criterion favoured lower frequency data since $|T(j\omega)|$ tends to be larger in this range, and for experimental data the coherence is smaller at higher frequencies were the noise is large.

The optimisation method followed the study of Gawthrop et al. [25]. The optimised vector θ was separated into two parts:

The time-delay parameters

$$\theta_\Delta = \begin{cases} [\Delta] & \text{for NPC and PC} \\ [\Delta, \Delta_{ol}] & \text{for IC} \end{cases} \tag{4.68}$$

and the controller design parameters

$$\theta_c = [q_v, q_p, q_o] \tag{4.69}$$

such that $\theta = [\theta_\Delta, \theta_c]$.

During the optimisation the time-delay parameters Δ for the NPC and PC and Δ, Δ_{ol} for the IC were varied over a pre-defined range with the restriction that $\Delta_{ol} > \Delta$ [39] and for each given set of time-delay parameters a set of corresponding optimal controller parameters $\theta_c^* = [q_c, q_v, q_o]$ were found to solve the constrained optimisation problem of equation

$$\theta_c^* = \arg\min_{\theta_c} J([\theta_\Delta, \theta_c]), \qquad \theta_c > 0 \tag{4.70}$$

In the identification method the elements θ should only be non-negative values, therefore the sequential quadratic programming (SQP) algorithm as described in [126] was used and it was implemented on the optimisation Toolbox of Matlab (Mathworks, USA) to solve equation (4.70) for each set of θ_Δ (equation (4.68)) for each participant.

The optimal cost function for each set of time-delay parameters, $J^*(\theta_\Delta)$ was calculated and the overall optimum cost function J^* was determined. During the analysis, the time-delay parameters corresponding to the optimal cost were determined, with Δ and Δ_{ol} combined to give the effective time-delay Δ_{eff} for the IC (equation (3.40)),

$$\Delta_{eff} = \begin{cases} \Delta & \text{for NPC and PC} \\ \Delta + 0.5\Delta_{ol} & \text{for IC} \end{cases} \tag{4.71}$$

4.3 System identification using simulations

A preliminary test using simulated data was applied to make sure that the identification method described in Section 4.2.5 was valid. In particular, three sets of simulated data were derived from simulations determined by the three closed-loop systems (Figs.3.1,3.2,3.3). In simulations the system to be controlled was the second-order unstable system (equation (3.60)) and the controller models were the NPC, PC and IC respectively. In all simulations the controller parameters were known a-priori.

The identification method (Sect.4.2.5) was used to identify the simulated data using the parametric models of each of the three control systems.

The controllers parameters that were used for the design of the controllers are described below along with the identification procedure that was applied for the preliminary test.

The design parameters for the controllers NPC, PC, IC were:

$$\Delta = 100\text{ms}, \quad q_v = 1, \quad q_p = 1, \quad q_o = 100 \tag{4.72}$$

with $\Delta_{ol} = 250$ms for the IC. During the simulations simulated data for each of the three closed-loop systems were generated by exciting the system with the disturbance signal $d(t_n)$ (equation (3.61)). The input signal $d(t_n)$ was periodic with amplitude $A_e = 1$ and random phase ϕ_e therefore the resulting control signal, for each control system was obtained as

$$u(t_n) = \sum_{e=1}^{N_e} |T(j\omega_e)| \cos\left(\omega_e t_n + \angle T(j\omega_e) + \phi_e\right) \tag{4.73}$$

Each simulation lasted for 100 sec resulting in $T_p = 10$ (equation (3.63)) periods of simulated data with a sample period $T_s = 0.01$ s.

Following section 4.2.6 the closed-loop frequency response functions, $T(j\omega_e)$ (equation (4.8)), for each control system, was calculated from the input and output simulated data.

During the identification procedure for each of the control systems NPC, PC the time delay Δ was fixed in the range of values $[0, ...400]$ms in steps of 10 ms and for each value a corresponding optimal set of controller design parameters θ_c^* (equation(4.70))

was determined together with the value of the cost function $J^*(\theta_\Delta)$. In addition, for the IC the intermittent interval Δ_{ol} was varied over the same range as Δ and for each value of Δ the intermittent interval which results in the lowest value of the cost function J was chosen and denoted as Δ^*_{ol}.

4.4 Results

4.4.1 System identification analysis results using simulated data

The simulated data (Sect.4.3) were defined according to the controller model structure that was used to generate them. **Simulation data:NPC**, **Simulation data:PC**, **Simulation data:IC** are the data generated from the closed-loop simulations of the NPC, PC and IC respectively (Figs.3.1, 3.2, 3.3).

Figure 4.7 shows a period of 30 sec of the input $d(t)$ and the control signal, $u(t)$ that were generated from the simulation of the closed-loop predictive control system.

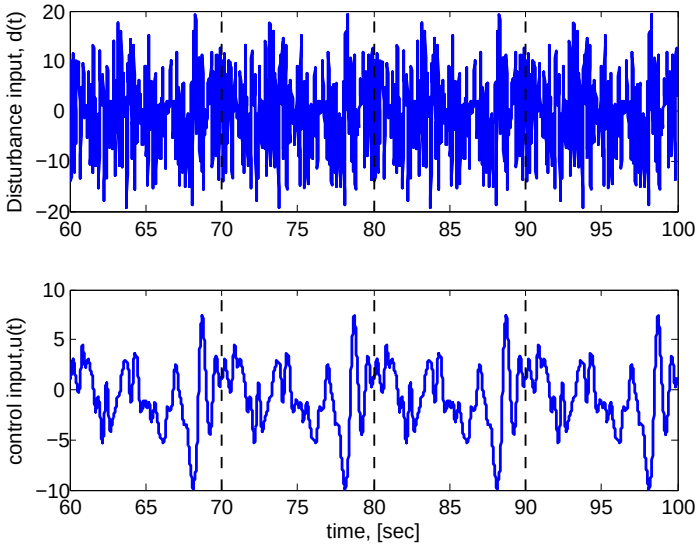

Figure 4.7: Simulated data generated from the PC control system. The vertical lines indicate periods of 10 sec duration. The top plot depicts the input signal $d(t)$ that excited the control system and the figure below depicts the simulated control signal $u(t)$ that was generated using the PC controller. The excited signal was multisine band-limited periodic signal with frequencies from $\omega_e = 0.1, ..10$ Hz and amplitude $A_e = 1$ for each frequency .The simulation lasted for 100sec.

Figure 4.8 depicts the cost function value J as a function of the time-delay Δ for each of the controllers NPC, PC, IC. In each sub-plot the minimum cost value $J^*(\theta_\Delta)$ which was achieved for each controller is indicated, by the bold mark, with the corresponding optimal delay Δ^*. From the sub-plots it is clear that the controllers were identified correctly for each of the simulated data generated by the same controller; a perfect fit was achieved at $\Delta = 100$ms. On the other hand, as expected, there was not a perfect match for each of the other two controller structures. What is important to mention here is that both PC and IC result in an optimal cost $J^*(\theta_\Delta)$ which is quite similar in all three sub-plots, however the NPC has optimal cost function higher that the other two controller structures. This shows that both of controllers PC, IC fitted the simulated data in a similar way, whereas, the NPC is shown to be unable to fit the simulated data satisfactorily. The optimal time delay Δ^* identified by the PC controller structure is shown to be larger than that identified by the IC model in all sub-plots. However, if the effective time-delay Δ_{eff} (equation (4.71)) is considered for the IC then the optimal delays for both controllers PC and IC are very similar for all three cases .

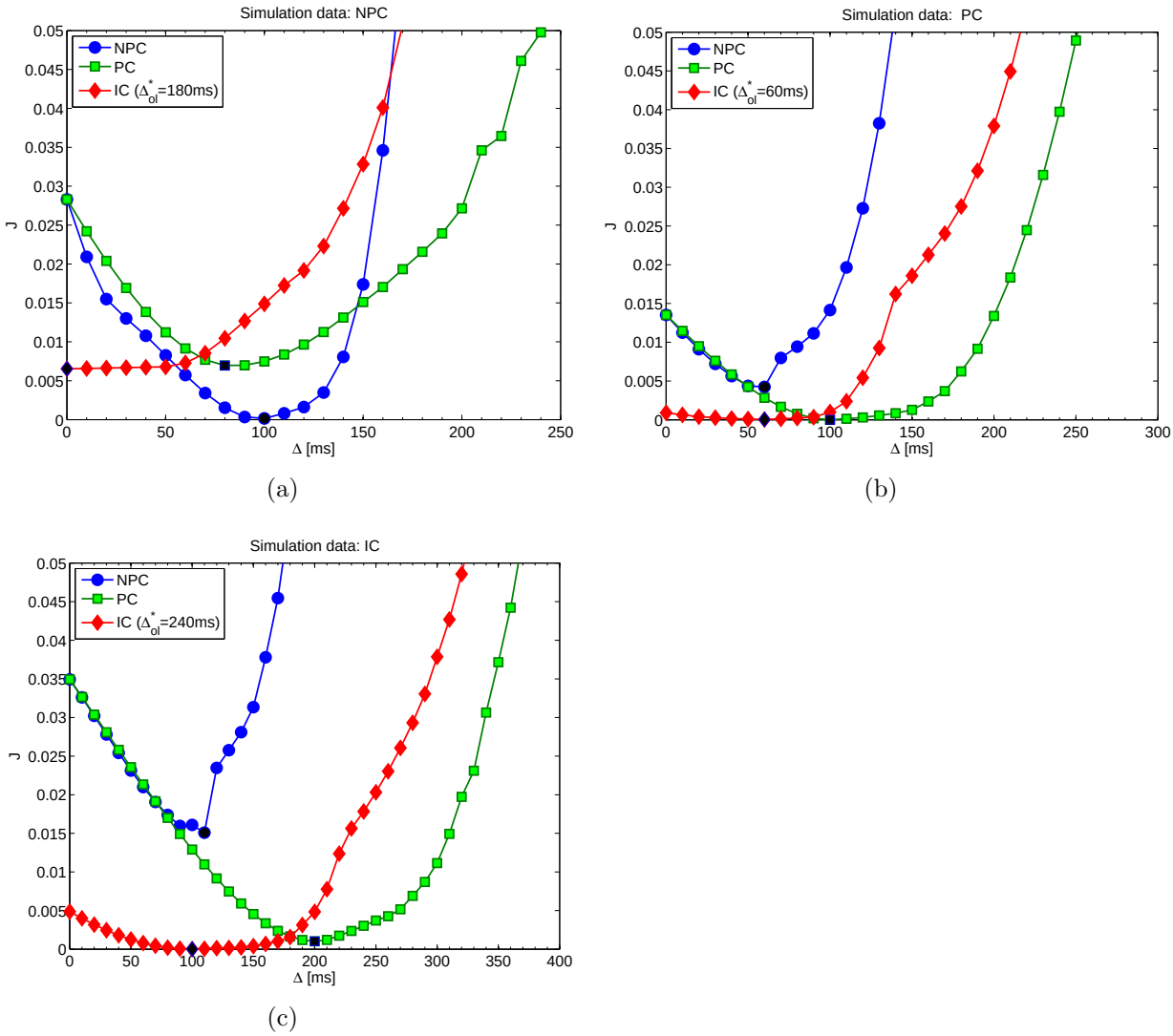

Figure 4.8: Simulated data: Cost function J as a function of the time delay Δ for the NPC, PC, IC controller structures, respectively. The bold marks indicate the minimum cost value $J^*(\theta_\Delta)$ for the corresponding controller structure. The title indicates the simulated data and the legend the controller structure that was identified for each of the simulated data. For the IC, the intermittent interval Δ_{ol}^* is shown in the legend of each sub-figure corresponds to the minimum J. The time delay used to generate the data was $\Delta = 100$ ms for all simulations. The effective optimal delay, for the IC, and for the **Simulation data:NPC** is $\Delta_{eff} = 90$ ms for the **Simulation data:PC** is $\Delta_{eff} = 90$ ms and for the **Simulation data:IC** is $\Delta_{eff} = 220$ ms.

Table 4.1 shows a summary of the optimal time delay Δ^* obtained during the identification procedure for each of the controllers. The table shows that the controllers identified an optimal time delay $\Delta^* = 100$ms for each of the simulated data generated by the same controller. The table also shows that the optimal delay Δ^* identified for the controller PC is always larger than that identified for the IC, however when the Δ_{eff} (equation (4.71)) is calculated then the optimal delays for both controllers PC and IC are very similar for all simulated data. On the other hand, the optimal time delay Δ^* identified by the NPC for the simulated data $2, 3$ is smaller to those identified by the other controllers PC and IC.

Simulated Data	NPC	PC	IC		
	Δ^* (ms)	Δ^* (ms)	Δ^*	Δ_{ol}	Δ_{eff} (ms)
1. Simulation data: NPC	**100**	80	0	180	90
2. Simulation data:PC	60	**100**	60	60	90,
3. Simulation data:IC	110	200	**100**	240	220

Table 4.1: Optimal time-delays Δ^* estimated from simulated data. The table shows that the optimal delay Δ^* for the controller PC is always larger than that identified for the IC, however when the Δ_{eff} is calculated then the optimal delays for both controllers PC and IC are very similar for all three simulated data . On the other hand the optimal time delay Δ^* identified for the NPC is smaller to those identified by the other two controllers for the Simulation data $2, 3$.

Figure 4.9 illustrates the estimated FRFs $T(j\omega_e)$ against the optimised frequency responses $\hat{T}(j\omega_e, \theta^*)$ and for each controller in the complex plane, for each of the simulated data. The results show that the optimised frequency responses resulted using the PC and IC controllers are very similar unlike the frequency responses resulted using the NPC controller it is clearly different. In a similar way Figure 4.10 depicts the impulse responses estimated from the frequency responses. Both Figures 4.9, 4.10 indicate that the PC and IC controllers generate frequency responses and impulse responses that are very similar (almost indistinquishable) to each other whereas the NPC controller structure gives different results.

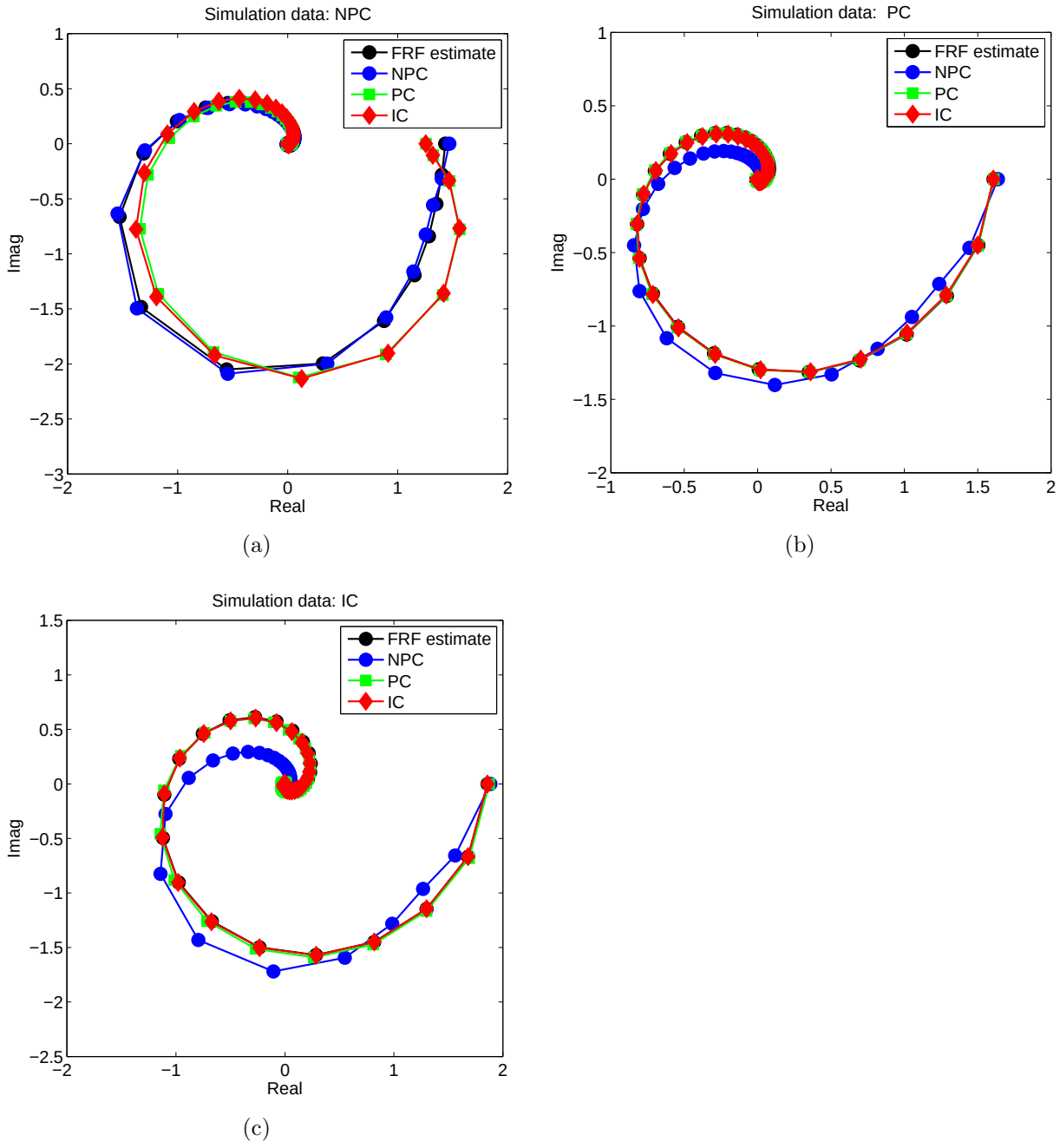

Figure 4.9: Closed-loop Nyquist plots of the estimated frequency responses and the fitted responses for the different controller structures. The black lines denote the estimated frequency response transfer function T. The other lines (blue, green, red) denote the fitted frequency responses $\hat{T}(j\omega_e, \theta^*)$ for the different controller structures NPC, PC, IC. The markers indicate the values at the discrete frequencies ω_e. Sub-plots: (a) correspond to Simulation data:NPC (b) Simulation data:PC and (c) Simulation data:IC.

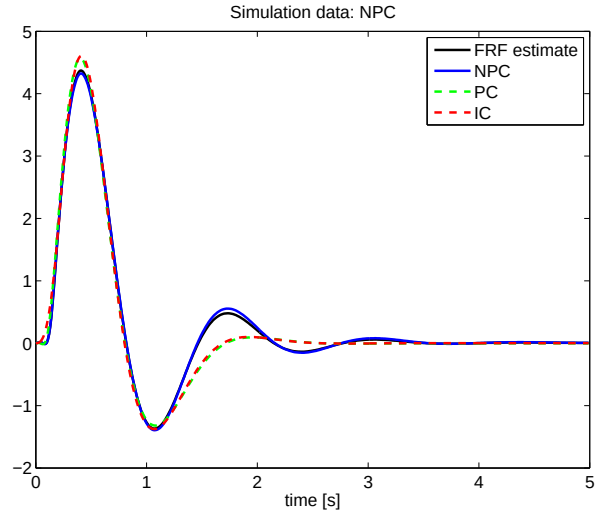

(a)

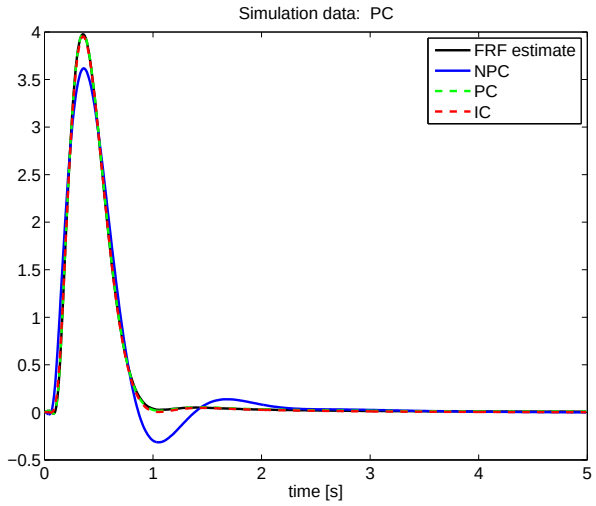

(b)

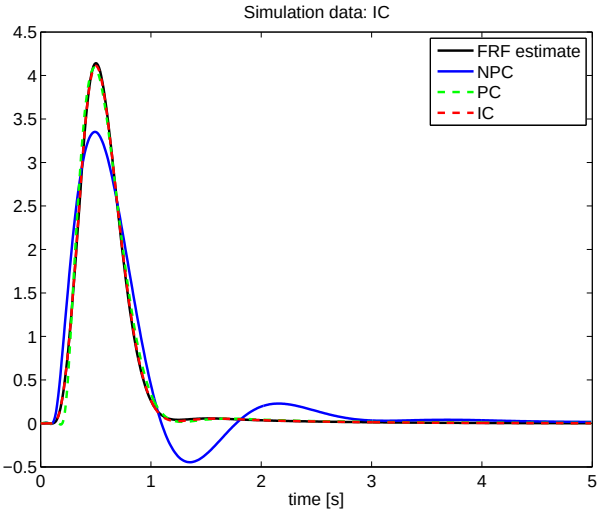

(c)

Figure 4.10: Impulse response plots obtained from the estimated frequency responses and from the fitted responses for the different controller models NPC, PC, IC. The black lines denote the estimated frequency response transfer function T. The other lines (blue, green, red) denote the fitted frequency responses $\hat{T}(j\omega_e, \theta^*)$ for the different controller structures NPC, PC, IC. The markers indicate the values at the discrete frequencies ω_e. Sub-plots : (a) correspond to Simulation data:NPC (b) Simulation data:PC and (c) Simulation data:IC.

4.4.2 Experimental results

The same identification procedure as in section 4.3 was applied using the experimental data derived from the visual-manual compensatory tracking task (Sect. 3.3). For the identification analysis the first two periods of the experimental data were discarded resulting in $n_a = 18$ periods (equation (3.69)). For each data the non-parametric FRF $T(j\omega_e)$ (equation (3.73)) was derived. Figure 4.11 shows a period of 40 sec of the input $d(t)$, the control signals $u(t)$, and the system position signal $y(t)$ that were recorded for one subject (Subject 3) when balancing the system. The vertical lines indicate periods of 10 sec. Figure 4.11a shows the recorded data from the experimental control strategy "minimise position" and Figure 4.11b shows the recorded data from the experimental control strategy "minimise velocity".

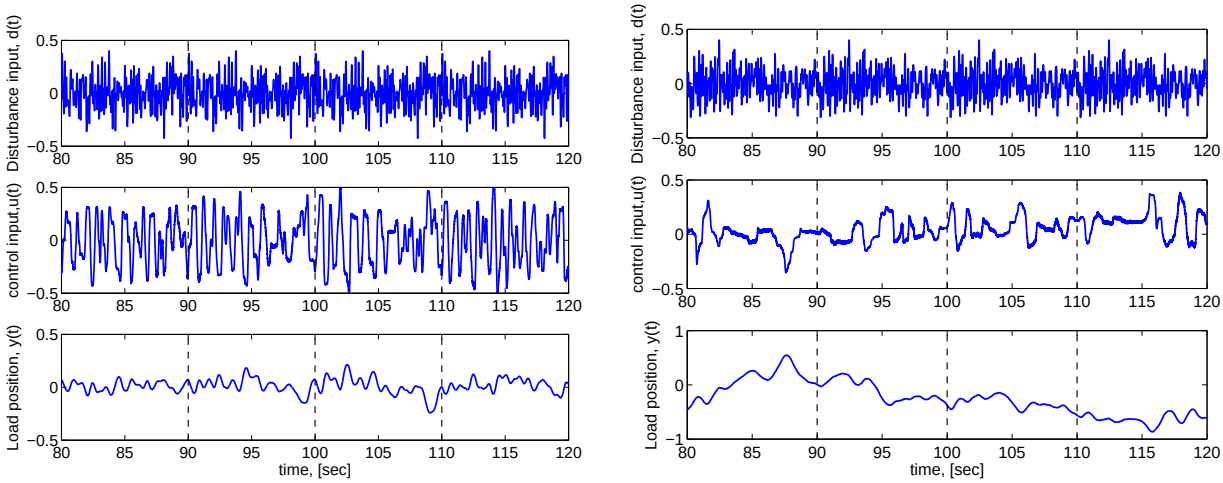

(a) "minimise position" (b) "minimise velocity"

Figure 4.11: Example of the experimental data that were generated during the experimental task, for subject 3. a) Represents raw data for the "minimise position" control strategy and b) depicts raw data generated for the "minimise velocity" control strategy. The vertical dashed lines indicate periods of 10 sec duration. In each sub-figure the top plot depicts the disturbance signal that was applied during the task. The middle plot depicts the control signal $u(t)$generated from the tasks and the bottom plot depicts the system response signal $y(t)$.

Table 4.2 shows the initial controller design parameters for each of the controller structures that were used for the identification study. This values were the controller parameters that were used as the initial parameters for the design of the controllers NPC,PC,IC.

Controller	NPC	PC	IC
q_c	0.1	0.1	0.1
q_v	0.1	0.1	0.1
q_o	0.1	0.1	0.1

Table 4.2: Initial controller parameters that were used for the identification procedure, for each of the controller structures.

Figures 4.12, 4.13 depict detailed results for a representative subject (Subject 3) for data obtained during the experimental control strategies: a) "minimise position" and b) "minimise velocity".

Figure 4.12 illustrates the cost function against the time-delay Δ derived for the subject and for each experimental control strategy :a) "minimise position" and "minimise velocity". Figure 4.12a depicts the results for the "minimise position" control strategy and Figure 4.12b depicts the results for the "minimise velocity" control strategy respectively. Both sub-figures show how the cost function J varies with Δ for all the NPC, PC, IC controller structures respectively where the optimal cost $J^*(\theta_\Delta)$ for each controller structure is depicted as a bold marker. Both sub-figures show that the cost function J, for the NPC controller, increases sharply as the time delay Δ increases. This is due to the fact that the closed-loop tends to be destabilised as the time-delay increases. The reason is that the feedback time delay Δ is not explicitly taken into account when designing the NPC controller. That doesn't appear for the IC and PC controllers. Looking at the results obtained from each experimental data there is always a different optimal time-delay Δ^* that minimises the cost function (equation(4.67)). The optimal cost J^* identified for the PC and IC result in similar values with similar identified effective time delays Δ_{eff} (equation(4.71)). On the other hand, the optimal effective time delays Δ_{eff} identified for the NPC is always smaller than that for the other two controller structures, for every subject and every control strategy either "minimise position" or " minimise velocity".

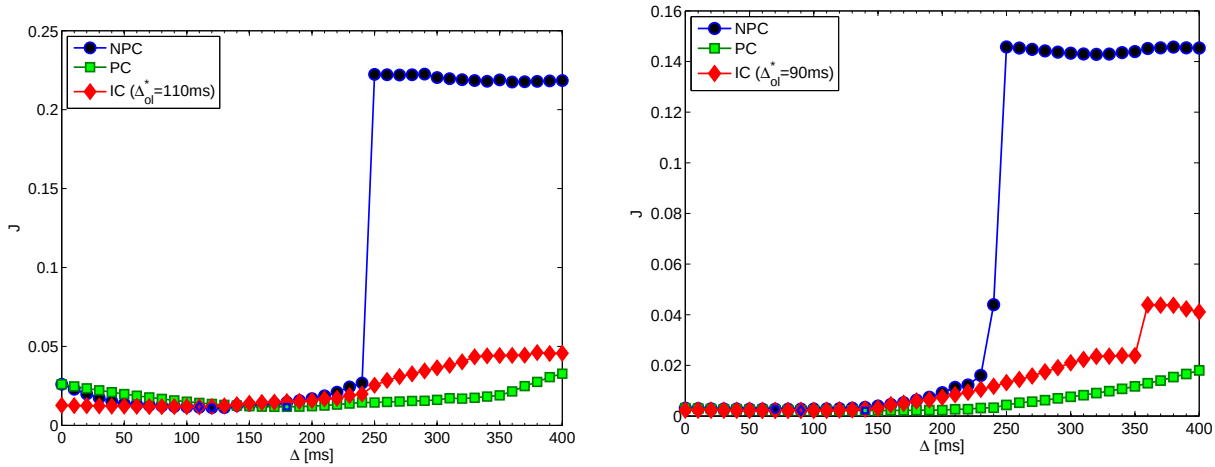

(a) "minimise position" control strategy for subject 3.

(b) "minimise velocity" control strategy for subject 3.

Figure 4.12: Cost function against time-delay resulted for subject 3 and for each of the control strategies "minimise position" and "minimise velocity". a) Represents the results for the "minimise position" control strategy and b) represents the results for the "minimise velocity" control strategy. The figures show the cost functions against the time delay Δ, for every controller structure NPC PC, IC. Blue line indicates the cost function derived from the identification of the NPC, the green line indicates the cost function derived from the identification of the PC and the red line indicated the cost function that derived from the identification using the IC. The bold markers indicate the minimum cost defined from the identification method for the corresponding controller structure. For the IC controller the intermittent interval Δ^*_{ol} corresponding to the minimum of J is given in the legend. Appendix A depicts the results obtained from the rest of the experimental data Figs A.1, A.4.

Figure 4.13 illustrates the closed-loop Nyquist plots of the estimated frequency responses T, for the subject, and the optimised responses $\hat{T}$ for the different controller structures, for each of the control strategies respectively. In both sub-figures the optimised frequency responses derived from the PC and IC controllers are indistinguishable whereas, the NPC controller results in different frequency responses. The graphical closed-loop Nyquist plots, derived using the frequency response functions, are confirmed from the impulse responses shown in Figure 4.14. The impulse responses obtained from the PC and IC are similar to each other for each of the control strategies. Also, the impulse responses identified from the PC and IC are closed to the estimated ones without excluding the impulse response derived from the NPC.

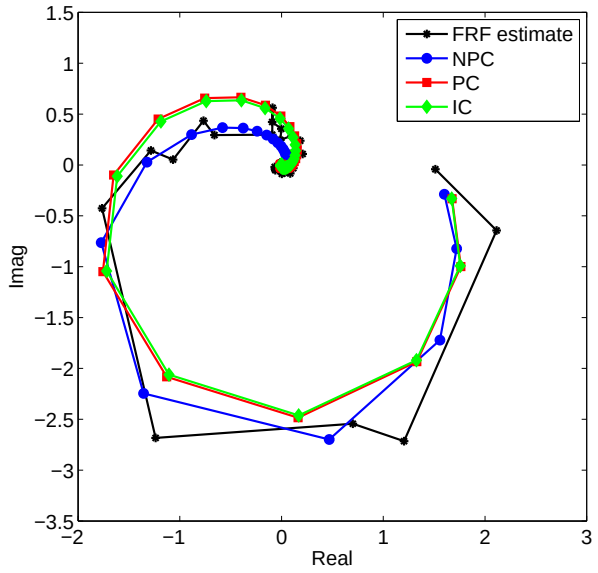

(a) "minimise position" control strategy for subject 3.

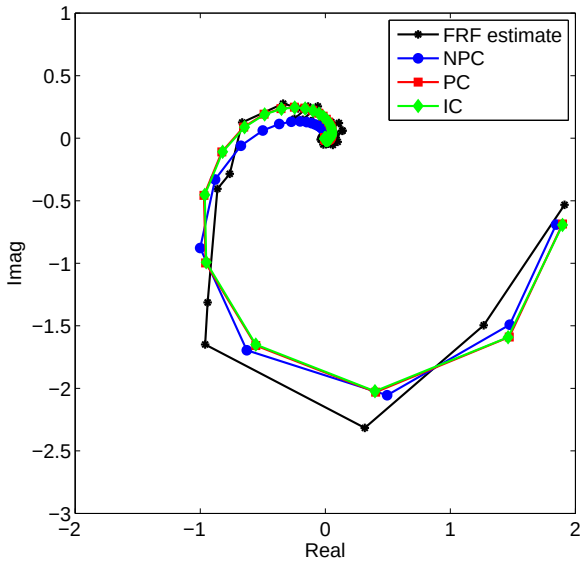

(b) "minimise velocity" control strategy for subject 3.

Figure 4.13: Closed-loop Nyquist plots of the estimated frequency responses T, for the subject, against the optimised responses $\hat{T}$ for the different controller structures, for each of the control strategies respectively. a) Represents the results for the "minimise position" control strategy and b) represents the results for the "minimise velocity" control strategy. In both sub-figures the optimised frequency responses derived from the PC and IC controllers are indistinguishable whereas, the NPC controller results in different frequency responses. Appendix A depicts the results obtained from the rest of the experimental data Figs A.2, A.5.

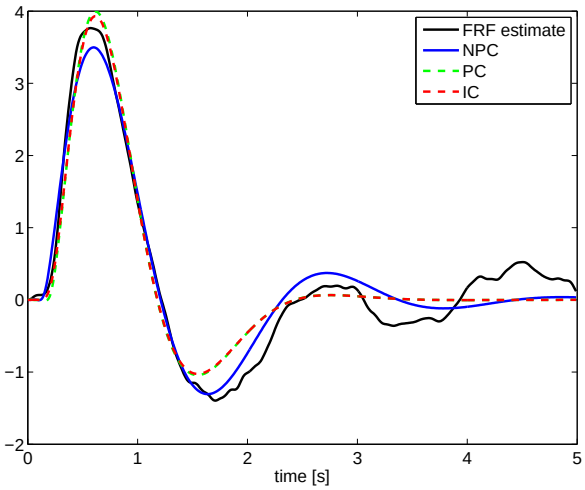

(a) "minimise position" control strategy for subject 3.

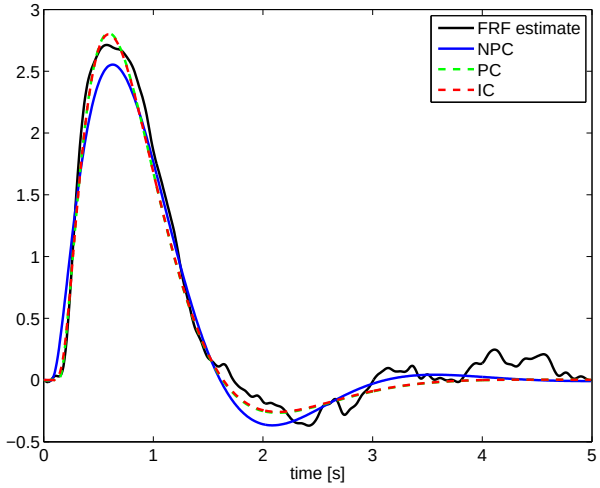

(b) "minimise velocty" control strategy for subject 3.

Figure 4.14: Impulse responses plots obtained from the estimated frequency responses (black line) and from the fitted responses for the different controller structures (coloured lines).Appendix A depicts the results obtained from the rest of the experimental data (Fig.A.3)

Figure 4.15 depicts the best values $J(\theta^*)$ obtained from the three controller structures for each of the participants and control strategies. The horizontal lines show the mean values of the best fit for each controller. The figures show that for both control strategies the IC and PC controllers result in a closed-loop which fit the experimental data in a similar way (The horizontal lines which correspond to the PC and IC controller results are very similar). On the other hand, the NPC controller result in closed-loop fit values which are slightly worse that the other two controllers.

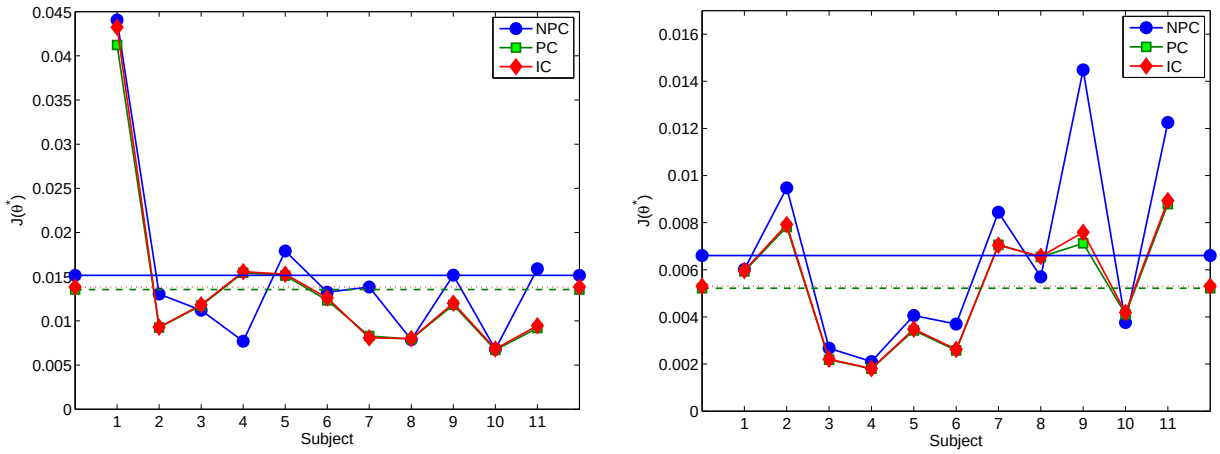

(a) "minimise position" control strategy (b) "minimise velocity" control strategy

Figure 4.15: Optimal fit values $J(\theta^*)$ for each subject. The horizontal lines show the mean value over all subjects for each control model.

Figure 4.16 shows the effective time delays Δ_{eff} which correspond to the best fit values for each the control strategies. The figures show that the optimal Δ_{eff} obtained for each of the PC and IC controller are similar to each other for both control strategies, whereas the NPC gives different optimal delays Δ_{eff} which are always smaller than that obtained from the other two controllers. Comparing the mean effective time delays which are denoted by the horizontal lines is seems that the mean Δ_{eff} obtained from the " minimise position" control strategy (Fig.4.16a) is smaller than that obtained from the "minimise velocity" control strategy (Fig. 4.16b).

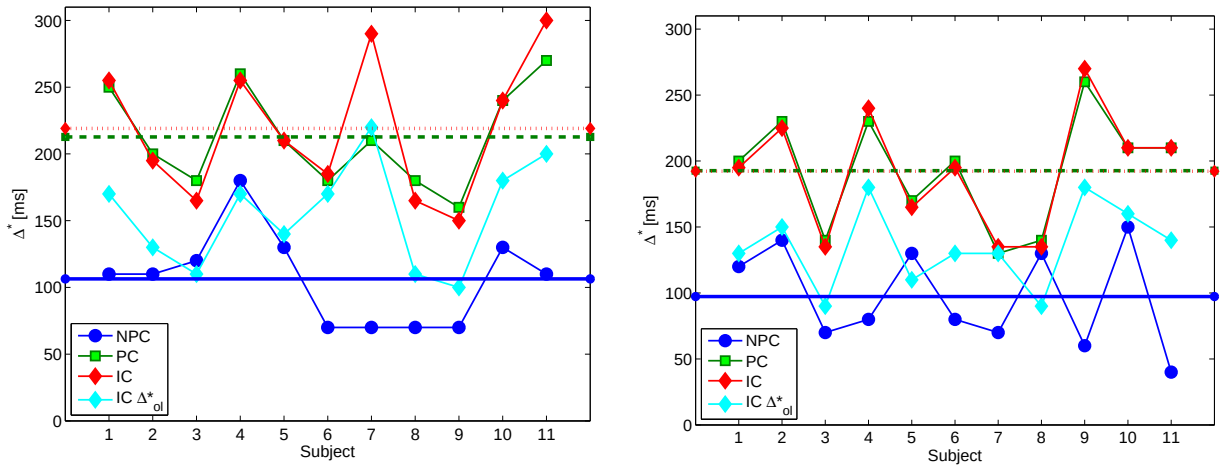

(a) "minimise position" control strategy

(b) "minimise velocity " control strategy

Figure 4.16: Optimal fit value Δ^* for each subject. The horizontal lines show the mean value over all subjects for each control model. The blue line indicates the results obtained from the NPC, the green line for the PC and the red line for the IC.

Tables 4.3, 4.4 summarise the optimal parameters values obtained for all subjects and for all three controller structures. The standard deviations are very large. However, that reflects the significant inter-subject variability, the subjects do not correspond in the same way in compensatory tracking tasks, therefore there is variability between them. If we compare the tables we see that the controller design parameter q_c is larger for "minimise position" control strategy (Table 4.3) than for the "minimise velocity" control strategy (Table 4.4). The controller design q_v is smaller for "minimise position " (Table 4.3) than for the "minimise velocity" (Table 4.4). The controller parameters q_c, q_v correspond to the weighted parameters of the matrix Q_c and therefore correspond to the weight associated with position and velocity control states respectively. The values of the optimised parameters reflect the control strategy adopted by each subject. That means that for the "minimise position" control strategy a larger weight is put on the position state while for the "minimise velocity" control strategy a larger weight is associated with the velocity state. The q_0 observer parameter appears to be unrelated to the control strategy. In addition the effective delay Δ_{eff} is slightly smaller for "minimise velocity" control strategy than for "minimise position" control strategy and the intermittent interval Δ_{ol} is slightly smaller for the velocity control than for position control task as it was shown in previous figures.

Ctr	NPC	PC	IC
q_c	9.0 ± 15.2	42.4 ± 63.4	51.1 ± 82.3
q_v	0.6 ± 1.1	0.4 ± 1.0	0.8 ± 2.1
q_o	136.2 ± 206.2	92.4 ± 168.3	470.9 ± 983.9
Δ_{eff}	106 ± 35	213 ± 37	219 ± 52
Δ_{ol}	–	–	155 ± 39

Table 4.3: Optimised parameters (mean ± standard deviation) for the "minimise position" control task

Controller	NPC	PC	IC
q_c	2.1 ± 4.3	13.1 ± 12.4	51.9 ± 16.1
q_v	0.8 ± 0.8	5.3 ± 12.0	6.7 ± 14.8
q_o	13.5 ± 22.5	275.4 ± 614.6	409.4 ± 984.7
Δ_{eff}	97 ± 37	193 ± 42	192 ± 45
Δ_{ol}	–	–	135 ± 31

Table 4.4: Optimised parameters (mean ± standard deviation for the "minimise velocity" control task

4.5 Discussion

The identification method was initially applied to simulated data derived from closed-loop simulations using each of the controller models NPC, PC, IC respectively to determine the efficacy of the system identification method. For each of the three sets of closed-loop simulation data the corresponding controller used for the design could perfectly be identified using the identification method of the study. Therefore, the method was found to be robust since there was always a clear minimum cost J (Fig.4.8) that corresponded to an optimal time delay Δ^*. On the other hand as was expected there was not a perfect match for the rest of the controller identifications. It is important to say that the identified parameters for the NPC controller were very different to those derived from the identification using PC and IC (Table 4.1). The NPC in all cases resulted in identified Δ^* parameters that were very different to that of the PC and IC. On the other hand, both the IC and PC resulted in similar identified parameters.

The same identification method was applied to experimental data. From the shape of the cost function the optimal cost J^* for all experimental data is distinguishable

(Figs. A.1, A.4), there is a clear minimum cost depicted in each plot for each experimental data and each control task. However, for the NPC there is always a jump which is due to the instability which occurs due to the delay in the closed loop system.

The consistency of the best fit J^* for all the eleven subjects for each of the control tasks (Fig. 4.16) clearly shows that the system identification method that was applied in the study is robust even when biological data are used, which is known to be noisy, non-linear and with high inter-subject variability. In addition the identification of the controllers PC and IC resulted in similar minimum costs J^* for all subjects (Fig. 4.15). However, it is important to note here that the optimisation using the NPC model was found to be problematic due to the unstable closed-loop system associated with some parameter values. This problem did not occur in the cases where a PC and IC were used.

Tables 4.3 and 4.4 show that the identified controller models reflect the control task conditions. For instance, for the "minimise position" control task the identified weighting factor q_c, which is associated with the position state, is larger than the identified q_v . For the "minimise velocity" control task the identified weighting factor q_v which corresponds to the velocity state is larger than the identified q_c. This shows that the identified parameters reflect the control strategy adopted by each subject during the tracking task [28].

The identified parametric FRFs fit the non-parametric FRFs in the complex plane in the same way (Figs.A.2, A.5). The identified FRF for the NPC model fit is not dissimilar to the other two controller models PC, IC. Only marginally favours the PC and IC. This is also confirmed from the impulse responses (Figs. A.3, A.6). This is not a surprise as other identification analysis studies using a NPC (eg. a PID) controller have shown to fit physiological data from a postural control tasks [11, 24]. Although the identified NPC fits the experimental data well the optimal delay Δ^*_{eff} (equation (4.71)) is consistently less that the optimal Δ^*_{eff} obtained for the other two controller model (Fig.4.16) for each subject. The same phenomenon was found for the simulated data.

Only the PC and IC resulted in optimal time delays Δ^*_{eff} which are in agreement

with the studies of Loram et al. [24,28]. Loram et al. [28] using the closed-loop impulse response functions relating disturbance to joystick signal (control signal) generated from the experimental data for the second order system with 85% stability found that the mean feedback time delay for the second order controlled system is 210 ± 30 ms for both control tasks "minimise position" or "minimise velocity". Table 4.3 shows that the identified Δ_{eff} for the PC and IC are in agreement with the feedback time delays derived in Loram et al. [28] except for the NPC controller model where the mean identified time delays Δ_{eff} is much smaller. This was also found in the time-domain identification method applied by Gawthrop et al. [25]. The optimal time delay identified by the NPC was smaller than that found from the experimental task. The above not only confirms the robustness of the identification method that was applied in the present study but also shows that the NPC results in time delay estimates which are consistently underestimated. The NPC model could not be considered a suitable model to describe physiological systems.

The identified closed-loop FRFs for both the PC and IC fit the estimated non-parametric FRFs in a very similar way, almost identically in most cases (Figs.A.2, A.5). In addition the identified time delays Δ_{eff} for the PC and IC (Figs. 4.16) for both control tasks are similar to each other for each of the experimental data. This indicates that the experimental data can be equally well explained using either the continuous-time PC or the intermittent control hypothesis [42]. The main reason for this is the masquerading property of the the IC [42]. The example in Section 4.2.4 has shown that the frequency response of the intermittent controller is almost indistinguishable to that of the corresponding predictive controller at lower frequencies and only diverges at higher frequencies.

It is essential to discuss the importance of local minima during the identification method procedure. In general, the choice of initial conditions may influence the identified parameters since the identification procedure may lead to a local minimum. In this study, we found that the identified parameters did not depend on the values of the initial condition, i.e. that the identification generally found the global minimum. For this reason, the initial parameter values were kept constant for the optimisations reported here.

4.6 Conclusions

The conclusions derived from the system identification study are:

1. The frequency domain identification method that was applied is robust even when biological data are used.

2. The identified controller parameters reflect the control task conditions.

3. The identified Δ_{eff} derived for the NPC is consistently less than the Δ_{eff} derived for the PC and IC respectively.

4. The identified Δ_{eff} derived for each experimental data for the PC are very similar to that derived using the IC.

5. The PC and IC resulted in optimal effective time delays which are in agreement with the studies of Loram et al. [24, 28].

6. The NPC model could not be considered as a suitalbe model to describe the physiological systems.

Chapter 5

Modelling Human Variability

5.1 Introduction

The computational modelling of the "human controller" during physiological mechanisms, such that of motor control tasks, must involve the modelling of the "human controller" considering both the deterministic and stochastic (random) response data that are generated by the controller during the task [27, 83]. Indeed, the "human controller" during sustained (i.e continuous) or discrete control tasks exhibit motor responses that contain both deterministic and stochastic data. Unlike the deterministic data, which are time-invariant and have the same pattern from repetition to repetition the latter are random data and are different from repetition to repetition. These random response signals are exhibited due to the inherent human variability [60]. For that reason, the "human operator" during sustained control tasks could not solely be modelled as a linear control system that describes only the deterministic human behaviour during the repetitive task however, the random behaviour that is due inherent human variability must be also be considered. Therefore, a "good" computational control model that describes the human behaviour is that which models both the deterministic and stochastic response signals that are exhibited during the human behaviour.

Human variability exhibits in all levels of human behaviour [27,83] and it is reflected in the motor control response signal of the "human controller" as a response signal which is random and its pattern is different from cycle to cycle in repetitive tasks. This

random signal is easily shown in tasks in which the "human operator" is asked to control a system which is excited over a range of discrete frequencies. The operator's response signal will contain components that reflect the input frequencies (i.e deterministic data), however components unrelated to the input frequencies will appear. The latter components will form a signal at non-excited frequencies which in engineering is called remnant and it is different from repetition to repetition (cycle to cycle).

So far, in computational modelling of the "human controller" during manual control tasks, the remnant signal has been treated as the portion of the continuous-time controller's response signal that is not related to the system input by the linear input/output transfer function [3,8,57,73]. In particular, the remnant signal in various computational modelling studies both in man-machine [8, 19, 53] and physiological studies [5, 12, 62] has been modelled as an observation noise model signal (i.e a noise process injected at the controller's input response signal) or motor noise (i.e a noise process injected at the controller's output response signal) or both. Most of the time these two noise signal models have statistical white Gaussian characteristics, or low-pass filtered white noise characteristics. In addition, most of the time the motor noise signal is described as signal-dependent on the mean level of the motor response signal during the control task [26]. The above remnant signal models has shown to fit simulated or experimental data from physiological mechanisms well.

The aim of this chapter is to investigate whether or not the variability that is exhibited during sustained control tasks can be represented by a remnant motor response signal which has an inherent structure of an intermittent controller. Human variability has been modelled as a structure of the IC model which is due to a varied intermittent interval Δ_{ol}, That is the human variability is due to the time-variation in which a reaction response is generated. This method of modelling the human variability has been compared against the method in which human variability is modelled as an observation white Gaussian noise or motor noise which is dependent on the controller's output signal and it is added to a continuous-time PC model.

In this study, during the sustained control experiment (Sect.3.3) the motor response signal that was generated by each subject was excited over a range of discrete frequencies. Therefore, from the response signal the deterministic signal (i.e response

signal at excited frequencies) can easily be distinguished from the remnant signal (i.e response signal at non-excited frequencies). So far, in Chapter 4 a system identification method ([111], Ch2) has been applied to identify the controller models (NPC,PC, IC) that best fit the deterministic data that were generated by the subjects during the control task experiment. In this chapter, controllers PC with noise and IC with varied intermittent interval are used to identify variability models that best describe the remnant signals generated by the subjects during the motor control task.

The computational modelling of human variability was implemented in two stages. In the first stage controllers PC and IC were identified based on the deterministic experimental data that were generated during the experimental task. The first stage has been implemented in chapter 4. In the second stage for each of the deterministic controller models a remnant signal model was considered. Then simulations took place to generate simulated data which are then analysed at both excited and non-excited frequencies. A cost function was applied between the simulated data for each of the control system models and the experimental data, at non-excited frequencies to define the best remnant signal model and variability parameter for each of the controllers.

Section 5.2 includes the materials and methods that were used for the study. In this section, the two stage approach that was applied is described in detail. Section 5.3 describes the results of the human variability study. Section 5.4 includes the discussion of the chapter and Section 5.5 concludes the chapter. The material presented in this chapter has been published in:

1. A. Mamma, H.Gollee, P.J. Gawthrop and I.D. Loram (2011) "Intermittent Control Explains Human Motor Remnant Without Additive Noise", In Proc $19th$ IEEE Mediterranean Conf Control Automation. Corfu, Greece, June 2011., pp.$558 - 563$

2. A. Mamma, H.Gollee, P.J. Gawthrop and I.D. Loram (2011) "Modelling the Human Remnant during Manual Control Tasks" In Proc. $6th$ Int. Posture Symposium. Smolenice Castle, Slovakia , September, 2011. , pp. 60.

3. P.J. Gawthrop, H. Gollee, A. Mamma, I.D. Loram and M. Lakie (2013), "Intermittency explains variability in human motor control", In NeuroEng 2013:

Australian Workshop on Computational Neuroscience. Melbourne, Australia , January, 2013.

5.2 Materials and Methods

This section presents analytically the materials and methods that were used for the modelling of the human variability during the sustained control balance task (Sect. 3.3).

Figure 5.1 shows the continuous-time predictive control system that was used for the remnant signal modelling. This figure is similar to Figure 3.2. Both PC controllers figures (Figs. 5.1, 3.2) consist of the same state Observer-Predictor-Feedback (OPF) model. However, Figure 5.1 has an extra signal $u^2(t)w_o(t)$ added to the control signal $u(t)$ and an additive signal $v(t)$ added to the system response. These extra signals in Figure 5.1 are considered the signal models which describe the non-deterministic data that have been generated during the sustained control task.

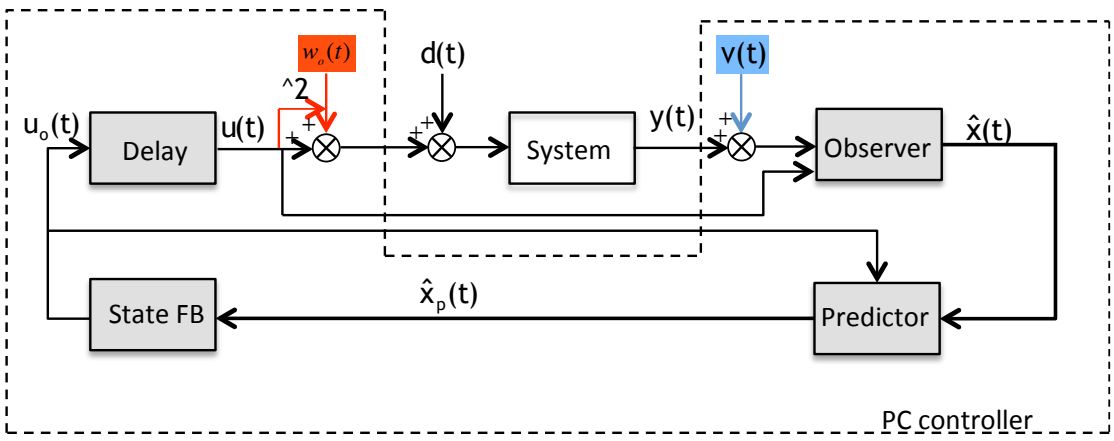

Figure 5.1: Predictive control structure that was used for the remnant signal modelling. The non-deterministic data (i.e remnant signal) were modelled firstly as an additive observation noise signal $v(t)$ (blue line) and secondly as as additive dependent motor noise signal $u^2(t)w_o(t)$ (red lines).

Therefore, for the continuous-time PC controller the remnant signal was modelled:

1. As an additive observation noise signal $v(t)$ [5, 8, 12, 18, 127, 128]. Or
2. As an additive dependent motor noise signal $u^2(t)w_o(t)$ [26, 129, 130].

The controller equations that correspond to the PC with additive noises (Fig.5.1) are given by:

$$\begin{aligned}\dot{\hat{x}}(t) &= A\hat{x}(t) + B[u(t) + u(t)^2 w_o(t)] - L[C\hat{x}(t) - y(t) - \nu(t)] \\ &= A_o\hat{x}(t) + Bu(t)[1 + u(t)w_o(t)] + L[y(t) + \nu(t)] \quad \text{(Observer)} \qquad (5.1)\end{aligned}$$

$$\hat{x}_p(t) = e^{A\Delta}\hat{x}(t) + \int_0^{\Delta} e^{A\tau} B u_0(t-\tau) d\tau \quad \text{(Predictor)} \qquad (5.2)$$

$$u_0(t) = -K\hat{x}_p(t) \text{(Controller)} \qquad (5.3)$$

where A_o is the observer matrix (equation (3.11)), $\hat{x}(t)$ is the estimated state (equation (5.1)) $\hat{x}_p(t)$ is the predicted state at time $t + \Delta$, $u(t)(1 + u(t)w_o(t))$ is the delayed control signal and $[y(t) + \nu(t)]$ is the system output.

When $w_o(t) = 0$ (Fig. 5.1) then a PC with an additive observation noise signal $v(t)$ is used whereas when $v(t) = 0$ then a PC with a dependent motor noise signal $u(t)^2 w_o$ is considered.

On the other hand, Figure 5.2 shows the intermittent control system that was used to model the non-deterministic data (i.e. remnant signal) that have been generated during the sustained control task. The equations of the IC with a varying intermittent interval are equal to the IC with fixed Δ_{ol} and have been presented in section 3.2.3.

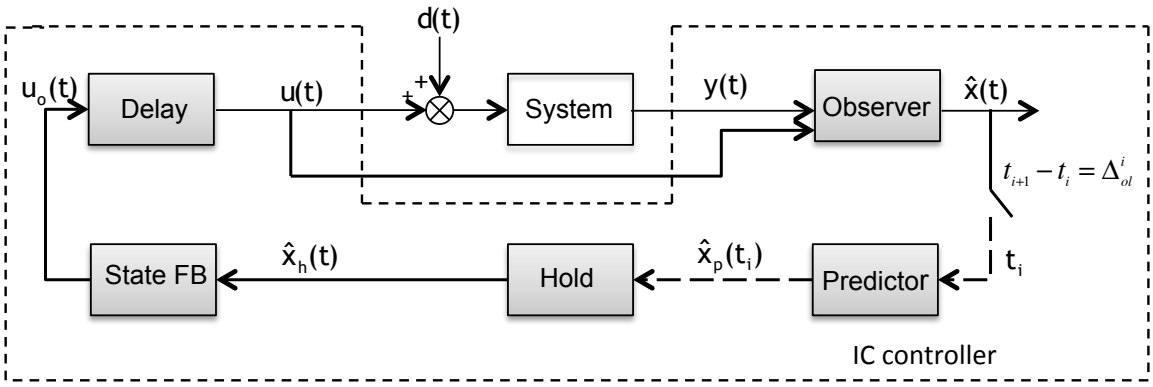

Figure 5.2: Intermittent control structure that was used for the remnant signal modelling similar to Figure 3.3. In this case, the variability that is exhibited was considered to be a structure of the controller which is due to the varying intermittent interval Δ_{ol}^{i}.

The computational modelling of the remnant signal for both controllers PC, IC was implemented in two stages.

1. In the first stage the artificial controllers PC, IC were parametirised at the excited frequencies ω_e (equation (3.67)) using the system identification method described in chapter 4. The two stage approach of Pintelon and Schoukens was followed for the case where $w_o(t) = v(t) = 0$ (Fig.5.1) for the predictive control system and for **fixed intermittent interval** Δ_{ol} for the intermittent control system (Fig.3.3). For every experimental data the optimal controllers parameters $\theta^* = [q_v, q_c, q_o, \Delta]$ (augmented for Δ_{ol} for the IC) were defined.

   Tables 5.1 and 5.2 show the optimal controller parameters that were identified for the "minimise position" control strategy.

Subjects	controller parameters θ^* (PC)			
S	q_c	q_v	q_o	Δ (ms)
S_1	185.7	0.001	185.9	250
S_2	14.7	1.8	77.2	200
S_3	4.2	0.001	4.2	180
S_4	6.8	0.001	6.9	260
S_5	11	0.01	11	210
S_6	114.8	3.06	2.2	180
S_7	1.8	0.01	152.7	210
S_8	7.9	0.01	7.8	180
S_9	108.6	0.03	0.7	160
S_{10}	8.3	0.01	8.3	240
S_{11}	2.7	0.01	559.4	270

Table 5.1: Optimal controller parameters identified for the PC controller using the system identification method described in Chapter 4. The PC controller was identified separately for every subject S using the identification methods described in Chapter 4.

Subjects	controller parameters θ^*(IC)				
S	q_c	q_v	q_o	Δ(ms)	Δ_{ol}(ms)
S_1	245.9	0.001	245.5	170	170
S_2	15.9	1.9	87.8	130	130
S_3	4.1	0.001	4.2	110	110
S_4	7.1	0.001	7.1	170	170
S_5	12	0.001	11.9	140	140
S_6	164.1	6.75	2.5	100	170
S_7	1.9	0.001	1849.5	180	220
S_8	7.8	0.001	7.7	110	110
S_9	91.9	0.001	0.7	100	100
S_10	8.6	0.001	8.6	150	180
S_11	2.9	0.001	2908.6	200	200

Table 5.2: Optimal controller parameters identified for the IC controller using the system identification method described in Chapter 4. The IC controller was identified separately for every subject S using the identification method described in Chapter 4.

2. In the second stage a remnant signal model was considered for each of the identified controller models PC, IC of the first stage. Therefore for the PC system (Fig.5.1)

   (a) A dependent motor noise signal $u(t)^2 w_o(t)$ was added to the PC system and

   (b) An observation noise signal $v(t)$ was added to the system output of the PC system.

   For the IC control system (Fig.5.2) a varying intermittent interval Δ_{ol} was considered. In this case variability is considered to generated due to the varying property of the intermittent interval Δ_{ol}.

The next section describes the second stage of the remnant signal modelling method.

5.2.1 Remnant signal modelling

This section describes the signal models that were used for the computational modelling of the remnant signal during the "minimise position" control strategy (i.e. keep the dot as close to the centre of the oscilloscope as possible). The remnant signal for the continuous-time PC control system was modelled as:

1. An additive white Gaussian noise signal $v(t)$ (Fig.5.1) with normal distribution $v(t) \sim N_g(0, \theta^2)$ with mean 0 and variance θ^2. The probability density function of the white Gaussian noise is given by

$$f(v(t); 0, \theta^2) = \frac{1}{\theta\sqrt{2\pi}} e^{-\frac{u(t)^2}{2\theta^2}} \tag{5.4}$$

   $\theta > 0$ is the standard deviation of the white Gaussian noise signal.

2. A motor noise signal $w(t) \sim N_l(0, (u(t)\theta)^2)$ (Fig.5.1) with mean zero and variance $(u(t)\theta)^2$. The variance $(u(t)\theta)^2$ of the signal depends on the amplitude of the control signal $u(t)$ and represents the signal dependent noise. The PDF of the signal $w(t)$ is given by

$$f(w(t); 0, (u(t)\theta)^2) = \frac{1}{u(t)\theta\sqrt{2\pi}} e^{-\frac{w(t)^2}{2(u(t)\theta)^2}} \tag{5.5}$$

On the other hand, for the IC controller the variabiltiy was modeled as single parameter θ which determined the variability of the intermittent interval Δ_{ol}. The variability was considered to be due to the fact that the intermittent interval was non-constant and it was given by

$$\Delta_{ol}^{i} = \Delta + \delta_i \tag{5.6}$$

where δ_i is generated by an inverse Gaussian distribution [131] $\delta \sim IG(\mu, \theta)$ with mean $\mu = \Delta_{ol} - \Delta$ and $\theta > 0$ is the shape parameter which in this study is varied. The probability density function (PDF) of the inverse Gaussian distribution is given by

$$f(\delta; \mu, \theta) = \sqrt{\frac{\theta}{2\pi(\delta)^3}} \exp \frac{-\theta\left(\delta - \mu\right)^2}{2\mu^2\delta} \tag{5.7}$$

An inverse Gaussian distribution was chosen to model the varied intermittent interval due to the fact that there was a need for a non-symmetrical distribution with a lower limit. The lower limit of the distribution was the optimal time delay Δ since the intermittent interval cannot be smaller than Δ. An example of the intermittent interval distribution is given in Figure 5.6b). Different non-symmetrical distributions could also be used.

5.2.2 Procedure

During the simulations for each control loop described above the independent parameter θ was varied over a pre-defined range and each system was simulated for each value. In particular, the parameter θ of the white Gaussian signal $\nu(t)$ was varied from [0,....,0.7] in increments of 0.002, for the PC with a dependent noise $w(t)$ the parameter θ was varied in the range $(1, ...9]$ in increments of 0.01. For the intermittent control system with a non-constant Δ_{ol} the parameter θ was varied in the range (0....0.2] in increments of 0.002.

All simulations and analysis algorithms were implemented in Matlab ($R2010a$, The Mathowrks, MA, USA). Simulations were defined by the type of the controller PC or IC, the noise signal, and for the IC the intermittent interval Δ_{ol}. The duration of each simulation was 200 sec and data was recorded with sample period $T_s = 0.01$ sec. The

output signal $\hat{u}(t_n, \theta)$ was generated for each control system and experimental data. The generated simulated data were then analysed at both excited ω_e (equation (3.67)) and non-excited frequencies ω_n (equation (3.68)) using a frequency domain method analysis. The best noise model and variability parameter for each of the controllers were defined.

To determine consistency and qualitative information, for every control system and every experimental data each simulation was repeated $r = 15$ times in which the initial seed of the random number generator was different.

5.2.3 Experimental data analysis

According to Pintelon and Schoukens ([111] Ch.4) the use of a sinusoidal excitation input signal facilitates the separation of remnant-induced signals from the linear response to the inputs, since signal power at other than input frequencies could arise only from controller remnant. Therefore in order to determine the non-excited frequency components, thus the remnant signal that exhibited during the experimental task, the analysis described in section 3.4.3 was followed.

For each experimental data, generated by the subjects during the control task, frequency domain analysis was applied by analysing data with duration, $n_p = 2$ times the disturbance period T_0, hence $T_p = 20$sec (equation (3.63)) resulting in 10 period chunks and $N_k = 200$ discrete frequency components ($\omega_k = [0.05, 0.15...., 9.95]$Hz) with a frequency resolution $\omega_k^0 = 0.05$ Hz (equation (3.64)). The extended time domain control signals, as expected, contained power data both at excited ω_e (equation(3.67)) ($\omega_e = [0.1, 0.2, ...10]$) and non-excited frequencies ω_n (equation (3.68)) ($\omega_n = [0.05, 0.15, ...9, 95]$ Hz). For the analysis and in order to avoid transients the first period was discarded resulting in $n_a = 9$ periods (equation (3.69)).

Figure 5.3 depicts the estimated power spectra density (PSD) (equation (3.75)) calculated from the control signal for one subject. The figure shows that during the motor control task variability is exhibited and it is reflected as the remnant signal (i.e the signal at non-excited frequencies). The same phenomenon has been shown in all experimental data; subjects exhibited human variability during the control task and that was depicted as the remnant signal in the PSD of the recorded control signal.

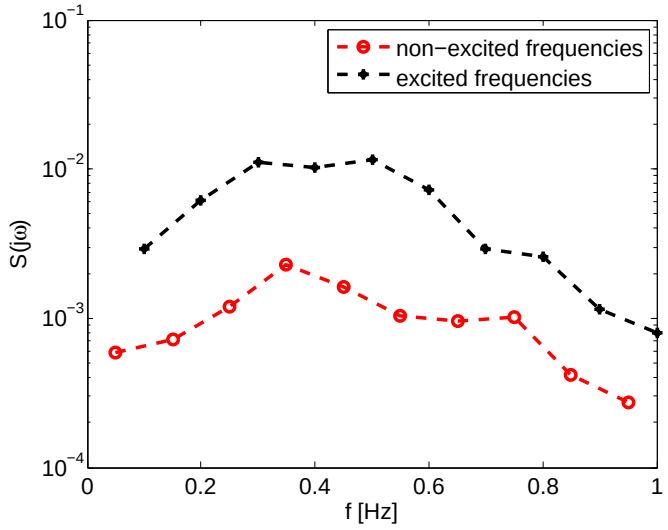

Figure 5.3: Power spectra density of the control signal that recorded during the control task for one subject. The spectrum shows that the control signal contains data both at excited (ω_e) and non-excited frequencies (ω_n). The dotted black line depicts the signal at excited frequencies and the dotted red line depicts the remnant signal.

For each period analysis l and each subject s the power spectra density (PSD), both at the excited (ω_e) and non-excited (ω_n) frequencies, followed by averaging over all periods are given by equations (3.74) and (3.75) respectively.

5.2.4 Computational data analysis.

The same frequency analysis as that applied for the generated experimental data (Sect.5.2.3) was used for the computational data that were generated usign the simulations. The control signal $\hat{u}_s(t_n, \theta)$ that was generated for each control system and repeat and for each experimental data was analysed in frequency domain with period $T_p = 20$ sec resulting in $n_a = 9$ periods (equation (3.69)). Every repeat n_b ($n_b = 1, 2, ..., r = 15$) of the simulated data contained n_a periods of the control signal, hence $R = rn_a = 135$ repeats (period chunks) over all frequencies, at excited ω_e and non-excited ω_n were derived for each simulated data for every parameter θ.

The DFT control signal that was generated for each experimental data and control system is denoted as $\hat{U}^{[kk]}(j\omega_k, \theta)$. This is the DFT control signal at the repeat kk (with $kk = 1, 2, ..., R = 135$) where ω_k can either be excited ω_e (equation (3.67)) or non-excited frequencies ω_n (equation (3.68)).

The estimated PSD, both at the excited and non-excited frequencies, followed by averaging over all repeats is given by, respectively

$$\hat{S}^{[kk]}(j\omega_k,\theta) = \frac{1}{\omega_k^0}|U^{[kk]}(j\omega_k,\theta)|^2 \quad \text{with,} \;\; \omega_k = 0.05, 0.1, ..., 10, \quad \text{Hz} \tag{5.8}$$

$$\hat{S}(j\omega_k,\theta) = \frac{1}{R}\sum_{kk=1}^{R} S^{[kk]}(j\omega_k,\theta) \tag{5.9}$$

where $\hat{S}^{[kk]}$ is the PSD at the kk^{th} period and $\hat{S}$ is the estimated PSD over all repeats generated using simulations for one subject. The PSD can be calculated at excited ω_e (equation ((3.67)) and non-excited frequencies ω_n (equation (3.68)) respectively.

From every simulation and control system the estimated simulated PSD control signal at each parameter θ, $\hat{S}(j\omega_k,\theta)$ was compared with the corresponding experimental estimated control signal $S(j\omega_k)$ (equation (3.75)) at non-excited frequencies $\omega_k = \omega_n$ and the error PSD at each parameter for every subject was calculated as

$$e(j\omega_k,\theta) = |S(j\omega_k)| - |\hat{S}(j\omega_k,\theta)|, \qquad \omega_k = \omega_n \tag{5.10}$$

For each experimental data the best fit $J^*(\theta)$ was determined as the minimum cost function J^*

$$J^*(\theta) = \min_{\theta} J(\theta) \tag{5.11}$$

where $J(\theta)$ is the squared error between the estimated generated PSD derived from the experimental data for each subject and its parametric fit, and it is given by

$$J_s(\theta) = \sum_{\theta=1}^{\theta=\theta_i} |e_s(j\omega_n,\theta)|^2 \quad \text{with} \quad \omega_n = 0.05, ..., 9.95 \tag{5.12}$$

The optimal parameter θ^* , for each subject, was determined and corresponds to the minimum cost function J^* (equation (5.11)). Therefore the optimal generated PSD control signal at non-excited frequencies is determined as $\hat{S}^{[kk]}(j\omega_n,\theta^*)$ for each period chunk kk. The estimated optimal generated PSD both at excited and non excited frequencies for each control system over all repeats R is given by

$$S^*(j\omega_k, \theta^*) = \frac{1}{R}\sum_{kk=1}^{R} |\hat{S}^{[kk]}(j\omega_k, \theta^*)| \qquad kk = [1, 2, ..., R] \tag{5.13}$$

5.2.5 Statistical analysis

Generally, for a noise-free linear system the response signal will be identical among its repetitions (i.e. periods), as the external disturbance is identical in each case. On the other hand, in the case where there is variability the response signal will be different from repetition to repetition (i.e. period to period), even when excited with the same disturbance. Therefore, in the study, a non-parametric one way statistical test (Kruskal-Wallis one way analysis of variance) [132] was performed in order to evaluate whether or not repetitions are statistically significantly different from one another. This was performed first on the response signal at each period using the experimental data, and secondly on the optimal simulated response signal at each repetition, for each control system (PC and IC). The statistical significance was determined for each statistical test the p-values were compared to $\alpha = 0.05$ which corresponds to 95% confidence level.

The non-parametric one way statistical test was applied to determine whether or not the median experimental PSD that was generated for every subject is statistically different ($p < 0,05$) between each period, both at excited and non-excited frequencies. The results from the statistical analysis showed that the median experimental PSD that was generated for every subject has been found to be different at each period ($p < 0.05$) both at excited and non-excited frequencies, except for two subjects ($p > 0.05$). This shows the variability during the manual compensatory tracking task experiment, as the response signal is variable and not repeatable at each frequency. Furthermore, for each control system PC and IC the same statistical one way test was applied to the optimal simulated PSD $\hat{S}^{[kk]}(j\omega_n, \theta^*)$ to determine whether or not the optimal median PSD at each repeat kk ($kk = 1, 2, , 135$) and subject s is statistically different from each other, both at excited and non-excited frequencies ω_n. The optimal simulated median PSD for the PC with added white Gaussian noise signal $v(t, \theta^*)$ has been found to be statistically the same ($p > 0.05$) for each repeat, at both excited and non-excited frequencies. On the other hand the optimal simulated median PSD for the PC

with a dependent Gaussian noise signal $w(t, \theta^*)$ has been found to be different at each repeat. For the IC with variable intermittent interval the optimal simulated median PSD has been found to be different over all frequencies at both non-excited frequencies ω_n and excited frequencies ω_e. Therefore, the IC with a varied intermittent controller can demonstrate both quantitatively and qualitatively the variability that is exhibited during motor control tasks without the need to add any external noise.

5.3 Results

Figure 5.4 depicts the simulated PSD control signals that were generated from the PC with no noise (i.e $w(t) = v(t) = 0$) (Fig.5.1) and IC controller with fixed intermittent interval Δ_{ol}, for subject S_3. The controller parameters are those identified using the first stage of variability analysis (Sect.5.2) and are given on tables 5.1 and 5.2 respectively. Figure 5.4a shows clearly that the PC controller without any noise cannot generate a control signal at non-excited frequencies (ω_n). As expected the PC controller generates data only at excited frequencies (ω_e). On the other hand Figure 5.4b shows that in the case where an IC system with a fixed intermittent interval Δ_{ol} is used the PSD control signal is generated both at excited and non-excited frequencies. From the above it is easily concluded that the IC controller can generate the remnant signal without the need of any additive noise signals unlike the continuous-time PC controller.

In the second stage of variability analysis a) two different noise models were added to the identified PC controller models and *b*) an IC controller with varied intermittent interval was used to fit the remnant PSDs derived from each of the experimental data.

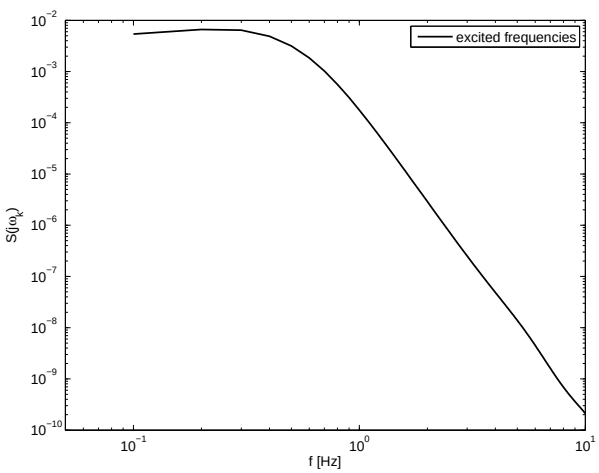

(a) PSD control signal generated using a PC system with neither observation nor motor noise added to the system during simulations.

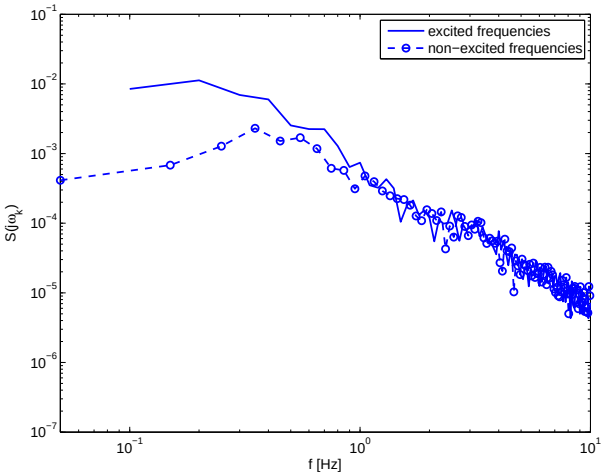

(b) PSD control signal generated using an IC with fixed intermittent interval $\Delta_{ol} = 0.15$ sec.

Figure 5.4: Example in which the PSD control signal is generated from simulations using: a) a PC system with no noise. The PSD control signal illustrates the signal at excited frequencies only. In this case the PSD control signal at non-excited frequencies is not depicted b) An IC with a fixed Δ_{ol}. The figure shows that the generated PSD control signal contains data both at excited (continuous line) and non-excited frequencies (dotted line). Therefore, the IC controller can generate the remnant signal without the need of any added signals to the system unlike the continuous-time PC.

Table 5.3 summarises the minimum cost function values J^* (equation (5.11)) along with the corresponding θ^* that were derived from the simulations using the artificial control systems. The parameter θ^* for both continuous-time control systems, PC with an additive observation noise or PC with a motor noise signal is the standard deviation of the Gaussian distribution of either the observation (equation (5.4)) or the motor noise signal (equation (5.5)) . For the intermittent controller IC the parameter θ^* depicts the standard deviation of the inverse Gaussian distribution of the variable intermittent interval (equation (5.7)). The small cost function values for each of the three different models indicate that they provide adequate fits to the remnant PSDs. The IC with a varied intermittent interval provides either a better remnant fit than the PC with $w(t) = 0$ (i.e PC with observation noise) (Subjects $S_1, S_2, S_3, S_4, S_5, S_7, S_{11}$) or slightly worse (subjects S_6, S_9, S_{10}. In addition, the IC with a varied intermittent interval is slightly worse to than the PC with $v(t) = 0$ (i.e PC with dependent noise signal).

Subjects	PC with $w_o(t) = 0$		PC with $v(t) = 0$		IC with variable Δ_{ol}	
a/a	θ^*	J^*	θ^*	J^*	θ^*	J^*
S_1	0.054	3.6×10^{-3}	1.91	1.9×10^{-3}	0.008	3.4×10^{-3}
S_2	0.092	5×10^{-4}	3.49	2.9×10^{-4}	0.05	4.2×10^{-4}
S_3	0.11	6.6×10^{-6}	2.85	1.5×10^{-6}	0.014	1.7×10^{-6}
S_4	0.554	1.2×10^{-2}	3.69	5.5×10^{-3}	0.108	7.6×10^{-3}
S_5	0.156	2.7×10^{-4}	3.23	8.5×10^{-5}	0.012	5.2×10^{-5}
S_6	0.076	5.5×10^{-5}	1.63	3.2×10^{-5}	0.194	9.2×10^{-5}
S_7	0.066	4.3×10^{-5}	6.1	1.6×10^{-5}	0.008	2×10^{-5}
S_8	0.288	4.6×10^{-4}	3.88	2.9×10^{-4}	0.03	7.7×10^{-4}
S_9	0.112	4×10^{-5}	1.86	2×10^{-5}	0.01	4.4×10^{-5}
S_{10}	0.212	8×10^{-4}	3.33	2.8×10^{-4}	0.012	3.8×10^{-4}
S_{11}	0.058	4.2×10^{-4}	6.63	1.8×10^{-4}	0.004	3.2×10^{-4}

Table 5.3: Optimal parameters θ^* that were derived for each of the artificial control systems using equation 5.11. The parameter θ^* for both continuous-time control systems, PC with an additive observation noise or PC with a motor noise signal is the standard deviation of the Gaussian distribution of either the observation or the motor noise signal. For the intermittent controller IC the parameter θ^* depicts the standard deviation of the inverse Gaussian distribution of the variable intermittent controller Δ_{ol}

The results of the best fits (θ^*) of noise models and varied intermittent interval to the remnant PSD for one experimental data (S_3) are shown below both in time and frequency domain.

Figure 5.5a shows a period of two seconds of the Gaussian white noise signal $v(t, \theta^*)$ and the corresponding control signal $u(t, \theta^*)$ that were generated during the remnant PSD fitting for the subject S_3. Figure 5.5b shows a period of two seconds for the dependent Gaussian noise signal $w(t, \theta^*)$ and the corresponding control signal $u(t, \theta^*)$ that were generated during the remnant PSD fitting of the subject S_3.

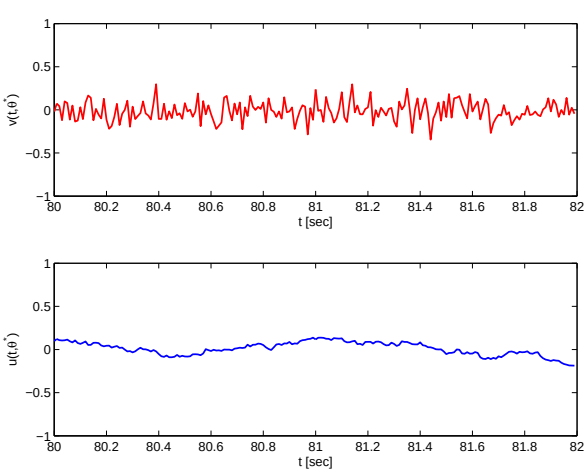

(a) PC with additive white Gaussian noise $\nu(t\theta^*)$

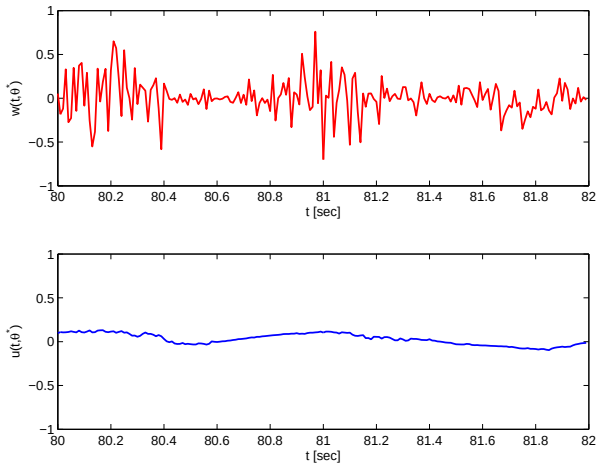

(b) PC with signal dependent noise $w(t, \theta^*)$

Figure 5.5: Noise model and simulated control signals that were derived for the PC with observation noise and PC with dependent noise respectively. The top figures show the noise signal models that correspond to the best remnant PSD fitting for the experimental data S_3 (Table 5.3). The bottom figures depict the control signals that were generated for the best fit model.

Figure 5.6 shows the control signal $u(t, \theta^*)$ and the optimal varied intermittent interval that were generated, for the IC, during the remnant PSD fitting of the subject S_3

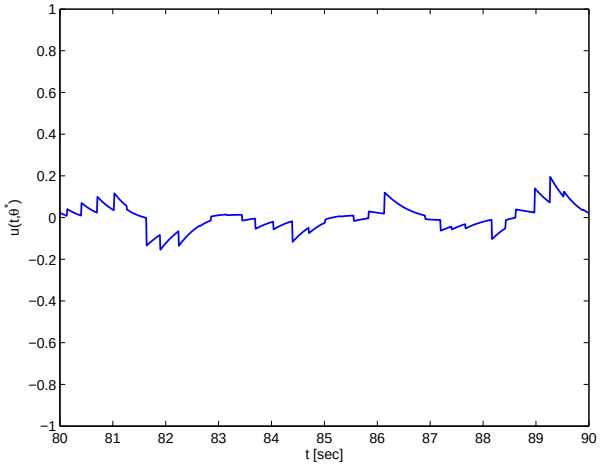

(a) Simulated control signal $u(t, \theta^*)$ generated for the IC with varied intermittent interval using the optimal θ^*

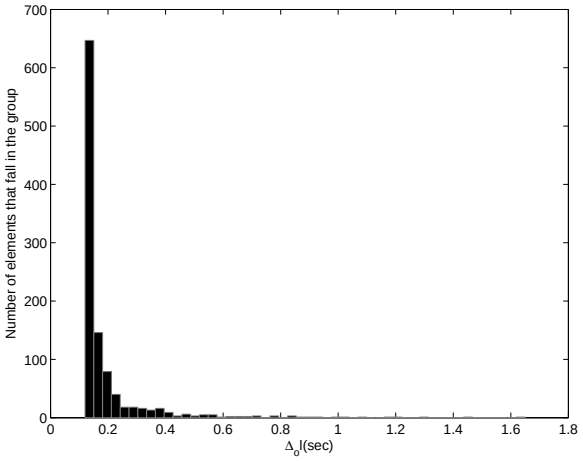

(b) Intermittent interval distribution for the optimal θ^*. Appendix B includes the results for all the experimental data and are shown in Figure B.1)

Figure 5.6: Simulated control signal $u(t, \theta^*)$ and optimal varied intermittent interval generated for the IC controller.

Figure 5.7 illustrates the optimal simulated PSDs, for each of the control systems against the PSDs generated from the subject S_3. The bottom subfigures depict the optimal simulated PSD of the control signals at non-excited frequencies (ω_n) against the remnant PSD (i.e PSD at non-excited frequencies ω_n) generated due to the human variability for the experimental data S_3. The bottom subplot of Figure 5.7c shows that the simulated PSD of the IC with the optimal intermittent interval controller fits the remnant PSD of the experimental data S_3 as well as the PC with a dependent noise signal (bottom plot of Fig.5.7b), especially up to 1Hz and slightly better than the PC with an observation noise signal. The IC controller using a varied intermittent interval could fit the remnant signal PSD experimental data without the need to add any noise unlike the continuous-time PC.

The top subfigures of Figure 5.7 illustrate the optimal simulated PSDs, at excited frequencies against the deterministic PSD for the experimental data S_3. All artificial models fit the deterministic PSDs generated by the experimental data S_3 equally well

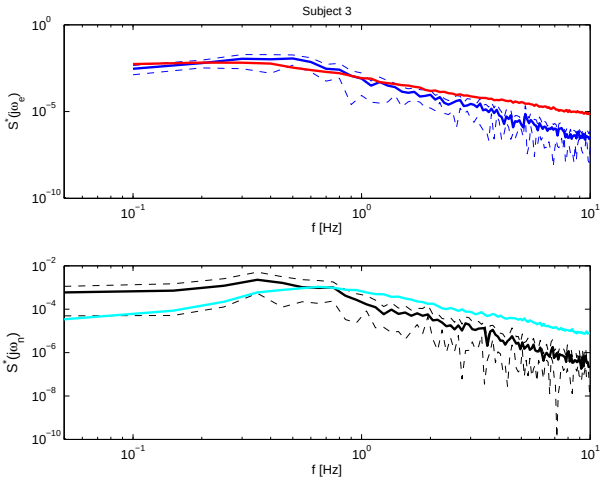

(a) PC with additive white Gaussian noise $\nu(t)$.

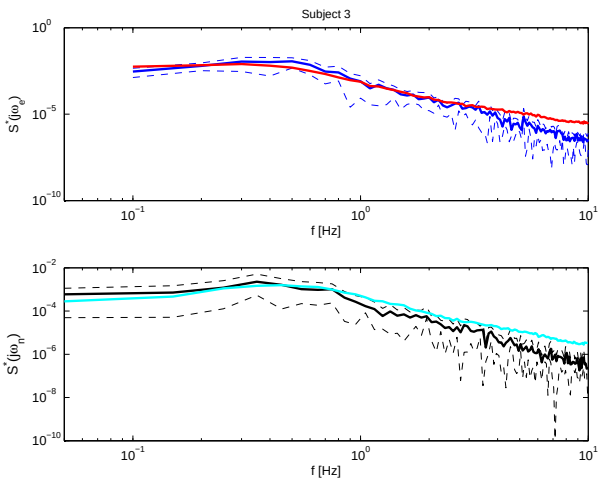

(b) PC with signal dependent noise $w(t)$.

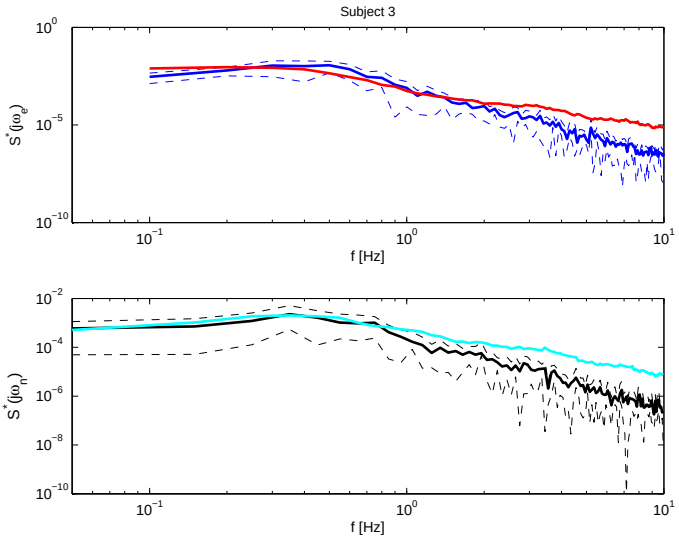

(c) IC with random intermittent interval.

Figure 5.7: Experimental PSD data S_3 against the optimal simulated PSDs for each of the control systems. The top subplots depict the optimal simulated PSDs (red line) at excited frequencies generated using each of the control systems a) PC with an observation noise signal $v(t, \theta^*)$ b) PC with a dependent noise signal $w(t, \theta^*)$ c) IC with an optimal varied intermittent interval Δ^i_{ol} against the PSD deterministic data (i.e PSD at excited frequencies) of the experimental data S_3 (blue line). The blue dashed line depicts the standard deviation of the PSD of the S_3. The bottom subplots depict the optimal simulated PSDs at non-excited frequencies ω_n for each control systems (cyan line)against the remnant PSD of the experimental data S_3 (black line). The dashed black line depicts the standard deviation of the experimental PSD. Appendix B includes the results for all subjects.

5.4 Discussion

In this chapter the aim was to determine whether or not human variability, which is depicted as a remnant signal in the response signal during human control tasks, could be modelled using an intermittent controller with a varied intermittent interval. The IC model was compared with the predictive controller in which variability is modelled as a noise source either dependent or independent.

Qualitatively the example in Figure 5.7 shows that the simulated PSD at non-excited frequencies for the IC with the most appropriate varied intermittent interval (Fig. 5.7c bottom subplot) fits the PSD remnant signal equally well as the PC with dependent noise (Fig. 5.7b bottom subplot) especially for frequencies up to 1Hz, whereas it worsens for higher frequencies. Looking at the rest experimental data the IC with a varied intermittent interval can model the remnant signals as well as the PC with a dependent noise signal with some exceptions in which the fitting in not very good. Probably, in order to describe all the remnant signals from all experimental data we need an IC controller with a varied intermittent interval plus an additive noise.

In human sustained motor control tasks the human response trajectory is different from repetition to repetition and this is due to human variability [3, 27, 60]. The statistical test showed qualitatively that the IC with a varied intermittent interval can show the variability that is exhibited during motor control tasks. From the non-parametric one-way statistical test it has been shown that the simulated median PSD both, at excited and non-excited frequencies, are statistically different ($p < 0.05$) among its repetitions except for one data. On the other hand, although the PC with an observation noise signal has been shown graphically to fit the PSD remnant signals for each experimental data, the statistical analysis has shown that the median optimal simulated PSD among its repetitions is not statistical different ($p > 0.05$). That shows that the variability during a repetitive task cannot be statistically explained using an observation white noise signal and the reason is that the variance of this signal is independent even if the signal varies by some amount, the variance is the same whether the signal has a small or large amplitude. The statistical method applied to the PC with a dependent motor noise signal has shown the variability among the repeats both at excited and non-excited frequencies for almost all subjects.

The above show that the remnant signal derived from the experimental data can equally be explained using a signal dependent noise to a PC system model or an intermittent controller with a varied intermittent interval.

The method applied in this chapter has shown that the PSD remnant signals could be fitted by either hypothesis. It has been shown that human remnant can be modeled either as an independent white Gaussian noise signal [8, 11, 12, 14] or a dependent noise signal to a deterministic continuous-time model [26]. In addition, Van de Kooij and Peterka [62] have suggested that a combination of an independent observation noise signal with a dependent motor noise signal fit remnant data better than having individual noise signals either observation or motor dependent. Although, human variability is modeled as a noise signal to a deterministic model there is still a debate on the physiological evidence of the characteristics of human variability relative to noise signals. Davids et al. ([63], chapter 1) support the view that the human variability in movement and posture is not white, either broadband or Gaussian. Also, Faisal et al. [27] concur that describing the variability that exhibits at lower levels of motor behavior as white Gaussian noise signal is convenient only to manipulate mathematical assumptions, since the structure of the noise is more complex. Although in literature physiological variability during manual control tasks is considered to be a source of noise, which exhibits in low levels of behavior such as perception, action and motor behavior [27] this study has shown that human variability can be explained due to the random intermittent behavior of the human during motor control tasks. Modeling human variability as an intermittent controller with a varied intermittent interval has a physiological basis. Van de Kamp et al. [96] have shown refractoriness in sustained visual-manual control tasks, which is directly related to the intermittent human behavior during these tasks. Therefore, explaining modeling human variability as an IC with varied intermittent interval has a natural and potentially testable basis since it adds evidence for the intermittent behavior of human during motor control tasks.

5.5 Conclusions

The conclusions derived from the human variability study are:

1. Human variability, could be described as a structure of an IC without the need to add any noise signal models, whereas the deterministic PC model cannot describe the remnant signal without any additive noise.

2. Modelling human variability as an intermittent controller with a varied intermittent interval has a physiological basis. Van de Kamp et al. [96] have shown refractoriness in sustained visual-manual control tasks, which is directly related to the intermittent human behaviour during these tasks.

3. Explaining modelling human variability as an IC with varied intermittent interval has a natural and potentially testable basis since it adds evidence for the intermittent behaviour of human during motor control tasks.

Chapter 6

Control of quiet standing

6.1 Introduction

Intermittent control [39,41] has been applied in continuous-time model-based predictive control systems (MPC) by replacing the continuous-time moving horizon by an intermittent moving horizon [47, 98, 133]. This allowed for on line computational optimisation which is used intermittently and in an open-loop fashion therefore it can handle cases in which the system is time varying. In addition, intermittent control has shown to be applied in modelling the human operator during physiological control mechanisms. Indeed in this study, intermittent control [39, 41] has been used in modelling the human operator in a compensatory balance tracking control task [28]. Using an identification method it has been shown that the optimal simulated data derived from the intermittent control model could fit the deterministic experimental data taken from subjects who took part at the compensatory tracking task. In addition, the variability, which is translated as a remnant signal during compensatory tracking tasks, has been shown to be described by the intermittent control system with a varied intermittent interval. So far, a compensatory manual control task has been described by the intermittent control system in a computational level.

This chapter describes a preliminary attempt to apply intermittent control in real time in the context of the physiological control mechanism of human standing balancing. Physiological studies [38, 134–136] have shown that human standing could be modelled as balancing an inverted pendulum with human dynamics in the saggital

plane. This chapter attempts to apply an experimental method following the study of Gollee et al. [137] to apply automatic artificial balance of an inverted pendulum, in the context of human standing, via functional electrical stimulation (FES) control of the lower leg muscles of a healthy subject. The lower leg muscles of the subject, Gastrocnemious (GA) and Tibialis Anterior (TA) were the actuators of the control system.

Potential instability of the controlled system required the feedback system must provide a certain minimum bandwidth. In engineering, a feedback structure that is usually used to overcome limitations in control performance due to actuator nonlinearities or modelling problems is a cascade control structure ([30],chapter 10). Previous studies on automatic balance control using FES technology on paraplegic people have used extensively the cascade structure [138–141]. Therefore this preliminary study uses a cascade control system ([30],chapter 10).

This chapter will describe an attempt to study automatic balance of an inverted pendulum with human dynamics using FES control using the intermittent control system model [39, 41]. Although the attempt failed the results of the experimental method are only indications that further study should take place in order for automatic balance control to be applied in real time. Subsequent to the experiment, simulations took place to test the sensitivity of the system output of the cascade control system: 1) to perturbations in the nominal dynamic actuator models 2) to state constraints and 3) to the sampling frequency.

Section 6.2 describes the materials and methods that were used in this study. Section 6.2.1 describes the apparatus, the modelling and control system design and the experimental procedure that were used. In addition section 6.2.2 describes the simulations that were applied to the cascade system. The parameters of the nominal dynamic actuator models that were perturbed are described in this section. In addition the state constraints and the sampling frequencies that took place in the simulations are described. Section 6.3 presents the results both from the experiment (Sec.6.3.1) and the simulations (Sec.6.3.2). Section 6.4 includes a discussion of the chapter and Section 6.5 concludes the chapter.

6.2 Materials and Methods

6.2.1 Experiment

Subject

The experiment was approved by the College of Science and Engineering Ethics Committee of University of Glasgow for non-clinical research involving human subjects, (project reference number $CSE00985$). The participant, $S1$ gave written, informed consent to this experiment. The male subject was fit and healthy, aged 40 years and, with no neurological deficit.

Apparatus

The apparatus used for the experiment were two biomechanic force platforms ($OR-6$ AMTI Biomechanics platforms, Massachusetts, USA). Throughout the experiment stood in a squad position with his feet on the two force platforms which allowed measurement of both force and ankle moment components about the XYZ axes in each platform respectively (Fig.6.1). The output signals were sent to a six-channel strain gauge amplifier and displayed to a computer through an A/D converter card (NI DAQCard $6024E$, National Instruments, UK). Calibration of the strain gauge amplifier took place in order for the measurement units of the force and moment signals to be in N and Nm respectively. During the experiment only the ankle moment M_x for each leg of the subject was measured (Fig. 6.1).

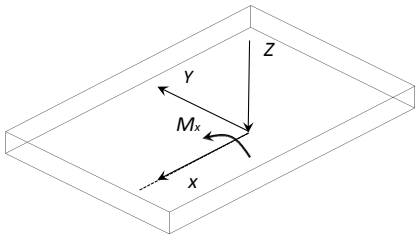

Figure 6.1: Schematic of the force platform used to measure the subject's ankle moment M_x.

In addition, a custom built frame which is similar to a standard rehabilitation standing frame was used. This frame supported the subject, while standing on the force platforms, at the knees and hip while preventing forward and backward movement of

the subject as well as falling. The frame was set up in such a way that the subject was in a slight squad position while his quadriceps muscles were relaxed.

For the stimulation of the lower leg muscles a neuromuscular stimulator device (RehaStim, HASOMED, Magdeburg, Germany) was used and it was connected to self-adhesive surface electrodes attached over the Gastrocnemious (GA) and Tibialis Anterior (TA) lower leg muscles for each leg respectively. The stimulator operated at a constant frequency of 50 Hz (sample interval 20 ms) which defined the sampling frequency f_s of the experiment. In addition, during the experiment the current intensity was kept constant. The stimulus pulsewidth was varied between 0 μs and a maximum level of 500 μs. The stimulator was driven directly via a serial line interface from the computer. All the signals were sampled at 50 Hz. Real-time data acquitision and control on the PC was implemented within Matlab/Simulink running the Real-time Toolbox.

The figure below shows a schematic example of the pulsewidth, the current intensity and the frequency of the stimulus applied during the experiment.

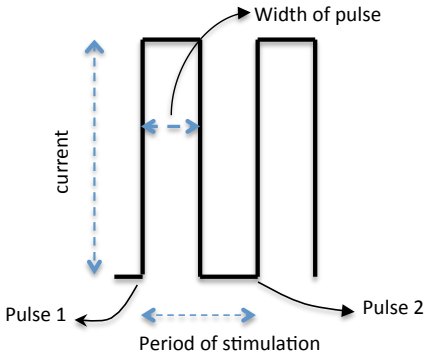

Figure 6.2: Schematic example of the puslewidth, current intensity and stimulation period (inverse of pulse frequency). Note that the ratio of pulsewidth to stimulation frequency is in practice much smaller than shown in the diagram.

Figure 6.3 shows a picture of the apparatus used in this study and Figure 6.4 shows a general form of the system apparatus used in order to measure the ankle moment of each leg of the subject during the experiment. A proportional controller defined the pulsewidth p that was applied by the stimulator in order functional electrical stimulation (FES) to be applied to each of the lower leg muscles of the subject while $S1$ was standing in the squad position on the force platforms. The total ankle moment m_t measured by the force platforms was then amplified and digitised via the AD card

and then sent to a computer.

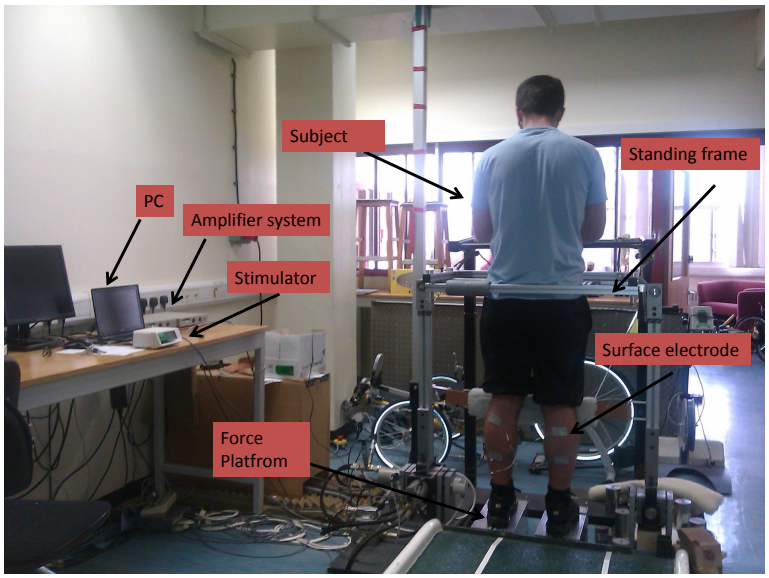

Figure 6.3: Schematic of the FES apparatus.

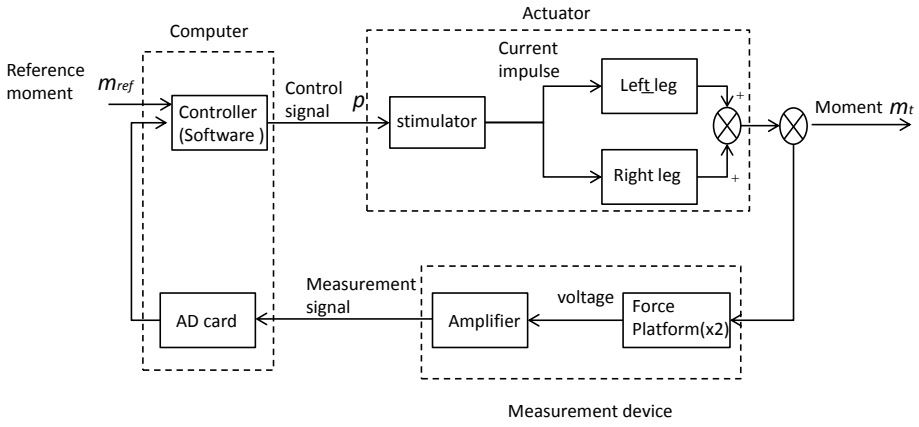

Figure 6.4: Schematic arrangement of the moment control.

Modelling and Control system design

Figure 6.5 shows the cascade control system that was used for the automatic balance of the virtual inverted pendulum in relation to human standing and Figure 6.6 shows the analytic representation of the cascade control system.

The block "P" (Fig. 6.5) represents the dynamics of the virtual inverted pendulum which include a response output constraint (Fig. 6.6) and block "NMSs" represents the dynamics, with a delay Δ, of the stimulated muscles GA or TA of the subject $S1$.

The block "C_m" represents the two inner proportional controllers $C_{m,GA}$ and $C_{m,TA}$ (Fig.6.6) that were designed for each muscle pair GA, TA respectively. The inner loop controllers regulated the total ankle moment m_t by applying appropriate stimulation $p(t)$ to each of the lower leg muscles of $S1$. A switching mode within the inner loop determined the inner loop muscle pair that was stimulated during the experiment (Fig. 6.6). The sign of the signal $m_{act}(t)$ determined which muscles would be stimulated and hence which inner loop will be switched on. Positive values of p indicated FES control of the GA muscle pair and negative values of p denoted FES control of TA muscle pair.

The outer controller C_θ (Fig. 6.5) regulated the virtual inverted pendulum (block P) inclination $\theta(t)$ by providing a desired moment $m_{ref}(t)$ for the inner loop. The outer controller C_θ describes the intermittent controller. Figure 6.6 shows the intermittent controller C_θ which includes an integrator. The integrator was added to the plant so that the derivative of the reference moment becomes the new input signal. This allows to compensate for constant disturbances. The IC system was designed as described in Chapter 3.5. For implementation purposes the integrator is included in C_θ. The reference angle $\theta_{ref}(t)$ was constant and equal to -4^o. The virtual inverted pendulum's angle position was constraint to $\pm 10^o$ during the experiment. In Fig. 6.6 $G_{m,GA}$ and $G_{m,TA}$ are the inverse steady state gains of each of the muscle models and were used in the modelling in order to ensure good tracking response during the experiment.

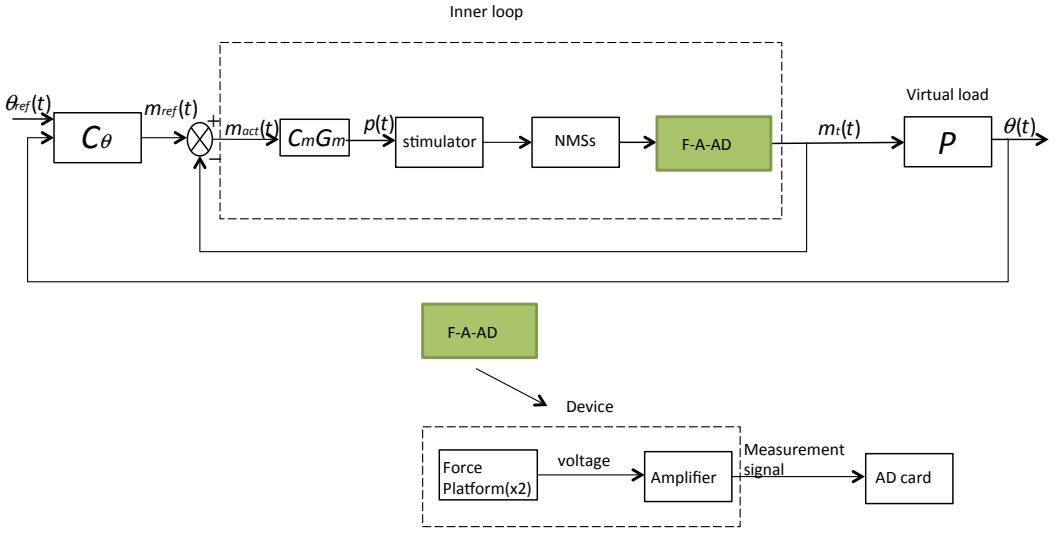

Figure 6.5: Schematic of the cascade control system design. C_θ describes the outer intermittent controller, C_m the inner proportional controller which is designed for each of the muscles GA and TA. G_m are the inverse steady state gains for each muscle pair which are used in order to ensure good tracking response and $NMSs$ describes the dynamics, which included a delay Δ, of the stimulated muscles GA or TA of the subject $S1$ and P is the the state constraint virtual inverted pendulum model.

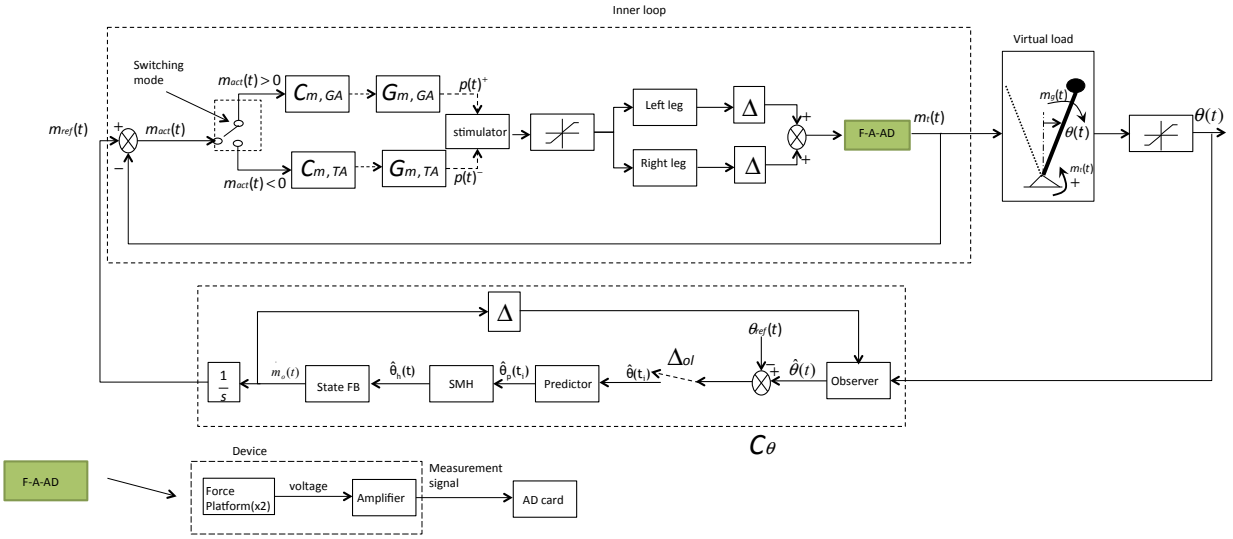

Figure 6.6: Analytic schematic of the cascade control system design.

The cascade control system structure allowed the overall feedback system to be designed and tested in steps, starting with the ankle moment control loop and moving to the inverted pendulum angle controller. The steps involved in system design are:

1. The muscle dynamics NMS_s were identified using an open-loop PRBS test described below (Test PRBS). That established dynamic models between the pulsewidth p and the ankle moment m_t for each muscle pair. In this test a series of PRBS stimulation signals were applied in open-loop at a range of mean levels and the total moment generated was recorded.

2. A Test moment tracking, described below (Test Moment tracking) was applied to design the proportional inner loop moment controllers $C_{m,GA}, C_{m,TA}$ for each of the linear dynamic muscle models. The design of the inner loop moment controllers (proportional controllers) were based on the empirical linear dynamic muscle models derived from Test PRBS.

3. The design of the outer loop position controller C_θ was based on the dynamics of the virtual inverted pendulum and the inner closed loop transfer function based on the linear dynamic model of the GA muscles. The contraction only of the GA muscles of the subject prevented the virtual load from falling over for that reason it was adequate to design the outer controller C_θ based on the inner closed loop system model using the nominal dynamic transfer function of the GA muscles. The design of the outer controller is described in Test balance.

Tests

During the experimental session a series of tests were carried out:

Test C: To measure the Maximum Voluntary Contraction (MVC) of each of lower leg muscles, the subject was asked to voluntarily apply an isometric contraction of his GA and TA muscles respectively. At the beginning the GA muscles were isometrically contracted and the applied total muscle moment was measured. In the same way the TA muscles were contacted and the applied moment was measured. Then the optimum stimulation current level was determined for each of the GA and TA muscles. Starting with a low current the isometric moment

for each muscle was measured. The current was then incremented by 10 mA and the stimulation pattern was repeated. This process continued until a current level could produce a 10% of the MVC for each of the muscles, with no pain for the subject. This current was then determined as the optimum current and set constant throughout the experiment. This procedure was carried out for each leg separately.

Test PRBS: This test was an open-loop test and it was applied to define the nominal transfer functions "NMSs" (Fig.6.5) of each of the muscles GA,TA of the subject respectively. Figure 6.7 shows a schematic representation of the test. An input signal, $p(t)$ where the pulsewidth had a PRBS form (Fig.6.8) was applied to both GA and TA muscles of each leg respectively and the total moment (left+right) moment m_t was measured. The amplitude of the input signal at each mean level was set at 35 μs with mean signal 200 μs. The PRBS which was used consisted of 4 periods with each period of 387.5 samples.

From the input $p(t)$ and output $m_t(t)$ data a linear system identification method was applied to identify the nominal transfer function models of the muscles of the subject using the system identification toolbox of MATLAB (Mathworks, USA).

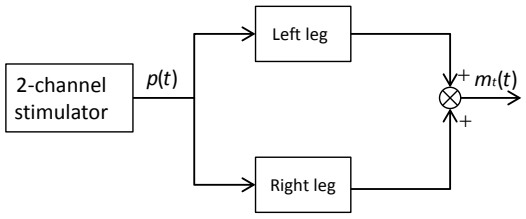

Figure 6.7: Structure of the system that was used to determine the nominal models of each of the actuator systems. A PRBS signal $p(t)$ was applied to the lower leg muscles of both legs of the subject. The output signal $m_t(t)$ was the total moment exerted by the left and right legs of the subjects. A system identification method was used to determine the transfer function of the system using the input/ output data.

The muscles are dynamical systems which posses non-linear as well as time-varying properties. However, the Hill-based muscle model [142] is a sufficient description and it is widely used in the computational modelling literature [28, 97, 130]. For that reason the nominal models of the calf muscles were identified as linear first order lag models with time delays Δ ([143],chapter 7).

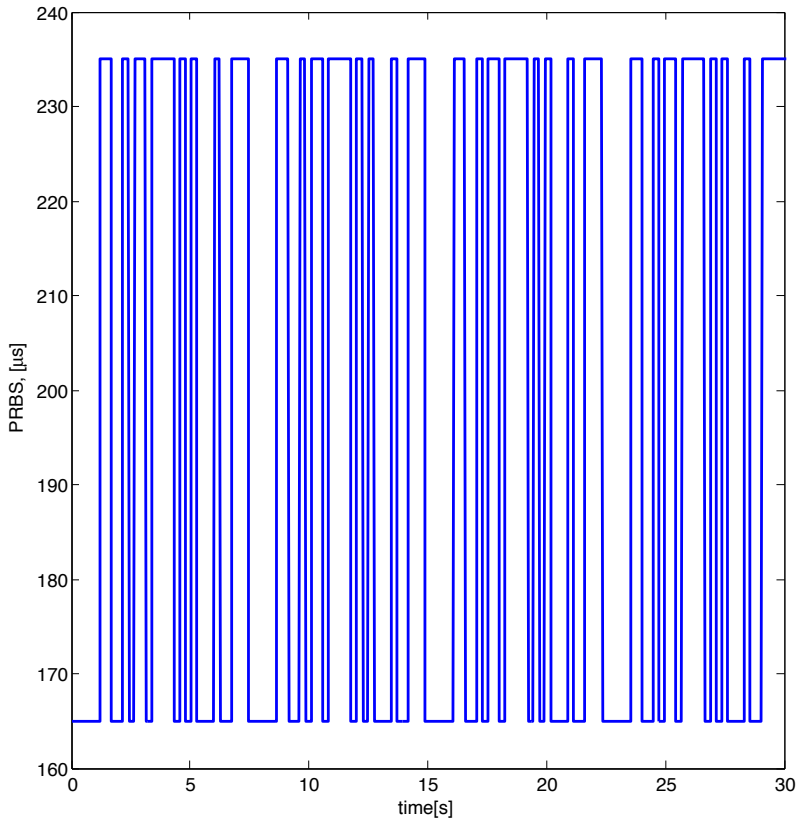

Figure 6.8: PRBS signal applied to the Test PRBS. The amplitude of the input signal at each mean level was set at 35 μs with mean signal 200 μs. The PRBS which was used consisted of 4 periods with each period of 387.5 samples.

Test Moment tracking: This test was applied to design the inner proportional controllers $C_{m,GA}$ and $C_{m,TA}$ (Fig. 6.6) for each of the nominal muscle models derived from Test PRBS. During the test moment tracking the inner loop control system was active only (Fig. 6.9). A negative square-wave reference moment m_{ref} with a given amplitude and frequency was predefined and directly applied (Fig.6.10). The inner proportional controllers $C_{m,GA}$ and $C_{m,TA}$ were tuned during this test. The switching mode within the inner loop determined negative and positive pulsewidth and hence stimulation of either the GA or TA muscles. In particular in case where $m_{act}(t) > 0$ that determined stimulation of the GA muscles and $m_{act}(t) < 0$ determined stimulation of the TA muscles.

The integral action in the inner loop would have ensured the error between the reference value and the measured value to approach to zero, however, in this control system design the integral was included only at the outer loop and not at the inner loop. This lead in an offset between the reference moment m_{ref} and the measured moment m_t (Fig.6.10) but this would be compensated in the outer loop with the integral action included at the IC controller.

The purpose of this test was to determine the proportional inner loop controller gains $C_{m,GA}, C_{m,TA}$ and also test whether or not control of both positive and negative moments could be achieved by a pair of proportional controllers switching between the GA and TA muscles.

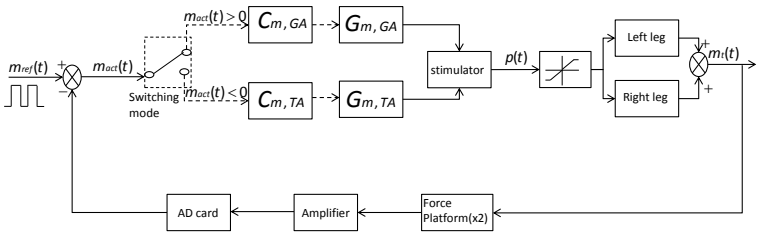

Figure 6.9: Moment tracking control. A switching mode mechanism translates positive values of m_{act} to GA stimulation and negative values ($m_{act} < 0$) to TA stimulation.

Figure 6.10 shows the results from the test moment tracking, which defined the inner loop gain controllers $C_{m,GA}, C_{m,TA}$ respectively. The inner loop gains that were determined were $C_{m,GA} = 3$ and $C_{m,TA} = 2$.

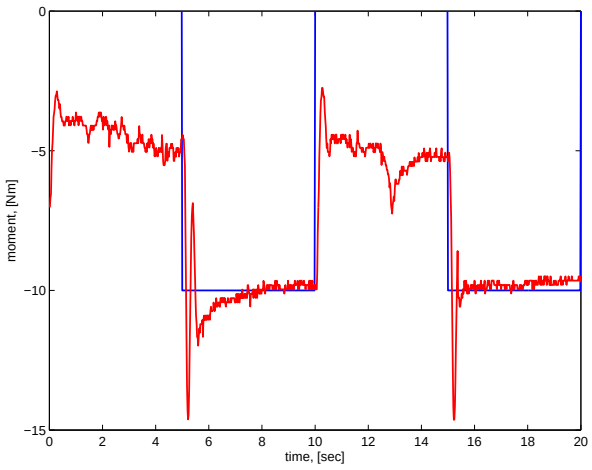

Figure 6.10: Muscle moment control with no integral action.

Test Balance: The dynamics of the virtual inverted pendulum is given

$$mgl\sin\theta(t) - k\theta - B\dot{\theta} - m_t(t) - m_d(t) = I\ddot{\theta} \tag{6.1}$$

θ is deviation of the virtual inverted pendulum, $\ddot{\theta}$ is the second derivative with respect to time. For small changes, $\sin\theta = \theta$; $m_t(t)$ is the total ankle moment and $m_d(t)$ is an external multisine disturbance moment signal which has been modified in such a way to fit in the experiment. The Laplace transfer function of the inverted pendulum is given as

$$\frac{\Theta(s)}{M(s)} = \frac{-\frac{1}{I_p}}{s^2 + \frac{B}{I_p}s - (1-c)\frac{mgl}{I_p}} \tag{6.2}$$

where $\Theta(s)$ is the Laplace transform of the angle $\theta(t)$, $M(s)$ is the Laplace transform of the total moment at the ankle $m_t(t) + m_d(t)$, and c denotes the ratio of spring stiffness to toppling moment due to gravity (see Section 3.3.2).

The outer IC controller was designed for the augmented system of the closed loop representation of the inner loop system based on the dynamics of the GA muscle model and the dynamics of the virtual inverted pendulum. The vector $x = [q_c, q_v, q_o, q_{int}, q_p, \Delta, \Delta_{ol})]$ was designed using the LQR method, where q_c, q_v are the position and velocity weighting factors for the states of the inverted pendulum, q_o is the weighting factor for the observer state, q_{int} is the weighting

factor for the integrator state, q_p is the weighting factor for the closed-loop inner system, Δ_{ol} is the intermittent interval and Δ is the delay of the system in which in this case is considered equal to the delay of the actuator model found from the identification method. Table 6.1 shows the design parameters for the IC controller used with the LQR method.

SMH IC Weighting factor	values
q_c	1000
q_v	100
q_p	0
q_o	6000
q_{int}	0
$\Delta_{ol}(sec)$	0.15
Δ(sec)	0.08

Table 6.1: Controller parameters of the IC. q_c is the weighting factor for the position of the pendulum, q_v is the weighting factor for the velocity of the virtual load, q_p is the weighting factor of closed-loop inner system, q_o is the observer weighting factor Δ_{ol} is the intermittent interval and Δ is the delay of the system.

Having designed the outer controller the final test was applied to provide artificial balance control of the inverted pendulum. The strategy was to balance the virtual load at a reference position of $\theta_{ref} = -4^o$ using ankle-joint moment control through FES stimulation of the lower leg muscles of the subject. The virtual pendulum angular position was constrainted between $\pm 10^o$. The controller IC provided the required ankle-joint moment signal m_{ref} needed to control the position of the inverted pendulum. This required moment was achieved by the proportional inner loop feedback controller which used the actual moment m_{act} and adjusted the stimulation intensity appropriately. The GA muscles were stimulated when there were positive values of p while the TA muscles were stimulated when negative values of p were required. The moment signal m_t which served as the control signal to the virtual load was the summation of the left+right moment signals measured from each leg. This signal was corrupted by a multisine periodic signal $m_d(t)$. The test was applied for 200 s.

Experimental Procedure

At the start of the session, a pair of self-adhesive surface electrodes were placed over the GA and TA muscles of each leg of the subject. The electrodes were connected to the neuromuscular stimulator device. The subject, stepped on the force platforms and was loosely fastened into the custom build frame. A Test C was applied to determine the optimum current intensity, applied to each of the muscles of the legs of the subject and then set constant. The current intensity did not exceed 60mA. A test PRBS was applied to determine the nominal models of the GA and TA muscles of the subject. Once, the nominal models of the GA and TA muscles were determined then a Test moment tracking was applied to determine the feedback inner controllers $C_{m,GA}$ and C_m, TA for each muscle nominal model. A Test Balance control was applied in which the outer-loop controller C_θ was designed and the complete structure shown in Fig. 6.6 was implemented. The aim for this test was to implement artificial balance control of the inverted pendulum in the context of "human standing" using the cascade control structure described above. The virtual inverted pendulum's state position was constraint at $\pm 10^o$. The moment applied to the virtual inverted pendulum was disturbed by an external multisine disturbance signal while the reference angle was constant at -4^o.

6.2.2 Simulations

Figure 6.11 shows the general control system form that was used for the simulations that we applied on the cascade system. The figure is similar to Fig.6.5 with the exception that in simulations the parameters of the nominal transfer function models NMS_s are perturbed. Figure 6.12 shows the analytic representation of the inner loop control system that was used in simulations. In this part of the study it was considered that there is a set of Π possible linear time invariant models $G'_{m,GA}(s,a), G'_{m,TA}(s,a) \epsilon \Pi$ which represent the transfer function models of the lower leg muscles (the actuators of the system); $a(t)$ determines the changes in the nominal parameters of the transfer function of the actuator models. The parameters were bounded within a region $[a_{min}, a_{max}]$.

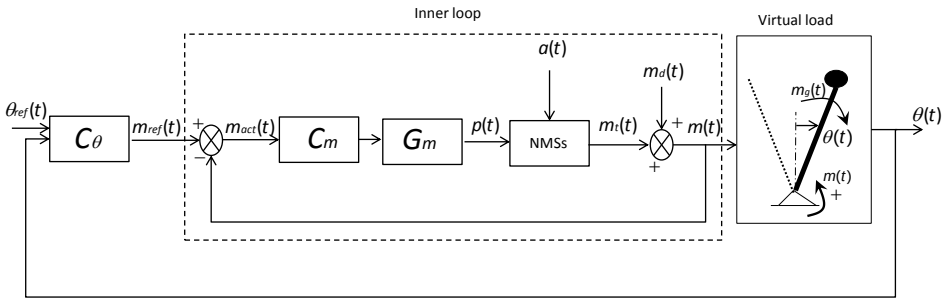

Figure 6.11: Cascade system structure that was used in the simulations. During the simulations it was considered that the parameters of nominal transfer function models NMS_s are perturbed within a region $[a_{min}, a_{max}]$

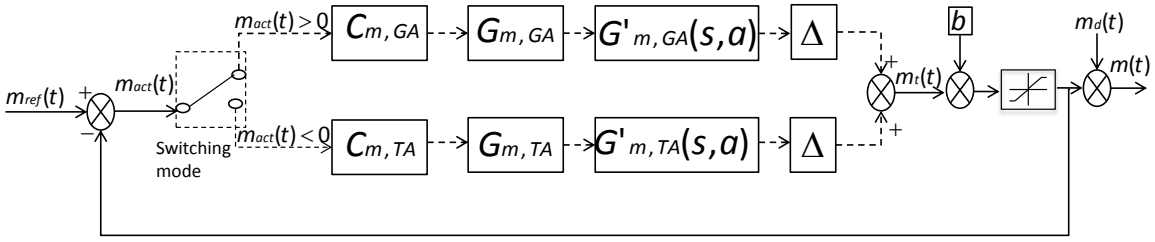

Figure 6.12: Inner loop structure that was used during the simulations.

Table 6.2 shows the parameters of the inner loop transfer functions $G'_{m,SA}$ and $G'_{m,TA}$ that were bounded during the simulations. These are: 1) the steady state gains G_{ss} for each of the inner loop models $G_{m,GA}, G_{m,TA}$, 2) the delay Δ of the nominal inner loop models and 3) the bias (an additional moment b that is added to the nominal models. The impact of constraints on the the inner loop output response state was studied along with the impact of the sampling frequency during the simulations. Therefore each parameter perturbation simulation was applied for sampling frequencies 1) 1 kHz, and 2) 50Hz with or without inner loop output response constraints as it shown on the table.

Perturbed parameters	$f_s = 1$ kHz	$f_s = 50$ Hz
steady state gain G_{ss}	$[0.1, 0.2, ...1]\%G_{ss_o}$	$[0.1, 0.2, ...1]\%G_{ss_o}$
bias, b (Nm)	$[0, 1, ..., 20]$	$[0, 1, 2...., 20]$
Delay Δ (sec)	$[0.08, 0.09, ..., 0.18]$	$[0.08, 0.09, ..., 0.18]$
Noise signal	Yes	Yes
actuator limitation	Yes, No	Yes, No

Table 6.2: Parameters that have been perturbed for the sensitivity analysis. f_s is the sampling time.

The duration of each simulation was 200 s and data was recorded with sampling frequency, f_s either 1 kHz or 50 Hz (Table6.2). Following Karnavas et al. [144] an empirical sensitivity analysis was performed. For the sensitivity analysis the steady state response signals $\theta(t)$ from each simulation were calculated. The mean output signals θ, θ_0 over all periods were calculated. The semirelative sensitivity function S was calculated by computing the difference between the nominal $\theta_0(j\omega_k)$ and the perturbed output response signals $\theta(j\omega_k))$ and this difference was divided over the change in the perturbed value (Δ_a). The ratio was then multiplied by the nominal parameter value a_0 (equation (6.3)).

$$S_a^{\theta}(j\omega_k) = \frac{|\theta_i(j\omega_k) - \theta_o(j\omega_k)|}{\Delta a} a_o \tag{6.3}$$

Matlab (Mathworks, USA) was used for the simulations and the analysis. Initially, a simulation was performed with the parameters of the feedback control system in nominal values. Then, a second simulation run was performed in which a parameter of the control system was changed (Table 6.2).

6.3 Results

6.3.1 Experimental results

Table 6.3 shows the current level intensities that were defined for each muscle for both legs, following test C.

Muscle	Current intensity [mA]
GA_l	35
GA_r	30
TA_l	25
TA_r	25

Table 6.3: Current levels defined for each muscle for both legs. The notation l, r denotes the left and right GA and TA muscles for each of the legs of the subject.

The input-output data recorded from the open-loop identification test (Test PRBS) are shown in Fig. 6.13. The top graph shows the PRBS stimulation pulsewidth p for a mean level of 200 that was applied to each leg calf muscles of the subject $S1$. The

total ankle moment m_t recorded for the GA and TA muscles separately are shown in bottom graph.

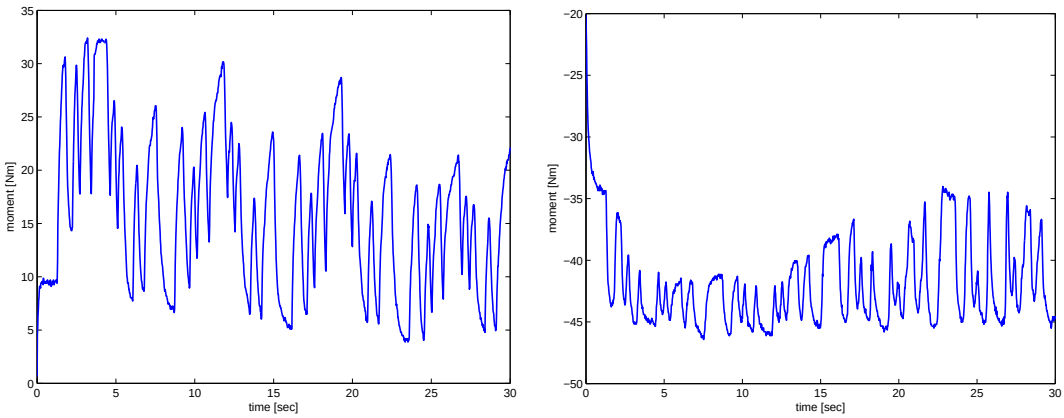

(a) Output moment recorded from the GA muscles for both legs.

(b) Output moment recorded from the TA muscles for both legs.

Figure 6.13: Input/output data recorded from the open-loop identification PRBS test. a)PRBS signal applied through a stimulator to the calf muscles of the subject. b) The figure represents the total moment (left+right) recorded from stimulation of each of the GA muscles. c) the figure represents the total moment (left+right) recorded from stimulation of each of the TA muscles.

Table 6.4 shows the first order linear transfer function models which were identified from the Test PRBS data.

mean pulsewidth μs	Muscle	Transfer function	DC gain	constraints (Nm)
200	NMS_{GA}	$\frac{2.912}{s+2.119}e^{-0.08s}$	1.37	$\pm$50
200	NMS_{TA}	$\frac{-0.425}{s+2.545}e^{-0.08s}$	0.17	$\pm$50

Table 6.4: Nominal dynamic models for the lower leg muscles.

Figure 6.14 shows the position and moment control signals along with the pulsewidths that were applied during the artificial balance control test using the intermittent controller as the outer controller in the cascade system. The top plot shows the virtual inverted pendulum angles, both reference θ_{ref} and measured angle θ. The second plot depicts the moments, both reference m_{ref} and actual m_{act} and the third plot shows the stimulation pulsewidths p. The top figure shows that automatic balance of the inverted pendulum was not succeeded using the control cascade system (Fig.6.6). A limit cycle behaviour of the system is shown, hence any disturbance could cause the system to be unstable which happened after few seconds as it shown in the top plot causing saturation in the pulsewidth (bottom plot).

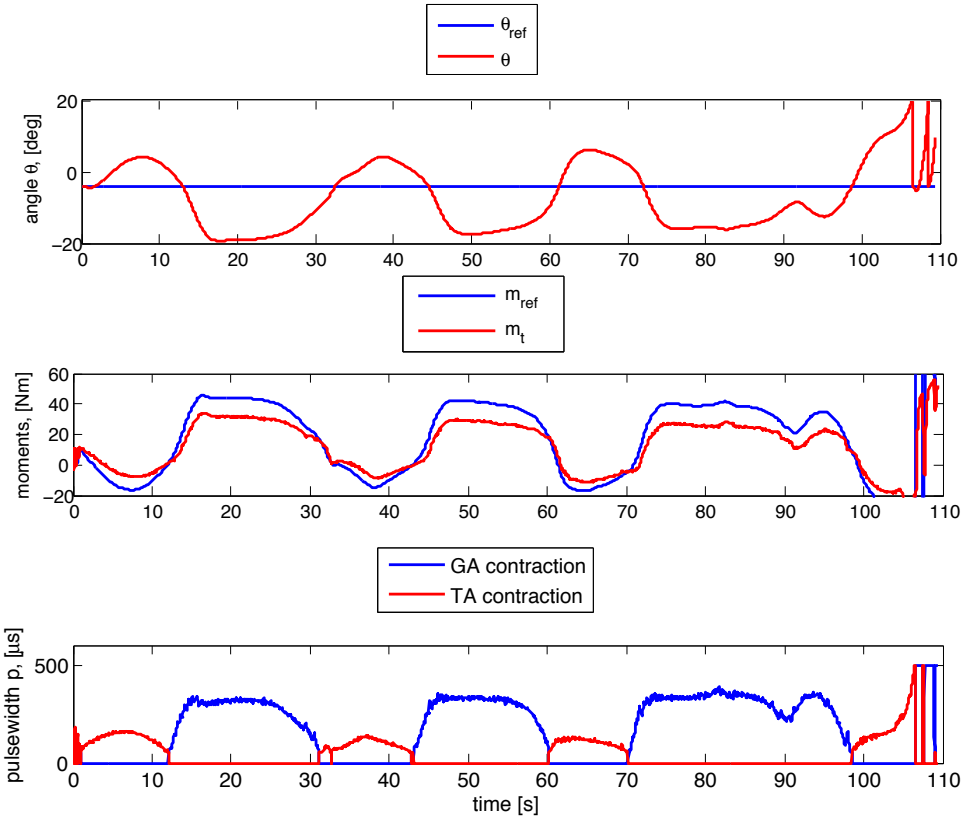

Figure 6.14: position and moment control results using an intermittent controller as the outer controller in the cascade system.

Two other independent trials using the same subject were applied showing the same results. In all three trials, artificial balance control was not implemented.

The same experiment was applied using the continuous-time predictive control (PC) as the outer controller in the cascade system in order to provide balance control in the inverted pendulum. Figure 6.15 shows the results from one trial. Unlike the intermittent control artificial balance of the virtual inverted pendulum was achieved using the continuous-time PC system however, that was not consistent. Other trials using the PC system did not provide artificial balance control.

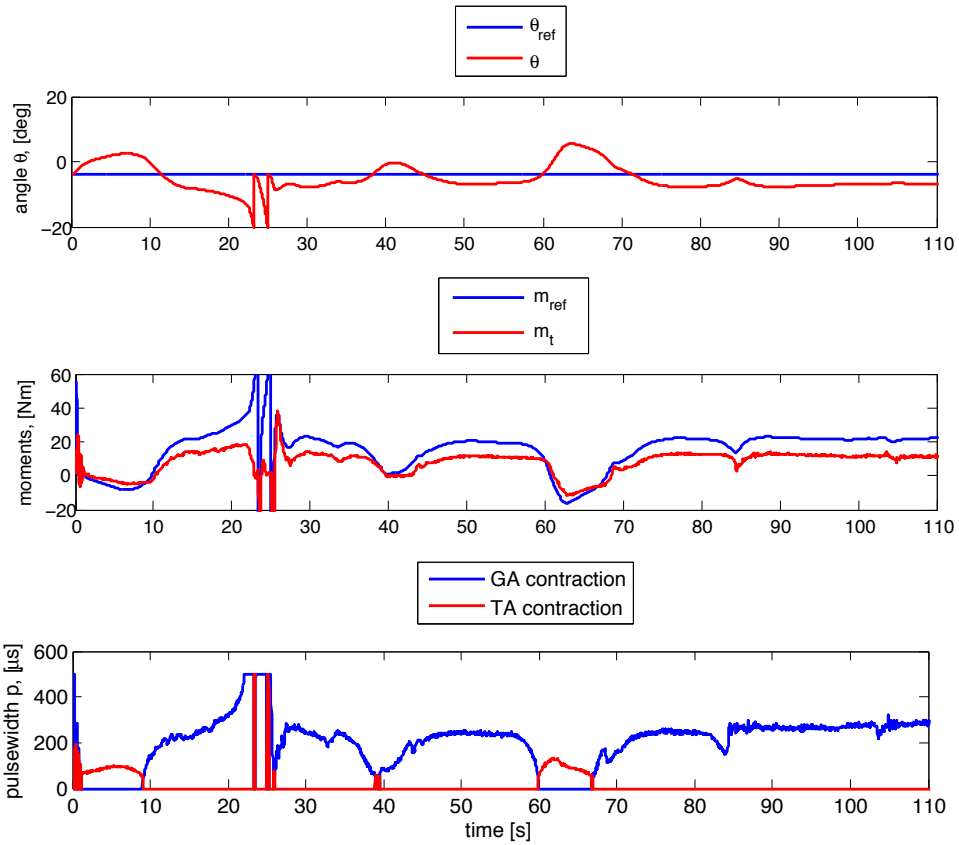

Figure 6.15: position and moment control results using a predictive controller as the outer controller in the cascade system.

6.3.2 Simulation results

The results presented in this section are the those in which no state constraints were applied in the cascade control system. The simulations that were derived when there were state constraints showed system response instability therefore are not presented.

Figure 6.16 shows the results from the simulations in which the steady state gains G_{ss} of the inner loop transfer functions of the nominal actuator models were perturbed based on Table 6.2. The figures shows that as the gain of perturbation increases the output response amplitude θ of the inverted pendulum increases for both sampling frequencies $f_s = 1$ Khz and $f_s = 50$ Hz. In particular, for sampling $f_s = 50$ Hz the simulations shows that the response output signal is more oscillatory (Fig.6.16b) in respect to that when the sampling is 1 Khz.

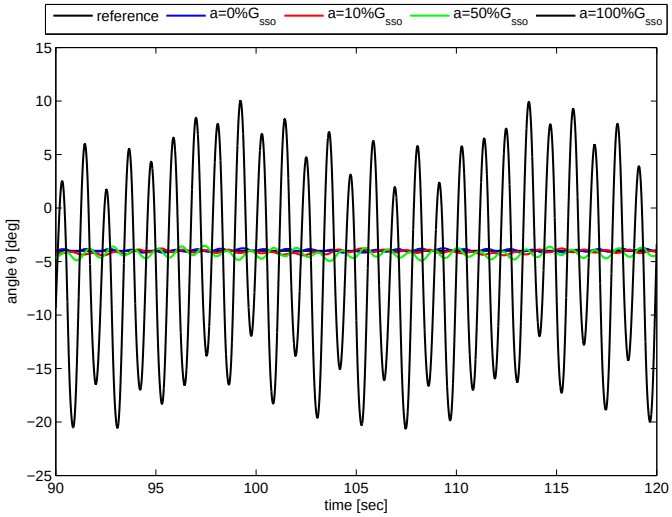

(a) Response output signal for $f_s = 1$ kHz

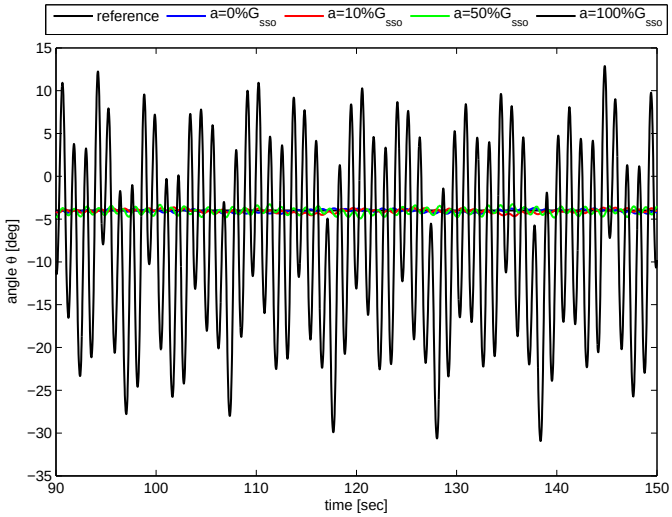

(b) Response output signal for $f_s = 50$ hz

Figure 6.16: Simulations: Response output signals in which the steady-state gain of the nominal inner loop transfer function is perturbed based on Table 6.2.

Figure 6.17 shows that the addition of bias in the inner loop nominal transfer

function actuator models does not increase the amplitude of the position response of the inverted pendulum, however, the response becomes oscillatory.

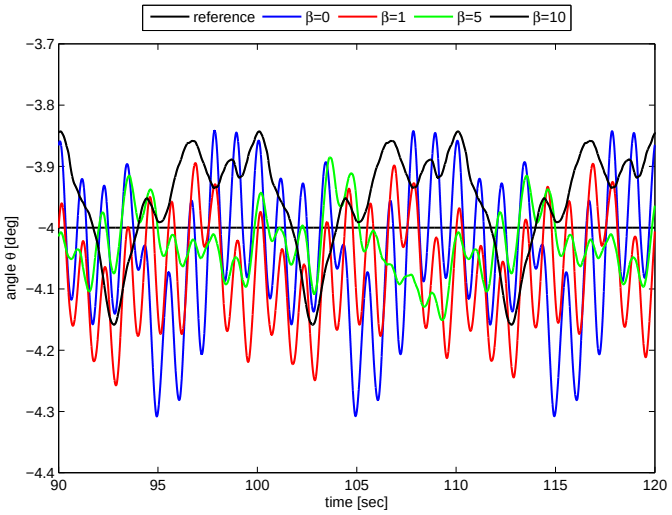

(a) Response output signal for $f_s = 1$ kHz

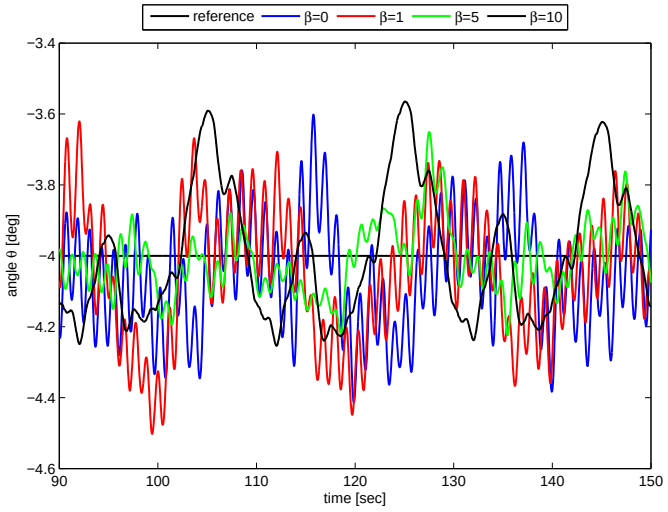

(b) Response output signal for $f_s = 50$ hz

Figure 6.17: Simulations: Response output signals when there is a bias on the nominal inner loop transfer functions based on Table 6.2.

Figure 6.18 shows that the addition of an extra delay causes the amplitude of the output response to increase.

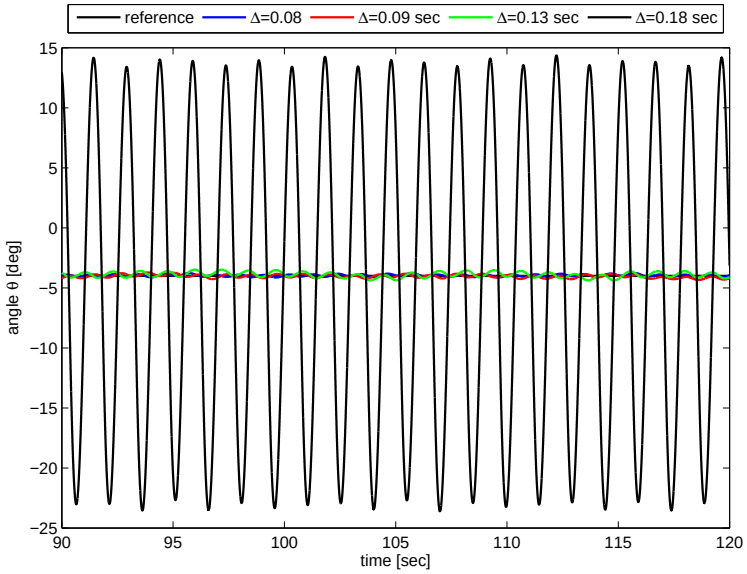

(a) Response output signal for $f_s = 1$ kHz

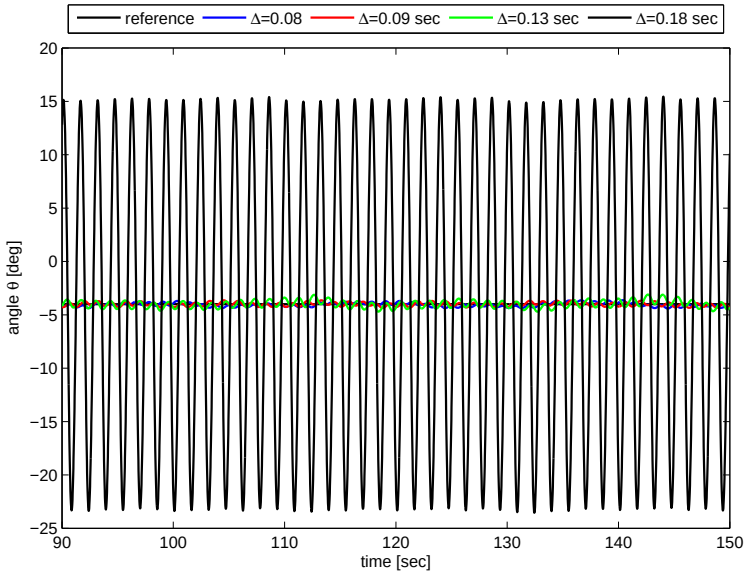

(b) Response output signal for $f_s = 50$ hz

Figure 6.18: Simulations: Response output signals when there is an additional delay on the nominal inner loop transfer functions based on Table 6.2.

Figure 6.19, shows the empirical relative sensitivity function of the output signal θ against changes the nominal transfer function of the inner loop actuator models. Figure 6.19a shows that the relative sensitivity function of the output response signal θ with respect to steady state gain G_{ss} increases in magnitude as the perturbation gets bigger. For ratios $\frac{G_{ss}}{G_{ss_o}} > 2$ the output signal is above the constraint limit $\pm 10^o$.

Figure 6.19b shows that the relative sensitivity function of the output θ with respect to steady state gain G_{ss} is parabolic, for sampling frequency $f_s = 50$ Hz. In these simulations only the first eleven perturbation values were used; above matlab was crashing.

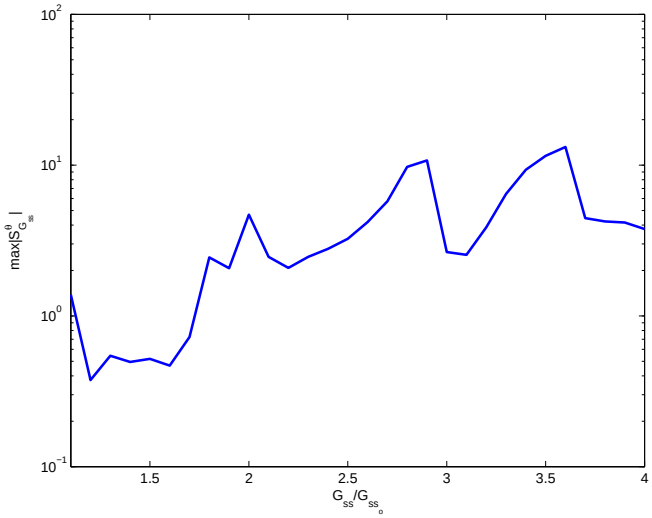

(a) Response output signal for $f_s = 1$ Khz

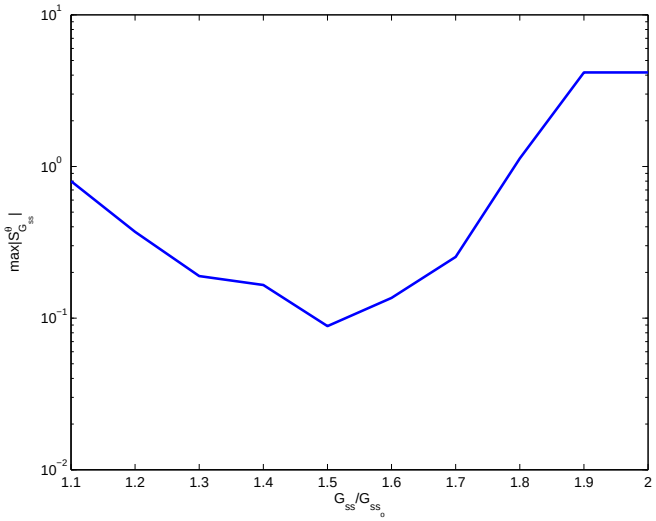

(b) Response output signal for $f_s = 50$ hz

Figure 6.19: Relative sensitivity function against changes in the nominal steady state gain of the inner loop models based on Table 6.2.

Figure 6.20 shows the relative sensitivity function of the output signal θ with respect to additional bias in the inner loop nominal transfer function models. The figures shows that the peak value of the relative selectivity function of the output response signal with respect to offsets in the nominal transfer function models is exponentially decreasing in magnitude as the offset value gets higher.

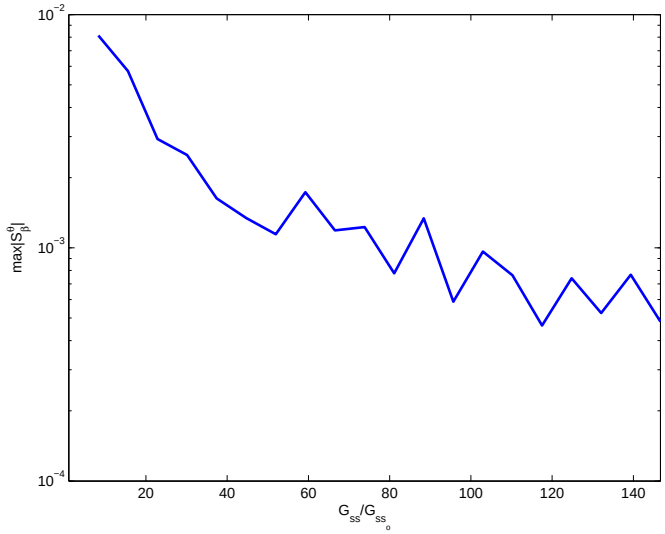

(a) Response output signal for $f_s = 1$ Khz

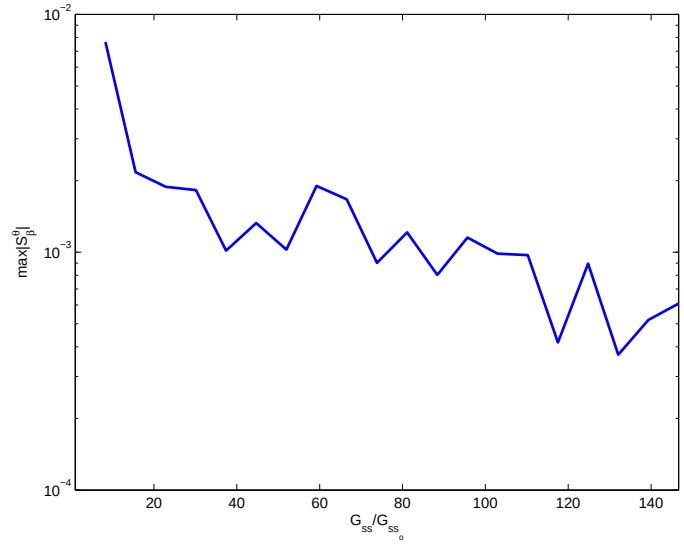

(b) Response output signal for $f_s = 50$ hz

Figure 6.20: Relative sensitivity function of the output signal θ against additional bias in the inner loop nominal transfer function models based on Table 6.2.

Figure 6.21 show the relative sensitivity function of the output signal θ against changes in the delay Δ of the nominal transfer functions of the actuator models. The

figures show that relative selectivity function of the output response with respect to additional delay Δ is parabolic both for sampling frequencies $f_s = 1$ kHz and $f_s = 50$ Hz. For additional delay above $\Delta > 0.18$ sec, the peak value of the sensitivity function increases in magnitude.

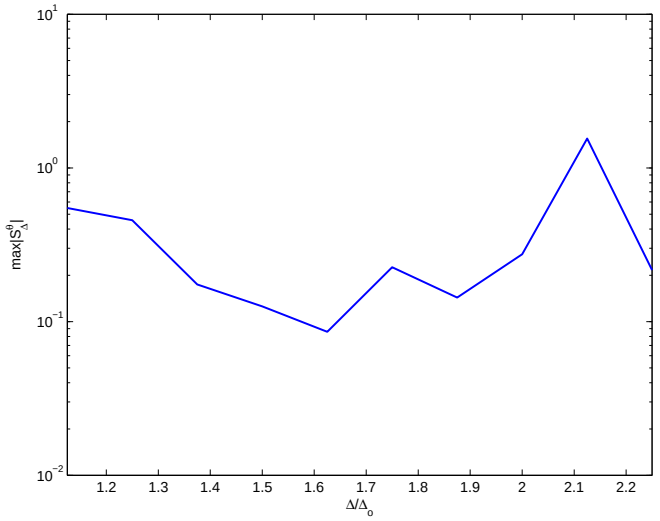

(a) Response output signal for $f_s = 1$ Khz

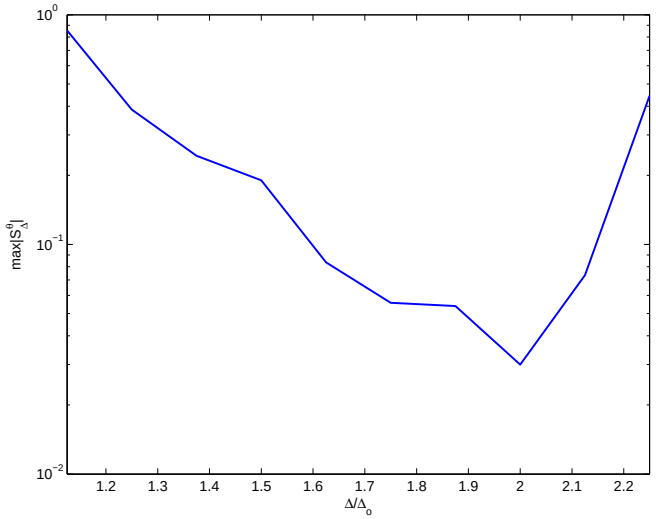

(b) Response output signal for $f_s = 50$ hz

Figure 6.21: Relative sensitivity function against changes in the delays Δ of the nominal inner loop transfer function models based on Table 6.2.

6.4 Discussion

A preliminary study has been applied to implement automatic balance control of an inverted pendulum with human dynamics using FES control of the lower leg muscles of a subject based on the experimental method of Gollee et al. [137]. The LQR method was used for the design of the IC controller as opposed to the use of pole placement. The reason was that using the LQR method it was possible to manipulate the weighting of the state matrices therefore control performance could be influenced. In particular, the relative weighting of the control signal could be adjusted. On the other hand, pole placement ensures stability by manipulating the poles based for example on the rise time, without consideration of control signal weighting.

The experiment showed that balance could not be implemented using the intermittent control system in real time. There is a limit cycle phenomenon which is due to closed-loop poles of the control system, hence any disturbance could have caused instability to the system. Indeed from the simulations it is shown that any perturbations in the steady state gains of the nominal inner loop transfer functions or additional delays could cause the system instability (Figs.6.16, 6.18, 6.19, 6.21).

An important contribution to the instability of the control system is the state constraints on the cascade control system. The simulations that were applied in which the actuator's control signal were constrained to ± 50 Nm resulted in instability of the control system. The control signal was constrained because physically the output signal, which is the output from the contraction of the calf muscles, must be within a limited range.

In addition, the initial condition of the internal (observer) model of the system did not correspond to that of the real plant, e.g. offsets in the ankle moment were present. This led to initially large control signals, which exceeded the constraints, although in steady-state the system could be controlled without exceeding the constraints. As a consequence it has been impossible to successfully apply automatic balance control using the existing modeling and control design of the cascade control system.

In this study, the intermittent controller was designed without including any constraints on the control system design or without having defined the initial conditions of the control system, the inverted pendulum. That according to Gawthrop et al.

[145] has as an effect on the state constraints of the system to be violated over the intermittent interval due to the use of the linear time-invariant feedback that is used in the unconstrained intermittent feedback. The intermittent controller should therefore be re-designed taking account of the constraints in the control system and to follow the method that has been suggested by Gawthrop and Wang [145].

Although the intergrator that was added at the controller design could reduce any effect of disturbances in steady-state, it generates a derivative state of the moment signal and that could be sensitive for the stabiltiy of the closed loop control system. An alternative way to using an integrator in the controller design is to use a disturbance observer whose aim is to estimate the constant disturbances and consider it in the controller. Another way could have been to use a disturbance observer with an intergrator action [40]. In this case, the disturbance observer adds another state which represents an estimate of the disturbance allowing the controller to compensate for that ([30] Sect. 18.7)

Furthermore, only one observer was used in the controller design, despite the fact that two different actuator models (i.e two different muscles) were used during the experiment. Therefore, probably switching observers could be have been a better solution for the design of the controller since both muscle actuators were firing at certain time during the experiment. However, the switching action needs to be optimised or improvised.

6.5 Conclusions

The theoretical sensitivity analysis has shown that the sampling frequency, the accuracy of the actuator model identification and the constraints on the states of the systems are important for the stability and performance of the intermittent controller. Further stability analysis is required in order the intermittent control to provide automatic balance in real time systems.

The conclusions derived from the automatic balance control study are:

1. The intermittent controller has to be redesigned taking account the contraints in the control system.

2. Switching observers could be another solution to the instability of the control system, since two muscle actuators are being used in the experiment.

3. The initial conditions of the controller model are important for the stability of the control system.

4. The integrator in the controller adds a derivative state representing the moment signal and that could be sensitive for the stabiltiy of the closed loop control system. An alternative way to using an integrator in the controller design is to use a disturbance observer whose aim is to estimate the constant disturbances allowing the controller to compensate for that.

.

Chapter 7

General Discussion

Although human sustained control movements are continuous in nature there is still a controversy on the mechanisms underlying such physiological systems. In compensatory tracking tasks the "human controller" is widely modelled as a continuous time system. Both in man-machine and physiological systems such that of human quiet standing the "human operator" is modelled as a continuous-time controller. Since the early years of human control modelling the servomechanism has been an adequate control model. For instance, the "human operator" in compensatory tracking tasks has been modelled as a lead-lag transfer function with a time delay plus a white noise with Gaussian characteristics signal to describe human variability [57, 91]. In addition, the non-predictive continuous-time PID model has been used either to simulate spontaneous sway [12] during human stance, or to fit experimental data taken from in tasks in which the surface is pseudo-randomly rotated [11] or translated [13,15]. Another continuous time system model that has been widely used to model sustained control tasks is predictive control [53] which is based on internal models [16] and includes prediction and optimisation. The continuous-time state Observer, Predictor, Feedback (OPF) structure of Kleinman [53] provides a paradigm for modelling human control systems. The OPF model has been shown to fit experimental data from simple man-machine visual-manual compensatory tracking tasks [17–19]. In addition, the same OPF model structure has been shown to fit experimental data from perturbed human balance control tasks [20,59] and experimental data from tasks in which subjects were required to balance an inverted pendulum which imitate human standing [25].

On the other hand, Craik [32, 33] and Vince [34] have suggested an intermittent basis for human control systems. Craik and Vince have shown that in ballistic control tasks humans respond to discrete stimuli at a constant frequency rate of two to three actions per second, therefore every 500 ms (i.e two Hz) unlike the frequency of the external disturbance signal. The operator's smooth response consists of a sequence of sub-movements, each planned in advanced using current information, however they are executed ballistically (open-loop), without being influenced by the feedback of the result. Although, the ideas of intermittency in human behaviour were suggested to explain tasks associated with discrete movements a series of sustained control physiological tasks have shown the intermittent control behaviour of humans during that tasks [37, 64, 81]. Using the materials developed in the third chapter of this thesis and in combination with the sustained control task of Loram et al. [28] it was possible to readdress the question of modelling sustained control physiological systems either as continuous-time or intermittent control systems.

The first step to answering the research question was taken in chapter 4 in which the deterministic part of each of the physiological experimental data derived from the visual-manual compensatory tracking balance task were modelled using the three different controller model candidates: a) non-predictive controller (NPC) b) predictive controller (PC) and c) intermittent controller (IC). This was achieved using the frequency domain identification method analysis based on the two stage approach of Pintelon and Schoukens [111], Ch.2). The two-stage frequency domain approach of Pintelon and Schoukens consisted of the following steps: First the non-parametric frequency response transfer function (FRF) was estimated from the experimental deterministic input/output data. Second, a parametric closed-loop FRF, for each of the three controller models, was fitted to the non-parametric FRF by adjusting the vector which included the weighted controller parameter factors, the feedback loop time delay and the intermittent interval for the IC.

The identification method has shown that the identified FRFs of the IC model fit the non-parametric FRFs only as well as the PC. The NPC didn't perform as well as the PC and IC. During the experiment the task was either i) keep the load position as close to the centre of the oscilloscope as possible i.e "minimise position" or ii) keep

the load position still and it does not matter where the load is on the screen, i.e "minimise velocity". The identified parameters for each of the control models reflected the control strategy adopted by the participant. In particular, for the position control task "minimise position" the weighting factor which corresponds to the position state was always larger than the weighting factor which corresponds to the velocity state and vice versa. On the other hand, numerically the identified NPC model resulted in optimal effective time delays, for all experimental data, smaller than the corresponding ones for the identified PC and IC. The same observation has been found in the study of Gawthrop et al. [25]. The non-parametric system identification method [25] resulted in the conclusion that although the simple non-predictive PID control system could fit well the experimental data from a visual-manual compensatory tracking task, the identified time-delays were found to be consistently less that those found from the experimental data. Also, other studies such that of Loram et al. [81] although they have shown that a PID controller with a time delay could fit very well experimental data taken from a tracking task, the optimised PID time delay was too low in relation to the mean response time delay found from the subjects who took part in the task. Also, Peterka [5] using simulations revealed that a PID feedback system with a time delay could be unstable if the system contained large loop time delays.

The mean optimal effective time delays for the PC and IC controller models were found to be very similar to each other and very close to that found from the physiological study of Loram et al. [24]. That indicated that the deterministic experimental data can be equally well explained using either the continuous-time PC of Kleinmann [53] or the intermittent control [42] excluding the NPC.

It is important to mention that during the identification method the local minima that were used palyed an important role in the identified results. It is true that any change in the initial conditions would change the identified delays in frequency domain identification using the experimental data. However, in this study, the local minima (i.e initial conditions) were kept the same throughout the procedure and also there was not any additional noise added during the identification procedure. Although the above is true the identified delays were found not only to be physiologically miningful as it has been discussed previously but also the resulted effective delays match with each

other which that shows that the procedure is not completely wrong. The identification method has been applied in frequency domain therefore any change in frequency domain would not affect the identifiction method, whereas if the method was applied in time domain the identification method would not be that straightforward in time domain.

Although the intermittent human control behaviour has been suggested for ballistic control tasks a series of sustained control tasks have shown the intermittent control behaviour of humans during that tasks. Lakie et al. [64] requested participants to manually balance a real inverted pendulum with human dynamics and low intrinsic stiffness. The experiment revealed that the load was balanced through discrete hand movements at a rate of about two to three adjustments per second. The rate of corrective actions observed in manually balancing a real inverted pendulum in the study of Lakie et al. [64] support that control is subject to the refractory period of two to three actions per second which is similar to that found in Vince [34] and Loram et al. [97]. The same low-frequency intermittent control behaviour has been observed in the study of Loram et al. [28]. The study has shown that tapping as opposed to continuously holding the joystick was more robust, more effective and natural and the response bandwidth was limited to one to two Hz which is based on the sampling process. Although this current study has not revealed a limited sampling bandwidth for the IC it has shown that the IC could fit the deterministic experimental data from a continuous process. The main reason for this is the masquerading property of the IC system matched hold [42]. The example in Section 4.2.4 has shown that the frequency response of the intermittent controller is almost indistinguishable to that of the corresponding predictive controller at lower frequencies and only diverges at higher frequencies.

The computational modelling of the "human controller" must consider both the deterministic and stochastic (random) response data that are generated by the controller during the task [27, 83]. For that reason, chapter 5 focused on the modelling of the non-deterministic experimental data. The remnant signal in the human response signal during the motor control task was modelled as an intermittent controller with a varied intermittent interval. The IC model was compared with the predictive controller in which variability is modelled as a motor-dependent noise or observation noise. An

indirect computational method was applied to determine the best variability model that described the remnant signals that were generated for every participant. In particular, the computational modelling of the remnant signal was implemented in two stages. In the first stage the artificial controllers PC and IC were parametrised at the excited frequencies and the optimal controller parameters for the experimental data were defined (the method is described in Ch.4). In the second stage a parameter for each of the variability models that describe the remnant signal was varied over a predefined range and each control system was simulated for each value. In particular, for the independent observation white Gaussian noise signal, the parameter was considered to be the standard deviation of the normal distribution. For the motor dependent noise signal model, the parameter was the standard deviation of the normally distributed noise signal. For the IC with varied intermittent interval the parameter was considered the shape parameter of an inverse Gaussian distribution which defined the distribution of the intermittent interval. The simulated data were then analysed at excited and non-excited frequencies. The parametric control power spectrum (PSD) at non-excited frequencies was compared against the experimental PSD remnant signal, and the best noise model and variability parameter for each of the controllers were defined based on the quadratic cost function. The study has shown that the PSD of the remnant signals generated from each subject can be described equally well either using an intermittent controller with a varied intermittent interval or a continuous-time predictive controller with noise. This was revealed by evaluating the minimum cost function values for each control systems and variability models. In addition, graphically the IC could fit the experimental PSD data equally well compared to the predictive control model with noise. The IC also showed qualitatively that it could model the variability that is exhibited during motor control tasks. A non-parametric one-way statistical test has shown that the simulated median PSD data both, at excited and non-excited frequencies, are statistically different ($p < 0.05$) among its repetitions.

For the first time in this study it was shown that an engineering control system model can describe human variability that is exhibited during motor control tasks as a structure of the controller model. Modelling human variability as an intermittent controller with a varied intermittent interval has a physiological basis and not a

statistical explanation as using added noise. In this study, human variability is linked to the intermittent behaviour of the "human controller" in which the intermittent interval is not constant but it varies over time. This means that the time it takes to respond to the stimuli is varied and it is not constant. This is connected to the refractory period which is not only observed in ballistic control tasks [32–34] but also in sustained control tasks [96]. Van de Kamp et al. [96] in their study have shown refractoriness in sustained visual-manual control tasks, which is directly related to the intermittent human behaviour during these tasks. Therefore, explaining modelling human variability as an IC with varied intermittent interval has a natural and potentially testable basis since it adds evidence for the intermittent behaviour of human during motor control tasks.

Having successfully modelled the human operator as an intermittent control system the last chapter of the analysis (Chapter 6) attempted to apply the intermittent control in real time in the context of the physiological control mechanism of human standing balance. This chapter aimed to apply an experimental method following the study of Gollee et al. [137] to apply automatic artificial balance of an inverted pendulum, in the context of human standing, via functional electrical stimulation (FES) control of the muscles of the lower leg of a healthy subject. The muscles of the lower leg of the subject, Gastrocnemious (GA) and Tibialis Anterior (TA) were the actuators of the control system. The experiment showed that balance could not be implemented using the intermittent control system in real time. A limit cycle phenomenon was observed in the time-domain results, which is due to closed-loop poles of the control system. The reason is that the closed loop poles of the control system were very close to the imaginary axis, hence any disturbance could have caused instability to the system. Indeed from the simulations it was shown that any perturbations in the steady state gains of the nominal inner loop transfer functions or additional delays could cause system instability.

However the most important factor causing the instability of the control system were the constraints imposed on the cascade control system. Therefore it looks impossible to apply automatic balance control using the existing modelling and control design of the cascade control system. In this study, the intermittent controller was designed

without including the actuator constraints. That according to Gawthrop et al. [145] has the effect the state constraints of the system are violated over the intermittent interval due to the use of the linear time-invariant feedback control signal that is used in the unconstrained intermittent feedback. In addition, the state constraints on the cascade system along with the initial conditions, which are difficult to control, are the main reason for the instability of the control system.

Although the intergrator that was added at the controller design could reduce any effect of disturbances in steady-state, it generates a derivative state of the moment signal and that could be sensitive for the stabiltiy of the closed loop control system. An alternative way to using an integrator in the controller design is to use a disturbance observer whose aim is to estimate the constant disturbances and consider it in the controller. Another way could have been to use a disturbance observer with an intergrator action [40]. In this case, the disturbance observer adds another state which represents an estimate of the disturbance allowing the controller to compensate for that ([30] Sect. 18.7)

Furthermore, only one observer was used in the controller design, despite the fact that two different actuator models (i.e two different muscles) were used during the experiment. Therefore, probably switching observers could have been a better solution for the design of the controller since both muscle actuators were firing at certain time during the experiment.

The intermittent controller needs to be re-designed taking account the constraints in the control system, following the methods that have been suggested by Gawthrop and Wang [145].

7.1 Limitations and future work

In the present section the limitations and future work in relation to computational modelling of sustained control mechanisms as intermittent control models is discussed.

Frequency response of the IC controller

In this research study, based on the ensemble average, for the first time, the IC controller was analysed and applied in frequency domain. The ensemble of the IC control system as it has been explained and described in Section 4.2.4 is applied only when the intermittent interval is fixed. Due to the ensemble average the frequency response of the IC controller's signal output can masquerade as the frequency response of the underlying predictive controller in low frequencies and only diverge in high frequencies due to the aliasing that occurs in the IC models because of the sampling rate which is the reciprocal of the intermittent interval. In future, it would be challenging to study the IC controller in frequency domain in the case where the intermittent interval varies. It would be interesting to study if the IC controller with varied intermittent interval could be analysed in frequency domain and if so how it behaves.

Controller model

The experimental data that were used in this study were taken from the study of Loram et al. [28]. During the experiment the subjects were asked to control the inverted pendulum by manipulating a single-axis joystick. In the design of the intermittent controller the dynamics of the hand were not considered. Therefore the control signal was generated by the artificial controller without considering the hand muscle dynamics. Usually, the hand dynamics are modelled as a first or second order linear system with a time constant of approximately 100 ms. The fact that in the IC modelling design we did not consider the muscle dynamics of the hand that manipulates the joystick did not has detrimental effects on the results. The time-domain control signal for the IC controller results typically in a jump of the control signal at the start of the intermittent interval, in the presence of a disturbance. In frequency domain, this jump results in high-frequency components. However, when calculating the ensemble average the individual jumps get averaged out, resulting in a smooth control signal which has less power at high frequencies. This has also been illustrated in the example given in Section 4.2.4. Therefore, this means that the ensemble average has the effect of

decreasing the response at high frequencies. This is similar to the effect of multiplying a high frequency response with a low-pass filter such that of the hand dynamics.

Human variability using an intermittent controller with a varied intermittent interval.

The human variability chapter (Chapter 5) has shown that the IC with a varied intermittent interval can describe the remnant signal that is generated at the frequency response of the human controller's signal response. The study has shown that human variability could be explained by random intermittency which is natural and has a physiological basis [96]. Although this model could describe human variability, future work is to study event-driven intermittent control based on a threshold, therefore the variation would be due to the event-triggering via threshold which is a more natural process to humans. The study could focus on how variation in intermittent interval is related to threshold, signal and system properties by studying different control models such as zero first or second order models and applying different signal models either periodic or random.

Connection of the control task with human balance. This study modelled a sustained motor control balance task that describes human quiet standing. The truth is that quiet standing is a more complicated process, however, experiments that study processes of that mechanism should not be considered as meaningless. A future work could be to apply the intermittent controller using multiple-input multiple-output (MIMO) dynamic systems which resemble the physiological mechanism of human quiet standing.

Control of quiet standing

It was attempted to apply the IC controller is real time in the context of the physiological control mechanism of human standing balancing, using FES control of the calf muscles of a subject. The attempt failed due to the design problems of the controller, important factors such as sampling rate and system constraints were not considered in the initial design. Future work is to redesign the controller taking into account the constraints of the system model and the available sampling rate which is based in the FES stimulator.

7.2 Conclusions

The study has arrived into some simple general conclusions. A human sustained control balance task could be modelled as an intermittent control system. The study has clearly illustrated that both the deterministic and non-deterministic responses that were generated during the physiological control mechanism could be modelled using an intermittent controller model [42] based on the underlying continuous-time predictive control model of Kleinman [53]. The intermittent paradigm behaviour originates in the study of Craik and Vince using discrete tracking control tasks [32–34], however, there is a large evidence of the human intermittent control behaviour in sustained control mechanisms [24, 28, 64, 81]. The study has shown in a computational level that a sustained control mechanism could be modelled as an intermittent control model.

In this study, intermittent control frequency domain identification has been applied to a human control task for the first time, and has shown that is can describe this as well as a predictive controller. In addition it has been shown that the IC can model remnant by implementing its source as a structural property of the controller, rather than as external added noise. This provides the basis for a more physiological meaningful explanation of human variability.

References

[1] M. L. Latash and V. M. Zatsiorsky, *Classics in Movement Science*. Human Kinetics, 2001.

[2] M. L. Latash, *Synergy*. Oxford University Press, Inc, 2008.

[3] R. A. Schmidt and T. D.Lee, *Motor Control and Learning: A behavioural emphasis*. 5th edn. IL Champaign Human Kinetics, 2011.

[4] D. M. Wolpert, Z. Ghahramani, and M. I. Jordan, "An internal model for sensorimotor integration," *Science*, vol. 269, pp. 1880–1882, 1995.

[5] R. J. Peterka, "Postural control model interpretation of stabilogram diffusion," *Biol Cybern*, vol. 83, pp. 335–343, 2000.

[6] I. D. Loram, C. N. Maganaris, and M. Lakie, "Human postural sway results from frequent, ballistic bias impulses by soleus and gastrocnemius," *J Physiol*, vol. 564, pp. 295–311, 2005.

[7] T. Kiemel, K. S. Oie, and J. J. Jeka, "Slow dynamics of postural sway are in the feedback loop," *J Neurophysiol*, vol. 95, pp. 1410–1418, 2006.

[8] W. H. Levison, S. Baron, and D. L. Kleinman, "A model for human controller remnant," *IEEE Trans Man – Machine Sys*, vol. 10, pp. 101–108, 1969.

[9] D. T. McRuer, "Human dynamics in man-machine systems," *Automatica*, vol. 16, pp. 237–253, 1980.

[10] R. Johansson, M. Magnusson, and M. Akesson, "Identification of human postural dynamics," *IEEE Trans on Biomed Eng*, vol. 35, pp. 858–869, October 1988.

[11] R. J. Peterka, "Sensorimotor integration in human postural control," *J Neurophysiol*, vol. 88, pp. 1097–1118, 2002.

[12] C. Maurer and R. J. Peterka, "A new interpretation of spontaneous sway measures based on a simple model of human postural control," *J Neurophysiol*, vol. 93, pp. 189–200, 2005.

[13] A. Alexandrov, A. A. Frolov, F. B. Horak, P. Carlson-Kuhta, and S. Park, "Feedback equilibrium control during human standing," *Biol Cybern*, vol. 93, no. 5, pp. 309–322, 2005.

[14] H. van der Kooij and E. de Vlugt, "Postural responses evoked by platform pertubations are dominated by continuous feedback," *J Neurophysiol*, vol. 2, pp. 730–743, 2007.

[15] T. D. J. Welch and L. H.Ting, "A feedback model reproduces muscle activity during human postural response to support surface translations," *J Neurophysiol*, vol. 99, pp. 1032–1038, 2008.

[16] D. M. Wolpert, R. C. Miall, and M. Kawato, "Internal models in the cerebellum," *Trends Cogni Sci*, vol. 2, pp. 338–347, 1998.

[17] S. Baron and D. L. Kleinman, "The human as an optimal controller and information processor," *IEEE Trans Man – Machine Sys*, vol. MMS-10, pp. 9–17, 1969.

[18] D. L. Kleinman, S. Baron, and W. H. Levison, "An optimal control model of human response.I: Theory and validation," *Automatica*, vol. 6, pp. 357–369, 1970.

[19] S. Baron, D. L. Kleinman, and W. H. Levison, "An optimal control model of human response part II: Prediction of human perrformance in a complex task," *Automatica*, vol. 6, pp. 371–383, 1970.

[20] H. van der Kooij, R. Jacobs, B. Koopman, and H. Grootenboer, "A multisensory intergration model of human stance control," *Biol Cybern*, vol. 80, pp. 299–308, 1999.

[21] E. Todorov and M. I.Jordan, "Optimal feedback control as a theory of motor coordination," *Nat Neurosci*, vol. 5, pp. 1226–1235, 2002.

[22] J. A. Doeringer and N. Hogan, "Intermittency in Preplanned Elbow Movements Persists in the Absence of Visual Feedback," *J Neurophysiol*, vol. 80(4), pp. 1787–1799, 1998.

[23] J. L. Cabrera and J. G. Milton, "On-off intermittency in a human balancing task," *Phys Rev Lett*, vol. 89(15), p. 158702, 2002.

[24] I. D. Loram, M. Lakie, and P. J. Gawthrop, "Visual control of stable and unstable loads: what is the feedback delay and extent of linear time-invariant control?," *J Physiol*, vol. 587.6, pp. 1343–1356, 2009.

[25] P. J. Gawthrop, I. D. Loram, and M. Lakie, "Predictive feedback in human simulated pendulum balancing," *Biol Cybern*, vol. 101, pp. 131–146, 2009.

[26] C. M. Harris and D. M. Wolpert, "Signal-dependent noise determines motor planning," *Nature*, vol. 394, pp. 780–784, 1998.

[27] A. A. Faisal, L. P. J. Selen, and D. M. Wolpert, "Noise in the nervous system," *Nat Rev Neurosci*, vol. 9, pp. 292–303, 2008.

[28] I. D. Loram, H. Gollee, M. Lakie, and P. J. Gawthrop, "Human control of an inverted pendulum : Is continuous control necessary? is intermittent control effective? is intermittent control physiological?," *J Physiol*, vol. 589, pp. 307–324, 2011.

[29] O. J. M. Smith, "A controller to overcome dead time," *ISA Journal*, vol. 6, pp. 28–33, 1959.

[30] G. C. Goodwin, S. F. Graebe, and M. E. Salgado, *Control System Design*. Prentice Hall, New Jersey, 2001.

[31] Y. Asai, Y. Takasa, K. Nomura, T. Nomura, M. Casadio, and P. G. Morasso, "A model of postural control in quiet standing: robust compensation of delay-induced instability using intermittent activation of feedback control," *PLoS One*, vol. 4, p. e6169, 2009.

[32] K. J. W. Craik, "Theory of the human operator in control systems I: The operator as an engineering system," *Brit J Phychol Gen Sect*, vol. 38, pp. 56–61, 1947.

[33] K. J. W. Craik, "Theory of human operators in control systems II: Man as an element in a control system," *Brit J Phychol Gen Sect*, vol. 38, pp. 142–148, 1948.

[34] M. A. Vince, "The intermittency of control movements and the physiological refractory period," *Brit J Phychol Gen Sect*, vol. 38, pp. 149–157, 1948.

[35] F. Navas and L. Stark, "Sampling or intermittentncy in hand control system dynamics," *J Biophys*, vol. 2, pp. 252–302, 1968.

[36] P. D. Neilson, M. D. Neilson, and N. J. O'Dwyer, "Internal models and intermittency: A theoritical account of human tracking behaviour," *Biol Cybern*, vol. 58, pp. 101–112, 1988.

[37] M. Lakie and I. D. Loram, "Manually controlled human balancing using visual, vestibular and proprioceptive senses involves a commmon low frequency neural process," *J Physiol*, vol. 557.1, pp. 403–416, 2006.

[38] R. Fitzpatrick, R. B. Gorman, D. Burke, and S. C. Gandevia, "Postural proprioceptive reflexes in standing human subjects: bandwidth of response and transmission characteristcs," *J Physiol*, vol. 458, pp. 69–83, 1992.

[39] P. J. Gawthrop and L. Wang, "Intermittent model predictive control," *Proc IMechE, Part I: J Systems and Control Engineering*, vol. 221(7), pp. 1007–1018, 2007.

[40] P. J. Gawthrop and L. Wang, "Event-driven intermittent control," *Int J Control*, vol. 82, pp. 2235 – 2248, 2009.

[41] P. J. Gawthrop and L. Wang, "The sytem-matched hold and the intermittent control separation principle," *Int J Control*, vol. 84, pp. 1965–1974, 2011.

[42] P. J. Gawthrop, I. D. Loram, M. Lakie, and H. Gollee, "Intermittent control: A computational theory of human control," *Biol Cybern*, vol. 104, pp. 31–51, 2011.

[43] T. Estrada, H. Lin, and P. Antsaklis, "Model-based control with intermittent feedback," *Contr Autom Med conference*, 2006.

[44] T. Estrada and P. J. Antsaklis, "Model-based control with intermittent feedback: bridging the gap between continuous and instantaneous feedback," *Int J Control*, vol. 83(12), pp. 2588–2605, 2000.

[45] M. Margaliot, "Stability analysis of switched systems using variational principles : an introduction," *Automatica*, vol. 42(12), pp. 307–324, 2006.

[46] H. Lin and P. Antsaklis, "Stability and stabilizability of switched linear systems: A survey of recent results," *IEEE Trans Autom Control*, vol. 54(2), pp. 308–322, 2009.

[47] E. Ronco, T. Arsan, and P. J. Gawthrop, "Open-loop intermittent feedback control: Practical continuous-time gpc," *IEE Proc Part D Control Theory Appl*, vol. 146, pp. 426–434, 1999.

[48] H. Demirciogly and P. Gawthrop, "Continuous-time Generalised Predictive Control (CGPC)," *Automatica*, vol. 27(1), pp. 5–74, 1991.

[49] D. W. Clarke, C. Mohtadi, and P. S. Tuffs, "Generalized Predictive Control - Part I. the basic Algorithm," *Automatica*, vol. 23(2), pp. 137–148, 1987.

[50] D. W. Clarke, C. Mohtadi, and P. S. Tuffs, "Generalized Predicitve Control- Part II. Extensions and Interpretations," *Automatica*, vol. 23(2), pp. 149–160, 1987.

[51] J. B. Rawlings, "Tutorial overview of model predictive control," *IEEE Control Syst Mag*, vol. 20(3), pp. 38–52, 2000.

[52] L. Wang, *Model predicitve control system design and implementation using MATLAB*. 1st ed. London, 2009.

[53] D. L. Kleinman, "Optimal control of linear systems with time-delay and observation noise," *IEEE Trans Automatic Control*, vol. 14, pp. 524–527, 1969.

[54] H. Gollee, A. Mamma, I. D. Loram, and P. J. Gawthrop, "Frequency-domain Identification of the Human Controller," *Biol Cybern*, vol. 106, pp. 359–372, 2012.

[55] A. Mamma, H. Gollee, P. J. Gawthrop, and I. D. Loram, "Intermittent control explains human motor remnant without additive noise," in *Proc 19th Med Conf on Control and Automation*, pp. 558–563, 2011.

[56] P. J. Gawthrop, "Frequency-domain analysis of intermittent control," *Proc IMechE Part I: J Systems and Control Engineering*, vol. 223, pp. 591–603, 2009.

[57] D. T. McRuer and H. R. Jex, "A review of quasi-linear pilot models," *IEEE Trans Hum Factors Electron*, vol. HFE-8, pp. 824–832, 1967.

[58] D. A. Winter, A. E. Patla, S. Rietdyk, and M. G. Ishad, "Ankle muscle stiffness in the contol of balance during quiet standing," *J Neurophysiol*, vol. 85, pp. 2630–2633, 2001.

[59] H. van der Kooij, R. Jacobs, B. Koopman, and F. van der Helm, "An adaptive model of sensory intergration in a dynamic environment applied to human stance control," *Biol Cybern*, vol. 84, pp. 103–115, 2001.

[60] A. B. Slifkin and K. M. Newell, "Is variability in human performance a reflection of system noise?," *Curr Dir Phychol Sci*, vol. 7, pp. 170–177, 1998.

[61] H. van der Kooij, E. van Asseldonka, and F. C. T. van der Helm, "Comparison of different methods to identify and quantify balance control," *J Neurosci Methods*, vol. 145, pp. 175–203, September 2005.

[62] H. van der Kooij and R. Peterka, "Non-linear stimulus-response behavior of the human stance control system is predicted by optimisation of a system with sensory and motor noise," *J Comput Neurosci*, vol. 30, pp. 759–778, 2011.

[63] K. Davids, S. Bennett, and K. Newell, *Movement system variability.* Human Kinetics, 2006.

[64] M. Lakie, N. Caplan, and I. D. Loram, "Human balancing of an inverted pendulum with a compliant linkage: neural control by anticipatory intermittent bias," *J Physiol*, vol. 551, pp. 357–370, 2003.

[65] R. Shadhmehr. and F. A. Mussa-Ivaldi, "Adaptive representation of dynamics during learning of a motor task," *J Neurosci*, vol. 14(5), pp. 3208–3224, 1994.

[66] J. R. Flanagan and A. M. Wing, "The role of internal models in motion planning and control: Evidence from grip force adjustments during movements of hand-held loads," *J Neurosci*, vol. 17(4), pp. 151–1528, 1997.

[67] M. Kawato, "Internal models for motor control and trajectory planning," *Curr Opin Neurobiol*, vol. 9(6), pp. 718–727, 1999.

[68] R. C. Miall and D. M. Wolpert, "Forward models for physiological motor control," *Neur Netw*, vol. 9, no. 8, pp. 1265–1279, 1996.

[69] D. M. Wolpert and Z. Ghahramani, "Computatioal principles of movement neuroscience," *Nature*, vol. 3, pp. 1212–1217, 2000.

[70] A. Karniel, "Open Questions in Computational Motor Control," *J Integr Neuro*, vol. 10, pp. 385–411, 2011.

[71] P. Morasso, "Spatial control of arm movement," *Exp Brain Red*, vol. 42(2), pp. 223–227, 1981.

[72] P. R. Davidson and D. M. Wolpert, "Widespread access to predictive models in the motor system: a short review," *J Neural Eng*, vol. 2, pp. s313–s319, 2005.

[73] E. Poulton, *Tracking Skill and Manual Control.* Academic Press,Inc, 1974.

[74] D. A. Winter, "Human balance and postural control during standing and walking," *Gait Posture*, vol. 3, pp. 193–241, 1995.

[75] D. A. Winter, A. E. Patla, F. Prince, and M. Ishac, "Stiffness control of balance in quiet standing," *J Neurophysiol*, vol. 80, pp. 1211–1221, 1998.

[76] D. Elliott, W. F. Helsen, and R. Chua, "A century later: Woodworth's (1899) two-component model of goal-directed aiming," *J Psychol Bull*, vol. 127(3), pp. 342–357, 2001.

[77] E. R. Hoffmann, "Contributions of pre-fitts Researchers to Goal-Directed Aiming studies," *J Mot Behav*, vol. 44(1), pp. 27–46, 2012.

[78] S. W. Keele and M. I.Posner, "Processing of visual feedback in rapid movements," *J Exp Pscyhol*, vol. 77(1), pp. 155–158, 1968.

[79] R. W. Pew, "Performance of human operators in a three-state relay control system with velocity-augmented displays," *IEEE Trans Hum Factors Electron*, vol. HFE-7(2), pp. 77–83, 1966.

[80] S. Skogestad and I. Postlethwaite, *Multivariable Feedback Control Analysis and Design*. Willey, New York, 1996.

[81] I. D. Loram, P. J. Gawthrop, and M. Lakie, "The frequency of human, manual adjustment in balancing an inverted pendulum is constrained by instrinsic physiological factors," *J Physiol*, vol. 577.1, pp. 417–432, 2006.

[82] R. C. Mial, D. J. Weir, and J. F. Stein, "Intermittency in human manual tracking tasks," *Motor Behav*, vol. 25(1), pp. 53–63, 1993.

[83] M. A. Rilley and M. Turvey, "Variability and determinism in motor behavior," *J Mot Behav*, vol. 34(2), pp. 99–125, 2002.

[84] R. A. Schmidt, H. Zelaznik, B. Hawkins, J. S. Frank, and J. T. Q. Jr, "Motor-Output Variability- A theory for the accuracy of rapid motor acts," *Psychol Rev*, vol. 86(5), pp. 415–451, 1979.

[85] R. J. van Beers, P. Haggard, and D. M. Wolpert, "The role of execution noise in movement variability," *J Neurophysiol*, vol. 91, pp. 1050–1063, 2004.

[86] A. B. Slifkin and K. M. Newell, "Noise, Information and Force Variability," *J Exp Phych*, vol. 25, pp. 837–851, 1991.

[87] E. Todorov, "Optimality principles in sensimotor control," *Nat Neurosci*, vol. 7, pp. 907–915, 2004.

[88] R. J. van Beers, P. Baraduc, and D. M. Wolpert, "Role of uncertainty in sensorimotor control," *Philos R Soc Lond B Biol Sci*, vol. 357(1424), pp. 1137–1145, 2002.

[89] P. M. Fitts, "The information capacity of the human motor system in controlling the amplitude of movement," *J Exp Psychol*, vol. 47(6), pp. 381–391, 1964.

[90] L. D. Metz, "A time-varying approach to the modeling of human control remnant," *IEEE Trans Syst Man Cybern*, vol. SMC-12, pp. 24–35, 1982.

[91] D. T. McRuer and E. S. Kredel, "The human operator as a servo system element," *J Franklin Institute*, vol. 267(5), pp. 381–403, 1959.

[92] M. Flanders, "What is the biological basis of sensimotor integration," *Biol Cybern*, vol. 104, pp. 1–8, 2011.

[93] P. J. Gawthrop, M. Lakie, and I. D. Loram, "Predictive feedback control and Fitt's Law," *J Biol Cybern*, vol. 98, pp. 229–238, 2008.

[94] C. W. Telford, "The refractory phase of voluntary and associative responses," *Exp Psychol*, vol. 14(1), pp. 1–36, 1931.

[95] H. Pashler, "Dual-task interference in simple tasks: data and theory.," *Psychol Bull*, vol. 116(2), pp. 220–244, 1994.

[96] C. van de Kamp, P. J. Gawthrop, H. Gollee, and I. D. Loram, "Refracroriness in sustained visual-manual control: is the refractory duration intrinsic or does it depend on external system properties," *PLoS Comput Biol*, vol. 9(1), p. e1002843, 2013.

[97] I. D. Loram, C. van de Kamp, H. Gollee, and P. Gawthrop, "Identification of intermittent control in man and machine," *J. R. Soc. Interface*, vol. 9(74), pp. 2070–2084, 2012.

[98] P. J. Gawthrop and L. Wang, "Intermittent predictive control of an inverted pendulum," *Control Eng Pract*, vol. 221(7), pp. 1007–1018, 2006.

[99] P. J. Gawthrop and H. Gollee, "Intermittent tapping control," *Proc IMechE, Part I: J Systems and Control Engineering*, vol. 226(9), pp. 1262–1273, 2012.

[100] T. Insperger, "Act-and-wait concept for continuous-time control systems with feedback delay," *IEEE Trans Control Syst*, vol. 14(5), pp. 974–977, 2006.

[101] P. J. Gawthrop, "Act-and-wait and intermittent control: Some comments," *IEEE Trans Control Syst Techol*, vol. 18(5), pp. 1195–1198, 2010.

[102] D. M. Wolpert, R. C. Mial, J. L. Winter, and J. F. Stein, "Evidence for an error deazone in compensatory tracking," *J Mot Behav*, vol. 24(4), pp. 299–308, 1992.

[103] S. Hanneton, A. Berthoz, J. Droulez, and J. J. E. Slotine, "Does the brain use slinding variables for the control of movements?," *Biol Cybern*, vol. 77(6), pp. 381–393, 1997.

[104] V. Squeri, M. L. Casadio, P. G. Morasso, and E. Vergano, "Force-field componsation in a manula tracking task," *PLoS One*, vol. 5(6), p. e11189, 2010.

[105] A. Bottaro, Y. Yasutake, T. N. M. Casadio, and P. G. Morasso, "Bounded stability of the quiet standing posture: An intermittent control model," *J Hum Mov Sci*, vol. 27, pp. 473–495, 2008.

[106] M. Smith, "Theories of the psychological refractory period," *J Psycol Bull*, vol. 67(3), pp. 202–213, 1967.

[107] P. D. Neilson and M. D. Neilson, "An overview of adaptive model theroy: solving the problems of redundancy, resources, and nonlinear interactions in human movement control," *J Neural Eng*, vol. 2, pp. S279–S312, 2005.

[108] R. Bye and P. Neilson, "The bump model of response planning: variable horizon predictive control accounts for the speed-accuracy tradeoffs and velocity profiles of aimed movement.," *J Hum Mov Sci*, vol. 27(5), pp. 771–798, 2008.

[109] M. A. Vince, "Corrective movements in a pursuit task," *J Psychol*, vol. 1, pp. 85–103, 13 March 1948.

[110] L. Ljung, *System Identification: Theory for the User*. NJ:Prentice Hall, 2nd ed. ed., 1987.

[111] R. Pintelon and J. Schoukens, *System Identification – a Frequency Domain Approach*. IEEE Press, 2001.

[112] G. C. Goodwin and M. Salgado, "Frequency domain sensitivity ffunction for continuous time systems under sampled data control," *Automatica*, vol. 30(8), pp. 1263–1270, 1994.

[113] P. Gatev, S. Thomas, T.Kepple, and M. Hallett, "Feedforward ankle strategy of balance during quiet stance in adults," *J Physiol*, vol. 514.3, pp. 915–928, 1999.

[114] R. C. Fitzpatrick, J. L. Taylor, and D. I. McCloskey, "Ankle stiffness of standing humans in response to imperceptible perturbation: Reflex and task-dependent components," *J. Physiol*, vol. 454, pp. 533–547, 1992.

[115] I. Loram and M. Lakie, "Human ballancing of an inverted pendulum :position contol by small, ballistic-like,throw and catch movements," *J Physiol*, vol. 540, pp. 1111–1124, February 2002.

[116] I. D. Loram, C. N. Maganaris, and M. Lakie, "Active non-spring like muscle movements in human postural sway: How might paradoxical changes in muscles length be produced?," *J Physiol*, vol. 564, pp. 281–293, 2005.

[117] P. Morasso, L. Baratto, R. Carpa, and G. Spada, "Internal models in the contol of posture," *Neur Netw*, vol. 12, pp. 1173–1180, 1999.

[118] I. D. Loram and M. Lakie, "Direct measurement of human ankle stiffness during quiet standing: the intrinsic mechanical stiffness is insufficient for stability," *J Physiol*, vol. 545, pp. 1041–1053, 2002.

[119] M. Casadio, P. G. Morasso, and V. Sanguineti, "Direct measurement of ankle stiffness during quiet standing: Impications for contol modelling and clinical application," *Gain Posture*, vol. 21, pp. 41–424, 2005.

[120] I. D. Loram, C. N. Maganaris, and M. Lakie, "Paradoxical muscle movement during postural control," *Med Sci Sports Exerc*, vol. 41(1), pp. 198–204, 2009.

[121] G. F.Franklin, J. Powell, and A. Emami-Naeini, *Feedback Control of Dynamic systems*. Pearson ,Prentice Hall, 2006.

[122] K. S. Oie, T. Kiemel, and J. J. Jeka, "Multisensory fusion: simulations re-weighting of vision and touch for the control of human posture," *Cogni Brain Res*, vol. 14, pp. 164–176, 2002.

[123] R. Pintelon, J. Schoukens, and Y. Rolain, *Frequency-Domain Approach to Continuous-time System Identification: Some Practical Aspects (Chapter 8).* Springer, 2008.

[124] I. D. Loram, S. M.Kelly, and M. Lakie, "Human ballancing of an inverted pendulum:is sway size controlled by ankle impedane?," *J Physiol*, vol. 532, pp. 879–891, 22 December 2001.

[125] H. Kwakernaak and E.Sivan, *Linear optimal control system.* Willey, New York, 1972.

[126] J. Nocedal and S. Wright, *Numerical optimization.* Springer series in operations research, 2nd edition, 2006.

[127] W. H. Levison and J. I. Elkind, "Two dimensional manual control systems with separated displays," *IEEE transactions on human factors in electronics*, vol. HFE, pp. 202–209, 1967.

[128] T. Dijkstra, "A gentle introduction to the dynamic set-point model of human postural control during perturbed stance," *Hum Mov Sci*, vol. 19, pp. 567–595, 2000.

[129] R. A. Schmidt, *Motor Learning & Performance.* Human Kinetics Books, 1991.

[130] R. Shadmeir and S. Mussa-Ivaldi, *Biological Learning and Control.* MIS Press Cambridge, Massachusetts London, Englan, 2012.

[131] J. L. Folks and R. S. Chhikara, "The inverse gaussian distribution and its statisitcal application- a review," *Journal of the Royal Statistical Society*, vol. 40, pp. 263–289, 1978.

[132] M. . Hollander and D. A. Wolfe, *Nonparametric Statistical Methods.* Hoboken, NJ, 1999.

[133] P. J. Gawthrop and E. Ronco, "Predictive pole-placement control with linear models," *Automatica*, vol. 38, pp. 421–432, 2002.

[134] R. Fitzpatrick, D. Burke, and S. C. Gandevia, "Task-Dependent reflex responses and movement illusions evoked by galvanic vestibular stimulation in standing humans," *J. Physiol*, vol. 478(2), pp. 363–372, 1994.

[135] R. Fitzpatrick, D. K. Rogers, and D. I. McCloskey, "Stable human standing with lower-limb muscle afferents providing the only sensory input," *J Physiol*, vol. 15, pp. 385–403, 1994.

[136] R. Fitzpatrick, D. Burke, and S. C. Gandevia, "Loop gain of reflexes controlling human standing measured with the use of postural and vestibular disturbances," *J Neurophysiol*, vol. 76, pp. 3994–4008, 1996.

[137] H. Gollee, K. J. Hunt, and D. E.Wood, "New results in feedback control of unsupported standing in paraplegia," *IEEE Trans Neural Syst Rehabil Eng*, vol. 12, pp. 73–80, 2004.

[138] K. J. Hunt, M. Munih, and N. de N. Donaldson, "Feedback control of unsupported standing in paraplegia- part I: optimal control approach," *IEEE Trans Rehabil Eng*, vol. 5, pp. 331–340, 1997.

[139] K. Hunt, M. Munih, N. de N. Donaldson, and F. D. Barr, "Optimal control of ankle joint moment: toward unsupported standing in paraplegia," *IEEE Trans Autom Control*, vol. 43, no. 6, pp. 819–832, 1998.

[140] K. J. . Hunt, H. Gollee, and R. P. Jaime, "Control of paraplegic ankle joint stiffness using fes while standing," *Med Eng Phys*, vol. 23, pp. 541–555, 2001.

[141] K. J. Hunt, H. Gollee, R. P. Jaime, and N. de N. Donaldson, "Design of feedback controllers for paraplegic standing," *IEE Proc Control Theory Appl*, vol. 148, no. 2, pp. 97–108, 2001.

[142] A. V. Hill, *First and last Experiments in Muscle Mechanics*. Syndics of the Cambridge University Press, 1970.

[143] R. Shadhmer and S. P. Wise, *Computational Neurobiology of Reaching and Pointing: A Foundation for Motor Learning*. MIS Press Cambridge, MA, 2005.

[144] W. J. Karnavas, P. J. Sanchez, and A. T. Bahill, "Sensitivity Analyses of Continuous and Discrete Systems in the Time and Frequency Domain," *IEEE Trans Syst Man Cybern*, vol. 23(2), pp. 488–500, 1993.

[145] P. J. Gawthrop and L. Wang, "Constrained intermittent model predictive control," *Int J Control*, vol. 82, pp. 1138–1147, 2009.

Appendix A

Figures chapter 4

In this Appendix individual results relating to chapter 4 are shown.

Figures A.1, A.2, A.3 show the results for the control strategy **"minimise position" control strategy**.

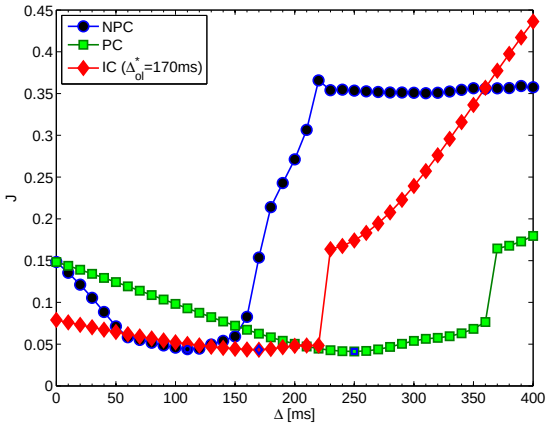

(a) Subject 1

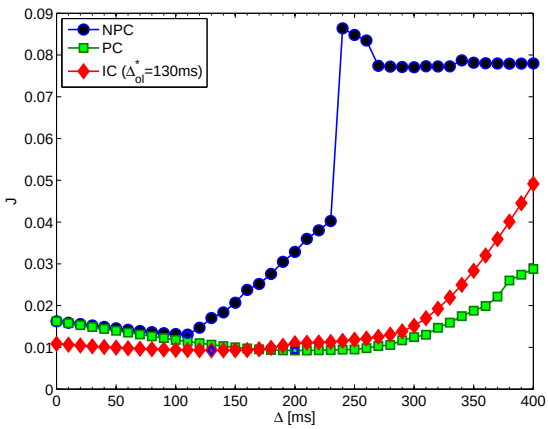

(b) Subject 2

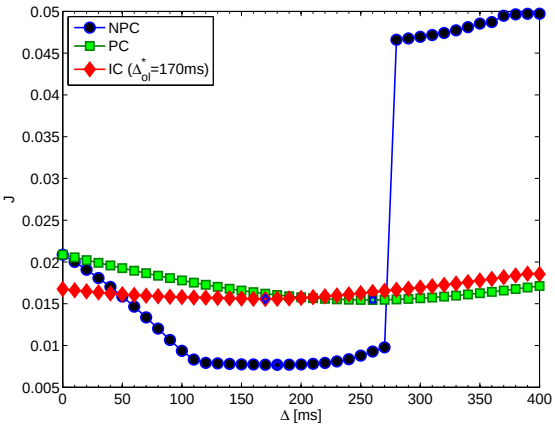

(c) Subject 4

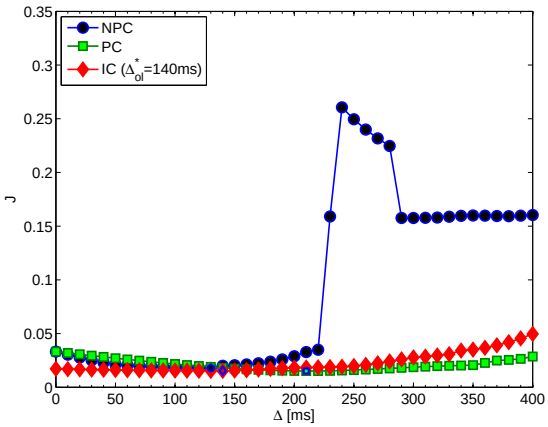

(d) Subject 5

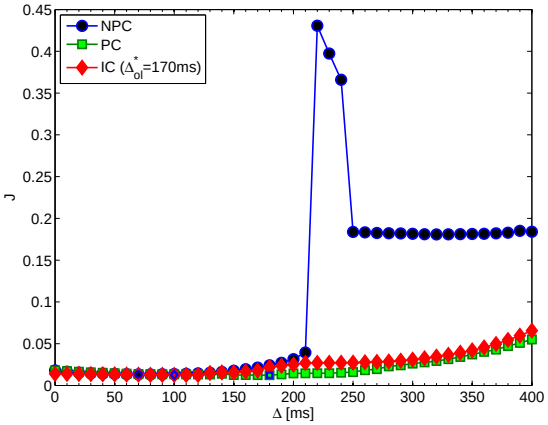

(e) Subject 6

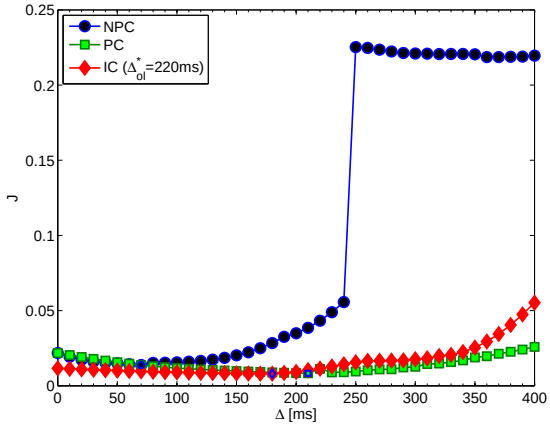

(f) Subject 7

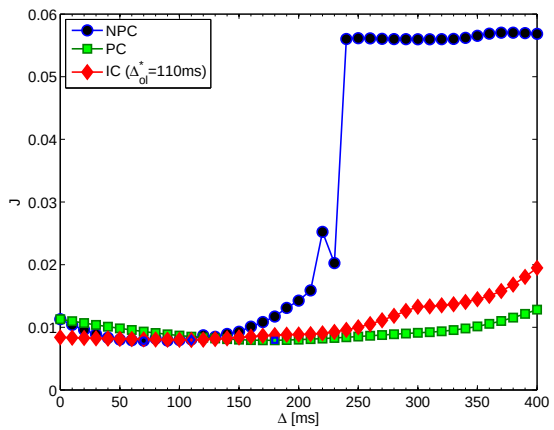

(g) Subject 8

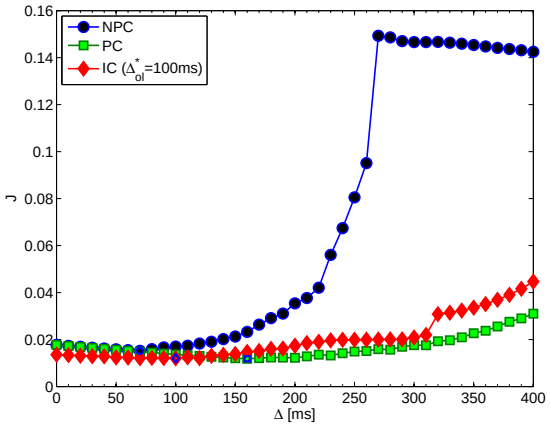

(h) Subject 9

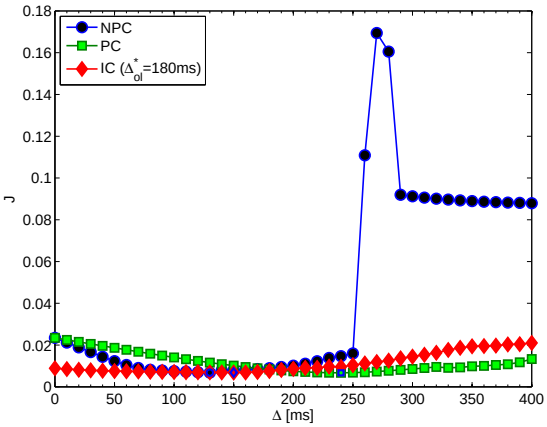

(i) Subject 10

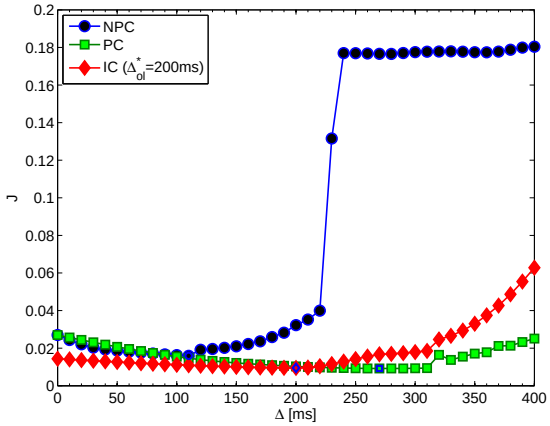

(j) Subject 11

Figure A.1: Cost functions against time delay for all subjects for the "minimise position" control strategy. The figures show the cost functions against the time delay Δ, for every controller structure NPC PC, IC. Blue line indicates the cost function derived from the identification of the NPC, the green line indicates the cost function derived from the identification of the PC and the red line indicated the cost function that derived from the identification using the IC. The bold markers indicate the minimum cost defined from the identification method for the corresponding controller structure. For the IC controller the intermittent interval Δ^*_{ol} corresponding to the minimum of J is given in the legend.

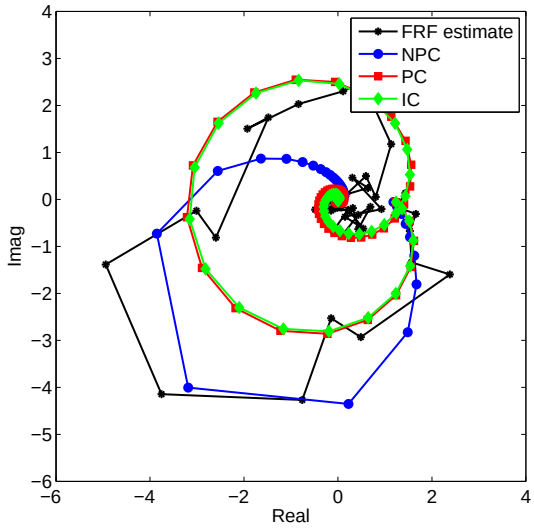

(a) Subject 1

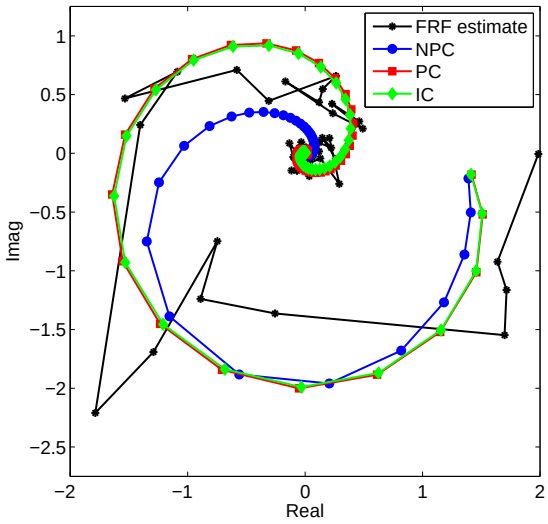

(b) Subject 2

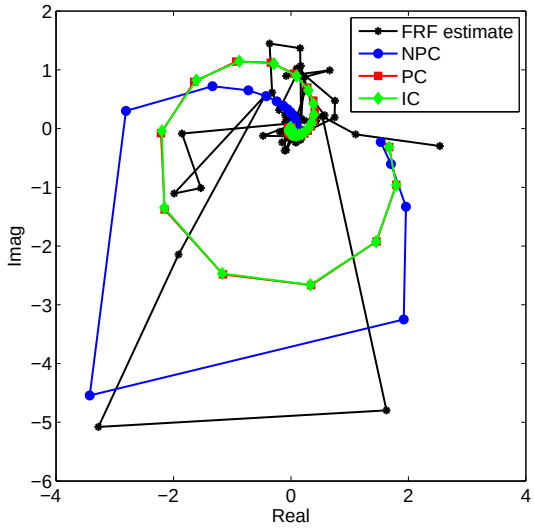

(c) Subject 4

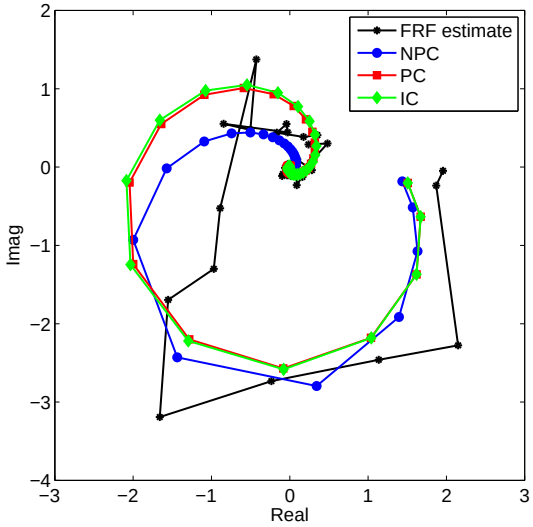

(d) Subject 5

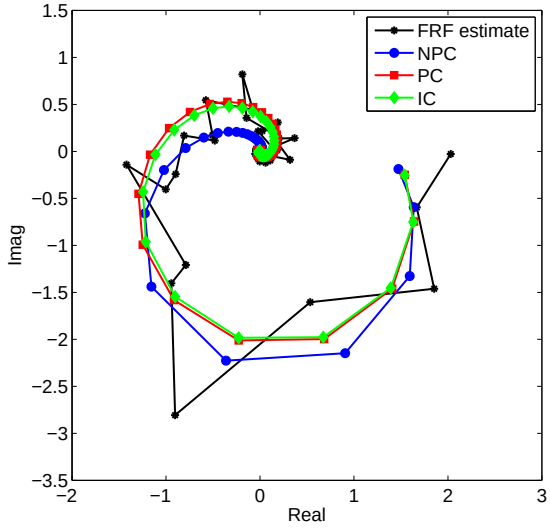

(e) Subject 6

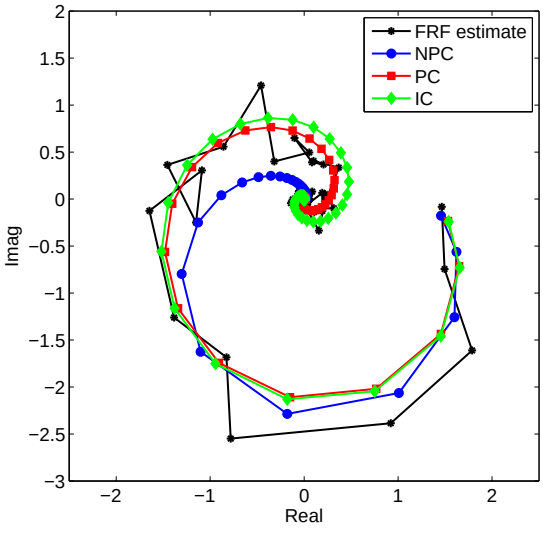

(f) Subject 7

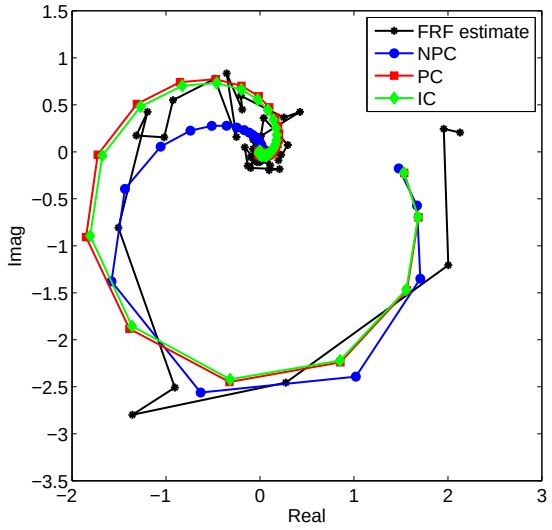

(g) Subject 8

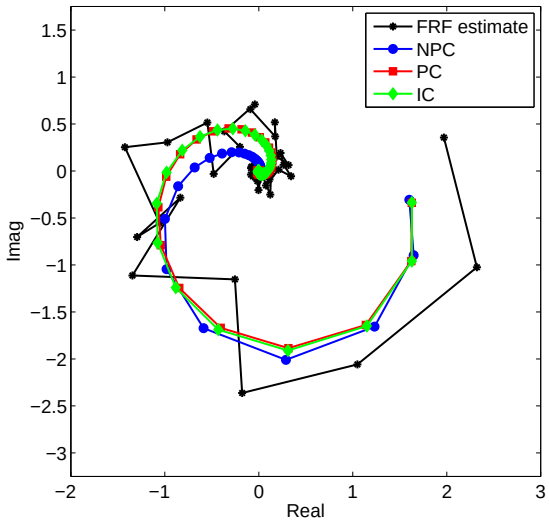

(h) Subject 9

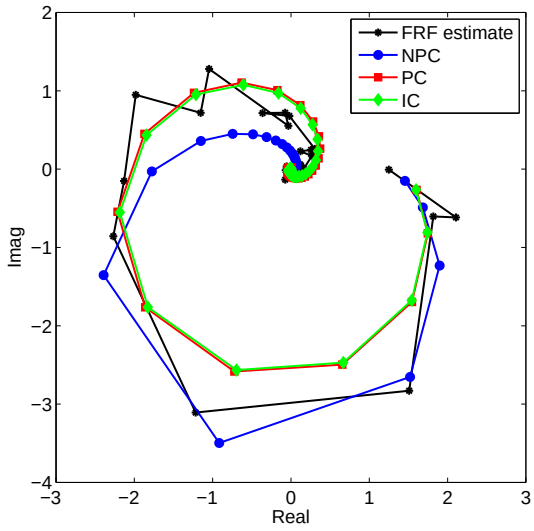

(i) Subject 10

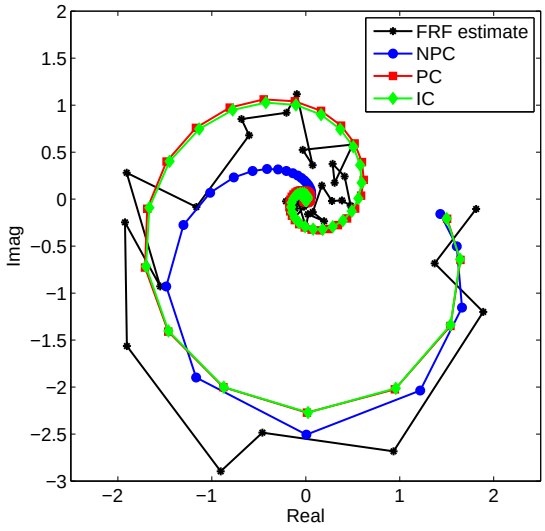

(j) Subject 11

Figure A.2: Closed-loop Nyquist plots of the estimated frequency responses T, for the subjects, against the optimised responses $\hat{T}$ for the "minimise position" control strategy.

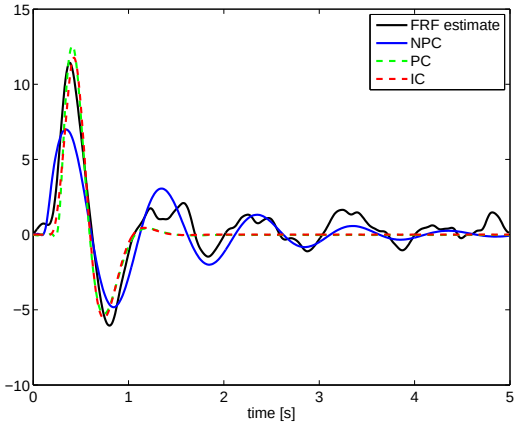

(a) Subject 1

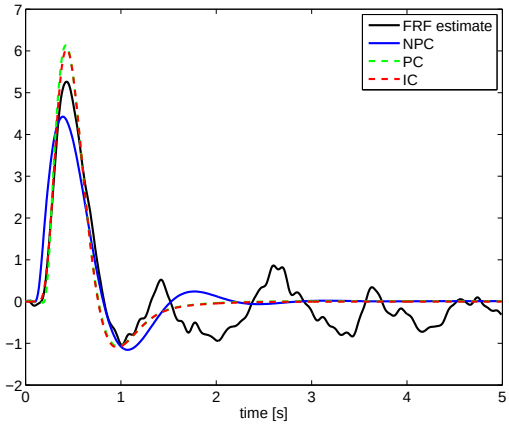

(b) Subject 2

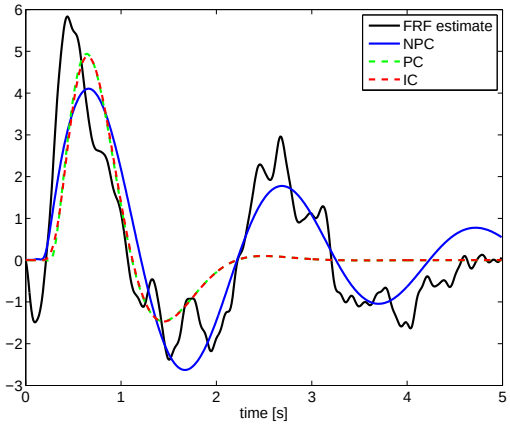

(c) Subject 4

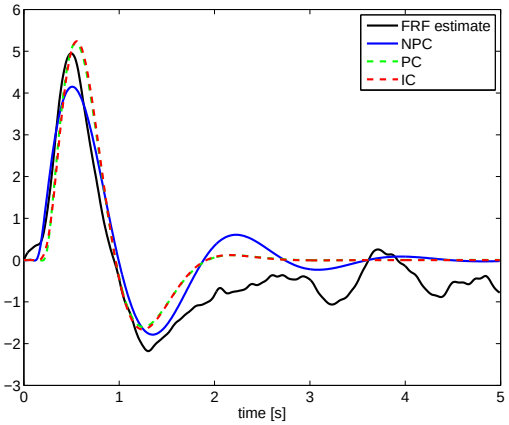

(d) Subject 5

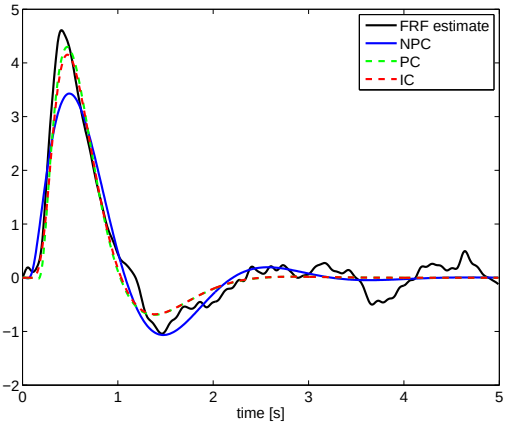

(e) Subject 6

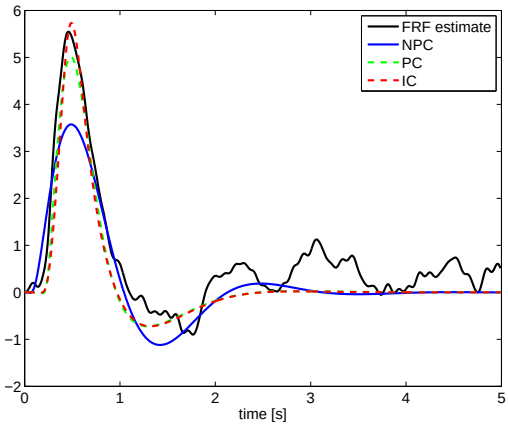

(f) Subject 7

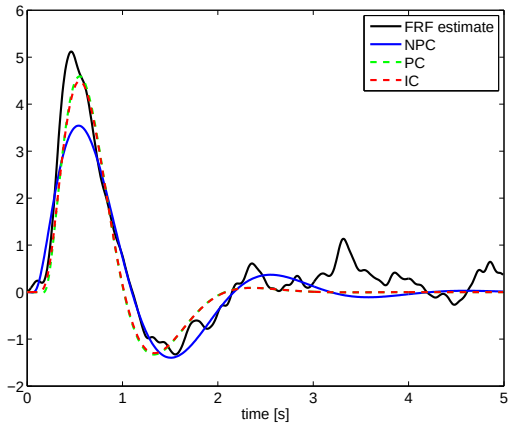

(g) Subject 8

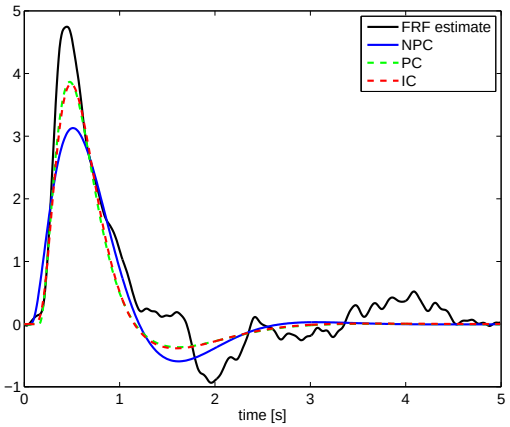

(h) Subject 9

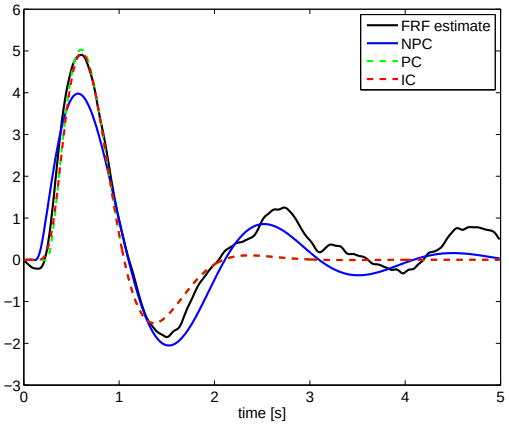

(i) Subject 10

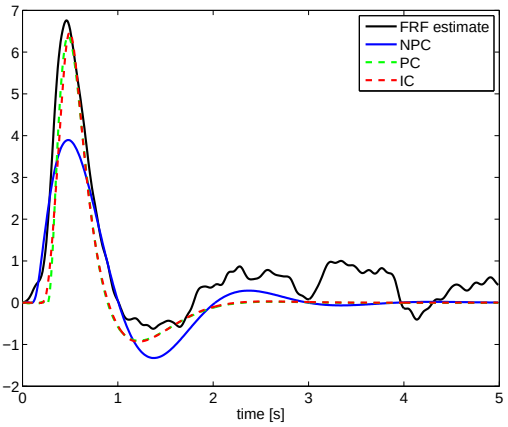

(j) Subject 11

Figure A.3: Impulse responses plots obtained from the estimated frequency responses (black line) and from the fitted responses for the different controller structures (coloured lines).

Figures A.4, A.5, A.6 show the results for the control strategy **"minimise velocity" control strategy**.

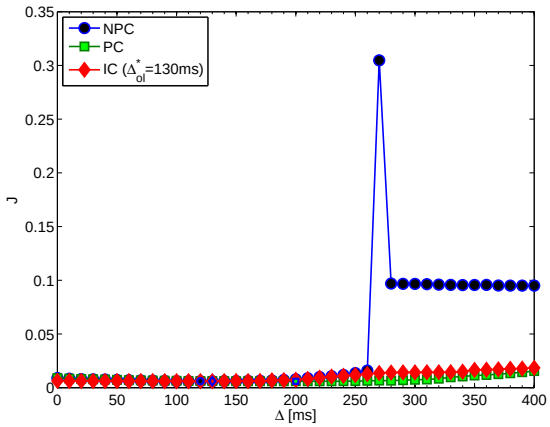

(a) Subject 1

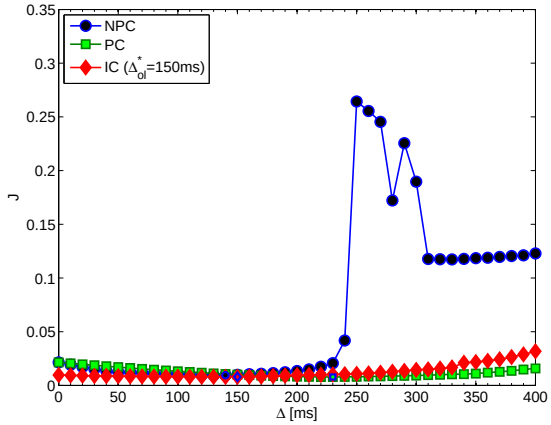

(b) Subject 2

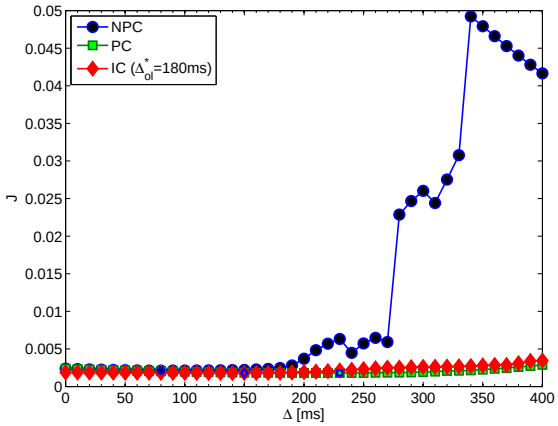

(c) Subject 4

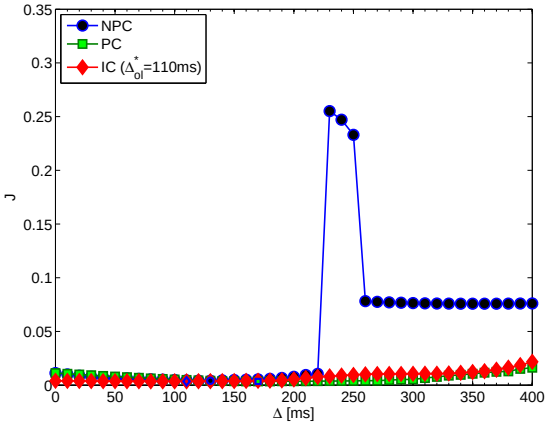

(d) Subject 5

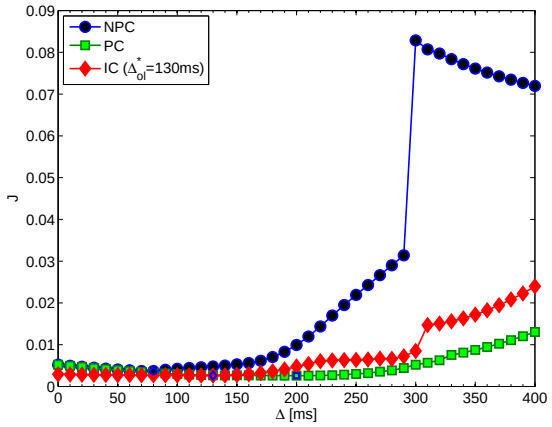

(e) Subject 6

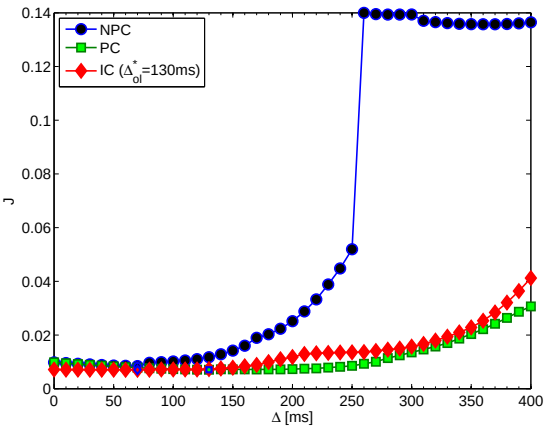

(f) Subject 7

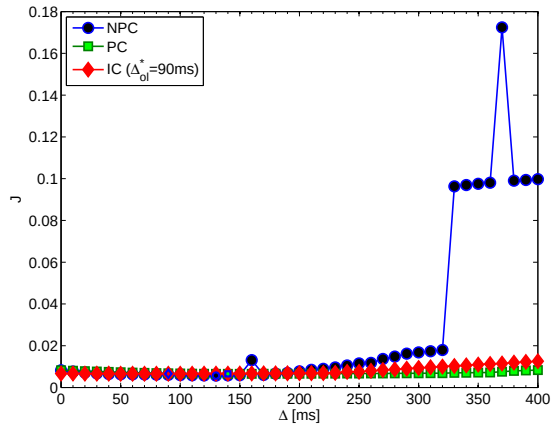

(g) Subject 8

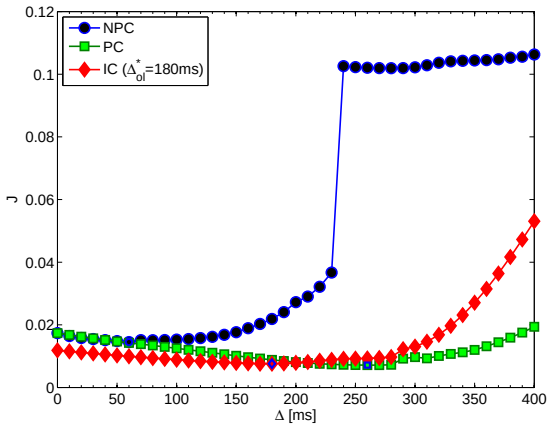

(h) Subject 9

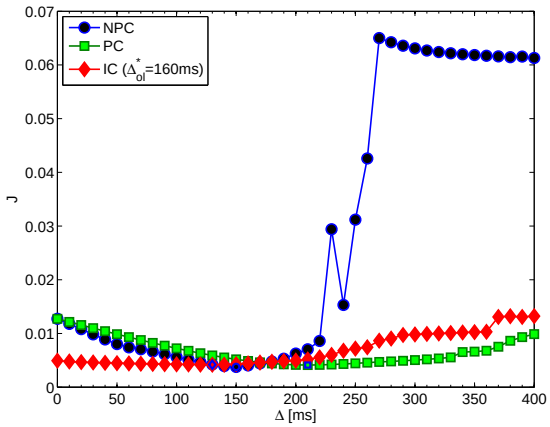

(i) Subject 10

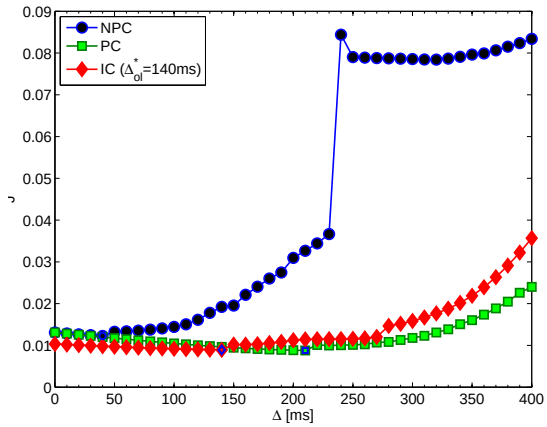

(j) Subject 11

Figure A.4: Cost functions against time delay for all subjects for the "minimise position" control strategy. The figures show the cost functions against the time delay Δ, for every controller structure NPC PC, IC. Blue line indicates the cost function derived from the identification of the NPC, the green line indicates the cost function derived from the identification of the PC and the red line indicated the cost function that derived from the identification using the IC. The bold markers indicate the minimum cost defined from the identification method for the corresponding controller structure. For the IC controller the intermittent interval Δ^*_{ol} corresponding to the minimum of J is given in the legend.

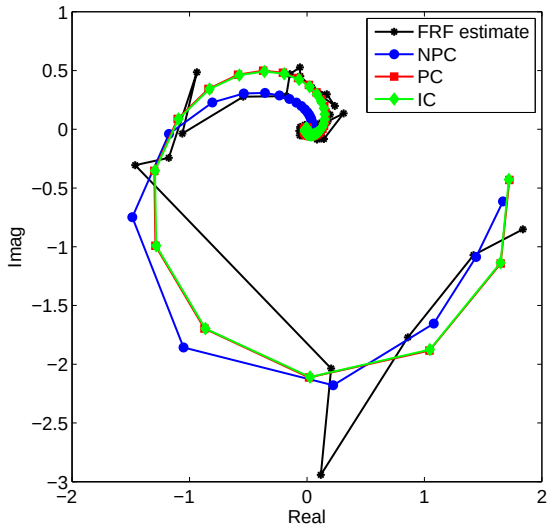

(a) Subject 1

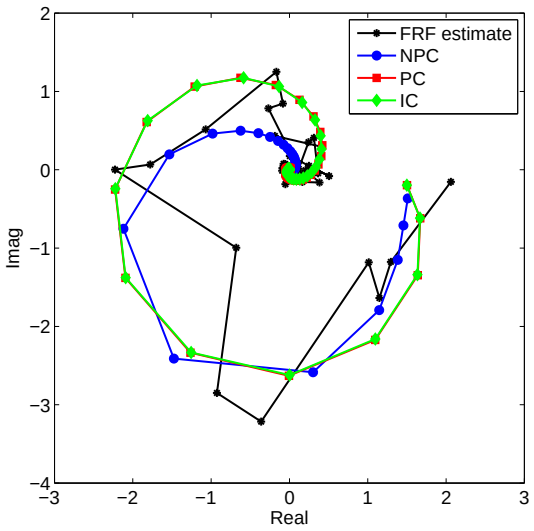

(b) Subject 2

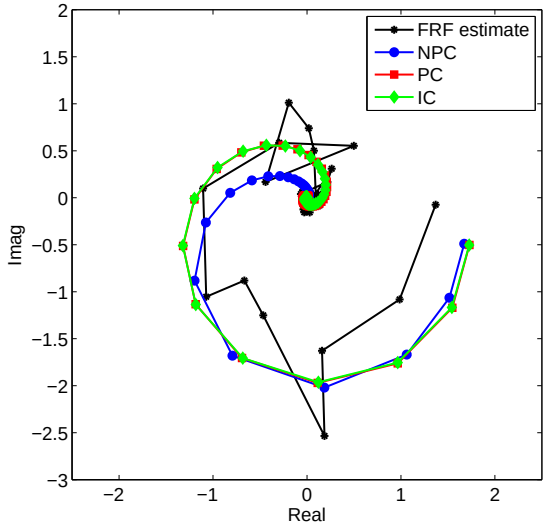

(c) Subject 4

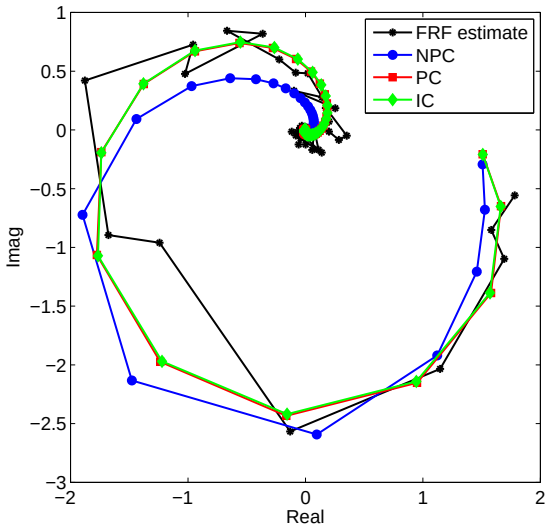

(d) Subject 5

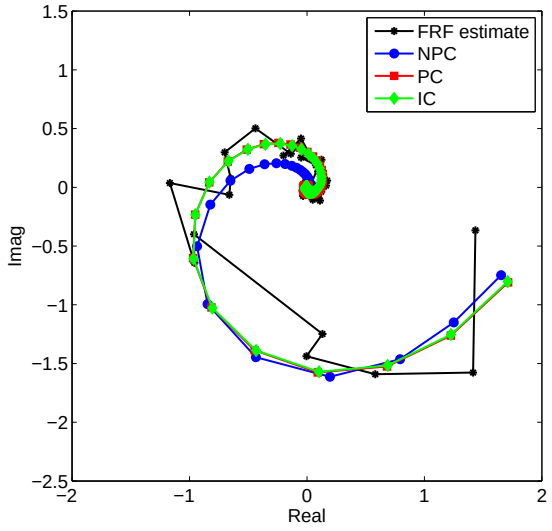

(e) Subject 6

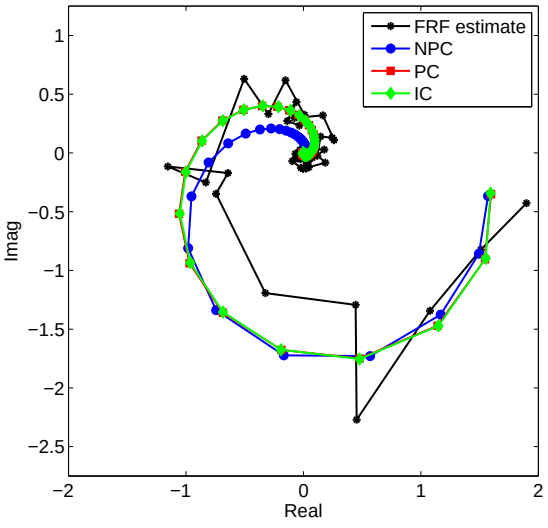

(f) Subject 7

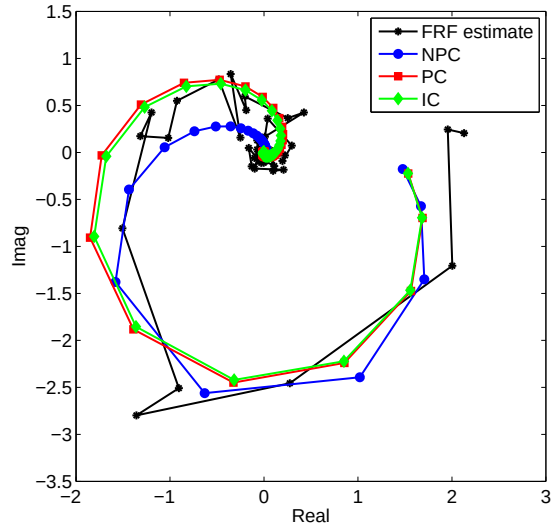

(g) Subject 8

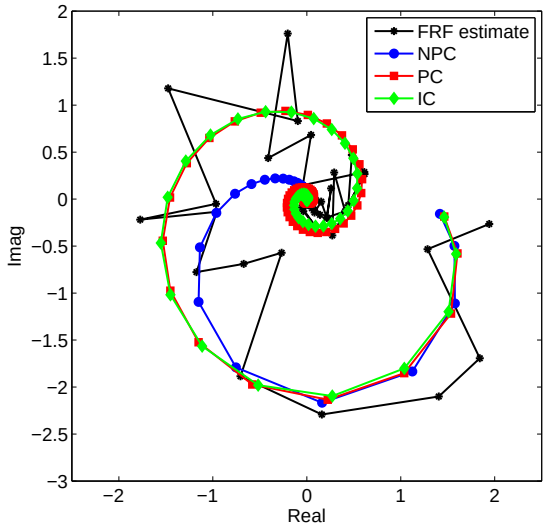

(h) Subject 9

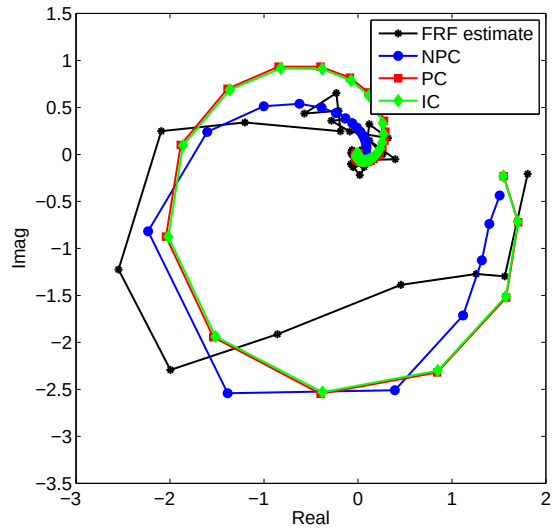

(i) Subject 10

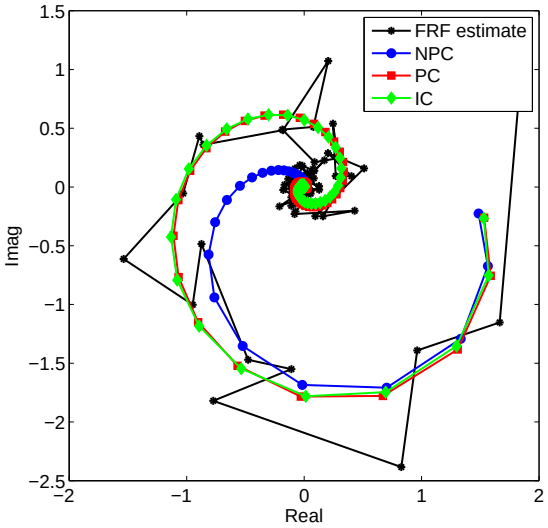

(j) Subject 11

Figure A.5: Closed-loop Nyquist plots of the estimated frequency responses T, for the subjects, against the optimised responses $\hat{T}$ for the "minimise position" control strategy.

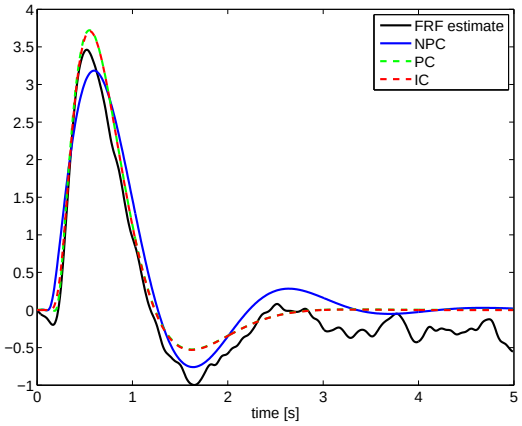

(a) Subject 1

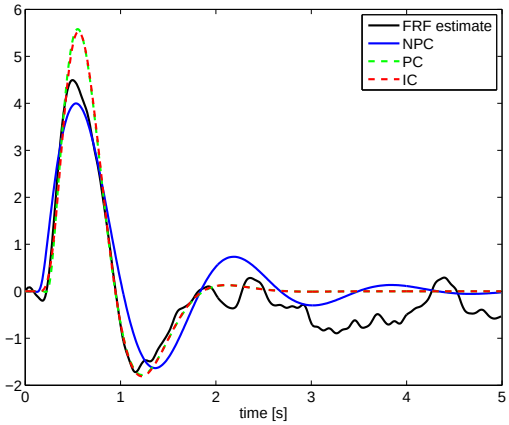

(b) Subject 2

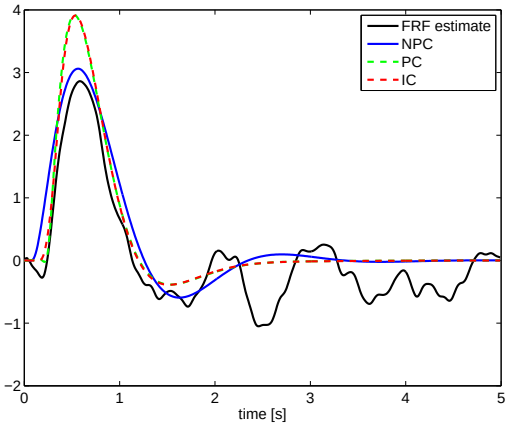

(c) Subject 4

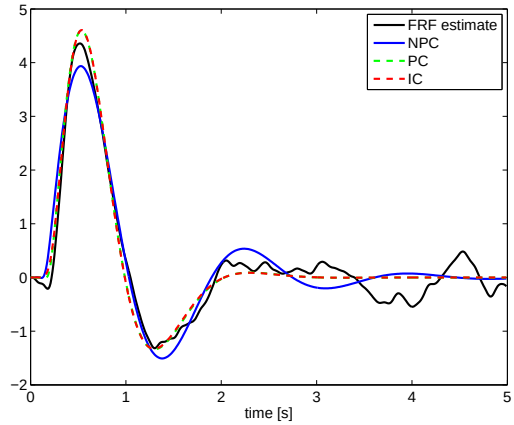

(d) Subject 5

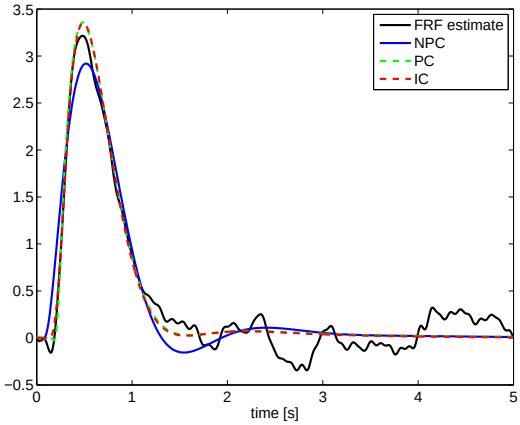

(e) Subject 6

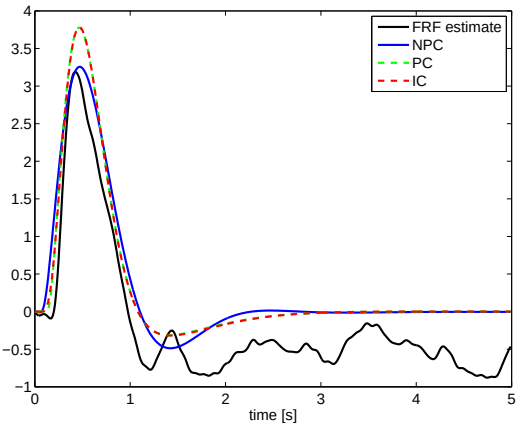

(f) Subject 7

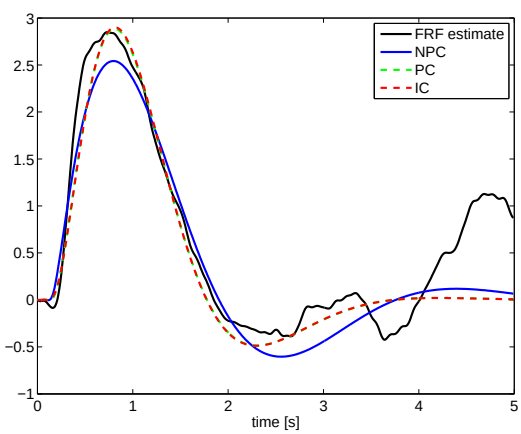

(g) Subject 8

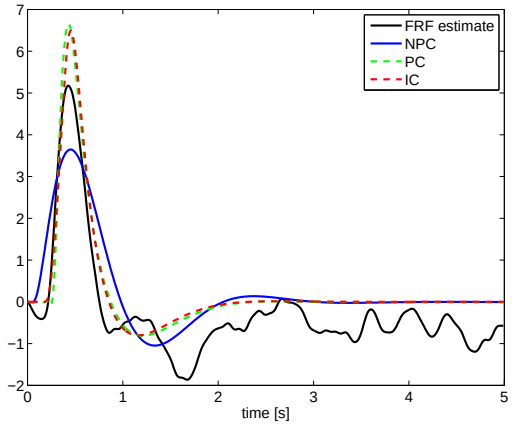

(h) Subject 9

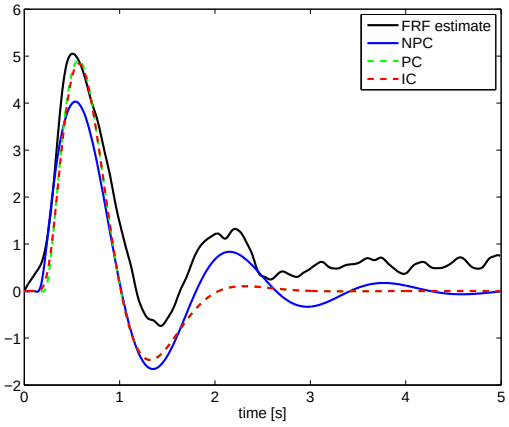

(i) Subject 10

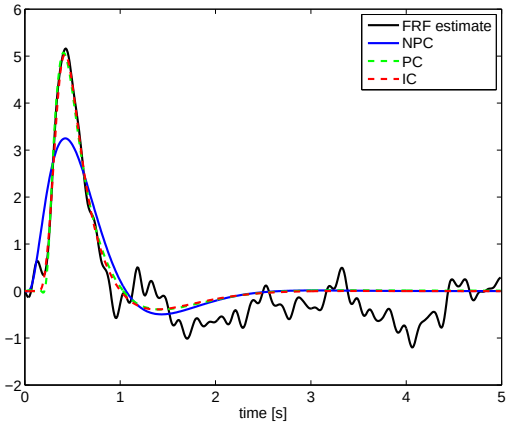

(j) Subject 11

Figure A.6: Impulse responses plots obtained from the estimated frequency responses (black line) and from the fitted responses for the different controller structures (coloured lines).

Appendix B

Figures chapter 5

In this Appendix individual results relating to chapter 5 are shown.

Figure B.1 shows the intermittent interval distributions that correspond to the optimal θ^* for each of the experimental data. This figure is related to Figure 5.6b.

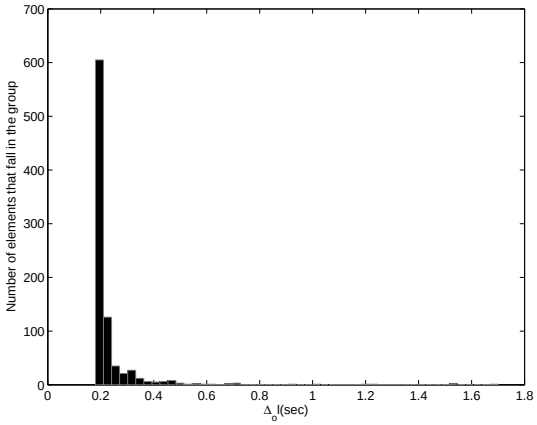

(a) Subject 1

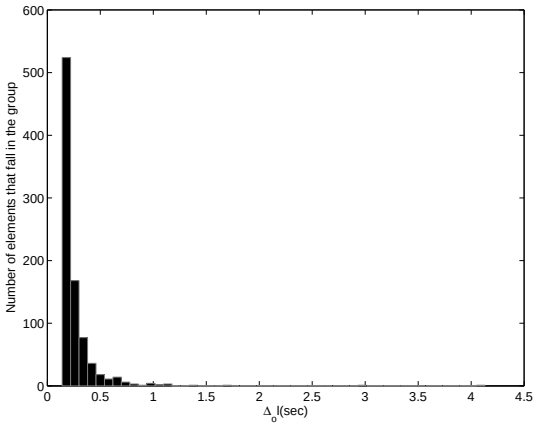

(b) Subject 2

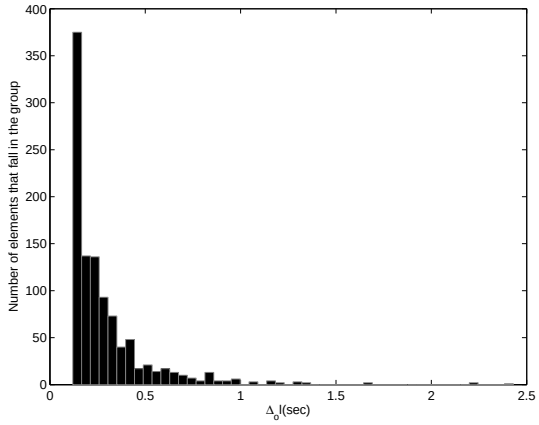

(c) Subject 4

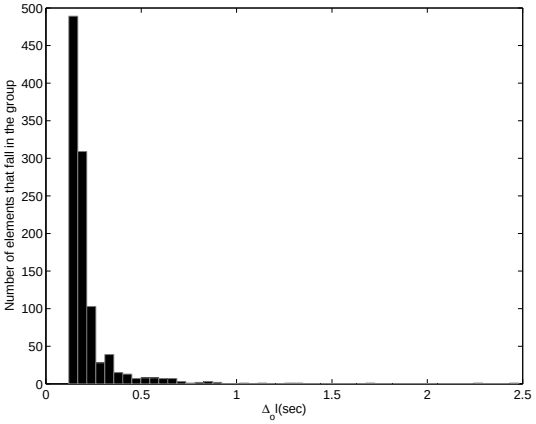

(d) Subject 5

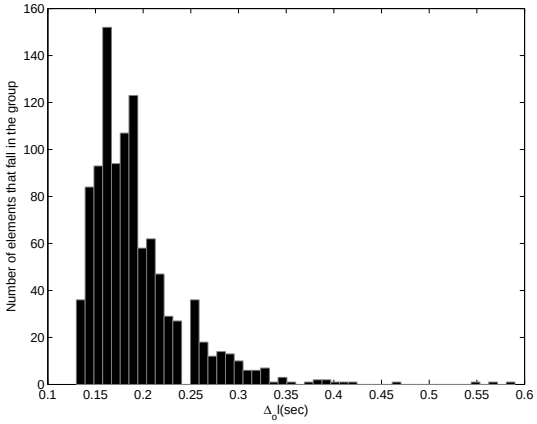

(e) Subject 6

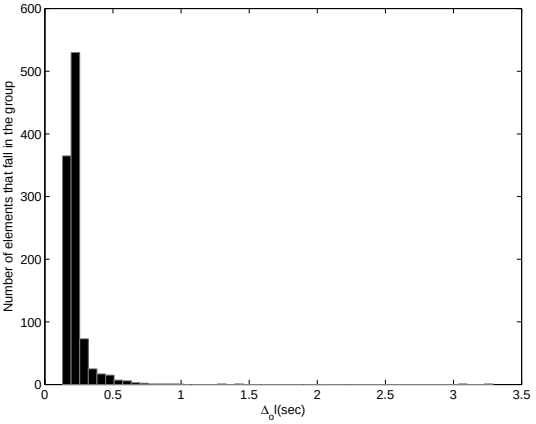

(f) Subject 7

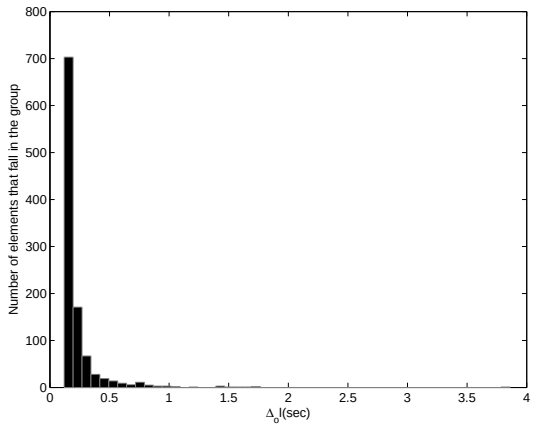

(g) Subject 8

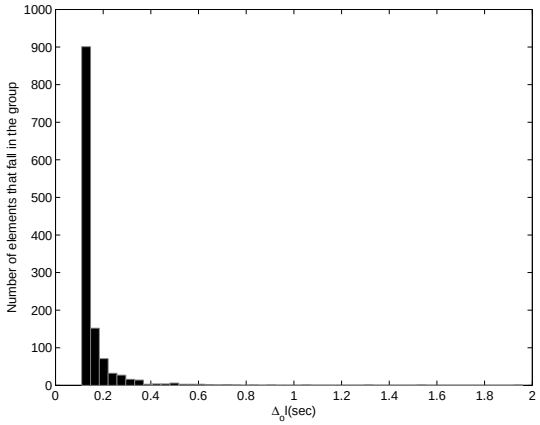

(h) Subject 9

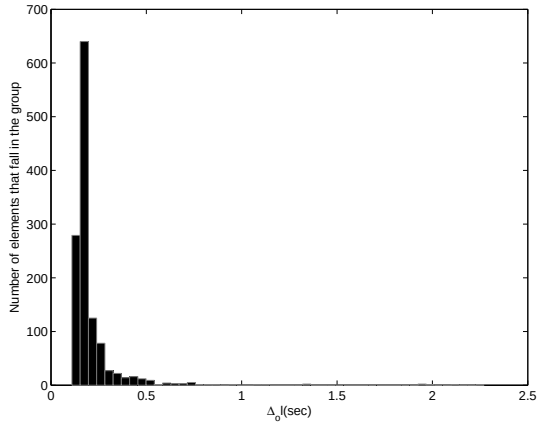

(i) Subject 10

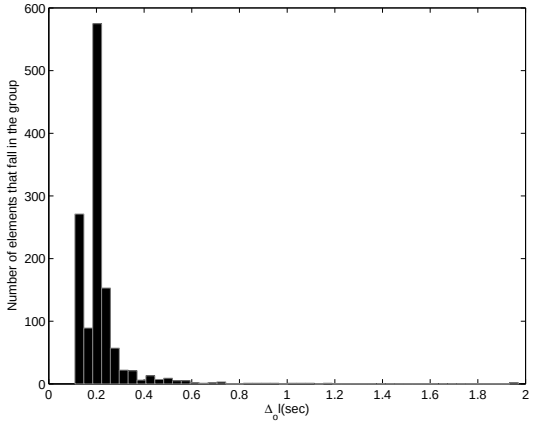

(j) Subject 11

Figure B.1: Intermittent interval distributions corresponding to the optimal θ^* which has been determined for each experimental data.

Figures B.2, B.3, B.4 show the experimental PSD data against the optimal simulated PSDs for each of the control systems. These figures are related to Figure 5.7.

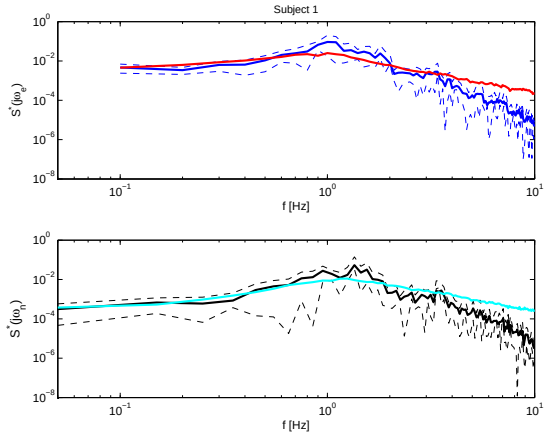

(a) Subject 1

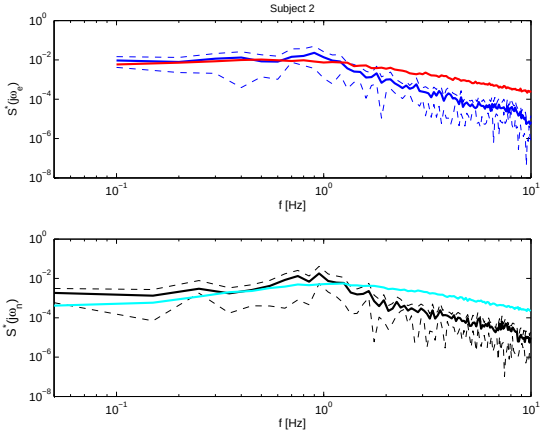

(b) Subject 2

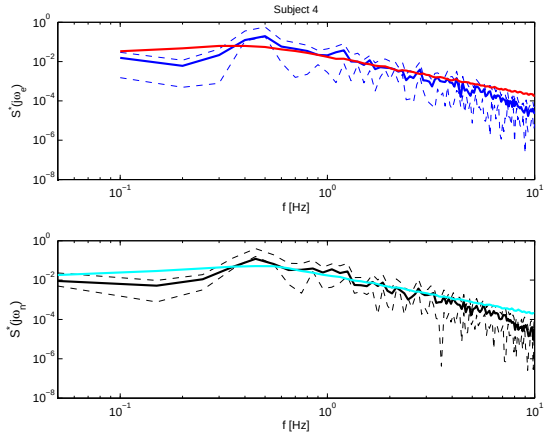

(c) Subject 4

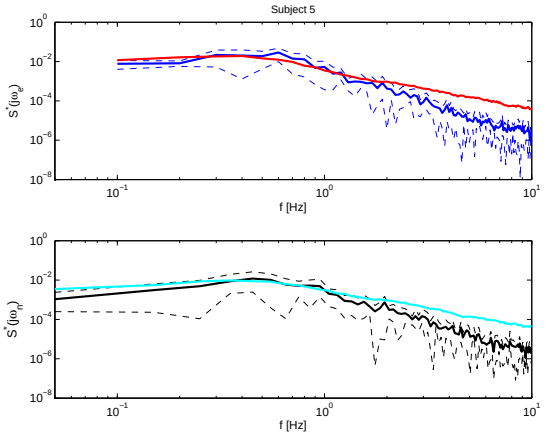

(d) Subject 5

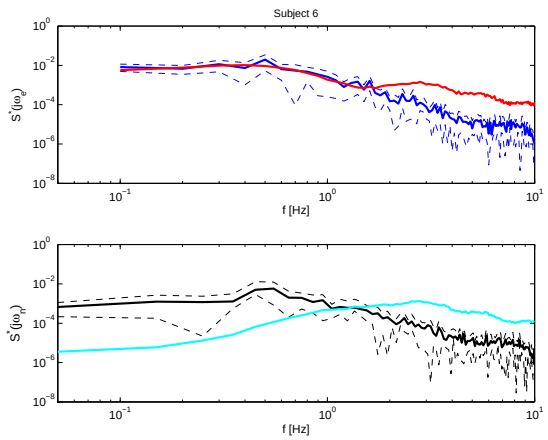

(e) Subject 6

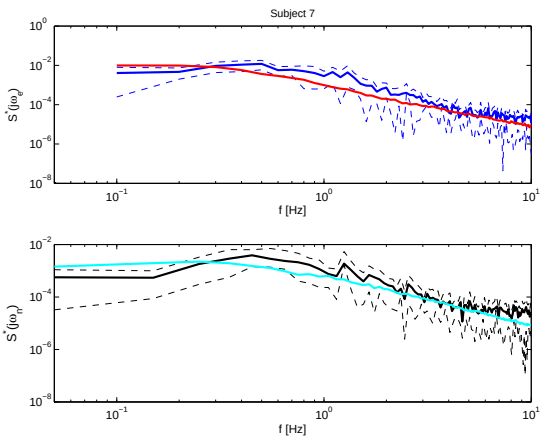

(f) Subject 7

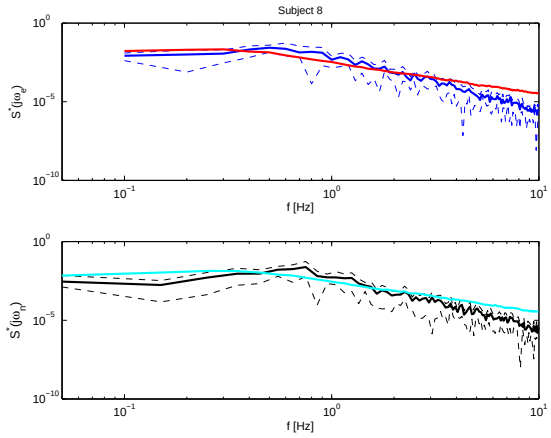

(g) Subject 8

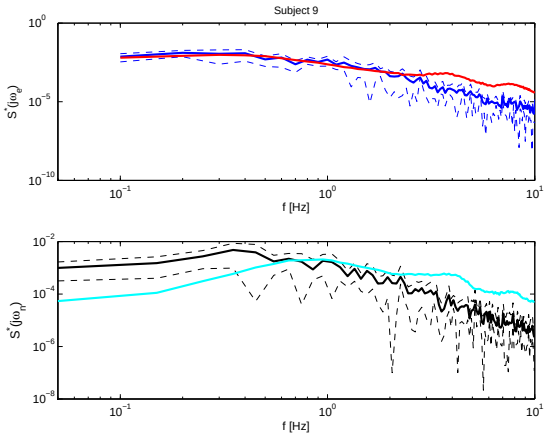

(h) Subject 9

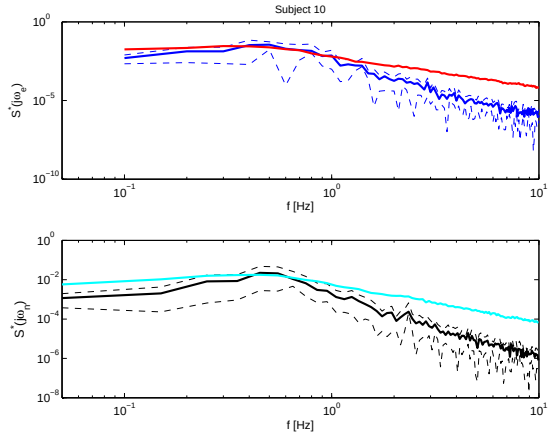

(i) Subject 10

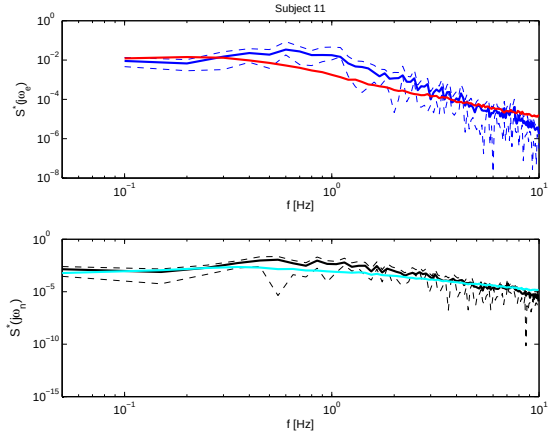

(j) Subject 11

Figure B.2: Experimental PSD data against the optimal simulated PSDs obtained using an intermittent controller with a varied intermittent interval. In each subfigure the top graph shows, at excited frequencies, the experimental PSD (blue line) against the optimal simulated PSD (red line), whereas in bottom graph shows, at non- excited frequencies, the experimental PSD (black line) against the optimal simulated PSD (cyan line). The dashed black lines depicts the standard deviation of the experimental PSD.

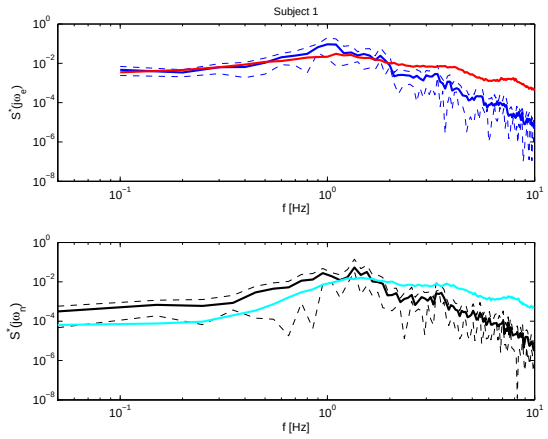

(a) Subject 1

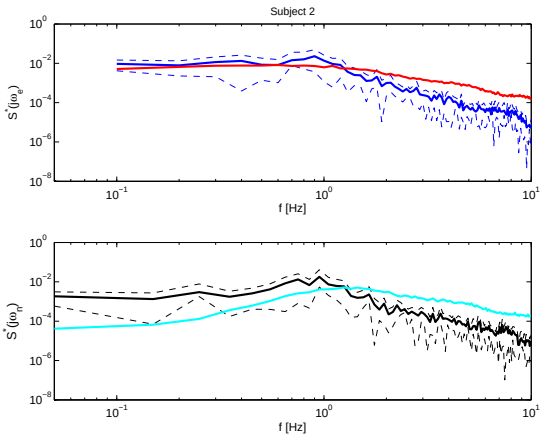

(b) Subject 2

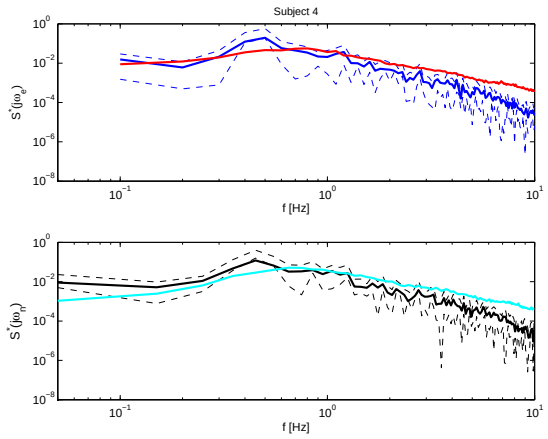

(c) Subject 4

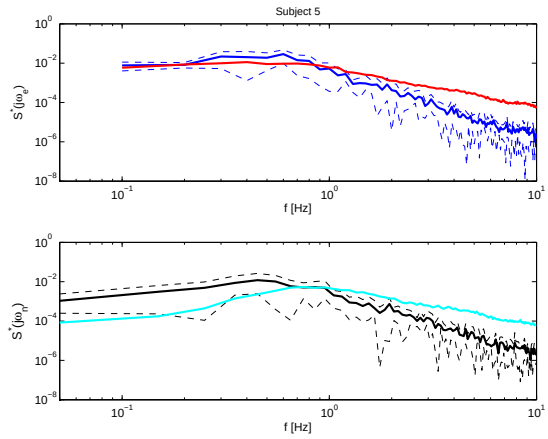

(d) Subject 5

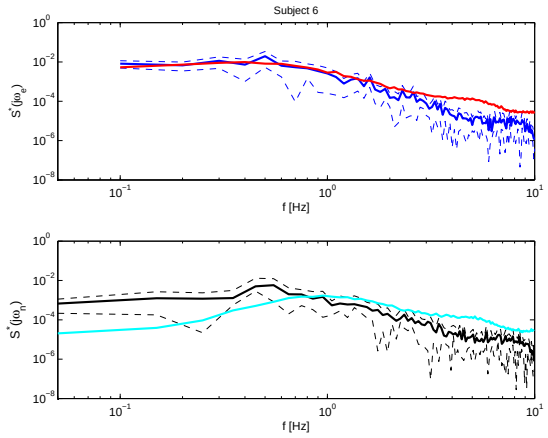

(e) Subject 6

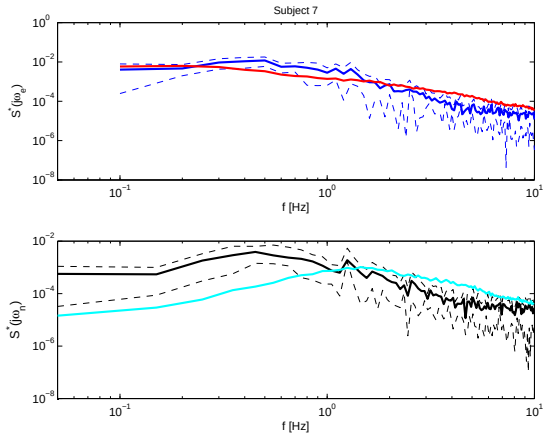

(f) Subject 7

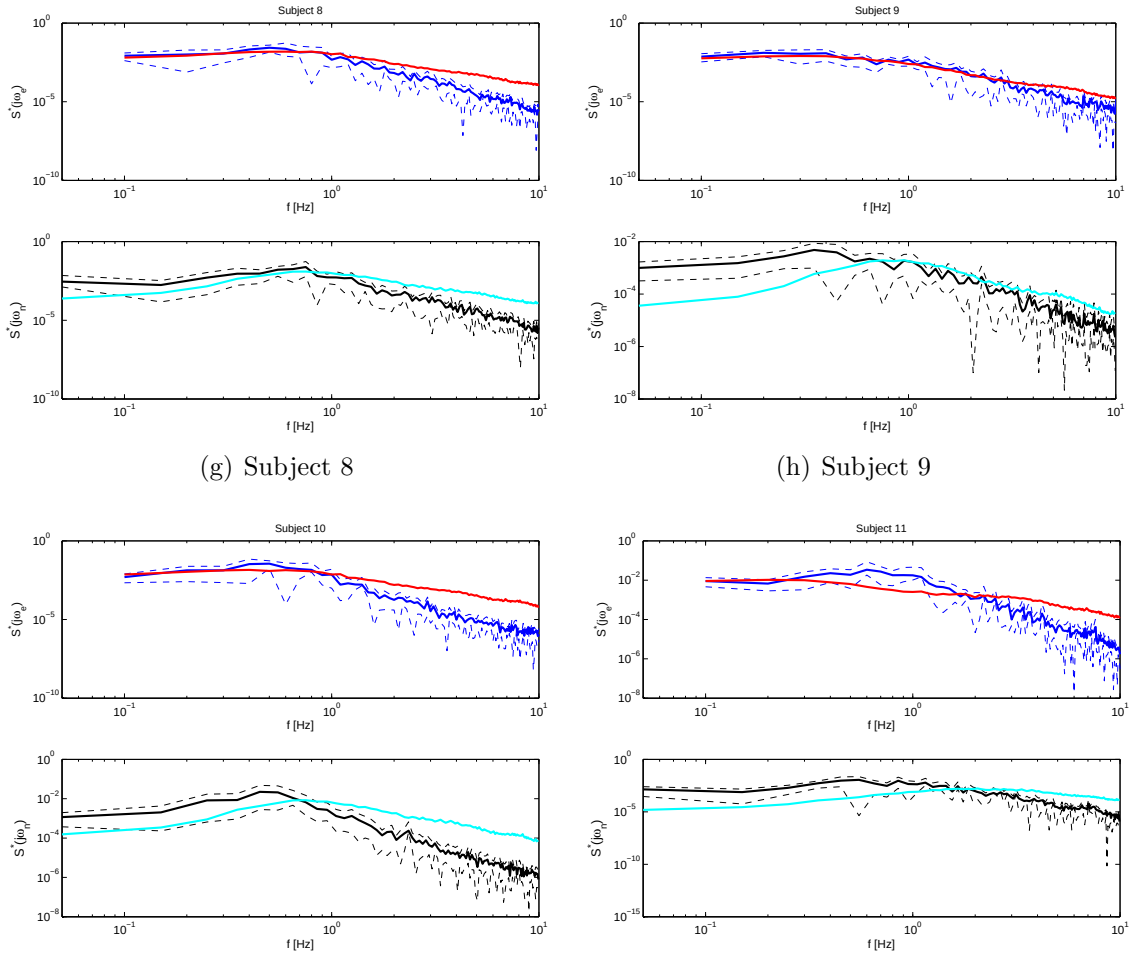

(g) Subject 8

(h) Subject 9

(i) Subject 10

(j) Subject 11

Figure B.3: Experimental PSD against the optimal simulated PSDs obtained using a continuous-time predictive controller with an observation signal added to the system. In each subfigure the top graph shows, at excited frequencies, the experimental PSD (blue line) against the optimal simulated PSD (red line), whereas the bottom graph shows, at non-excited frequencies, the experimental PSD (black line) against the optimal simulated PSD (cyan line). The dashed black lines depicts the standard deviation of the experimental PSD.

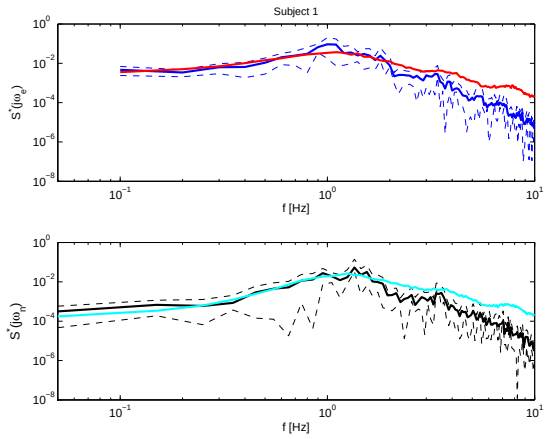

(a) Subject 1

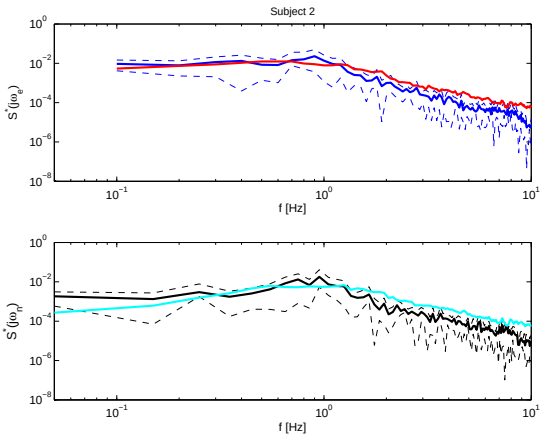

(b) Subject 2

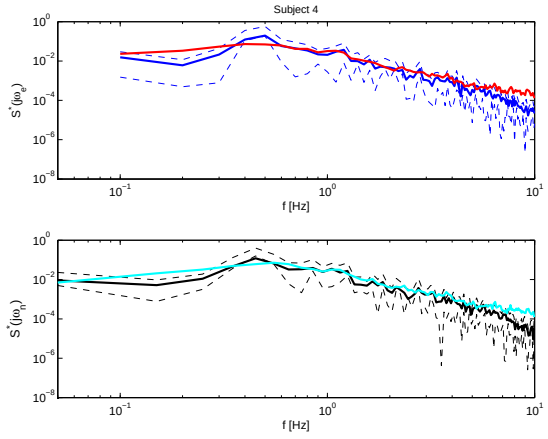

(c) Subject 4

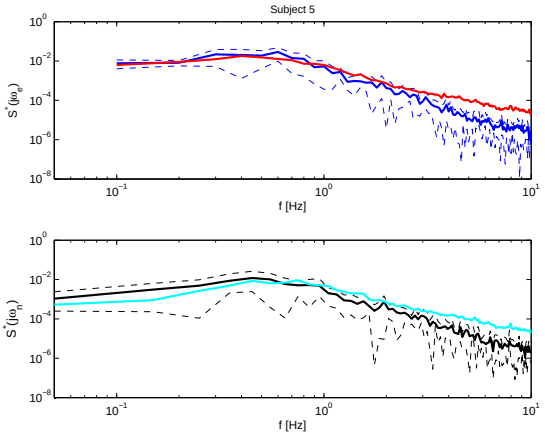

(d) Subject 5

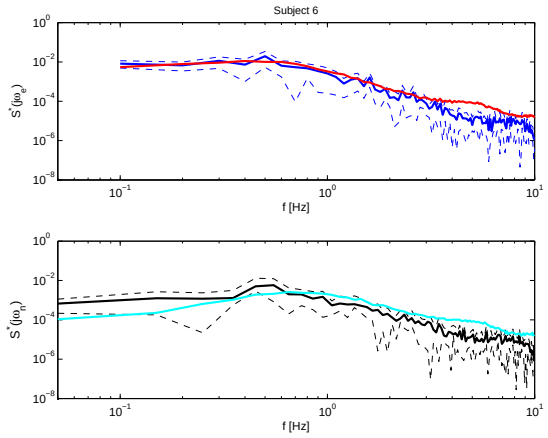

(e) Subject 6

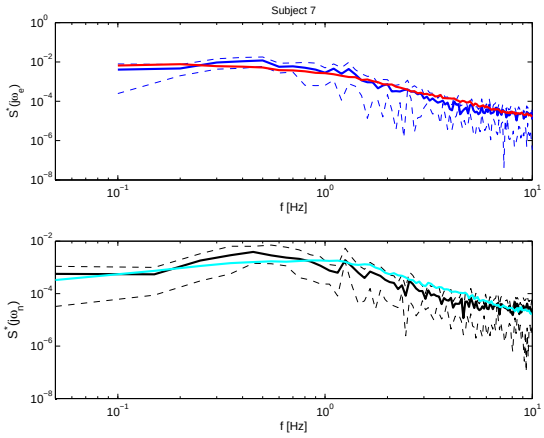

(f) Subject 7

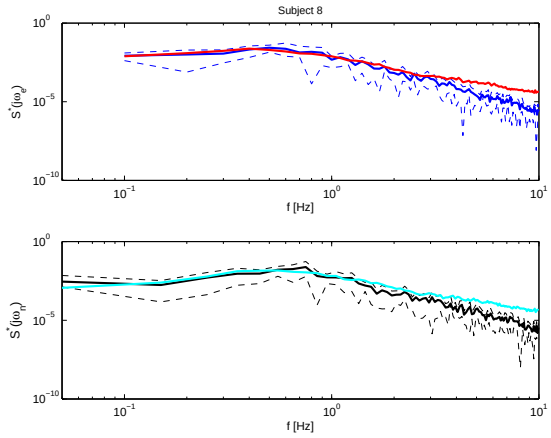

(g) Subject 8

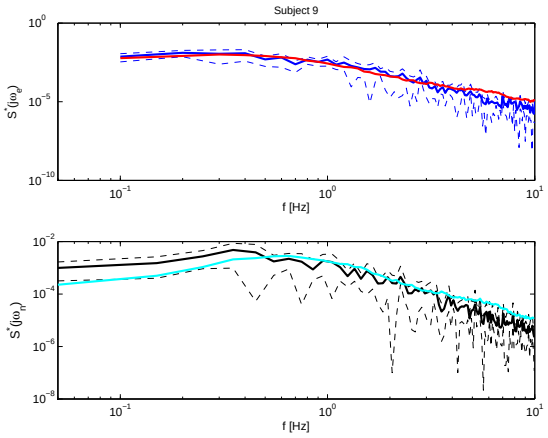

(h) Subject 9

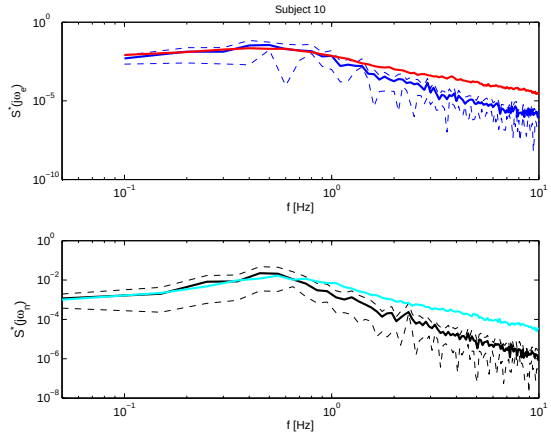

(i) Subject 10

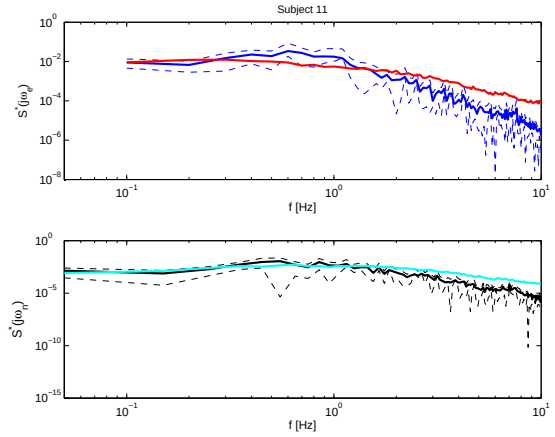

(j) Subject 11

Figure B.4: Experimental PSD against the optimal simulated PSDs obtained using a continuous-time predictive controller with a dependent motor signal added to the system. In each subfigure the top graph shows, at excited frequencies, the experimental PSD (blue line) against the optimal simulated PSD (red line), whereas the bottom graph shows, at non-excited frequencies, the experimental PSD (black line) against the optimal simulated PSD (cyan line). The dashed black lines depicts the standard deviation of the experimental PSD.

[This page is intentionally blank]